



**The University of
Nottingham**

UNITED KINGDOM • CHINA • MALAYSIA

Modelling of Biomass Milling

Gary Newbolt, BSc (Hons)

Thesis submitted to the University of
Nottingham for the degree of Doctor of
Engineering

May 2018

Abstract

Strategies to combat climate change focus on every industry and has led to government policies to reduce electricity generation through coal combustion. Switching to biomass provides an opportunity to use infrastructure constructed for coal combustion with carbon neutral fuels; however, the process of grinding biomass pellets as fuel in pulverised fuel combustion is not well known. 1% of energy generated at a power plant is utilised to achieve the required size for the fuel. Improvements in the understanding of biomass pellet milling could lead to optimisation of operating conditions and minimisation of energy consumption. The process could aid generators determine appropriate fuels and costs for each; this represents a potential opportunity to elongate the life of current power stations, which is more cost effective than construction of new biomass specific plants.

This research has developed a population balance equation (PBE) model simulation to predict the output of biomass pellet grinding for Lopulco E1.6 mill and a Retsch PM100 planetary ball mill; this has never been published in literature. It has proven it can predict the output particle size distribution of a Lopulco E1.6 mill, a scale model of an industrial mill, for biomass pellet PSD's. It has shown that the simulation parameters can be based on axial and flexure deformation testing results, and that it can predict the PSD to within an average 88% accuracy against blind test. A novel technique in evaluating a PSD has been achieved using an overlapping coefficient, a measure better suited to PSD analysis than conventional model validation techniques. The PBE simulation has also shown that back calculating parameters can separate mill and material contributions when utilising a popularly used selection function and a breakage function developed in this research based on the Rosin-Rammler equation. This has been shown for the Lopulco mill and a lab scale planetary ball mill for axial and flexure deformation tests respectively.

The research shows that emphasis should be placed on understanding classifier dynamics due to unexpected behaviour in the Lopulco mill experiments. Further conclusions show that energy consumption can be related to axial deformation energy that can be explained by the action of a Lopulco mill's application of compressive force on and the orientation of pellets against the rollers.

Acknowledgements

I would like to thank my colleagues that assisted me throughout this research project; these include Dr Pete Connor and his assistant Kevin Bersch, Mr Daniel Fallows, Mr Salvatore La Rocca, Mr Patrick Whitelaw and Dr Lee Stevens all of whom aided in the collection and training for me with regards to the experimental research completed.

For the support and entertainment that grounded me throughout this EngD programme I would like to thank all my friends, which includes those above, with special mentions for two of the best, Mr Chris Bridge, and for providing a soundboard for ideas and problem solving, Mr Scott Russell. For all those who helped guide me to peruse a doctorate in engineering, my parents, and my lecturers at Sheffield Hallam University, notably Dr Ian Halliday, I would also wish to express my thanks.

I would like to thank the Biomass and Fossil Fuel Research Alliance for providing financial support and access to industrial specialists. Especially the supervision team provided by them, from GE Power, Dr Dave Waldron, Mr Greg Kelsall, from the BF2RA Mr Peter Sage, as well as those who have taken part from the BF2RA members. All of whom were a valuable contact to help guide the project and build foundation knowledge of the biomass milling subject. I would also like to thank the Engineering Physical Sciences Research Council for their financial support for the project.

I would like to thank Dr Orla Williams for helping to develop my knowledge in the subject, for assistance in experimental work and her valued friendship. And lastly, I would like to thank Dr. Carol Eastwick and Dr. Paul Langston for their supervision, guidance, support, ideas and feedback they have provided to me throughout the last 4 years.

Contents

Abstract	i
Acknowledgements.....	ii
List of Tables	ix
List of Figures.....	xii
Chapter 1 - Introduction.....	1
1.1 Anthropogenic CO ₂ Emissions.....	1
1.2 Grinding Processes and Pulverised Fuel Combustion	1
1.2.1 Process Overview	2
1.2.2 Industrial Mills	3
1.3 Motivation for the Research and Research Objectives	7
Chapter 2 - Literature Review	10
2.1 Properties of Biomass.....	10
2.1.1 Microstructure of Biomass.....	11
2.1.2 Biomass Properties	12
2.1.3 Pre-Treatment of biomass.....	13
2.2 Grindability of Biomass	15
2.2.1 Grinding Theory.....	15
2.2.2 Fracture Mechanics of Biomass	16
2.2.3 Single Particle Fracture	17
2.2.4 Particle Breakage Mechanisms.....	19
2.2.5 Material Comminution Indexing.....	19
2.3 Particle Characterisation.....	21
2.3.1 Distribution Analysis.....	21
2.3.2 Methods of Particle Analysis	23
2.4 Milling Options in Power Stations	24
2.4.1 Biomass Combustion Options	24
2.4.2 Dedicated Biomass Combustion.....	25

2.4.3 Coal to Biomass Conversions	26
2.5 Circuit Operation	26
2.6 Mills	27
2.7 Size Classification.....	28
2.8 Safety Aspects of Mill Operation.....	29
2.8.1 Dust Ignition.....	29
2.8.2 Design Features for Safe Operation	29
2.9 Mill wear	30
2.10 Effects of Mill Operating Variables	31
2.11 Modelling approaches.....	34
2.11.1 Empirical Modelling.....	35
2.11.2 Numerical Simulation Modelling	39
2.12 Up-Scaling Methods	44
2.13 Literature Review Conclusions	45
Chapter 3 - Modelling Technique Evaluation and Ranking	47
3.1 Data Analysis	47
3.1.1 Literature.....	47
3.1.2 Industrial Partner Information	52
3.1.3 Sister Project Experiment Information.....	54
3.1.4 Data Analysis Conclusions.....	56
3.2 Evaluation Framework.....	57
3.2.1 Modelling Score Card Areas	57
3.3 Modelling Techniques	61
3.3.1 Artificial Neural Networks.....	62
3.3.2 Population Balance Equation Method	65
3.3.3 Discrete Element Method.....	68
3.3.4 Finite Element Method	72
3.3.5 Finite Volume Method	75

3.3.6 Particle Finite Element Method	78
3.3.7 Smoothed Particle Hydrodynamics Method	80
3.3.8 Hybrid Modelling Techniques in Literature	82
3.4 Model Ranking Results.....	83
Chapter 4 - The Population Balance Equation Method.....	86
4.1 General Theory.....	86
4.1.1 Background	86
4.1.2 The Breakage Population Balance Method	87
4.1.3 Method of Solution	89
4.2 Selection and Breakage Functions	91
4.3 Simulation Implementation	91
4.3.1 Method Validation.....	91
4.3.2 Parameter Back Calculation Method	92
4.4 The Overlapping Coefficient.....	92
4.5 Steady-State Simulations	93
4.6 Simulation Experimental Process	95
4.6.1 Domain Separation.....	95
4.6.2 Feed generation.....	95
4.6.3 Optimised Selection and Refinement.....	96
Chapter 5 - Experimental Methodology.....	98
5.1 General Analysis Methods	98
5.1.1 Particle Analysis.....	98
5.1.2 Mass Fraction Oversize Sieve Analysis	98
5.1.3 Volume Fraction Undersize Dynamic Analysis	99
5.1.4 Energy Consumption Data Logging.....	100
5.1.5 Mass Output Analysis	100
5.2 Lopulco E1.6 Mill	101
5.2.1 Mill.....	101

5.2.2 Air Flow Rates	104
5.2.3 Experimental Design	105
5.3 Material Characterisation	107
5.3.1 Sister Project Characterisation Summary	107
5.3.2 Skeletal Density Measurements	109
5.3.3 Surface Area Analysis via Kr Gas Adsorption	109
5.4 Statistical Analysis and Error.....	110
5.5 Conclusion	110
Chapter 6 - Experimental Results.....	111
6.1 Lopulco Ring and Roller Mill.....	111
6.1.1 Initial Observations.....	113
6.1.2 Response to Mill Table speed.....	115
6.1.3 Response to Change in Feed Rate	119
6.1.4 Response to Change in Classifier Vane Angle	124
6.1.5 Response to Fuel Type	129
6.2 Material Characterisation	134
6.3 Conclusions.....	137
Chapter 7 - Population Balance Modelling Results.....	140
7.1 Model Validation.....	140
7.1.1 Discretised Matrix PBE.....	140
7.2 Batch Process Model	145
7.2.1 Determining Appropriate Selection and Breakage Functions, Batch Processing.....	146
7.2.2 Extracting Material Differences, Batch Simulations	148
7.3 Lopulco Milling Modelling	154
7.3.1 Classifier Function.....	154
7.3.2 Material Differences.....	155
7.3.3 Operational Difference.....	160

7.4 Blind Testing of the Steady State Model.....	165
7.4.1 Blind Testing Operational Conditions	165
7.4.2 Blind Testing Materials	167
7.5 Conclusions.....	167
Chapter 8 - Single Impact Testing and a Master Curve Population Balance Model.....	169
8.1 Background	169
8.1.1 Experimental Process	170
8.2 Experimental Results	173
8.2.1 Master Curve	173
8.2.2 Comparison with Material Characterisation Tests.....	175
8.3 Simulation Results.....	177
8.4 Conclusions.....	179
Chapter 9 - Conclusions and Future Work	180
9.1 Objectives.....	180
9.2 Modelling Review.....	180
9.3 The Population Balance Equation Method.....	181
9.4 Experimental.....	182
9.5 Recommendations for Future work	182
Appendix A: Mill Types.....	I
Appendix B: Modelling Technique Evaluation and Ranking Analysis Paper Summary	XXI
Appendix C: Modelling Technique Evaluation and Ranking Industrial Partner Survey	XXX
Appendix D: Modelling Technique Evaluation and Ranking Scorecard	XXXV
Appendix E: Modelling Technique Evaluation and Ranking Results ...	XL
Appendix F: Particle Characteristics	XLII

Appendix G: Overlapping Coefficient Calculation MatLab™ Script	
XLVIII	
Appendix H: Biomass Materials Used in the Research.....	XLIX
Appendix I: Lopulco Experiment Mean Results.....	LII
References	LIX

List of Tables

Table 2.1 showing the different circuit operations usable in milling, source: adapted from (Coulson, 1999; Green, 2008).....	27
Table 2.2 showing the grinding mechanisms applicable to the type of mill.	28
Table 2.3 lists the energy laws and describes their differences.	36
Table 3.1 displays industrial milling manufacturers and models used or manufactured by BF2RA members for grinding different fuels.....	52
Table 3.2 displays the independent variables used by the industrial generators as controlled variables for milling.	53
Table 3.3 displays the dependent variables in relation to industrial milling practices.	53
Table 3.4 displays the laboratory mills used within the sister project and variables that were tested as part of the experimental process.	55
Table 3.5 displays the dependent variables for which experimental results have been collected within the scope of the sister project.	56
Table 3.6 displays the secondary variables of interest to the research but not primary to the objectives of the project.	58
Table 3.7 displays the modelling techniques that are considered for use under the research project.	62
Table 3.8 displays the scorecard for the Artificial Neural Network method.....	65
Table 3.9 displays the scorecard results for PBE methods.	68
Table 3.10 displays the nomenclature for equations 3.3 and 3.4.....	68
Table 3.11 displays the scorecard results for DEM.....	72
Table 3.12 displays the scorecard for the FEM.	75
Table 3.13 displays the scorecard for FVM.....	77
Table 3.14 displays the scorecard for PFEM.	80
Table 3.15 displays the scorecard for SPH.	82
Table 3.16 displays examples in literature of hybrid modelling techniques.....	83
Table 5.1 displays the independent and dependent variables for the Lopulco mill experiments.	102
Table 5.2 displays the sensors used for the Lopulco milling experiments.....	103
Table 5.3 displays the Venturi tube specification from the Lopulco E1.6 mill....	104

Table 5.4 displays the experimental settings used in the Lopulco mill experiments.	106
Table 6.1 displays the deformation energies in the various orientations taken from the sister project for the biomass pellets used in the material variation Lopulco rperiments.....	129
Table 6.2 displays which tests were carried out as part of which project; this one, “Modelling of Biomass Milling” or the sister project, “On Biomass Milling for Power Generation”.....	135
Table 7.1 displays the selection functions used in the population balance equation simulations.	141
Table 7.2 displays the breakage functions used in the population balance equation simulations.	142
Table 7.3 displays the optimisation values to which the optimisation process back calculated the parameter values to. Included is a measure of the time taken to complete the back calculation and for providing a solution when handed a set of values.....	145
Table 7.4 displays the initial optimisation optimal models, along with the second and third ranked model for each biomass species.....	147
Table 7.5 displays the deformation energies in the different axis for each of the biomasses used in in the PM100 batch milling trials.	149
Table 7.6 displays the values of the selection and breakage model parameters established after the optimisation programme for material differences has been completed. χ indicates the axial deformation energy.....	160
Table 7.7 displays the initial optimisation values for the operational differences study into the parameters for the selection and breakage model S3, B1 as was as the initial constraints on them.	160
Table 7.8 displays the various model relationships that have been found for the S3, B1 population balance model.....	164
Table 7.9 displays the overall statistics of the operational conditions blind tests.	165
Table 7.10 displays the accuracy of the simulation because of the operational conditional settings. The model is unaffected by operational conditions.	165

Table 7.11 displays the overall statistics of the blind test on Eucalyptus after reconfiguring the model to account for operational conditions.	167
Table 8.1 displays the improvements in accuracy of the Single Impact Testing based Population Balance Equation simulation with reductions in the iteration step size.....	178
Table 8.2 displays the statistics of the OVL results for the SIT PBE simulation training.....	178

List of Figures

Figure 1.1 displays the process of pulverised fuel combustion for electricity generation, (World Coal Association, 2014).2

Figure 1.2 displays the concept of ball and tube mill from the viewpoint of the end of the mill. The illustration is specific for a lab scale Bico ball mill however the function is the same, other than the scale, differences include the insert of wear plates along the circumference and grinding balls of uniform size.3

Figure 1.3 displays the concept of the vertical spindle mill, specifically a ring and roller Lopulco style mill.....4

Figure 1.4 displays the concept of a hammer mill, whereby a rotating core swings flailing hammers to cause size reduction through shearing and abrasion....5

Figure 1.5 displays several variations for industrial classification processes; top right, whizzer blade classifier, top left, gravitational inertial air classifier, image source: <http://www.metso.com/products/separation/gravitational-inertial-air-classifier>, bottom left, perforated and serrated screen classifiers, image source: http://www.marksutton.co.nz/perforated_metal.htm, bottom right, rejecter blade design, image: <http://www.sturtevantinc.com/products/product/whirlwind-air-classifier>.6

Figure 2.1 displays the classification of biofuel sources by different characteristics source: (Food and Agricultural Organization of the United Nations, 2004)10

Figure 2.2 shows the configuration of wood tissues. **A** Adjacent cells. **B** cell wall layers. S1, S2, S3 secondary wall layers, P primary wall, ML middle lamella. **C** Distribution of lignin, hemicellulose, and cellulose in the secondary wall (Pérez, Munoz-Dorado, de la Rubia, & Martinez, 2002).11

Figure 2.3 displays the difference in energy requirements necessary to grind Miscanthus and Switchgrass through various size screens, comparisons of the effect of moisture content is also made. Note ‘Air-dry’ has moisture content between 7-10%, source: (Miao et al., 2011).13

Figure 2.4 showing modes of crack propagation, mode I: opening, mode II: in-plane shear, mode III: out-of-plane shear, source: (Schreurs, 2009).16

Figure 2.5 showing the principle systems of crack propagation in wood, source: (Barrett et al., 1981).....	17
Figure 2.6 displays the factors affecting the breakage of a particle, source: (Green, 2008).....	17
Figure 2.7 shows an example of particle size distribution plots on normal (top) and logarithmic scales (bottom), source: (Green, 2008).	22
Figure 2.8 (left) displays a laboratory mechanical sieving apparatus, source: http://www.retsch.com/dltmp/www/2058-1ca7f28fb7bb/brochure_sieving_en.pdf . (Left) displays the outline of the sieving technique, image source: http://www.scryptirenews.com/crumb.php#prettyPhoto/4/	23
Figure 2.9 outlining the processing routes biomass and coal can take for combustion in a pulverised fuel boiler, source: (Livingston, 2013).....	24
Figure 2.10 showing the factors affecting the combustion of dust particles, source: (Kauffman, 1981).....	29
Figure 2.11 highlighting the hierarchy of modelling approaches, at the higher level more detail about milling is discovered but at the expense of computational time, source: Extracted from (Herbst & Fuerstenau, 1980).	34
Figure 2.12 provides an illustration of the principles of DEM, (P. W. Cleary, 2009).	39
Figure 2.13 displays a liquid flow modelled with the SPH technique, image source: http://www.itm.uni-stuttgart.de/research/pasimodo/video_gallery_de.php	42
Figure 2.14 displays the UCM model structure, source: (Powell et al., 2008).	43
Figure 3.1 displays the survey results for the types of mills used in published literature on biomass milling.	48
Figure 3.2 displays the biomass species and form of the biomass that has been used to study biomass milling in the literature surveyed.	49
Figure 3.3 displays the survey results of the independent variables that are tested in literature based on the milling of biomass material.....	50
Figure 3.4 displays the most frequently collected dependent variables in published biomass milling literature.	51
Figure 3.5 displays the concept of an Artificial Neural Networks neuron complete with inputs, weights, bias, summation, activation function and output.....	62

Figure 3.6 displays the architecture of artificial neural networks inclusive of input, hidden and output layers.....	63
Figure 3.7 displays the process flow algorithm of DEM.....	69
Figure 3.8 displays the 2 stated methods of breakage modelling in DEM, particle packing and replacement (left), and the bonded particle method (right)...	69
Figure 3.9 displays how domains are discretised in finite element simulations, here the stresses on a tumbling ball and tube type mill liner are simulated (Jonsén, Pålsson, & Häggblad, 2012).....	73
Figure 3.10 displays the concept of the finite volume method.....	76
Figure 3.11 displays a representation as how PFEM works, detailing the meshing, solution, and updating of nodal position in the process (E Oñate et al., 2011).....	78
Figure 3.12 displays a representation of the smoothed particle hydrodynamics method.....	81
Figure 3.13 displays the final total scores from the model technique evaluation process.	84
Figure 4.1 displays the concept of the overlapping coefficient, which is used in comparing distributions and as an objective function for optimisation. ...	93
Figure 4.2 displays the concept of the steady state PBE model.	93
Figure 5.1 displays the particle size ranges for which various particle analysis techniques are effective.	98
Figure 5.2 displays the concept of the CAMSIZER P4 and how it captures and analyses particle information.	100
Figure 5.3 displays pictures of the Lopulco E1.6 mill used in the project and based at the University of Nottingham.....	101
Figure 5.4 displays the set up for the Lopulco mill experiments including, mass output, temperature and pressure tapping points.	102
Figure 5.5 displays the close-up schematic of the pressure transducer mounting on the Lopulco mill.	103
Figure 5.6 displays a representation of the adjustable vanes on the Lopulco mill classifier system; (upper) the rotating core, (lower) individual vanes.	105
Figure 5.7 displays the central composite circumscribed experimental design philosophy.....	106

Figure 5.8 displays the axial orientation Instron mechanical testing arrangement.	108
Figure 5.9 displays the diametric orientation Instron mechanical testing arrangement.	108
Figure 5.10 displays the flexure Instron mechanical testing arrangement.	109
Figure 6.1 displays the relation between the residence time and the specific effective energy. It shows that there is no relation between the two. The triangular data points represent the star points of the CCC DoE regime.	113
Figure 6.2 displays the feed rate against the output rate of the milling experiments to highlight that using the experimental mill, it becomes difficult to achieve a steady state experiment.	114
Figure 6.3 displays the Rosin-Rammler characteristic size parameter with variation in mill speed for the Lopulco milling experiments. It shows there seems to be either no or a quadratic relationship.	115
Figure 6.4 displays the Rosin-Rammler spread parameter with variation in mill table speed for the Lopulco mill experiments. Again, it shows that there is no or a possible quadratic relationship.	116
Figure 6.5 displays the variation in residence time with mill speed for the Lopulco milling experiments. It shows that there is little variation except where other parameters are factored into the argument.	117
Figure 6.6 displays the variation in mass output of the Lopulco mill experiments with the mill speed. Here it shows that the mass output is likely a product of the mill speed with the classifier vane angle.	118
Figure 6.7 displays the Specific Effective Energy consumption attributed to the Brites wood pellets with varying mill speed. Whilst mill speed seems to have little effect on the result there is high variation in between experimental repeats.	118
Figure 6.8 displays the Rosin-Rammler characteristic size parameter with variation in feed rate for the Lopulco milling experiments, again showing the potential quadratic relationship.	119
Figure 6.9 displays the variation of the Rosin-Rammler characteristic spread parameter with feed rate. It shows again a possible quadratic relationship.	120

Figure 6.10 displays the residence time variation with feed rate in the Lopulco mill experiments. Only small variation is observed that could be a consequence of experimental error. Outside effects of high mill speed and a fully open classifier shows signs of a greater effect.	121
Figure 6.11 displays the variation in mass output rate with feed rate. As there was no one to one relationship, there are indications that steady-state conditions were not achieved.....	121
Figure 6.12 displays the Specific Effective Energy to mill the pellets at varying feed rates into the mill. A decaying exponential relationship is observed in increasing feed rates.....	122
Figure 6.13 displays the running energy consumption, mass throughput, air flow and temperature for the 3rd experimental run of conditions whereby, feed rate: 0.014 kg s^{-1} , mills speed: 202 RPM and the classifier vane is 90°	123
Figure 6.14 displays the 1st experimental run energy consumption, air flow and mill outlet air temperature for the running conditions of feed rate: 0.006 kg s^{-1} , mill speed: 202 RPM and classifier vane angle: 90°	124
Figure 6.15 displays the variation in the Rosin-Rammler characteristic size variation with the classifier vane. The correlation seems strong as expected however it seems to in a contrary relation to that which was expected.....	124
Figure 6.16 displays the variation in the Rosin-Rammler characteristic spread parameter with the classifier vane. The graph shows a narrower spread at smaller angles as expected, yet there is much higher spread of results with a fully open classifier vane.	125
Figure 6.17 displays the concept of how the fully open classifier vane in the Lopulco mill might allow larger particles through when at narrow angles and reject them when fully open.....	126
Figure 6.18 displays the variation in the residence time with classifier vane angle. It shows a consistent time except when the classifier is fully open, and a vast elongation when coupled with a fast mill speed.....	127
Figure 6.19 displays the variation in the mass output rate with classifier vane angle. It displays the only small variation until the vane angle is fully open at which point it seems to significantly slow the output when the speeds are high.	127

Figure 6.20 displays the variation in the specific effective energy with the classifier vane angle. It reinforces the evidence that material is staying in the mill longer with the fully open classifier and subsequently being milling for longer.	128
Figure 6.21 displays the variation in the Rosin-Rammler characteristic size with material axial deformation energy. The figure alludes to a possible relation.	129
Figure 6.22 displays the variation in Rosin-Rammler characteristic size with flexure deformation energy. Here the relation seems to have far less relevance on the output.	130
Figure 6.23 displays the variation in the Rosin-Rammler characteristic spread parameter with axial deformation. Here a strong correlation seems to exist.	131
Figure 6.24 displays the variation in the Rosin-Rammler characteristic spread parameter with flexure deformation. Here again strong correlation seems to exist however it is not as strong as in figure 5.23.	131
Figure 6.25 displays the residence time variation with axial deformation energy. A strong relationship seems present with this.	132
Figure 6.26 displays the variation in residence time with flexure deformation energy. Here again the relationship looks likely but not as strong as the axial deformation.	132
Figure 6.27 displays a conceptual diagram showing how axial deformation energy may provide better correlations with the product of milling over diametric deformation energy.	133
Figure 6.28 displays the flexure deformation energy variation with the specific effective energy. The results suggest that flexure energy provides good correlation in this regard.	134
Figure 6.29 displays the variation in the deformation energies with surface area. As no relation with flexure is observed the error bars have been omitted. A reasonable correlation between the surface area and axial deformation energy is present.	136
Figure 6.30 displays the deformation energy variation with skeletal density. Here potential relationships may exist with the diametric and axial deformation energies.	136

Figure 6.31 displays the variation in deformation energy with the variation in the particle density.....	137
Figure 7.1 displays the validation of the Matrix BPBE model against publicised results for the same scheme.....	140
Figure 7.2 displays a top down conceptual diagram of the motion of a PM100 planetary ball mill. Material is only loaded into a grinding vessel with 8 stainless steel grinding balls that follow similar motion to that indicated. Loaded material is ground between the balls and the grinding vessel walls as well as through interactions with other material in there.	145
Figure 7.3 displays the OVL values for the initial back calculation of the parameter values for all the selection and breakage functions when trained against experimental runs for Eucalyptus wood pellets.....	146
Figure 7.4 displays the frequency chart for the selection and breakage function combinations when optimised against the PM100 planetary ball mill experiments for raw biomass species. Included are the average OVL scores for the combinations of high frequency.	147
Figure 7.5 displays the parameter values for the 4 parameters of the selection and breakage combination S3, B1 to indicate the variance and why when studying the material difference effect on the parameters it was concluded to peruse parameters α and γ as material parameters.....	148
Figure 7.6 displays the evolution of the average OVL scores as changes to the optimisation constraints were imposed. It displays how independent OVL accuracy is sacrificed for the ability to improve the model for all species.	150
Figure 7.7 displays the study of the relation between the parameter α and the material deformation energy tests completed within the sister project regime. The final observations suggest a relation to the flexure deformation energy for this mill. Due to the strong relationship, it was hypothesised that that α may be material linked.....	151
Figure 7.8 displays the final relationship observations between the deformation energies for each material with the initial optimised β parameter. It shows that there is not clear relation and why the decision to suggest β might be a machine linked parameter.	151

Figure 7.9 displays the final relationship between γ and the material deformation energies. Again, it shows a link between it and the flexure energy and reason to suggest that it is material linked.....	152
Figure 7.10 displays the concept of how the flexure deformation may be linked to the grinding mechanism in a planetary ball mill.	153
Figure 7.12 displays the frequency of the optimum selection and breakage models across the different biomass species when used under the material study for the steady state simulation.	156
Figure 7.13 displays the relationship observations between β and the various deformation energies. Here a strong relation was initially observed between the axial and parameter β	157
Figure 7.14 displays the initial relations between the parameter γ and the various deformation energies. Here a strong correlation was observed between γ and both the axial and flexure energies.....	157
Figure 7.15 displays the progression of the OVL scores as constraints on the modelling parameters increased. It shows that the reduction in the model accuracy was manageable.	158
Figure 7.16 displays the relationships between β and the deformation energies after the 7 steps of optimisation, whilst the relationship is not as strong as it was initially there is still good evidence to use it as a potential model.....	159
Figure 7.17 displays the relationship between the parameter γ and the deformation energies after 7 steps in optimising.	159
Figure 7.18 displays the relationships of the mill speed to the S3, B1 PBE model parameters after initial optimisation over A and α	161
Figure 7.19 displays the relationships between the feed rate and the S3, B1 model after the initial optimisation over A and α	162
Figure 7.20 displays the relationships between the mill speed and the S3, B1 parameter values after the first step in optimisation over A and α . There is still a strong relationship between α and the mill speed. Beta remains at a constant value but lower than predicted.....	163
Figure 7.21 displays the relationships between the feed rate and the S3, B1 parameter values after the first step in optimisation over A and α . Here the relationship with feed rat and A persists. Beta remains constant as before.	163

Figure 7.22 displays the OVL values as optimisation progression pushed beyond 1 st step, OVL's significantly reduce as optimisation is squeezed beyond the 1 st step, hence why the 1st step was used as the model.....	164
Figure 7.23 displays the worst case fit to the experimental results in the blind test, feed rate: 0.014 kg s ⁻¹ , mill speed, 202 RPM and the classifier vane angle of 20°. The OVL on the blind test was 0.82.	166
Figure 7.24 displays the best case fit to the experimental results in the blind test, feed rate: 0.014 kg s ⁻¹ , mill speed, 282 RPM and the classifier vane angle of 90°. The OVL on the blind test was 0.92.	166
Figure 8.1 displays a Retsch ZM200 mill, set up with no screen so that particles when passed through experience only 1 impact before size analysis is completed.	170
Figure 8.2 displays the single impact testing results for Brites wood pellets, shown are the results from sieve analysis, CAMSIZER P4 analysis for minimum and maximum chord, along with the fitted master curve models; standard deviations in the models signified by the dotted lines.	173
Figure 8.3 displays the <i>f_{mat}</i> and <i>xW_{m,min}</i> results for the single impact tests completed on 3 different biomass pellet species. The assessment shows the results from the mass based sieve analysis and the volume based CAMSIZER P4 dynamic particle analysis.	174
Figure 8.4 displays the materials used in this research in context with the literature from (Vogel & Peukert, 2003) and (Miguel Gil et al., 2015b). The patterned bars are the results from this research. All results here are presented on mass basis from sieve analysis.	175
Figure 8.5 displays the correlation of the minimum breakage energy <i>W_{m,min}</i> from the single impact testing correlated to the deformation energy results from the sister project for the 3 materials tested in the SIT regime.	176
Figure 8.6 displays the correlation of <i>f_{mat}</i> to the deformation energies in the various orientations.	177
Figure 8.7 displays the Single Impact Testing PBE based simulations against the experimental results for a Lopulco E1.6 mill experiment results, 0.006 kg s ⁻¹ , 202 RPM, 90° vane angle.	178

Chapter 1 - Introduction

1.1 Anthropogenic CO₂ Emissions

Global warming and climate change are concepts to which there is significant evidence, whereby human activity is affecting the climate and ecology of the planet. In the last IPCC report (Allen et al., 2014), significant evidence is presented to confirm this and projections of the necessary steps to slow and remediate the climate have been presented. Various gasses contribute to the effects of global warming based on their potential of trapping energy from the sun within the atmosphere; these gasses include but are not limited to: Halo-Carbons (CFCs, HCFCs and Ozone, O₃), Nitrous-oxides, NO_x, Carbon Monoxide, CO and one of the major contributors, Carbon Dioxide, CO₂. These gasses have increased in production since combustion of fossil fuels became the driver for growth in industrial process and transportation needs. To decrease their production all aspects of their production require review.

1.2 Grinding Processes and Pulverised Fuel Combustion

It is estimated that approximately 2% of the electricity generated on the planet is consumed by grinding processes (Napier-Munn, 2015). This encompasses a variety of different industries that spans metallurgy, ore processing, cement manufacturing, food processing and many more. Of the electricity consumed in comminution, 41% is utilised in the grinding of coal and some other fuels (Napier-Munn, 2015; World Coal Association, 2014) for the purposes of fuel preparation in pulverised fuel combustion, the most common technology used for electricity generation globally (International Energy Agency, 2014). As one of the most energy intensive activities in a power station, up to 1% of energy generated in the power plant is used to pulverise coal to the required size, therefore there is a great deal of emphasis placed on ensuring the process of grinding is as efficient as possible.

1.2.1 Process Overview

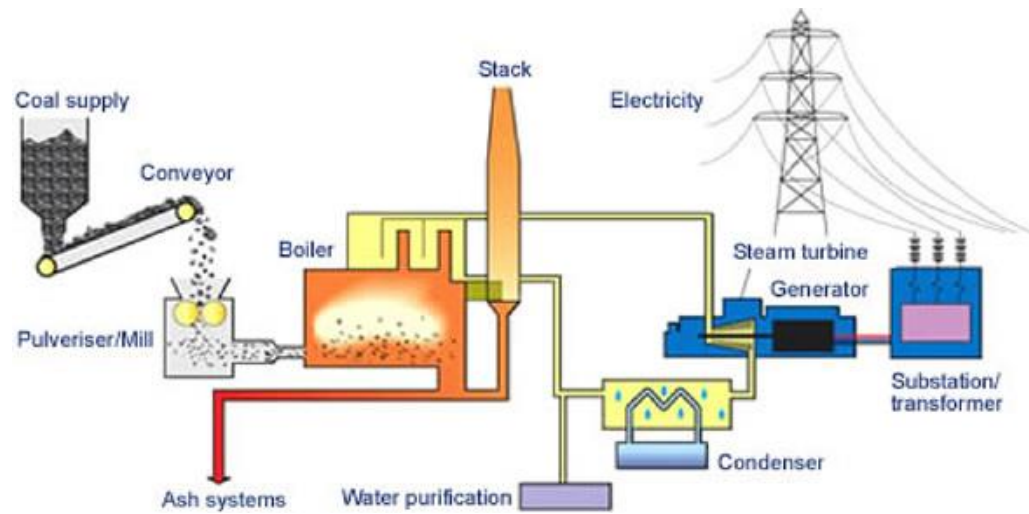


Figure 1.1 displays the process of pulverised fuel combustion for electricity generation, (World Coal Association, 2014).

In PF combustion, crushed coal is conveyed via belt and ramp conveyors to the top of feed chutes. Once released, the fuel is fed under gravity into hoppers that lead either directly in to the mill or to other conveying mechanisms like screw feeders. Once in the milling chamber, the interaction of grinding media, mill walls, balls, rollers, flailing hammers etc. (see 1.4) interact with the fuel and cause breakage through several kinds of mechanisms (see chapter 2.6) to reduce the particles in size. In many systems, fans and heating elements create a primary hot air stream through the mill that serves two purposes; the first is to assist in lowering moisture content, the second is to sweep up particles that have reached a sufficiently small enough size to be carried away; for coal, the target size is for 75% of particles passing the classifier at below $75\mu\text{m}$ and less than 2% above $300\mu\text{m}$ (International Energy Agency, 2014). After passing the classification system the air fuel mix is transported to the boiler for combustion and completion of the electricity generation process as shown in figure 1.1.

1.2.2 Industrial Mills

There is a large variation on the type of mill used in different industries, even more so within the fuel preparation industry. Historically mills are selected and constructed depending upon which type of coal was the expected source at the plant when it was designed (Colechin, Malmgren, & Britain, 2005). A classification device also accompanies mills, for which there is again a large variation in design. This section provides a conceptual illustration and description of some of the technologies in use at the plants.

Ball and Tube Mills

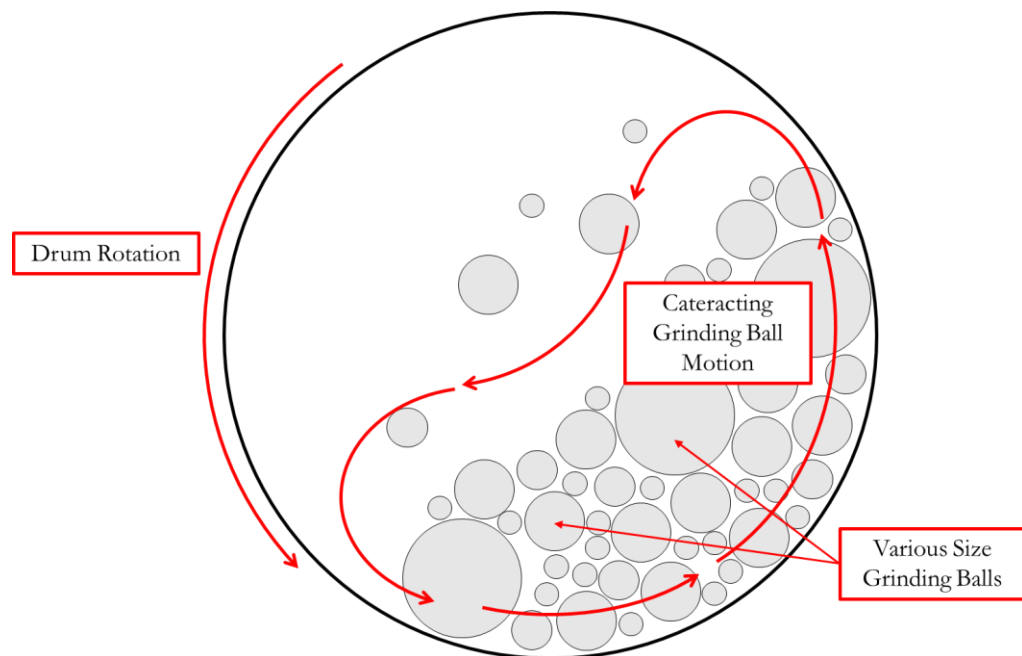


Figure 1.2 displays the concept of ball and tube mill from the viewpoint of the end of the mill. The illustration is specific for a lab scale Bico ball mill however the function is the same, other than the scale, differences include the insert of wear plates along the circumference and grinding balls of uniform size.

Ball and tube mills have fuel and replacement grinding media loaded through one end of the tube, either through screw feeders or gravity chutes mounted through the axis. The rotation of the tube rises the fuel and grinding media up to a level where they begin to fall in a cascading and cataracting motion. This action causes impact and compression upon the fuel that aids in reducing it in size before transport by the air flow to the classifiers.

Vertical Spindle Mills

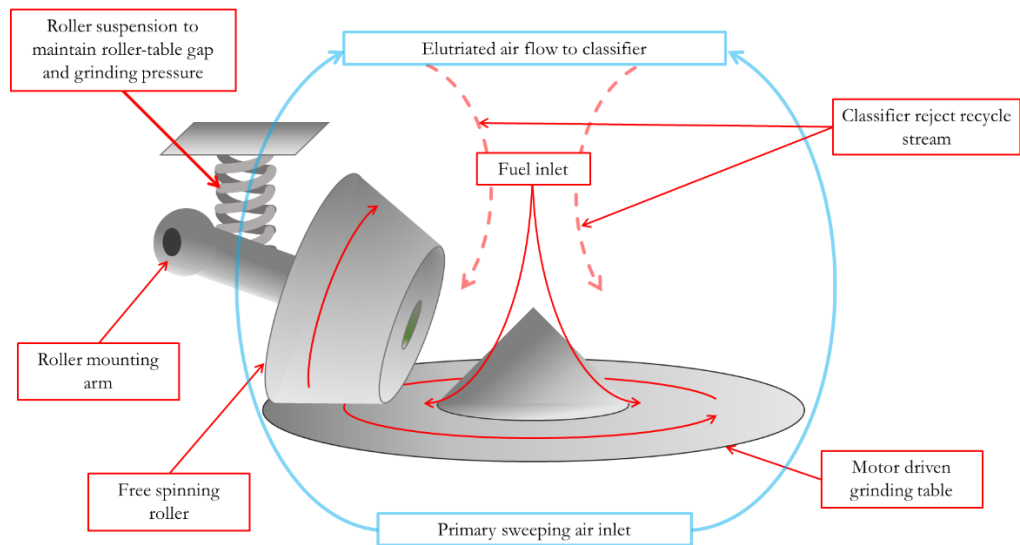


Figure 1.3 displays the concept of the vertical spindle mill, specifically a ring and roller Lopulco style mill.

A table onto which fuel is unloaded rotates to cause the feed to move to the circumference due to centrifugal forces. Mounted on the edge of the table are the grinding media; either heavy duty tyres, concrete balls with a race or rollers (see figure 1.3). The grinding media are pushed down towards the table and either maintain a gap with the table (roller mills) or held against the table (ball and race). The feed is forced under the grinding media where it is compressed and crushed. As the size reduces the material is forced further to the edge and off the table and into the air flow to be carried to the classifier.

Hammer Mills

The mill consists of a central rotating core (that can be mounted horizontally or vertically), to which are fixed rows of swinging metal bars (hammers). As the central core rotates the hammers orientate to a radial position with centrifugal action. A serrated screen encloses the grinding chamber. Feed is also carried to the screen through centrifugal action and through impact and shearing forces between the screen and hammers, the feed is broken down in size. After falling through the serrated screen, the particles are picked up and carried off to the boiler in the primary air stream.

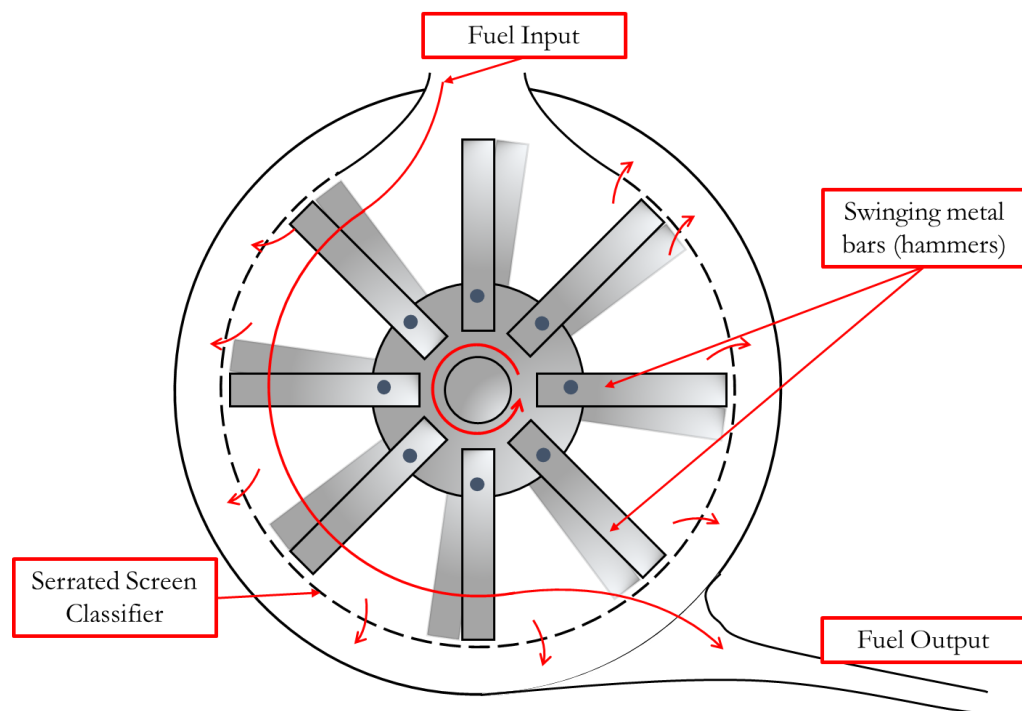


Figure 1.4 displays the concept of a hammer mill, whereby a rotating core swings flailing hammers to cause size reduction through shearing and abrasion.

Classification Systems

Classification systems provide a key role in ensuring that particle sizes are of the appropriate size to be combusted in the boiler of the power plant. The objective, is to screen the particles and return the particles that are rejected to the grinding media for further processing. As with mills, there is multitude of different classification systems that are available (Coulson, 1999) which are tailored to the specific application. Figure 1.5 displays a few examples of different classification mechanisms.

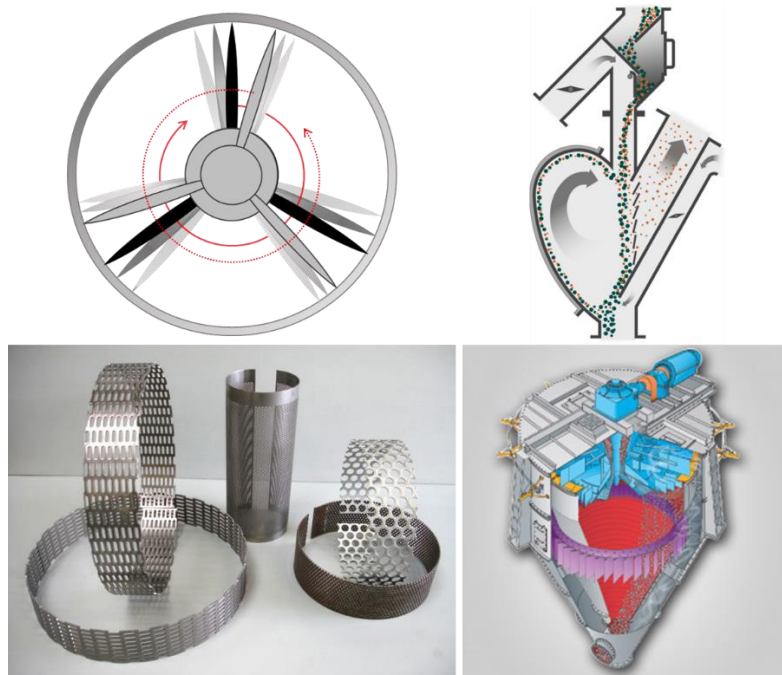


Figure 1.5 displays several variations for industrial classification processes; top right, whizzer blade classifier, top left, gravitational inertial air classifier, image source: <http://www.metso.com/products/separation/gravitational-inertial-air-classifier>, bottom left, perforated and serrated screen classifiers, image source: http://www.mark.sutton.co.nz/perforated_metal.htm, bottom right, rejecter blade design, image: <http://www.sturtevantinc.com/products/product/whirlwind-air-classifier>.

Biomass as a Fuel Source

Combustion of biomass as a fuel for electricity generation is attractive as, according to (Demirbas, 2004), “Biomass consumes the same amount of CO₂ from the atmosphere during growth as is released during combustion” hence, omitting transportation and pellet production related emissions, biomass is considered to be a carbon neutral fuel source. The effect of substituting coal for biomass is the reduction of CO₂ emissions from anthropogenic sources. Biomass includes all kinds of materials that were directly or indirectly derived not too long ago from contemporary photosynthesis reactions (Van Loo & Koppejan, 2007). It is also considered renewable if the fuel source is sustainably produced (Food and Agricultural Organization of the United Nations, 2004), so with adequate sources, biomass energy generation can be a carbon neutral renewable energy source.

Use of biomass also provides opportunity that no other renewable source can match; utilising the current infrastructure in power plants with very little modification to accommodate the change, dry biomass can direct substitute coal

and provide significant emission savings. This can be achieved via direct co-firing, either through dedicated biomass milling or co-milling; the latter has a limitation, a ratio of up to 10% on a mass basis is possible (Livingston, 2005). Downstream processes could have addition expense in the form of biomass burner modification or installation. Parallel co-firing, whereby the biomass combustion is used to preheat the steam before coal combustion is used to upgrade the steam to higher temperature and pressure; it is more expensive, due to the construction and installation of dedicated biomass milling and boiler equipment. Dedicated biomass power stations are possible; these options are often less desired due to long development times and significant cost. They do, however, offer opportunity to optimise design for biomass combustion (Colechin et al., 2005).

1.3 Motivation for the Research and Research Objectives

As many governments around the world have decided to act on the issue of climate change (see the Paris Agreement 2016) (UNFCCC, 2016), mechanisms for inducing the adoption of carbon free or neutral fuel sources have been implemented . For a comprehensive list one can be found at (IEA, 2013); as an example, in the UK, renewable obligation certificates whereby large scale electrical power generators are obliged to source increasing proportions of the electricity from renewable sources and are penalised if they do not meet the criteria (Ofgem, 2017) and Contracts for Difference, CfD, that provides long term revenue stabilisation for new and low carbon initiatives (Ofgem, 2017). Other initiatives have been enforced over greater territories, such as the Industrial Emissions Directive (IED), which supersedes the previous Large Combustion Plant Directive (LCPD), places a requirement on power stations to limit the emissions of certain gasses and particulate matter during generation; the former has led to the consequence that several power stations have had to close as conversion to enable clean generation has not been economically feasible. Further to this, the UK government announced that they plan to cease unabated coal power generation by 2025 (Department of Business, 2016) that ends the use of many PF power stations in the UK for coal generation.

It then becomes apparent, that despite the legislation imposed by international agreements and government policy, options do exist to maintain the use of the power station by switching the fuel used. Conversions to biomass of some UK power stations has already been completed, (see chapter 2.4.3 for details) and, although many UK power stations are approaching or surpassed their life expectancy, the millions of pounds of infrastructure could still be used to provide electricity through combustion of biomass. The difficulty in doing so, is developing understanding of the handling, and preparation of biomass as a fuel source.

Using biomass with the current infrastructure is by no means the most efficient method and is filled with difficulty due to the high variation in characteristics of biomass fuels. There is however, significant cost savings in doing so (Colechin et al., 2005; Livingston, 2013). To reliably predict the outcome of the biomass consumption requires in depth understanding as to output of the individual components of the power station. One such component is the power station mills, which as stated earlier, were often built for a local coal source. Therefore, to increase understanding of the biomass pellet grinding process, the Biomass and Fossil Fuel Research Alliance, BF2RA, instigated a research project under grant number 5, with the title “On Biomass Milling for Power Generation” (Williams, 2016). The research completed undertook experiments with lab scale mills; a Retch PM100 planetary ball mill, a Bico ball and tube mill, a Retsch SM300 cutting mill and a Lopulco E1.6 ring and roller mill. A variety of milling activity analysis was completed and is summarised in chapter 3.1.3 with an objective of characterising the link between the resulting product and energy consumed to achieve the result. Further analysis is completed to characterise a variety of biomass fuels. As a follow on from that project, this research has been commissioned to where possible utilise the previous research, determine appropriate methods and subsequently develop simulations of the biomass grinding process at the power station. The objective of which is to maximise biomass throughput, with the required product grade and to minimise the energy consumption in doing so. By increasing knowledge and developing simulations to aid decision makers, opportunity to make biomass combustion a more lucrative and cost-efficient process may encourage the generators to invest in biomass generated power. The benefit is that the mills will not need to be taken off-line to complete extensive trials, and possible downtime in cleaning and repair if a simulation helps to identify

the reaction of the mill to a fuel based on simple characteristics, which represents a cost saving. This would aid in reducing further anthropogenic CO₂ emissions and help to maintain power generation capacity in the face of generation capacity reduction through plant closure. Additionally, since PF combustion is used worldwide, the research could be utilised extensively.

Chapter 2 - Literature Review

2.1 Properties of Biomass

		woody biomass	herbaceous biomass	biomass from fruits and seeds	others (including mixtures)
		WOODFUELS		AGROFUELS	
Energy crop		- energy forest trees - energy plantation trees	- energy grass - energy whole cereal crops	- energy grain	
By-products*	direct	- thinning by-products - logging by-products	crop production by-products: - straw	- stones, shells, husks	- animal by-products - horticultural by-products - landscape management by-products
	indirect	- wood processing industry by-products - black liquor	- fibre crop processing by-products	- food processing industry by-products	- biosludge - slaughterhouse by-products
End use materials	recovered	- used wood	- used fibre products	- used products of fruits and seeds	MUNICIPAL BY-PRODUCTS - kitchen waste - sewage sludge

*The term "by-products" includes the improperly called solid, liquid and gaseous residues and wastes derived from biomass processing activities.

Figure 2.1 displays the classification of biofuel sources by different characteristics source: (Food and Agricultural Organization of the United Nations, 2004)

Biomass is classified in many ways, the Food and Agricultural Organization of the United Nations classifies biofuels as in figure 2.1; these classes are based on the source of the biomass with the terms direct, indirect and recovered used to identify the journey of the fuel to the end user, straight from the source, waste from processed material and material reclaimed at a product's end of life respectively. Woody biomass includes the trees, bushes, and shrubs, including the bark root and leaf. It is characterised by the longer growing times and higher lignin content (Saidur, Abdelaziz, Demirbas, Hossain, & Mekhilef, 2011). Due to the lower levels of ash and volatiles, wood is more suitable for direct combustion (Jaya Shankar Tumuluru, Sokhansanj, Wright, Boardman, & Yancey, 2011).

Herbaceous biomass, as defined by the European Standard EN 14961-1 (Solid biofuels – Fuel specifications and classes Part 1: General requirements) is "... from plants that have a non-woody stem and which die back at the end of the growing season. It includes grains or seeds crops from food processing industry and their by-products such as cereal straw". They often have higher percentages of

cellulose and hemicellulose compared to the lignin content. In addition, they have a quick growth rate. This has the effect that they have lower heating values compared to woody biomass and often have a higher content of elements and materials that are problematic for combustion (Bioenarea, 2012). Fruit biomass is the seeds or the section that holds seeds in the plant (Alakangas, 2010).

2.1.1 Microstructure of Biomass

Plant originating biomasses such as wood, energy crops or agricultural waste, have cell walls that consist of cellulose, hemicellulose, and lignin. Study into the differences between the numerous biomass species has been completed in literature (Demirbas, 2004; Demirbaş, 1997; Grammelis, 2010; Vassilev, Baxter, Andersen, Vassileva, & Morgan, 2012) and in other BF2RA literature reviews (Hussain, 2015; Jenkinson, 2012) to which the author would direct the reader for further information. The anisotropic growth of biomass is due to the shape and nature of the cell growth and the individual cells are joined through the middle lamella, this also has the consequence that when size reduction processes are completed on biomass the result is of larger fibrous final product.

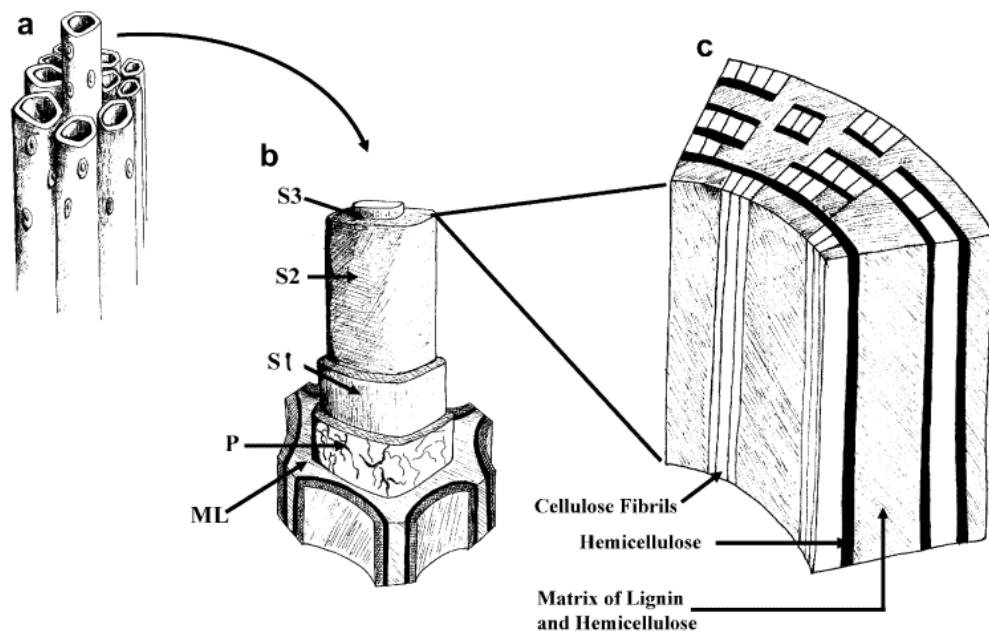


Figure 2.2 shows the configuration of wood tissues. **A** Adjacent cells. **B** cell wall layers. S1, S2, S3 secondary wall layers, P primary wall, ML middle lamella. **C** Distribution of lignin, hemicellulose, and cellulose in the secondary wall (Pérez, Muñoz-Dorado, de la Rubia, & Martínez, 2002).

Cellulose provides the mechanical strength of the cell wall and chemical stability; during photosynthesis, solar energy is absorbed and stored as cellulose (Harmsen, Huijgen, Bermudez, & Bakker, 2010). Cellulose is a polysaccharide that forms chains, called elemental fibrils, consisting of several hundred to thousands of molecules linked together via hydrogen bonds and van der Waal forces (Pérez et al., 2002), creating the fibrous and tough plant structure (Lope, Phani, & Mahdi, 2011). At each level in the cell wall the primary wall, S1, S2, S3, the microfibrils have different orientations. Cellulose comprises between 40 – 60% of the dry mass of biomass (Lope et al., 2011). The polymer structure is crystalline in nature (Lope et al., 2011).

Hemicellulose is again a polysaccharide this time in a matrix structure. Whilst hemicellulose provides structure to the cell and contributes to between 20-40% of the cell, the structures of the molecules are more random. It is amorphous and has less strength than cellulose (Lope et al., 2011), thus it can be broken down with lower energy levels. Lignin is a chemically complex compound that has no defined structure. It fills the gaps between the hemicellulose and cellulose (Lope et al., 2011), binding the polysaccharides and providing strength to the cell wall and plant structure (Chabannes et al., 2001). It requires more energy to breakdown lignin than required for cellulose or hemicellulose (Dutta, n.d.). It also exhibits thermosetting properties if heated and cooled (Van Dam, van den Oever, Teunissen, Keijsers, & Peralta, 2004) that aids in the pelletisation of biomass fuels. Plant cells are held together via the middle lamella, a material composed of pectin and lignin (Bailey, 1936).

Moisture content plays a significant part in the combustibility of biomass, anything above 67% moisture content is considered to completely inhibit combustion, approaching that level requires more energy to vaporise the water (Bushnell, Haluzok, & Dadkhah-Nikoo, 1989). By having initially low moisture content, less of the input energy used in the combustion of the fuel is utilised in moisture evaporation and more energy can be recovered (Hanning et al., 2012).

2.1.2 Biomass Properties

Moisture Content

In several studies the effects of moisture on the specific energy requirements required to mill biomass was investigated (Esteban & Carrasco, 2006;

Miguel Gil, Arauzo, & Teruel, 2013; M Gil, González, & Gil, 2008; Miao, Grift, Hansen, & Ting, 2011; Repellin, Govin, Rolland, & Guyonnet, 2010). All report that the requirements increase if the moisture content increases, as is displayed in figure 2.3. This is also reflected in the food processing industry (Bhandari, Bansal, Zhang, & Schuck, 2013).

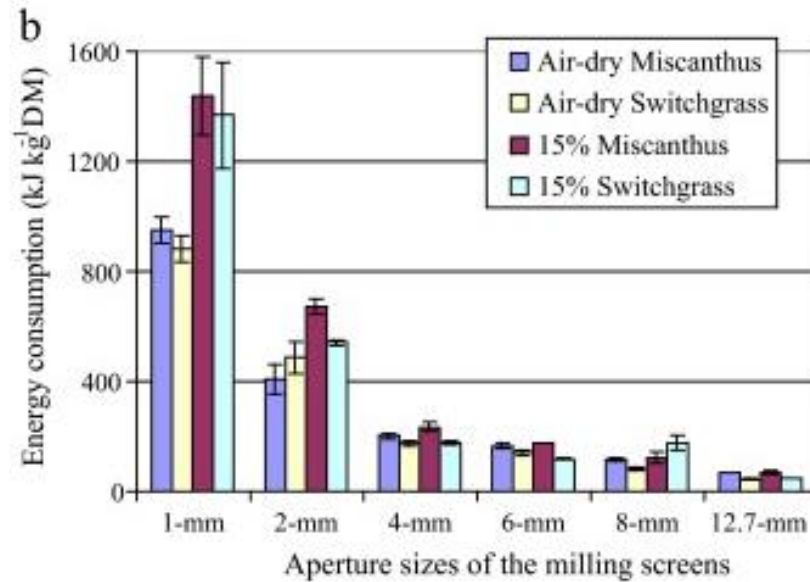


Figure 2.3 displays the difference in energy requirements necessary to grind Miscanthus and Switchgrass through various size screens, comparisons of the effect of moisture content is also made. Note ‘Air-dry’ has moisture content between 7-10%, source: (Miao et al., 2011).

Biomass Species

The species of plant that is ground also is a factor in the energy requirements necessary to grind biomass to the required size; again, the variation in one study is shown in figure 2.3. In several studies (Esteban & Carrasco, 2006; M Gil et al., 2008; Miao et al., 2011; J. S. Tumuluru, Tabil, Song, Iroba, & Meda, 2014) the energy requirements for different species has been reported; a detailed analysis of the reported literature is given in (Kratky & Jirout, 2011) along with the type of mill used in the process; this does however apply to the raw biomass and not pelletised biomass.

2.1.3 Pre-Treatment of biomass

Pre-treatment of biomass is used to change the fuel characteristics in such a way that it becomes more favourable for use. A few of the most common techniques are described below with a comment on how the pre-treatment method

can affect the milling process. These three also specifically aid grinding, although other pre-treatments are used for other reasons.

Pelletisation

Pelletisation is used in order to increase the bulk density of biomass (Uslu, Faaij, & Bergman, 2008); this aids in reducing transportation costs and increases the energy density of the fuel. In (Ryu et al., 2006) it is generalised that many biomass sources have a bulk density of less than 150 kg/m^3 with and post-pelletisation this can be over 600 kg/m^3 . Biomass particle size is reduced by an initial milling of the raw material (Van Loo & Koppejan, 2007). Following milling the product should be of a more uniform size and shape (Kallis, 2012), the surface area increases as a result of the milling facilitating inter-particle bonding (Sokhansanj, Mani, Bi, Zaini, & Tabil, 2005). The particles of biomass undergo compression that increases the interfacial forces, this causes interlocking of the fibres of the biomass (Tabil, Sokhansanj, & Tyler, 1997) in a pellet press. This can be supplemented by using other binding agents if necessary to improve the tensile strength of pellets (Razuan, Finney, Chen, Sharifi, & Swithenbank, 2011). In the work by Temmerman et al. (Temmerman, Jensen, & Hebert, 2013) experimental results conclude that the energy requirement in milling biomass pellets is lower than that of wood chip of the same species. The energy input into milling the pellets is used mostly in breaking the bonds caused by the pelleting process with little used in further particle comminution. This is a key point of note to the project as the mills we are modelling with have material provided in pellet form for most applications.

Torrefaction

Torrefaction is a mild form of pyrolysis. This usually takes place at temperatures of $200\text{-}300^\circ\text{C}$ for about 30-60 minutes in an inert or low oxygen atmosphere. When applied to biomass, this produces a product that has material properties closely related to coal (Yan, Acharjee, Coronella, & Vásquez, 2009). The final product has a higher calorific value, up to increases of 1.46 times the original HHV values have been observed, e.g. willow in a raw form has a HHV of 19.609 MJ/kg , torrefied at 290°C increases this to 28.611 MJ/kg (Chen, Cheng, Lu, & Huang, 2011); as given by Channiwala and Parikh the range for coal HHV is from 21 MJ/kg to 35 MJ/kg (Channiwala & Parikh, 2002). Torrefied product is also hydrophobic, is more homogenous and has improved grindability (Dutta, n.d.;

Topell Energy, 2014; van der Stelt, Gerhauser, Kiel, & Ptasinski, 2011). Torrefied material can also be pelletised to create a product with higher bulk density.

Steam Exploded

Steam explosion is where the biomass is subjected to a high pressure environment in a temperature range of 180-230°C for a period of time, normally around 10 minutes (Lope et al., 2011). The release of the steam causes explosive decompression of the environment (Lavoie, Beauchet, Berberi, & Chornet, 2011) subsequently causing the rapid expansion of water in the biomass, degrading the cellulose, hemicellulose and lignin bonds (Avellar & Glasser, 1998). This creates biomass that has enhanced grindability and aids in pelletisation (Biswas, Yang, & Blasiak, 2011).

2.2 Grindability of Biomass

2.2.1 Grinding Theory

To help build a model that can simulate the processes that occur in the mill it is important to understand what the particles are subject to. The key process in a mill is that of grinding. Application of the theory of grinding and the ability to incorporate the principles within a model will help to make a simulation that is more predictive and useful in understanding the interactions of the feed material and the mill in question. Grinding theory describes the process of material failure and their causes.

As described in (Coulson, 1999) when a particle of material is subject to sudden impact the resulting progeny are in the order of a few large particles and a number of fine product particles, very few intermediate sized. Also if the impact force is increased the size of the larger fragments is reduced whereas the size of the fines is relatively unchanged. The conclusion of which is that the size of the large particles is related to the process of size reduction and the size of the fines is related to the internal structure of the material.

Given the link to the internal structure of the material, grinding consists of two parts; opening any small fractures within the material and then creating new surface area of the material. The energy from impact on a particle induces a stress field on the particle (Green, 2008), as long as the stress remains, subject to the material properties size reduction will start, exploiting micro-cracks and flaws in the

material. The cracks grow both internally and on the surface until fracture occurs; all the time this causes the creation of new surface area. Thus, the link between energy and new surface area can be seen. In fracture mechanics the propagation of cracks proceeds via three modes as displayed in figure 2.3.

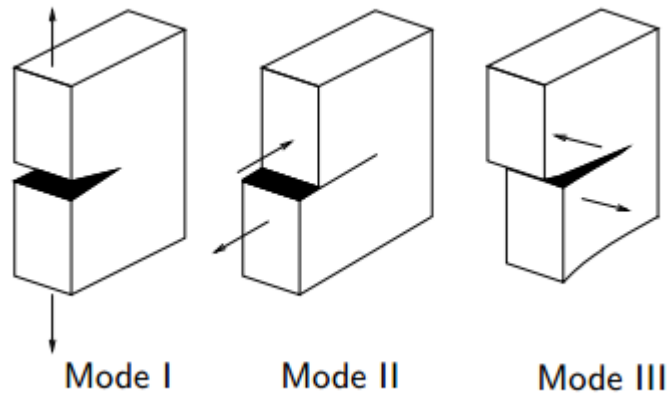


Figure 2.4 showing modes of crack propagation, mode I: opening, mode II: in-plane shear, mode III: out-of-plane shear, source: (Schreurs, 2009).

Two stages present themselves during size reduction processes (Coulson, 1999); the grinding of the coarse material, where the flaws are exploited, followed by the second mode that develops at a particular size, this mode is characteristic of the material properties of the material and known as the persistent mode. Each machine used for size reduction will also have a grind limit at which point, continued processing yields little or no further grinding of the product.

2.2.2 Fracture Mechanics of Biomass

The anisotropic structure of wood creates three orthogonal planes of material symmetry, radial, tangential and longitudinal (Barrett, Haigh, & Lovegrove, 1981). Strength and stiffness are great in the longitudinal direction and relatively low in the tangential and radial directions. This structural design contributes to the formation of natural cleavage planes and crack propagation typically occurs along the grain and makes it difficult to induce cracking across the grain. Due to this, characterisation of the propagation of cracks in wood via the three modes manifests via six different systems, identified by the letters t (tangential), l (longitudinal) and r (radial), as outline in figure 2.4. The first letter indicating the direction normal to

the crack surface and the second indicating the direction of propagation (Barrett et al., 1981).

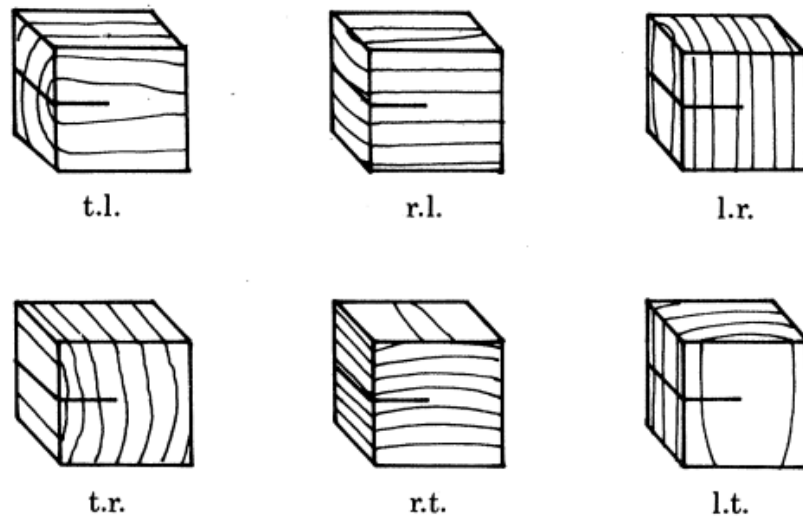


Figure 2.5 showing the principle systems of crack propagation in wood, source: (Barrett et al., 1981).

2.2.3 Single Particle Fracture

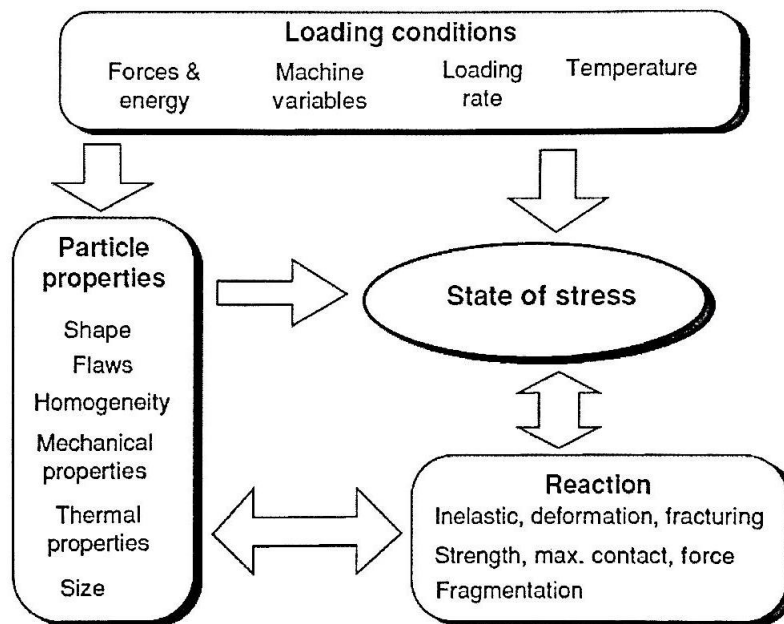


Figure 2.6 displays the factors affecting the breakage of a particle, source: (Green, 2008)

The magnitude of the load, the manner, and the nature in which it is applied are critical factors in the fracture of a single particle (see figure 2.5). Insufficient load can cause only elastic deformation and once the load is removed the

deformation is reversed thus creating an inefficient utilisation of the input energy. If the load is not sufficient to overcome the elasticity of the particle, the energy is stored until the load is removed, at which point it will return to its previous state (Coulson, 1999) without completing any useful work. Plasticity in biomass is also very low, some species are totally lacking as described in the work by Maiti et. al. (Maiti, Dey, Purakayastha, & Ghosh, 2006). Additionally, pre-processed biomass undergoing drying processes, as most are for use as fuel, become hard and lose plasticity if they have it (Ryu, Finney, Sharifi, & Swithenbank, 2008); this is a favourable characteristic when grinding biomass as the input energy is consumed in comminution. For efficiency in the breakage mechanisms of a particle, is it useful to apply a load only just greater than the elasticity limit. Additionally, a greater rate of application of force results in the production of a higher number of fines and may be inefficient for the intended purpose of the product. A lower rate of application for a longer amount of time may be beneficial, however, this may not in some instances be sufficient to overcome any viscoelastic properties where a high rate is preferential.

Single particle testing can be useful in that information about fracture mechanics and milling can be determined with a small amount of material (Meier, John, Wieckhusen, Wirth, & Peukert, 2009), avoiding the need for additional cost. It is possible to complete the tests via specialised machinery. The work by Vogel and Peukert (Vogel & Peukert, 2005) uses single particle breakage tests for establishing the parameters of the material constant and minimum breakage energy, later used for the modelling of two different impact mills.

Furthermore in the work by Meier et al (Meier et al., 2009) the use of indentation testing on single particles is used for establishing the same material constants. These tests determine hardness, Young's modulus and fracture toughness allowing the extrapolation of a brittleness index and subsequently a breakage probability function that is used to model the behaviour of impact milling. In a study on the resistance to impact milling of cement clinker by Genc and Benzer (Genc & Benzer, 2009), single particle fracture mechanisms were assessed via drop weight testing.

Reviewing the literature, a conclusion drawn is that mechanical testing of biomass and biomass pellets could play a part in developing a more predictive

model for biomass milling. Determination of the breakage energies would be a key objective; additionally, it may be useful to study aspects such as the stress/strain curves through the application of forces to biomass material and pellets. The ability to correlate the behaviour of a material through simple testing such as these would be idealistic if their performance in a mill can be determined from them, alleviating the requirement for time consuming and potentially expensive experimentation.

2.2.4 Particle Breakage Mechanisms

Materials can be subjected to forces via several different modes during the process of size reduction. These are summarised as (Coulson, 1999; Green, 2008):

- Impact – impact against a target, forces acting on the particle are normal to the plane of the rigid body.
- Compression – The force is applied via slow compression between two planes or between a surface and impact with a target.
- Attrition – when the normal force from impact is not large enough to affect the whole of the particle, however is large enough to affect a volume at the surface of a particle.
- Shear/abrasion – caused by the scraping of fluid-particle interaction or particle-particle interaction.
- Cutting – a variation in shearing whereby the opposing forces are applied acutely, the cutting implement generates stress in the object inversely proportional to the area over which the force is applied; therefore, a smaller area creates greater stress.

It is noted in (Green, 2008) that when grinding certain materials problems are encountered when the material is ductile, and the grinding machinery is designed for brittle material, this is especially true when the breakage mode is primarily compressive or abrasive.

2.2.5 Material Comminution Indexing

There are many methods that have been devised in order to characterise and quantify the properties of materials in relation to their comminution; generally, the energy required to reduce the material to a target size. This section provides a summary of several of these methods that relate to the project.

Bond Work Index

The Bond Work index (Bond, 1954) test procedure uses a small-scale locked cycle ball and tube mill and a screening process to simulate recirculating

condition of a full scale mill with classification (Prasher, 1987). The method is used to determine an index value, W_I , for a material which can subsequently contribute to a calculation of energy required, W , to produce d_{80} of the particles passing a target size (determined by the W_I calculation) when starting with a feed size, F_{80} , (see equation 2.1). The full process details can be found in (Prasher, 1987; Williams, 2016; Williams et al., 2015).

$$W = 10W_I \left(\frac{1}{\sqrt{d_{80}}} - \frac{1}{\sqrt{F_{80}}} \right) \quad (2.1)$$

The Bond Work Index process is targeted for application in ball and tube mills; Bond has a similar version for rod and tube mills. For different mills however, the application of the method is inappropriate. In (Williams et al., 2015) it is shown that the application of the BWI method still maintains its integrity with biomass materials. Shortcomings of the method are listed in (Prasher, 1987) and include aspects such as: not explicitly accounting for classifier effectiveness, variation in residence time; also for assuming specific energy is not a function of ball load, which is contrary to a known fact; not accounting for over/under filling; and causes of inefficiencies are not explored.

Hardgrove Grindability Index

The Hardgrove Grindability Index (HGI) is a method for determining the grindability of coal using a vertical spindle mill type mill; a ball and race laboratory mill. Small samples are ground within the mill for 60 revolutions. The sample is then sieved through a 200-mesh sieve ($0.75\mu\text{m}$) and the passing sample is weighed. The weight of the sample is compared to the US Department of Energy standard coal indices for determination of its own HGI (Coulson, 1999).

For mills with similar grinding processes, such as vertical spindle mills, and ball and race mill, the HGI has proven to be a good reference point. When utilising the HGI index as a reference point for milling. Shortcomings with the use of the method in determining the correct mill and milling parameters to use are encountered. Scale effects and variation in commercial coal pulverising practices on occasion deviate from predictions based on the HGI references, additionally a variation in the type of mill used also displays deviation. Influences to the process include: unrepresentative coal, moisture content, size classification and recycle,

product sizing differences for modern pulverised coal (Coulson, 1999). Further to this, in (Williams et al., 2015) it is concluded that HGI does not correspond well when applied to biomass pellets.

Other Grinding Index Systems

Other grindability indexing methods have been developed however there are limitations in their application due to insensitivities to heterogeneous properties in materials, hence given the variation in biomass species and defining characteristics a suitable indexing system has proved difficult to develop (Bridgeman, Jones, Williams, & Waldron, 2010; Van Essendelft, Zhou, & Kang, 2013). In tackling the problem Van Essendelft et al. (Van Essendelft et al., 2013) developed a Hybrid Work Index, combining the Resistance to Impact Milling (RIM) technique used to measure fungal decay in wood with the Bond Work Index technique. RIM is used to determine the mass of compromised integrity wood due to fungal decay but was theorised this could be applied to milled product.

An adapted version of the HGI was used for analysis of grindability in biomass and torrefied biomass fuel in the paper by Bridgeman et al (Bridgeman et al., 2010). The adaptation used a volumetric measure of the fuel rather than a mass measure, and then calibrates the results with the standard HGI references.

2.3 Particle Characterisation

The objective of milling in the power sector is to reduce the particles to a size and shape that is suitable for pneumatic conveyance in a power station transport system and subsequently consistent combustion in a PF boiler. As seen in section 2.2.5 the energy consumption is linked to the degree of size reduction. It is therefore necessary to have methods of quantifying the size of the particles.

2.3.1 Distribution Analysis

As particulate systems consist of many particles as opposed to individuals, analysis methods often enact data reduction methods (Green, 2008). This comes in the form of particle size distributions and cumulative distribution (see figure 2.7). These provide broad data characterising the ranges of particle sizes resulting from the milling practices, thus identifying whether a desired range is achieved and the effectiveness of the mill in producing consistent product, e.g. narrower size

distributions. Much of the provided data for the project will be in this form, hence understanding how and why it presented in this manner is essential.

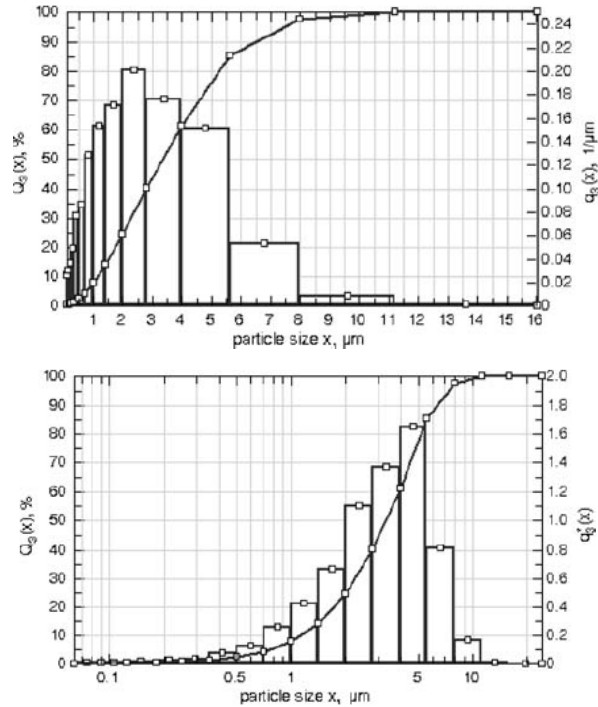


Figure 2.7 shows an example of particle size distribution plots on normal (top) and logarithmic scales (bottom), source: (Green, 2008).

Many different size distribution equations are used in comminution analysis. Two of the most prevalent in the mineral liberation are the Gates-Gaudin-Schuhmann equation and the Rosin-Rammler equations. The latter of the two was designed specifically for coal and used extensively in the coal analysis and energy generating sector uses it almost entirely in the measurements of the fuel grade (Coulson, 1999; Prasher, 1987).

Rosin-Rammler Distribution

The particle size distributions, $R(d)$, is governed by the characteristic passing size, d' , and the characteristic spread parameter, n . The distribution is described by the cumulative density function (Brezani & Zelenak, 2010) as in equation 2.2.

$$R(d) = 100e^{-\left(\frac{d}{d'}\right)^n} \quad (2.2)$$

To determine values for d' and n , linear regression of data to fit equation 2.2 can be completed or linearisation techniques can be used by transformation to log-log plots. Details of how to complete such analysis is given in the paper by Brezáni and Zelenák (Brezani & Zelenak, 2010).

2.3.2 Methods of Particle Analysis

Sieve Analysis

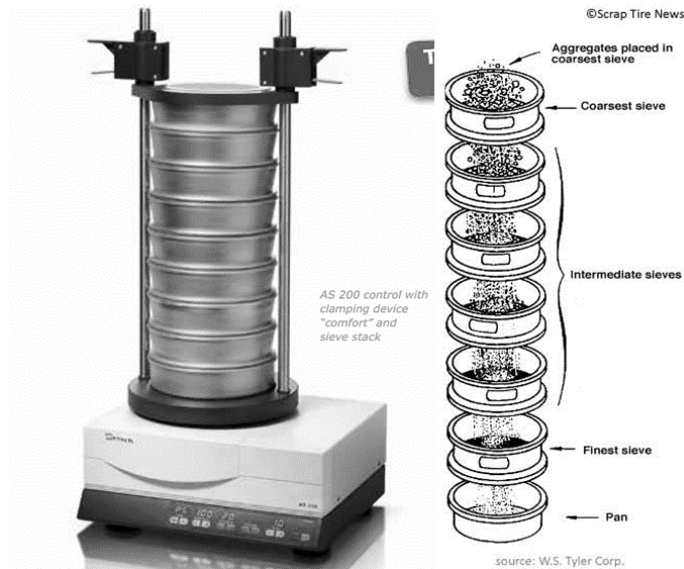


Figure 2.8 (left) displays a laboratory mechanical sieving apparatus, source: http://www.retsch.com/dlmp/www/2058-1ca728fb7bb/brochure_sieving_en.pdf. (Left) displays the outline of the sieving technique, image source: <http://www.scraptirenews.com/crumb.php#prettyPhoto/4/>.

One of the simplest techniques in particle size analysis is sieving (Coulson, 1999). This can be achieved manually or using specialised equipment such as in figure 2.7 where the general principle is outlined. Sieves can be obtained for sizes ranging from very large through sub $50\mu\text{m}$; the effectiveness of the sieve does diminish for sizes below $150\mu\text{m}$ (Green, 2008). Sieve stacks often increase in size by approximate multiples of $\sqrt{2}$ (Prasher, 1987), this is based on the unit square of the sieve aperture having a maximum distance of a multiple of $\sqrt{2}$.

Image Analysis

Whilst the standard for particle size analysis is a mass-based sieve analysis, other particle analysis techniques exist that offer more than measure of the minimum size to pass a screen aperture. In the paper, (Miguel Gil, Teruel, & Arauzo, 2014), biomass particle images are subjected to manipulation with MatLab™ image analysis techniques. Scanning electron microscopes were used in

with a back scattered electron mode to study particle morphology (Motte, Delenne, Rouau, & Mayer-Laigle, 2015) and showed this to be effective to 250 μm for determining particle size and shape. A Retsch CAMSIZER, which uses dynamic image analysis techniques has been used in several biomass particle analysis papers (Cardoso, Oliveira, Junior, & Ataíde, 2013; Göktepe, Umeki, & Gebart, 2016). This has been shown to be a good method based on the ability to capture and analysis the particles in a short space of time, providing both distribution size and shape data. Additionally, the samples can be passed through non-destructively, whereas SEM and other microscope technologies destroy or render the sample unusable.

2.4 Milling Options in Power Stations

2.4.1 Biomass Combustion Options

Within pulverised fuel power stations there are different strategies that can be implemented that utilise biomass. Figure 2.9 provides an illustration of the possible options open to generators.

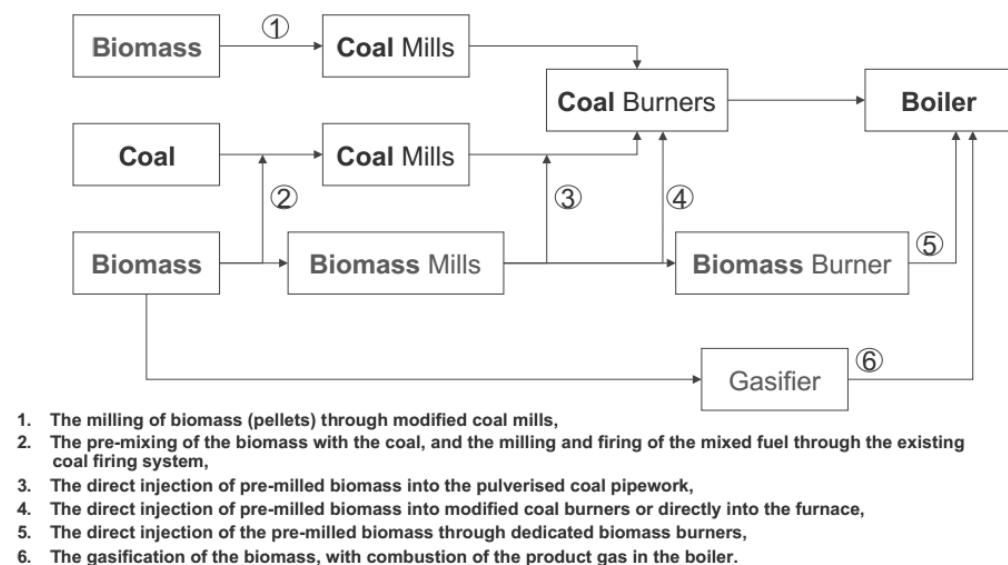


Figure 2.9 outlining the processing routes biomass and coal can take for combustion in a pulverised fuel boiler, source: (Livingston, 2013).

Co-milling (route 2 in figure 2.9) is sometimes practiced where the intention is for direct co-firing of biomass and coal (Livingston, 2005). The lower calorific value of biomass creates limitations in the ratio of biomass to coal that can be co-milled. Firing through the existing coal mills can be achieved for up to 10% (Khorshidi, Ho, & Wiley, 2014; Lester, Gong, & Thompson, 2007; Livingston,

2005) of the mill capacity; approaching levels as high as 20% requires dedicated milling and burner systems. For torrefied biomass, as the characteristics are more like coal, this can be increased to as much as 40% (Khorshidi et al., 2014).

Problems occur with the use of biomass due to its breakage behaviour and moisture content (Grammelis, 2010; Livingston, 2007). These include the particles causing unstable flames at the burners, variation in fuels requires different optimisation in the mills, some mills cannot process certain types of biomass (Lester et al., 2007). It has been noted that on vertical spindle mills, increased differential pressures have occurred (Livingston, 2007) due to the use of biomass. There are also safety concerns in that the hot air used to dry the coal could cause ignition of biomass which releases combustible volatile matter into the mill at temperatures lower than coal, indicating a need to modify the operating procedures (Livingston, 2005).

Route 1 in figure 2.9 requires modification; this seems to be more prevalent in vertical spindle mills and the modifications include reducing the internal volume of the coal mills in order to be suited to biomass fuel, installation of baffles in the mill to help maintain air flow in the mill (Livingston, 2012). Rotary inlet valves are installed at the fuel entry point and reduction in the mill throat size (where the pyrite spills over the grinding table in a vertical spindle mill when grinding coal) are used to create an air seal and aid in air flow within the mill respectively. Due to the lower combustion temperature of biomass, it is also necessary to reduce the temperature of the inlet air, which should also reduce outlet air temperature. Furthermore, in order to increase safety, changes to explosion suppression systems such as installation of systems to release chemicals like sodium bicarbonate (Montgomery, 2013) have been introduced. Even with the modifications there are restrictions so that only certain possible fuel sources such as biomass pellets are suitable, few raw fuels are.

2.4.2 Dedicated Biomass Combustion

Dedicated biomass plants have been constructed and many more planned with generation capacities in excess of 100 MW_e (Biomass Energy Centre, 2013). Polaniec Biomass Power Plant in Poland offers 205 MW_e (see: <http://www.power-technology.com/projects/polaniec-biomass-power-plant-poland/>) and although

the project is no longer proceeding Drax Power in the UK had planned to build several 300 MW_e power plants (see: <http://processengineering.theengineer.co.uk/environment/drax-axes-new-biomass-plans/1011957.article>). When developed these standalone plants do not use pulverised fuel favouring circulating fluidised bed boiler designs that do not require such small particle sizes in the feedstock.


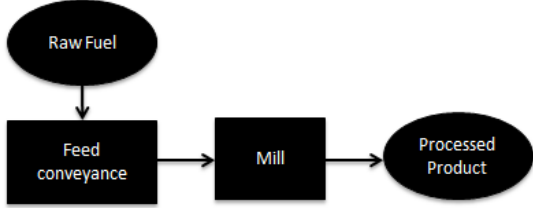
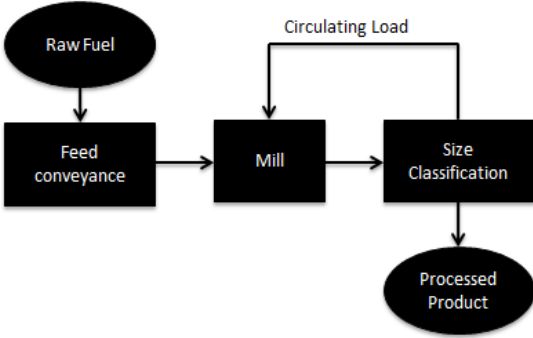
2.4.3 Coal to Biomass Conversions

Several examples of coal-to-biomass conversions include Ironbridge B; Foster Wheeler D9 tube and ball mills were used for coal grinding. Small scale trials were conducted with wood pellets; these proved the mills can grind them however energy output of the boiler was reduced due to the lack of throughput coupled with the lower energy density of biomass fuels. In order to increase material throughput, the mills were changed to hammer mills (Zwart, 2012) which proved far more effective on this particular issue. For the conversion at Fiddler's Ferry power station Bühler DFZK2 hammer mills were installed for biomass grinding instead of using the Lopulco LM 45 ring and roller mills used for coal grinding, this is due to the rapid build-up of material on the grinding table of the mill that reduces output severely (Rigoni, 2012), again the hammer mills reduced the effect of this problem. Installation of hammer mills for the biomass fuel stream also took place in with the conversion at Drax power station, where they have previously ground coal with ball and race mills (Greensmith, 2013).

2.5 Circuit Operation

Depending on the application of the milling, operations can be completed as described as in table 2.1. Each different approach has a different application and scenario for when and where appropriate, as given in column 3 of table 2.1, the need for increased complexity is often a result of industrialisation of the process. With the option of circuit operation mills and in industrial practices it is important to know what effects these might have on the processes and final product they have.

Table 2.1 showing the different circuit operations usable in milling, source: adapted from (Coulson, 1999; Green, 2008).

Operation	Description	Application
Batch		<ul style="list-style-type: none"> • Small samples • Laboratory • No size control
Open-cycle continuous		<ul style="list-style-type: none"> • Industrial • No size control
Closed-cycle continuous		<ul style="list-style-type: none"> • Industrial • Size control

2.6 Mills

The breakage mechanisms that occur in a mill is dependent the working principles of the mill in question. There is a high variation in the design of milling machinery; the fundamentals of mill design include the application of the grinding mechanisms, such as a rotating grinding table interacting with weighted rollers creating compression in the particles, or a rotating tube vessel loaded with free to move grinding media creating impact, such as in a ball and tube mill. Appendix A provides a summary of some of the mills that are currently used in the power industry can be found, that provide correlation to mills used in the power industry or have application for the milling of biomass. Their working principles along with some comments on their operation are provided. Table 2.2 provides a summary of the breakage mechanisms in the various types of mill.

Table 2.2 showing the grinding mechanisms applicable to the type of mill.

<i>Mill Type</i>	<i>Grinding Mechanism</i>				
	<i>Compression</i>	<i>Impact</i>	<i>Abrasion/ Shear</i>	<i>Attrition</i>	<i>Cutting</i>
Tube and Ball	✓	✓			
Tube and Rod	✓	✓			
Ring and Roller	✓				
Ball and Race	✓				
Hammer		✓	✓	✓	
Knife			✓		✓
Disk	✓		✓		
Rotary					✓
Roller	✓		✓		
Centrifugal		✓	✓		
Planetary Ball	✓				

The mechanism by which a mill breaks particles may be relevant in the project as certain biomass material may be comminuted more efficiently given a certain type of grinding mechanism. The ability to characterise and specify this within a model would increase its usefulness.

2.7 Size Classification

The milled product is often carried from the mill via a flow of air pumped through the mill or released in to a flow of air via gravity. The flow of air facilitates pneumatic conveyance of the fuel through (in certain circumstances) classification units and on to the PF boiler. An overview of particle size classification processes used in power station classification is given in table 2.3. Understanding of the effects of classifiers is important. In the literature it has been discussed that inefficient performance of classifier units, effects overall mill performance; notably the throughput and capacity of the circulating load of mills can be reduced, as well as the quality of the final product (Jankovic & Valery, 2013). Some diagrams of different classification systems are shown in chapter 1.2.2, in an industrial setting, almost all work on an elutriating air principle. Some operate through physical separation using spinning blades of some fashion, set to different angles of rotational velocities to determine the screening size; others using gravitational inertia separation to remove oversize particles, similar in principle to cyclone separators.

2.8 Safety Aspects of Mill Operation

2.8.1 Dust Ignition

The possibility of dust ignition is always present wherever dusts are produced, stored or processed and are considered explosive if there is a sufficient mix of the fuel dust and air (Abbasi & Abbasi, 2007). In the fuel preparation processes in a power station this will be relevant in the conveyance of the fuel to the mills, during comminution in the mills, the elutriated air flow from through the classifier and in the pneumatic conveyance processes from the mill to the boiler. The factors affecting the combustion of dust are described in the dust explosion pentagon (Kauffman, 1981) in fig 2.10.

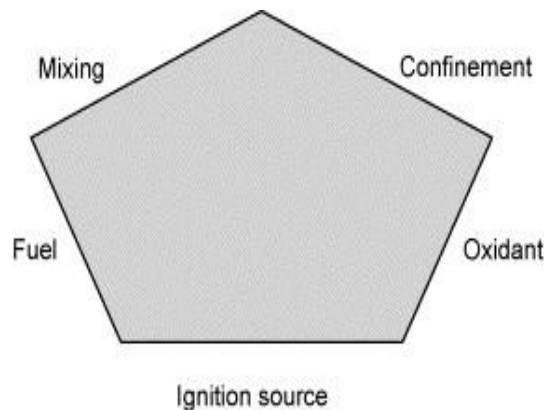


Figure 2.10 showing the factors affecting the combustion of dust particles, source: (Kauffman, 1981).

The rapid combustion of fuel takes place once the fuel has been ignited in a gas stream, propagation of the flames will depend on several factors, importantly the nature of the dust, the particle size and the geometry of the environment (Abbasi & Abbasi, 2007). Described in the work (Abbasi & Abbasi, 2007), methods of ignition and strategies for prevention and damage control covering a broad range of industries is given; these include the coal, food processing, mineral processing and wood processing industries, all of which are applicable to this project.

2.8.2 Design Features for Safe Operation

Mill Inerting

As outlined in (Abbasi & Abbasi, 2007), mill inerting can be used to eliminate the risk of combustion and therefore explosion in a mill. The principle is

that by milling in an inert gas, such as CO₂ or nitrogen or more commonly steam, the lack of oxygen prevents combustion. The choice of gas would depend on the fuel and would require study to ensure that there are no undesired chemical reactions. Inerting can be complete or partial in the gas elutriating air stream, again depending on the conditions of the mill and fuel.

Explosion Suppression

Upon detection of a flame within the milling environment, explosion suppression can be used to prevent flame propagation by creating an inert atmosphere within the mill. The sudden injection of inert gas and the dowsing of flames via the release of chemicals such as sodium bicarbonate (Montgomery, 2013) are two such strategies used.

Explosion Vents

Many mill types can be made sufficiently strong to withstand an explosion of dust within, as is the case with some hammer and ball and tube mills; care of adjoining plate sections should be taken as the joints may not be as robust. However, for those that cannot, the installation of explosion vents is an option. The principle behind which is the release of pressure within the mill to protect it from reaching destructive levels (Abbasi & Abbasi, 2007). When designing appropriate vents, consideration of the unit geometry, initial pressure, temperature, dust concentration, turbulence and ignition source must be given.

Start-Up and Shut-Down

During the start-up and shutdown phases of a coal fired power station, there is a higher risk of explosion of fuel (Guo, Wang, Wei, & Zachariades, 2014; Jianlin, Jihong, & Shen, 2009). This is caused by the static deposits of fuel heating up over time, in addition the air to fuel ration is in the flammable range. Identification of the potential for fires in the mill is difficult to achieve. In the papers by Guo et al. (Guo et al., 2014) and Jianlin et al. (Jianlin et al., 2009) software programs are developed to help maintain and control mill variables to limit the potential for such events.

2.9 Mill wear

Wear of mill consumables, such as grinding media, mill liners and classifier rotor blades causes significant cost incurred due to the shutdown of mills when components require replacement (P. W. Cleary, 1998; Salzborn & Chin-Fatt, 1993).

The wearing of mill components also affects the efficiency of the mill; should the grinding elements not retain the correct concentricity, physical dimensions and contours affect the ability to grinding. This causes the residence time to increase in order to achieve the accepted particle size and has the consequence of increased power consumption. Another repercussion of worn grinding elements is that the product size also increases.

The primary cause of wear is from the abrasive mechanisms acting on the grinding media and shells (Durman, 1988), also damage is caused from impact with sufficiently hard particles (Moore, Perez, Gangopadhyay, & Eggert, 1988). As well as the cost of the consumables and down time of the mills, the function can also be affected, such as variation in the flow patterns of the mill charge and the grinding processes (P. W. Cleary, 1998).

Measures taken to minimise such wear on the mills consist of study into materials that provide resistance to the wear mechanisms. These include study into abrasion resistant steels, non-metallics such as natural rubber, polyurethane, ceramics, and alloyed cast irons (Durman, 1988; Salzborn & Chin-Fatt, 1993).

2.10 Effects of Mill Operating Variables

Operating parameters of mills, for example rotational speed, grinding media load, feed rates and load, and variation in grinding media etc. have a direct influence on the final product and energy consumption. Optimisation of the parameters would increase overall efficiency with potential to save on energy utilised in the grinding of biomass. In an evaluation of the operating conditions taken from various industries several key similarities are present.

In multiple studies across several types of mill it has been determined that the particle size distributions reduce in mean size with increases of residence time in the mills (L. G. Austin, Luckie, & Shoji, 1982; L. G. Austin, Shah, Wang, Gallagher, & Luckie, 1981; Jindal & Austin, 1976; Meghwal & Goswami, 2014; Naik, Malla, Shaw, & Chaudhuri, 2013; Nath, Jiten, & Singh, 2010). In mills with tumbling grinding media, i.e. ball and tube, rod and tube, planetary ball mills etc. this follows an exponential decay to the mean particle size (Mandal, Mishra, Garg, & Chaira, 2014; Nath et al., 2010) suggesting a limit to size reduction. This occurs

for both brittle and fibrous material, i.e. both coal and biomass. In other mills this is not as clear based on different breakage mechanisms or by the removal of product under a certain size through internal classification, as is common on rotary, knife, hammer, vertical spindle and centrifugal mills.

The operational speed of the mill, defined in revolutions per minute (RPM), also influences the mean particle size of the final product. It has been concluded from studies (L. G. Austin et al., 1981; Naik et al., 2013; Nath et al., 2010) that there is a direct relation to the finer particle size with increases in the operational speed, these studies are about ball and race, tube and ball (exponential size reduction), and rotary mills. In the case of tube and ball type milling it was determined by (Mandal et al., 2014) that there is a critical speed, defined as a percentage of the maximum operational speed of the mill, that is optimal for comminution. A speed that is too high or too low can affect size reduction efficiency as the cataracting motion that causes shearing and impact is diminished.

The load in the mills is also linked to several characteristics of mills and final product. In (Naik et al., 2013), once the load within the knife mill built up to a certain volume, the primary grinding mechanism changed to attrition, rather than cutting, due to the lack of room to move in the mill and the shearing forces of friction causing breakage. The work by (L. G. Austin et al., 1981) determines that for a ball and race mill there is a peak load at which the maximum rate of breakage of particles is achieved.

The variation in grinding media within the mills can also affect the final product. In the studies by (Mandal et al., 2014) and (L. G. Austin et al., 1981) both state that the increase of the number of grinding balls in a planetary ball mill and ring and race mills increase the rate of the breakage. Mandal also states with a higher ball to material weight ratio the product will be finer. However larger diameter balls produce a coarser product. In the study of hammer milling (Jindal & Austin, 1976), fatter and sharper hammer blades increased the rate of breakage of particles. In knife, centrifugal, hammer and other mills that incorporate internal classification all can control the passing particle maximum size, therefore with screen aperture decrease, the particle size decreases (M Gil et al., 2008; Meghwal & Goswami, 2014; Miao et al., 2011). The trade off with the decrease in screen size though is that

greater energy consumption is brought about through increased residence time or RPM.

The mill feeding systems will vary based on the type of mill in use. In the study by Austin et al (L. G. Austin, Jindal, & Gotsis, 1979) into continuous grinding in a laboratory hammer mill, higher feed rates increased the hold up in the mill, their evaluation also concluded that only small increases in the feed rate could bring about instability in the operation of the mill, causing the maximum hold up of product in the mill to be exceeded. In agreement with Austin's results an explanation of why this occurs is given in (Naik et al., 2013) who concluded with a knife mill that at higher feed rates the mechanisms of particle breakage changed from impacting forces to attrition. Furthermore, the particle size distribution of the product varied more, due to the attrition producing a higher proportion of fines. Hence the ability to control the feed rate is an important factor in the product quality and safety aspects of mill operation.

Other milling attributes that affect the energy consumption of a mill are RPM, feed rate, mill load and grinding media charge (through the increase total mill load) (L. G. Austin et al., 1982; L. G. Austin et al., 1981; Magini, Iasonna, & Padella, 1996; Mandal et al., 2014). The product size requirement (through necessity for higher RPM or greater residence time) is also a factor and is linked to the creation of new surface area of the particles consistent with the energy laws for grinding (Meghwal & Goswami, 2014).

2.11 Modelling approaches

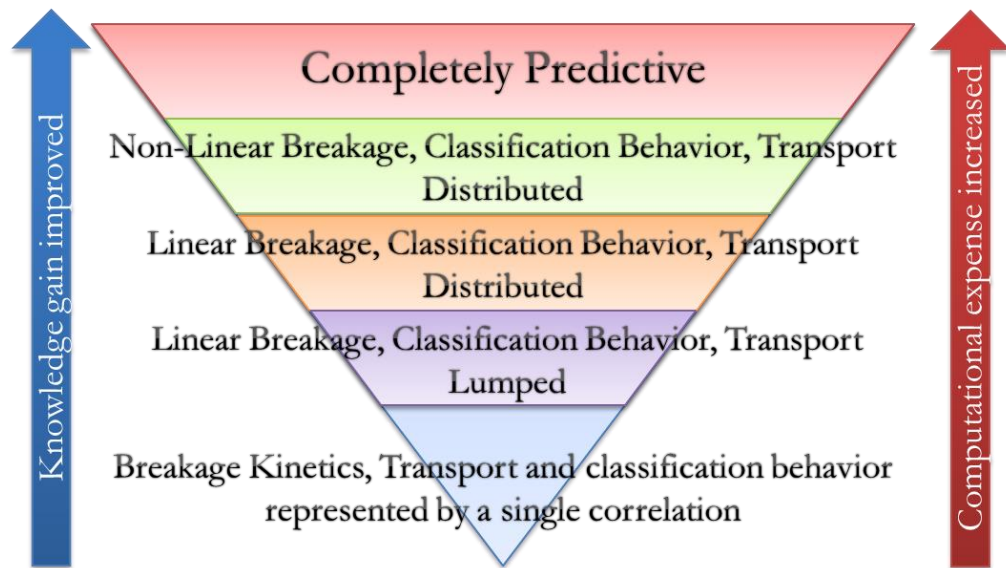


Figure 2.11 highlighting the hierarchy of modelling approaches, at the higher level more detail about milling is discovered but at the expense of computational time, source: Extracted from (Herbst & Fuerstenau, 1980).

Modelling approaches are conveniently summarised in the paper by Herbst and Fuerstenau (Herbst & Fuerstenau, 1980) indicating a hierarchy based on the physical detail they contain and the experimental and computational difficulty associated with their usage; details of this are shown in figure 2.11. Complexity of a simulation is governed by the ability to account for properties of the feed material, the stress application environment existing in the mills and for the mathematical structure which would be required for the model.

Identified by Herbst and Fuerstenau are the behaviours in the mill that need to be accounted for on an individual basis. These include:

- **Breakage kinetics:** how the particles in the model break, linear breakage defines a directly proportional relationship between mill parameters, e.g. rotational speed, input energy etc. and the rate at which the particles are comminuted. Non-linear breakage considers the repercussions of other mill dynamics such as development of a particle bed cushioning impacts and absorbing some of the impact energy, thus the breakage may or may not occur. Here the rate of breakage will not fit a linear relationship.
- **Classification Behaviour:** this is how the particles are assessed and how the decision is made for them to move on and exit the system. The classifier

behaviour would also govern the throughput of the mill and the circuit load of any milling process.

- **Transport Behaviour:** the flow of particles into, through and out of the mill may also not be as straight forward a process in milling. A modelling approach would ideally handle how the particles behave in the mill and a transport function in a mill may govern the spatial movement of particles, thus enabling prediction of material build up in areas of the mill as well as complications in feed and exit of the mill.

Whilst comminution modelling has been of considerable interest, much of the research completed has been for brittle materials that are generally homogeneous in nature and have a more crystalline structure than biomass. The practice of modelling biomass comminution has received very little research. Where studies have been completed, the studies have focused on relation to the energy laws and looked to upscale processing based on energy utilisation. As the primary focus of the project is to create a model that is as predictive as possible a review of modelling techniques is necessary to determine which will be most appropriate to use and can incorporate as many of the features of as identified by Herbst and Fuerstenau as possible.

2.11.1 Empirical Modelling

Energy Law Modelling

For the purposes of milling several theories are in existence. The objective of these theories is to quantify the energy required for the breakage of particles of a given material. The theories in existence are encompassed in a differential equation proposed by Walker et. al. (Walker, Lewis, McAdams, & Gilliland, 1923) in equation 4.1; each of the separate laws has a different value for the exponent of the particle size variable in the denominator, see table 2.3.

$$dE = -C \frac{dX}{X^n} \quad (4.1)$$

Table 2.3 lists the energy laws and describes their differences.

<i>Energy Law</i>	<i>Exponent Value</i>	<i>Governing Philosophy</i>
Kick's $E = C_K f_c \log\left(\frac{X_P}{X_F}\right)$	$n = 1$	Energy requirement is proportional to Kick's coefficient (C_K), it indicates the work required for a 10-fold reduction in size (L. G. Austin, 1973).
Rittenger's $E = C_R f_c \left(\frac{1}{X_P} - \frac{1}{X_F}\right)$	$n = 2$	Energy required for size reduction proportional to the new surface area created by the fracture of the particle (Temmerman et al., 2013). C_R is von Rittenger's constant.
Bond's Law $E = 100E_i \left(\frac{1}{\sqrt{X_P}} - \frac{1}{\sqrt{X_F}}\right)$	$n = \frac{3}{2}$	Energy required to grind a feedstock to 80% of the product passing 100 μm grade sieve (Green, 2008). E_i is the Bond Work Index.
f_c – is the specific crushing strength of a material	X_F – the size of the feed material	X_P – the final product size

It is the conclusion of a review paper on the subject of the power laws that “... these laws are empirical fits to the batch grinding data, and cannot be applied except as the crudest approximation to a continuous mill circuit with recycle”, hence for an overall model they may be of limited use (L. G. Austin, 1973). They have proven useful for in batch experimentation for determining the performance of grinding devices when difficulty has arisen in calculating the stresses on particles in them (Green, 2008); in general though, the energy laws have not been successful in practice, it is speculated that this is due to the inefficiency in transferring the input energy to the grinding mechanisms, most of the energy is converted to noise and heat through friction.

Despite the comment from Austin, development is still being pursued in developing energy-size reduction models in order to produce them so that up-scaling to industrial application will be adequate (Morrell, 2004; Nomura & Tanaka, 2011; Temmerman et al., 2013); these models are specific in their application, both to the type of mills used and the specific energy law that is used.

Population Balance Equation Modelling

As described by (Ramkrishna, 2000), “In the application of population balances, one is more interested in the distribution of particle populations and their effect on the system behaviour”. Applied to the application of milling, the ability of the population balance equation methods (PBE) to describe the physical characteristics of the particulate system, e.g. mass, volume, size distribution, promotes its candidacy as a suitable modelling technique. Applied to the processes of particle size reduction the PBE method has been implemented extensively. Some early work on mineral processing has been completed by (L. G. Austin et al., 1979; Jindal & Austin, 1976; Klimpel & Austin, 1977) all of which apply the PBE method solved through ODE solvers. Matrix forms of the PBE are implemented in (Miguel Gil, Luciano, & Arauzo, 2015b; Herbst & Fuerstenau, 1980; Petrakis & Komnitsas, 2017; Prasher, 1987) that all simplify the algorithms somewhat. The PBE method uses a back-calculation of parameters for governing functions, the selection and breakage functions, a process that requires nonlinear optimisation (Bilgili, Yepes, & Scarlett, 2006; Miguel Gil et al., 2015b; J. Kumar, Peglow, Warnecke, Heinrich, & Mörl, 2006; S. Kumar & Ramkrishna, 1996a, 1996b). except for all but the paper by Gil et. al., they deal with brittle material and form more spherical particles on impact. This leads to smooth curves and particle analysis results that are less affected by high aspect ratios. Other works look to increase the ability of the PBE to maintain information, through the moments of particle size distributions, these are maintained through different mathematical schemes such as Finite Element schemes (Mantzaris, Daoutidis, & Sreenc, 2001b; Nicmanis & Hounslow, 1996, 1998), Finite Volume schemes (J. Kumar et al., 2006; S. Kumar & Ramkrishna, 1996a, 1996b), and direct quadrature method of moments (Daniele L Marchisio & Fox, 2005). They aim to preserve other information such as particle number as well as mass or volume conservation. Chapter 4.1 provides a fundamental formulation of the PBE method and subsequent method of solution used in this research.

Artificial Neural Networks

Inspired by natural neurons, Artificial Neural Networks (ANN) is a method that is used when large data sets are available and is highly dependent on that data to cover the extremes of operation. With a suitable training process the data sets can use the data sets to generate an accurate model for the network (Shuiping, Hongzan, Zhichu, & Jianzhong, 2002). Input parameters for a process are multiplied by weightings constituting the contribution of the input to the model. ANN has been used in comminution modelling to generate models that have resulted in accurate non-linear models leading to the desired outputs. In comminution modelling ANN has been used in optimising electricity consumption based on operational conditions of the mills (H. Wang, Jia, Huang, & Chen, 2010), in addition the use with biomass milling based on variables, both of the mill and fuel properties, was used to characterise mill energy consumption (Miguel Gil et al., 2013). Many of the implementations of ANN for grinding circuits focus on using neural networks to control the mill as opposed to building a predictive tool (Chelgani, Hower, Jorjani, Mesroghli, & Bagherieh, 2008; Stange, 1993).

The modelling methodology can also be used with other techniques to further optimise the comminution processes, such as in the work by (Shuiping et al., 2002) that couples the process with fuzzy logic to deal with the uncertainty and genetic algorithms to optimise the model once trained.

Genetic Algorithm Optimisation (GA)

The optimisation via the genetic algorithm method has been used in conjunction with other empirical modelling efforts (Farzanegan & Vahidipour, 2009; Shuiping et al., 2002; Su, Wang, & Yu, 2010; Tang, Zhao, Zhou, Yue, & Chai, 2010; H. Wang et al., 2010; Y. G. Zhang et al., 2002). The process of genetic algorithm optimisation is given in (Datta, 2011). The uses of the technique include optimising ball milling circuit simulators (Farzanegan & Vahidipour, 2009), optimisation of artificial neural network generated models (Shuiping et al., 2002; H. Wang et al., 2010) and for optimisation of mill parameters, mainly mill load (Su et al., 2010; Y. G. Zhang et al., 2002).

The stochastic optimisation of a model uses a set of all potential solutions to the problem, then evaluates the performance of each candidate solution with respect to the objective (Pelikan, 2005). Continuous iterations and progeny

generation cause the convergence of the candidate solutions to a single solution whereby the fitness evaluation cannot be improved.

The crossover stage of the GA processes takes two sets from the promising solutions, a combination of the two parent sets is then used as the progeny to be utilised in the next fitness evaluation. Mutation is used in genetic algorithms, based on a programmable probability function in the GA framework representing random change and diversity in the set, thus ensuring that parameter strings do not get too similar to each other and prevents fixation on a particular locus (Mitchell, 1998).

2.11.2 Numerical Simulation Modelling

Discrete Element Modelling

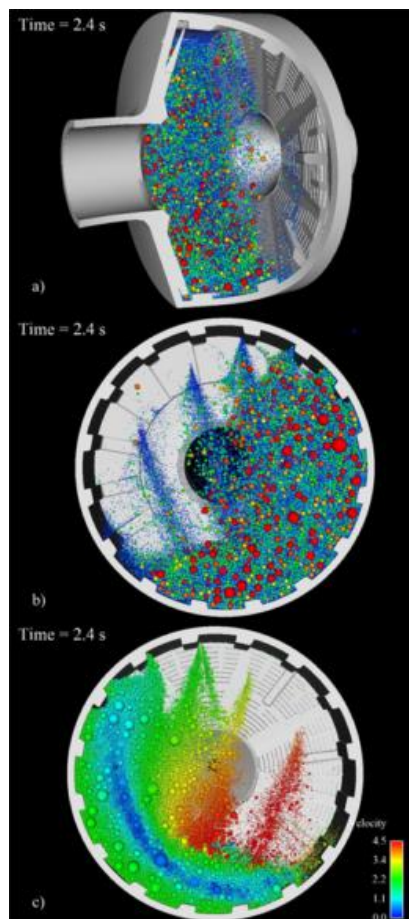


Figure 2.12 provides an illustration of the principles of DEM, (P. W. Cleary, 2009).

Developed by Cundall and Strack (Cundall & Strack, 1979), DEM is a numerical method for determining the behaviour of granular assemblies using

algorithms based on Newton's second law of motion (Mishra & Rajamani, 1992). The modelling technique requires the resolution of inter-particle and particle-boundary resolution.

The use of DEM has been varied since its inception, including crowd dynamics (H. Singh et al., 2009; Smith et al., 2009), particle flow problems in hoppers (J. Li, Langston, Webb, & Dyakowski, 2004), pneumatics conveyance in pipes (Sakai & Koshizuka, 2009) and interaction with ground soil (Horner, Peters, & Carrillo, 2001) to name but a few. DEM has seen extensive use in modelling comminution (P. Cleary, 2001; Mishra & Rajamani, 1992; Weerasekara et al., 2013), usually, again for mineral processing of brittle materials or in mining. Use for biomass does has yet been considered due to the homogenous non-spherical shape for which complications are encountered in DEM and so in general using it to model milling could lead to quantitative drawbacks (P. W. Cleary, 2009). In DEM the shape of particles can be generated through the bonded particle method (BPM) that creates bonds between groups of spheres that represent the material characteristics. These spheres have to be arranged in different geometries (Mair & Abe, 2011). Other approaches use construction of ellipses, polygons or super-quadratics and hyper-quadratics (P. W. Cleary, 2009; Džiugys & Peters, 2001; J. Wang, Yu, Langston, & Fraige, 2011). Modelling of complex geometries does present difficulties with the contact detection, force and torque calculation, extension to 3D and the bonding of particles as these can all become complicated and computationally expensive (Y. Wang & Mora, 2009).

Comminution modelling in DEM can be achieved using a bonded particle method (BPM), with the particle bonds breaking when subjected to forces exceeding the mechanical bonding strength (Khanal, Schubert, & Tomas, 2007; Naik et al., 2013; Weerasekara et al., 2013). Alternative methods use a routine whereby when subjected to a force sufficient to break the particle it is removed and replaced by smaller progeny particles (Paul W Cleary, Prakash, Sinnott, Rudman, & Das, 2011; Delaney, Cleary, Sinnott, & Morrison, 2010).

Finite Element Method (FEM)

FEM uses functions to determine approximate solutions to variational problems with differential equation (Reddy, 1993). Complex domains are represented by collections of simple subdomains (the finite elements). Over each

element the functions are derived based on the idea that any continuous function can be represented by a linear combination of algebraic polynomials. The functions are derived using concepts from interpolation theory.

There is no direct use of FEM in comminution that the author has been able to find in literature however the use of FEM in the scope of the project is suggested for modelling of other components that may arise. These include calculation of the effects of the fuel on the mill components as was investigated in (Jonsén, Pålsson, Tano, & Berggren, 2011). The wear on mill surfaces, breakage modelling of biomass fuels, material stress, strain, and breakage, has seen an extensive history of FEM modelling (Özcan, Bayraktar, Şahin, Haktanir, & Türker, 2009; Sarris & Constantinides, 2013).

Finite Volume Method (FVM)

FVM is a discretised modelling technique for the solution of partial differential equations arising from the laws of conservation. It uses a volume integration formulation problems, partitioning a set of volumes into discrete equations (Long, 2013). It is often used as a technique in the solution of computational fluid dynamics (CFD) simulations.

Whilst not used directly for comminution, it has been used to describe fluid motion in stirred bead milling (Graeme, 1999b) and for the elutriating air flow through a vertical spindle variation mill, a bowl mill, and accompanying classifier unit (Bhasker, 1999).

Smooth Particle Hydrodynamics (SPH) and Moving Particle Semi-Implicit Method (MPS)

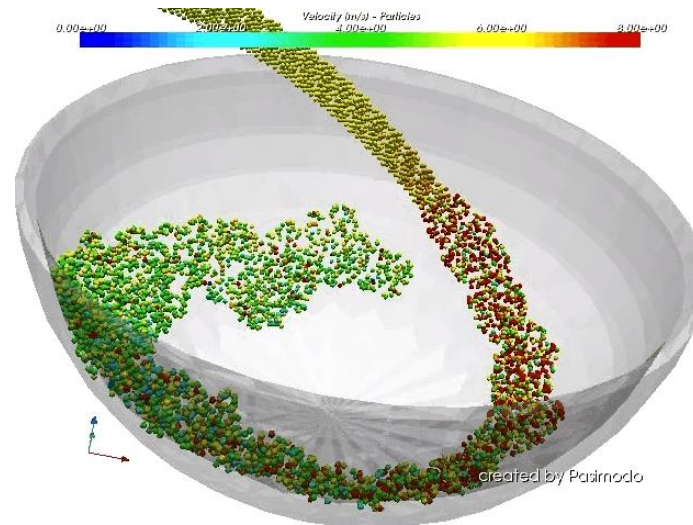


Figure 2.13 displays a liquid flow modelled with the SPH technique, image source: http://www.itm.uni-stuttgart.de/research/pasimodo/video_gallery_de.php

With SPH, assemblies of particles represent fluids. The particles hold the physical quantities such as velocity, pressure, mass and move according to the Lagrangian material velocity (Sun, Sakai, & Yamada, 2013). A smoothing kernel is used with the interpolation of SPH approximations and is related to the numerical stability. Uses of SPH extend beyond fluid mechanics, the dynamics of impact, fracture and fragmentation have also been studied using the method given in (Randles & Libersky, 1996). When SPH has been used to model action in a mill, it has been to model the liquid phases of wet milling (Paul W Cleary & Morrison, 2012; Paul W Cleary, Sinnott, & Morrison, 2006; Jonsén¹, Häggblad, & Pålsson, 2014). MPS is like SPH except it can only be used in the case of an incompressible fluid. The smoothing function is also different (Vorobyev, 2012).

Hybrid Models

Linking of modelling techniques can provide a way to overcome some of the shortcomings that individual methods have. This highlights alternative directions that the project can take. In several works, linking PBE to DEM models, allows the particle level detail to be integrated into the model. Different implementations have captured certain information such as, particle velocity and trajectories (Sen, Dubey, Singh, & Ramachandran, 2013). Also, the impact energies have been used to correlate to a specific breakage of particles (M. Capece, E. Bilgili, & R. Davé, 2014; Lee, Cho, & Kwon, 2010). The benefit of this approach over a

purely DEM approach is that the computational time and resources are considerably less (Sen et al., 2013). The interaction between the grinding media and mill liner for a rotating drum was also the motivation for a coupled DEM-FEM model by (Jonsén et al., 2011). Here it was chosen as FEM would better allow assessment of the response of the mill liner on the mill charge. The use of SPH and MPS to model the fluid phases in wet milling has been utilised in several studies (Paul W Cleary & Morrison, 2012; Paul W Cleary et al., 2006; Jonsén¹ et al., 2014; Jonsén et al., 2011; Sun et al., 2013; Yamada & Sakai, 2013). DEM was also used in conjunction with FVM in the paper by (Yamada & Sakai, 2013). DEM was used to model the particle motion in a rotating drum whilst the FVM was used to model the heat transfer between the drum, the gas and the balls in the drum.

Jonsén et al. used SPH, DEM and FEM in conjunction to model the milling components of slurry, charge and mill structure respectively (Jonsén¹ et al., 2014). The virtual comminution machine, targeted at reducing development and integration time of new machinery with accurate simulation, fully integrate two way coupling of DEM and SPH methods (Morrison & Cleary, 2008). The unified comminution model looks to utilise all of the unique features of the methods described to aid in the understanding of the milling processes (Powell, Govender, & McBride, 2008), figure 2.14 provides a representation of its working.

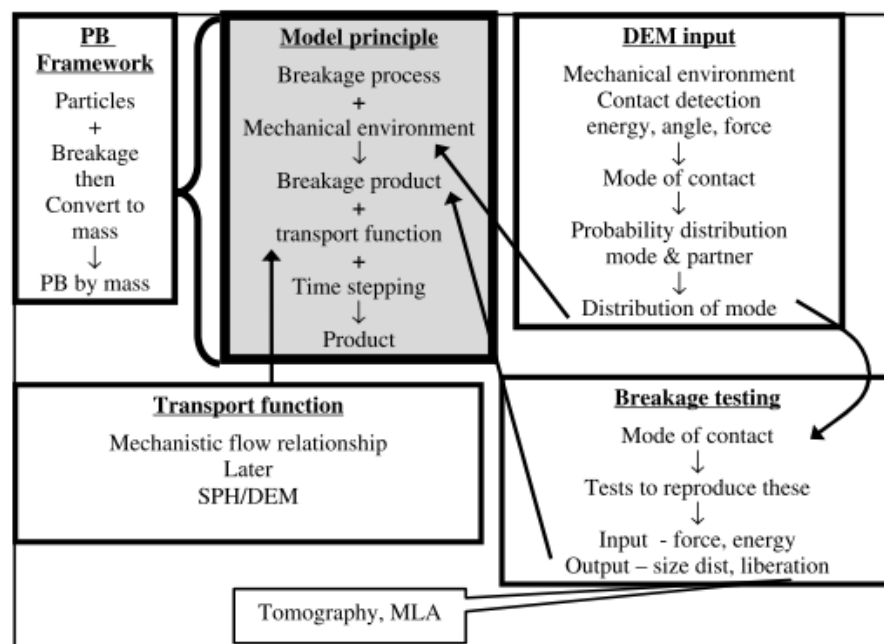


Figure 2.14 displays the UCM model structure, source: (Powell et al., 2008).

2.12 Up-Scaling Methods

Up-scaling simulations to model industrial scale mills based on simulations for laboratory mills has been achieved in a few different ways. Scale up based on the energy requirements has historically been one method for determining energy required to power industrial milling practices. Using the theories such as Bond's law, upscaling has been achieved by the introduction of parameters that represent characteristics of the milling operation (Coulson, 1999), and to characterise the energy loss that is not attributed to the breakage of material in the mill (Tanaka, 1972). Upscaling using these methods have not proven successful, primarily down to the collating of a 'one-for-all' variable related to the mill and milled material (L. G. Austin, 1973). Predicting the energy requirements, throughputs and product size distribution has been completed for the case of a high pressure grinding roll type mill (Daniel & Morrell, 2004) based on the physical parameters of the mill. For a ball mill, work towards a predictive energy map that could be used to upscale energy requirements has been completed (Magini et al., 1996), this map depends on the grinding media physical parameters. Both studies recognised that this method of upscaling became dependent on the feed material and whilst good correlation with validation data was achieved, the models are sensitive to accuracy of the parameters. Furthermore, the unforeseen mechanical influences, such as slippage of the rollers in the former paper also influenced the performance of the model calculations.

Scale-up methodology experimentation was completed in (Iwasaki, Yabuuchi, Nakagawa, & Watano, 2010). Here the theory with ball milling is based on the principle that to achieve the same size fine product as achieved in the bench mark testing, the same impact energy per unit mass must be provided by the larger scale milling machinery. Using a DEM simulation, verified against observations of ball movement within the mill, they could extract impact energy information. This was based on a sectional area where the shear flow field within the grinding region was evaluated. With increases in the diameter of mill shell, the region of the shear flow field under scrutiny needed to be expanded and it is necessary to maintain similarity in the shear flow field. To maintain the shear flow field similarity, for a smaller mill it was necessary to increase the rotational speed to critical speed ratio due to larger diameter of grinding media to mill shell ratio in order to maintain validation.

In the work by Herbst and Fuerstenau (Herbst & Fuerstenau, 1980), development of a PBE technique is used for the up-scaling of laboratory ball mill to a commercial continuous closed circuit ball mill. Here they identify the breakage rate function to be independent of mill design and operating variables. Furthermore, the breakage distribution functions are invariant with the changes in the mill design and operating conditions. These two observations allow the prediction of optimal design based on laboratory testing. It has also allowed the study to account for transport and classification behaviour through the mill. More importantly it has allowed the study of deviation from the optimal conditions as the study indicates when assessing the efficiency of the classifier on the circulating load residence time. This highlighted the danger of using lumped parameter approaches for mill design, for example against the Bond Work Index method that assumes perfect classification and plug flow conditions.

2.13 Literature Review Conclusions

From reviewing the literature, it has been determined that any model that is to be taken forward for development will need to be adaptable to account for several parameters. These can be summarised as the fuel parameters and mill type and operating conditions. Fuel parameters would contain descriptive variables that contribute to understanding the required energy to break the fuel and how it breaks once exposed to that energy, i.e. specific breakage energy and breakage distribution. Previously studies in such regard have generally been applied to mineral processing and do not provide consideration for the cellular structure and anisotropic rigidity that is inherent with biomass material. Therefore, such characteristics may need to be considered. Milling parameters would be expected to contribute to a model that accounts for the energy transfer to the fuel. Furthermore, the mill design and breakage mechanisms would contribute to the efficiency of that energy transfer. This however could be different based on the interaction of the breakage mechanism and the biomass fuel type.

When upscaling, it will become necessary to increase the complexity of the model to account for other milling factors. These will include circuit operation, accounting for fuel entering and leaving the system. Additionally, effects of the way in which this is facilitated should be considered, e.g. the pneumatic conveyance used with classifiers and the efficiency of the classifier.

Implementation of the model will also need to be carefully decided. It is clear from the literature that an empirical approach to modelling will yield benefits in a reasonable time scale, fully appreciated for industrial purposes. This will however only be possible with extensive experimental research and has very limited predictive ability when considering the variety of both biomass and mill type.

The numerical method approach has scope to increase the understanding of the fundamentals of milling, specifically in terms of the material/grinding media interaction. Furthermore, the ability to model other aspects of particle behaviour, e.g. velocity, energy, mass, at the particle level is possible; this would aid in understanding the fundamentals and potentially modelling additional considerations of mill operation, such as how and why or where potential for dust explosion may occur. Drawbacks to such model development are the likelihood of extensive computational resources and computational time. One positive discovery regarding limiting the flaws in both approaches, that has been drawn out of the literature review, is the ability to couple multiple techniques, an empirical method with a numerical method, to compliment the shortfalls in any one individual technique.

Chapter 3 - Modelling Technique

Evaluation and Ranking

Whilst the milling of biomass material has been studied and grinding process simulations, in general have been devised and implemented, the specific application of a modelling technique to evaluate the comminution of biomass pellets has not been covered in detail. To select the most appropriate method, a framework for ranking techniques that could offer advances in predicting the results of biomass grinding has been created and implemented.

Prior to the development of the ranking framework a suitable level of knowledge is required regarding: the data available to hand on which to base the simulations, understanding as to the how comminution is achieved and the objectives of doing so in an industrial setting, and the constraints upon the research project. To this end the first stage is to acquire the relevant knowledge more than that obtained in the literature review.

3.1 Data Analysis

3.1.1 Literature

The following survey of information on mill type, fuel type and comminution variables is a summary of 21 papers about biomass milling from various fields, such as agriculture, food, and fuel preparation. The survey is a quantitative analysis of the papers and of the three areas stated. All papers surveyed are summarised in appendix B of this thesis. The survey is a collection of papers that focus specifically on the grinding of biomass material. Plenty of literature is available on the study of biomass as a material however research into biomass for use in pulverised fuel combustion is rare hence the need to draw upon other sectors for information on practices and procedures and relate that knowledge to the context of what the research project is trying to achieve.

Mills

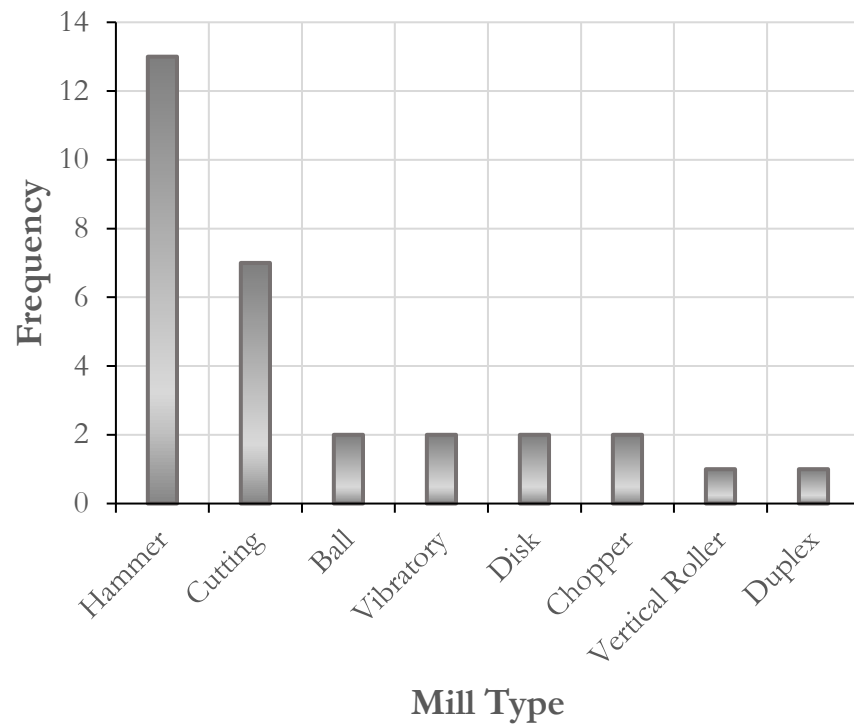


Figure 3.1 displays the survey results for the types of mills used in published literature on biomass milling.

From the analysis of the review of published literature for mills used to reduce biomass particle size there is a preference for hammer style mills, followed by the cutting mill type (figure 3.1). This is in no part a coincidence as the ductility in biomass leads a preference of cutting and shearing action when under comminution and inhibits effectiveness of compression and impact mechanism. Where mills with actions such as compression and impact are the main grinding mechanism, application is generally for biomass species with more anisotropic growth structures, e.g. some seed species (Too, Yusof, Chin, Talib, & Aziz, 2012), or where temperatures of the biomass is reduced to sub-zero temperatures in order to enhance grindability (Goswami & Singh, 2003).

The shortcomings in the analysis is with regards to industrial size mills. In the survey only (Miao et al., 2011) uses an industrial scale mill; all others are laboratory scale or pilot scale. Literature on industrial scale milling of biomass could not be found beyond this.

Biomass Species and Form

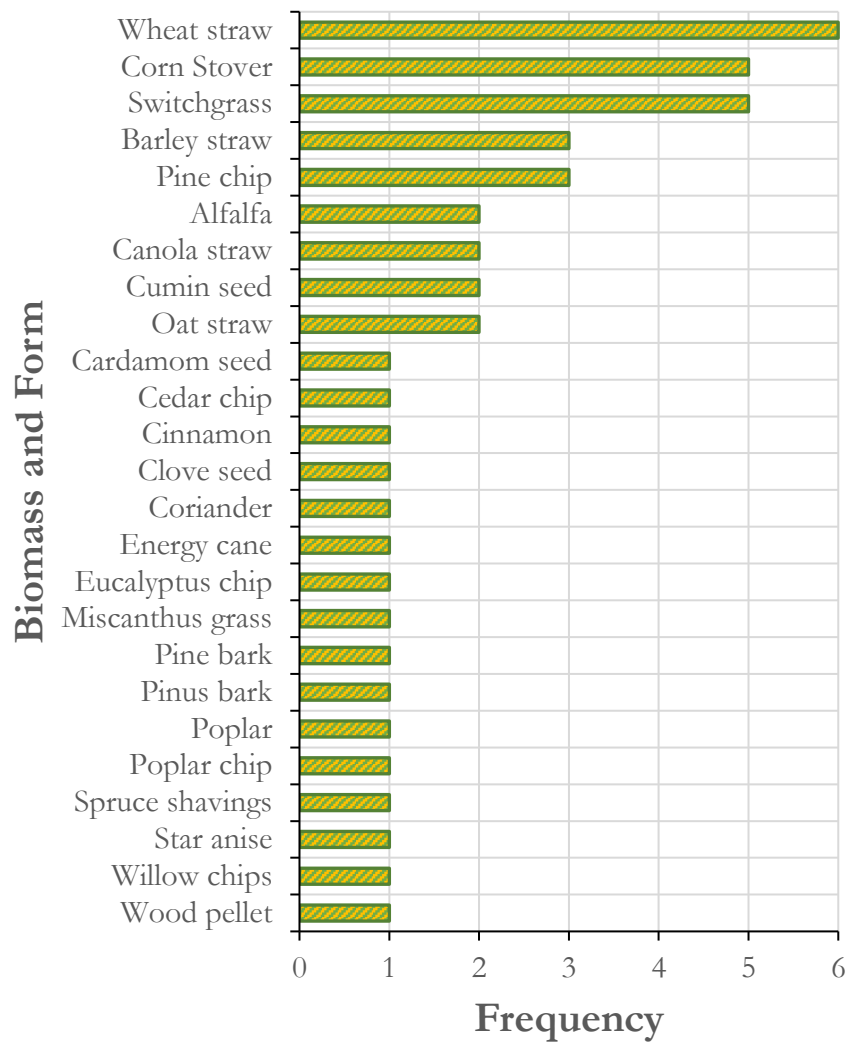


Figure 3.2 displays the biomass species and form of the biomass that has been used to study biomass milling in the literature surveyed.

The biomass species within the literature (figure 3.2) is linked to the field of application for the paper. As comminution in the agriculture sector comes at such a high cost, constant research has been commissioned hence much of the literature comes from there and understanding as to the implications upon the research project can be gathered from this sector, however as biomass combusted in pulverised fuel heat and power systems arrives in pellet form, other factors should be considered. Only 1 of the papers surveyed contained information on biomass

pellet milling for an unspecified wood species (Tamura, Watanabe, Kotake, & Hasegawa, 2014).

Independent Variables

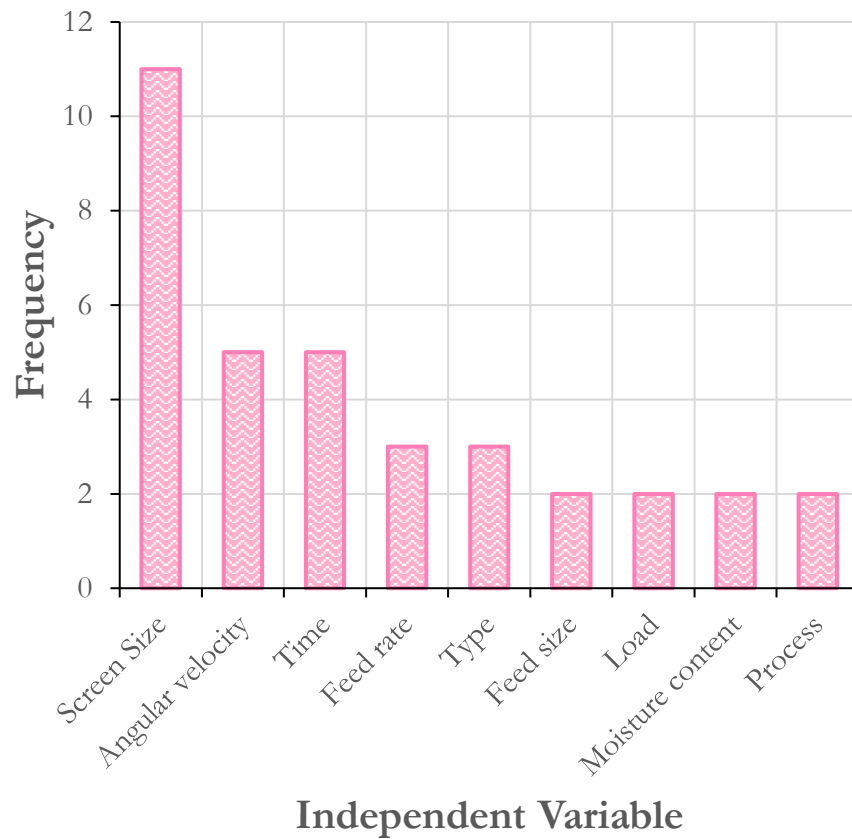


Figure 3.3 displays the survey results of the independent variables that are tested in literature based on the milling of biomass material.

Figure 3.3 again shows only the 9 most frequent independent variables. Given the preference of hammer and cutting mills for biomass milling, it is unsurprising that screen size is the most frequent. The helpful aspect of the majority of papers concerning hammer and cutting type mills is that they follow the cycle milling process seen in power stations and the most frequent variables of screen size, angular velocity and feed rate are comparable with industrial practices. Milling time as a variable occurs in papers where batch milling takes place, likewise for mill load; whilst the context of the papers does not factor in continuous cycle milling practices in power station fuel preparation, they offer insight in to the analysis of particles and grinding efficiency measures.

Dependent Variables

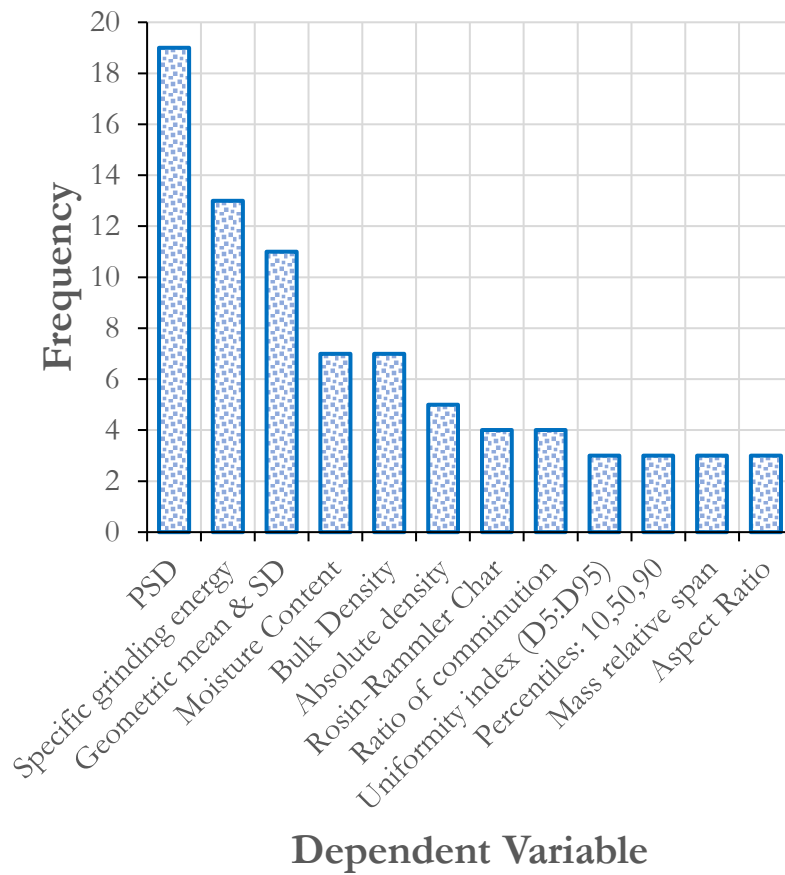


Figure 3.4 displays the most frequently collected dependent variables in published biomass milling literature.

The survey results for the dependent variables (figure 3.4) reaffirm that particle size distributions and specific grinding energy are of prime importance. Further physical characteristics such as moisture content, bulk and absolute density are also popular measures. The bulk of statistics then transfers to the characterisation of particle size distribution features and what can be inferred from them. Figure 3.4 shows only the top 12 surveyed parameters; particle shape parameters such as circularity, sphericity and roundness are surveyed however are more infrequent. Other characteristics of a more fundamental nature are also obtained from further experiments such as, but not limited to, Ultimate analysis, Thermogravimetric analysis (TGA) and bomb calorimetry that provide the elemental composition, combustion relevant characteristics and heating values respectively. In appendix B, details of the papers and what they survey can be found.

3.1.2 Industrial Partner Information

The following information is collection of the limited information available in literature, information available in the public domain and information shared by the members of the BF2RA who are involved either directly as generators or indirectly as equipment manufacturers. Information sourced from the latter 2 are because of the lack of published information on industrial scale mills. Appendix C includes a small survey presented to the BF2RA members for their response to enhancing understanding of the problems faced when milling in general.

Mills

Table 3.1 shows a list of mills in use at BF2RA member power stations and the fuel for which they are used to grind. Appendix A contains illustrations of a variety of mills along with details of their grinding mechanisms.

Table 3.1 displays industrial milling manufacturers and models used or manufactured by BF2RA members for grinding different fuels.

<i>Manufacturer/ Model</i>	<i>Type</i>	<i>Fuel</i>	<i>Grinding mechanism</i>
Babcock 10E	Vertical Ball and Race	Coal	Compression/Abrasion
Foster Wheeler D9	Horizontal Ball and Tube	Coal	Impact/Abrasion
Lopulco	Vertical Spindle Ring and Roller	Coal	Compression/Abrasion
Raymond	Vertical Tyre Roller	Coal	Compression
Champion	Horizontal Hammer	Biomass	Impact/Shearing
Loesche	Vertical Spindle Ring and Roller	Biomass /Coal	Compression/Abrasion
Andritz	Horizontal Hammer	Biomass	Impact/Shearing
Bühler	Horizontal and Vertical Hammer	Biomass	Impact/Shearing
Christy-Turner	Horizontal Hammer	Biomass	Impact/Shearing

As with the survey results from the literature, there is a preference for the use of hammer mills for grinding of biomass. However, in literature the bulk of the fuel is in an unprocessed form, much of the material combusted in power stations arrives pelletised and grinding of the biomass pellets results in the unpacking of the densified pellet back into the particles used to form them. In conversation with the industrial partners, advice was given that whilst the observation stated above is largely true, some additional comminution does ensue.

Independent Variables

Table 3.2 displays the independent variables used by the industrial generators as controlled variables for milling.

<i>Independent Variable</i>	<i>Association</i>
Primary air inlet temperature	Mill
Primary air flow rate	Mill
Pressure differential across the mill	Mill
Feed rate	Mill
Classification size (defined by screen size, classifier vane angle, separator speed, etc.)	Mill
Mill operating speed †	Mill
Moisture content (inlet)	Fuel
Bulk density	Fuel
Particle size (feed)	Fuel
Hardgrove Grindability Index (HGI)	Fuel

† In power stations mills generally have a set operating speed, however since the mills are often built to order the speed varies from one mill to the next hence should still be considered a variable for modelling purposes.

Like in literature, variables (see tables 3.2 and 3.3) can be grouped in to mill operating conditions and the characteristics of the fuel; many of those variables are shared. The ones that are not, namely the primary air inlet temperature and primary air flow rate provide additional actions that are not captured in most laboratory milling. These include, the pneumatic conveyance of pulverised fuel to the boilers burners; the primary air also provides further moisture content release from the fuel (L. G. Austin et al., 1982). Lastly the air input contributes to the stoichiometric mixture required for the combustion of the fuel in the boiler of the power station.

Dependent Variables

Table 3.3 displays the dependent variables in relation to industrial milling practices.

<i>Dependent Variable</i>	<i>Association</i>
Primary air outlet temperature	Mill
Pressure Differential across the mill	Mill
Energy consumption	Mill
Throughput	Mill
Particle size distribution	Fuel
Moisture content (product)	Fuel
Bulk density (product)	Fuel

Again, the dependent variables exhibit resemblance to the laboratory milling experiments. Energy consumption, throughput and particle size distribution are key

variables. Again, the other variables are constraints on the milling system that are designed to allow monitoring and influence the entire energy generation system. The monitoring of primary air temperature and pressure differential across the mill provides valuable information for the operating status of the mill load and throughput; higher mill pressure differential pressure indicates a higher mill load (Shoji et al., 1998). Moisture content of the product is also of importance as a higher level in the fuel will reduce the heat output from the boiler due to the energy required to evaporate it before combustion can initiate (van den Broek, Faaij, & van Wijk, 1996).

3.1.3 Sister Project Experiment Information

The BF2RA project, “On Biomass Milling for Power Generation” (Williams, 2016) completed an experimental research project with the objective of characterising biomass fuels and gathering insight in to the factors that affect the milled product and energy consumption in a variety of different mill types. The experimental analysis included a large amount of characterisation of thermal and mechanical properties of biomass as well as the results of milling experiments. This summary provides an overview of the milling experimental results that were available for use in this project.

Mills

Each of the mills used in the study (see table 3.4) were utilised due to their availability at the University of Nottingham. It should be noted that the mills used in the project, except for the Lopulco mill, do not simulate the industrial scale mills due to the difference in the grinding mechanisms, however each has similar attributes. The SM300 cutting mill is like a hammer mill in terms of the grinding mechanism. Additionally, they also have a screen surrounding and forming part of the grinding mechanisms as well as the closed cycle style of operation, due to the internal screen. The Lopulco E1.6 mill is a scale model of a Lopulco LM16 mill operating with 2 rollers instead of 3. The Bico ball mill is a mill designed to determine the BWI value for tested materials. It has a fixed rotational speed and no internal classification. The Bond work index includes a stage where undersize material is screened and removed outside of the milling environment and the mass removed is replaced with unmilled material. Through this a continuous closed cycle

process is simulated. The charge of grinding balls also varies in size, where as a Foster Wheeler D9 industrial mill uses balls of the same size as its grinding media.

Table 3.4 displays the laboratory mills used within the sister project and variables that were tested as part of the experimental process.

<i>Mill Type</i>	<i>Circuit Operation</i>	<i>RPM</i>	<i>Experimental Parameters</i>			
			<i>Feed Rate</i>	<i>Classif- ication</i>	<i>Residence Time</i>	<i>Material</i>
Retsch PM100 Planetary ball	Batch	✓	✓ ^a		✓ ^b	✓
Retsch SM300 Cutting	Closed cycle	✓	✓	✓		✓
Lopulco E1.6 Ring-Roller[†]	Closed cycle					✓
Bico Ball and tube[‡]	Closed cycle (simulated)					✓

[†] Whilst the mill is capable of alternative feed rates, table speed and classifier variation, no time was left to investigate these, reducing the experiments to simply material variation.

[‡] For this mill, as it has a fixed speed and no internal classification, it was used in the context of the project for its purpose as a Bond Work Index (BWI) investigative resource only.

^a For the PM100 mill, no feed rate as such was investigated as it is a batch milling machine, however batch load was investigated in its place.

^b Residence time was measured through 2 parameters, standard time, but also through milling energy input, controlled by settings on the mill.

Independent Variables

As specified in table 3.5, the variables tested under the sister project include those similar in nature to those required by the industrial partners and those tested by other researchers and documented in literature. As specified in the table some constraints were observed in both the capability of the mills in question and as in the case of the Lopulco mill, the project simply ran out of time to complete more experiments. Further characterisation of the product of the milling includes the premilled volume.

Dependent Variables

Table 3.5 displays the dependent variables for which experimental results have been collected within the scope of the sister project.

<i>Variable</i>	<i>PM100</i>	<i>SM300</i>	<i>Lopulco</i>	<i>Bico</i>
Bulk volume	✓	✓	✓	
Mass difference	✓	✓	✓	
Specific grinding energy	✓	✓	✓	✓ ^b
Particle size distribution	✓	✓	✓	✓
Particle shape characteristics	✓	✓	✓	✓
Throughput		✓	✓	✓ ^c
Grinding media temperature	✓	✓ ^a		
Milled biomass temperature	✓			
Differential pressure			✓	
Environmental temperature			✓	

^a The temperature of the SM300 experiment grinding media was determined via a thermal imaging camera in some instances.

^b The Bond work index process calculates a specific grinding energy requirement whereas the other mills the energy draw is measured.

^c The Bond index provides a simulated steady-state conditions and mass throughput can be calculated from this.

The collection of the dependent variables is also consistent with the literature and the practices followed by the industrial partners. Where some of the mills have additional variables collected, they have been done so in an investigatory capacity as an alternative method to the standard approach and to see what insight might be gathered from doing so. Shape characteristics of the samples have measured using dynamic imaging processes that will be outlined in appendix F. Consistency in recording what look to be some of the key processes in milling in general have also been gathered where appropriate; mill throughput, particle size distribution and energy consumption are recorded throughout the experimental regime.

3.1.4 Data Analysis Conclusions

From analysis of milling literature, industrial information, and sister project experiments, it has been determined that the objective of any model should be to achieve the appropriate grade product with the minimum expenditure of energy, hence the key dependent variables should be as follows:

- Throughput
- Particle Size distribution (product)
- Energy consumption

Wherever possible any model should be driven towards the output of these

3. Had there been time remaining in the project, additional application to industrial milling could have focused on the areas of:

- Mill differential pressure
- Primary air temperature

The dependent variables that should be used to drive the models, in order of importance as drawn out of the literature, are:

1. Operational Speed
2. Feed rate
3. Screen aperture size (or classification parameters)
4. Particle size distribution (Feed)
5. Residence time (where applicable, mainly in used for lab-scale in certain mills)
6. Moisture content
7. Grindability (as determined by certain grindability indices)
8. Primary Air inlet flow rate

3.2 Evaluation Framework

To compare different modelling techniques a method of evaluation has been determined that covers the key aspects of the project. This accounts for the needs of the industrial partners, the budgetary constraints, and the methods by which the modelling can be implemented and validated. The following section provides a commentary on the key aspects and how each modelling technique is scored under this evaluation program. Points allocation for the different areas of the scorecard along with a description of criteria for the awarding of points is given in appendix D.

3.2.1 Modelling Score Card Areas

Ability to Model the Scenario

This section is to assess the capability of the modelling technique to provide solutions to the key variables as identified in section 3.1.4. The score is based on the following:

1. How well the technique can model the key variables of the project:
 - a. Particle size distribution
 - b. Energy consumption
 - c. Mill throughput
 - d. Pressure differentials across the mill (industrial simulations)
 - e. Air temperature differential (industrial simulations)
2. The capability to model secondary features of milling; table 3.6 displays the secondary variables of interest in a simulation of milling.

Table 3.6 displays the secondary variables of interest to the research but not primary to the objectives of the project.

<i>Category</i>	<i>Feature</i>
<u>Physical environment</u> Creation of the milling environment and its evolution as milling takes place	Mill Geometry
	Grinding media geometry
	Temperature (gas)
	Pressure (gas)
<u>Motion</u> As applied to the fuel, grinding media and air flow within the mill. The objective of which is to assess where and how comminution takes place.	Mill Geometry
	Grinding media geometry
	Temperature (gas)
	Pressure (gas)
	Velocity
	Translation
	Rotation
	Contact forces (boundaries)
	Contact forces (inter-particle)
	Contact forces (grinding media)
	Entrance
Exit	
<u>Particle Properties</u> The evolution of the particles whilst in the milling circuit	Temperature (solids)
	Stresses
	Particle Geometry
	Fracture/breakage (single particle)
	Fracture/breakage (multi-particle)

Computational Requirements

It is necessary to evaluate the technique in relation to the ease of implementation at the end user. Information for the likely run times and computational resources is required to appropriately evaluate implementation of the simulation. To this end the following assessments are made:

1. What computational resources, beyond those of a standard desktop computer, are required to run the simulation based on the modelling technique under evaluation?
 - a. The optimal scenario is a standard desktop computer
 - b. Other considered cases are a high specification desktop computer or a something more powerful, e.g. high-performance cluster (HPC) of which one is available at the University of Nottingham.
2. How long is the simulation expected to last?
 - a. The optimum case on agreement with the industrial partner is no longer than 7 hours for suitability for their use. Anything longer than this can be considered but scored lower.

Software Availability

If suitable software packages are not available through the university, 2 options remain as to how to implement the modelling technique. These would be either to purchase appropriate software packages, incurring a cost against the research budget, or code the software directly; the latter of which increases the time required to develop the program. To this end, for this category the technique is scored on the following:

1. Is software that is capable of facilitating the elements of the simulation available?
 - a. Ideally the software should at least be able to fulfil modelling using the key variables, hopefully including some of the secondary.
2. If a cost is required to obtain the software, how much will it be?

- a. Budget concerns are on whether or not the university currently has any licenses available for the use of the software identified. If so whether a contribution to the licencing would be required from the project budget.
- b. If a license is not available from the University, the price would also dictate whether it could be purchased for use in the project.

Dependency on Data

As discussed in chapter 1.3, to take mills and boilers off-line to set up for experimental tests of new fuels and operating conditions is not a preferred option to a generator due to the cost implications of doing so; increased time in cleaning out mills and searching for optimal settings results in a loss of output and eventually income. The value of the simulation increases if a scheme can predict a mill behaviour based on training with a small data set. Therefore, the modelling technique will also be subject to evaluation for:

1. The reliance on experimental investigation to provide the foundations of a simulation.
2. Whether the simulation can predict sufficiently when based on physical principles that may relieve the need for experimental data.

Ease of Validation

Once a simulation has been created, the necessary step will be to validate the output. It is required that this be completed either using analytical solutions or for through experimental data. Therefore, analysis of the implemented technique requires sufficient and suitable data on which validation can take place, hence a technique will also be evaluated on:

1. Whether the data is suitable to validate the variables for which the technique is utilised for.
 - a. Scores in the evaluation are weighted to the primary variables of interest as opposed to the secondary.
2. If not, how much additional experimental work would be required to collect the required data?

- a. This would also include evaluation as to the complexity of the experimentation should it take place.

Adaptability to Industrial Scale

As the research is focused on answering a question posed by industrial partners the development of a simulation should be concerned with how it can be applied to industrial practices after development on laboratory condition simulations. As previously mentioned laboratory grinding can have significant differences from industrial milling beyond simply the scale of the operation. Techniques are therefore also evaluated on:

1. If it is applicable for the industrial scale milling variables.
2. What is the expected workload required in implementing a scale up simulation?

3.3 Modelling Techniques

From the literature search (chapter 2.11), table 3.7 lists the techniques that have been identified as potential candidates for the project due to varying capabilities to model the facets of milling. This section provides a review of each technique. Using the framework outlined in 3.2 each of the techniques has been evaluated and presented with a score. The techniques have been grouped 2 categories, stochastic and numeric to differentiate the fundamental basis; driven by experimental testing and results and based on physical principles respectively.

In addition to the techniques evaluated individually, some have also been assessed as a hybrid system. Used in such ways, the strengths of one technique aims to offset the limitations of another to create a better system. Potential hybrid systems are also listed in table 3.7.

Table 3.7 displays the modelling techniques that are considered for use under the research project.

Method Type	Method
Stochastic	Artificial Neural Networks (ANN)
	Population Balance Methods (PBE)
Numerical	Discrete Element Methods (DEM)
	Finite Element Methods (FEM)
	Finite Volume Methods (FVM)
	Particle Finite Element Methods (PFEM)
	Smoothed Particle Hydrodynamics (SPH)
Hybrid	PBE-DEM
	FEM-DEM (where FEM analysis is on each discrete element)
	DEM-FEM (where FEM analysis is on structures because of contact with discrete elements)
	DEM-FVM
	DEM-SPH
	SPH-FEM

3.3.1 Artificial Neural Networks

General Theory

ANN is based on the summation of weighted inputs to a system, being applied to an activation function to generate an output as in figure 3.5 and stated in equation 3.1. On occasion a bias is added to the output prior to summation and conveyance through the activation function. Activation functions themselves regulate the output to a range [0, 1].

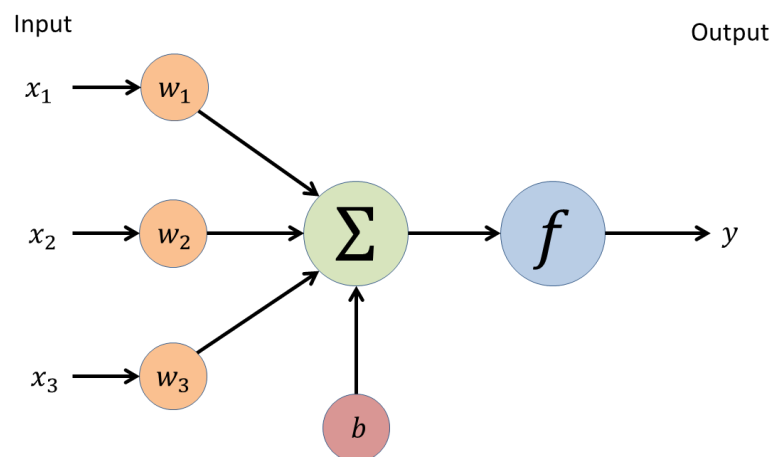


Figure 3.5 displays the concept of an Artificial Neural Networks neuron complete with inputs, weights, bias, summation, activation function and output.

$$y = f\left(\sum_i x_i w_i + b_i\right) \quad (3.1)$$

Layers of neurons (sometimes known as perceptrons, see figure 3.6) add further manipulation to the model that help to refine the accuracy of the model; each layer has additional weights. Model evaluation via techniques such as Least Mean Squared (LMS) is completed and tolerances in errors determine the application of optimisation routines like Steepest Descent gradient search algorithms (Graupe, 2007).

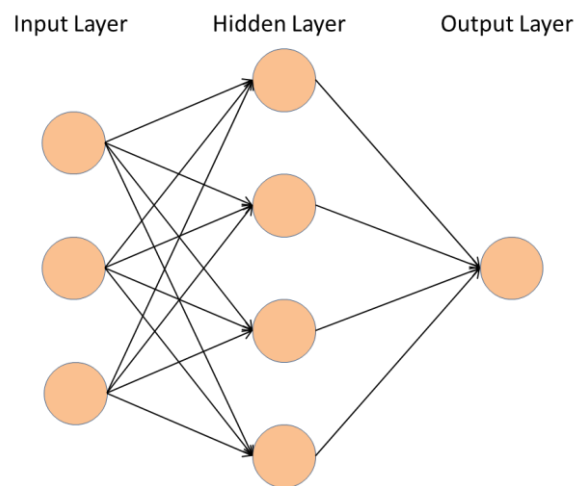


Figure 3.6 displays the architecture of artificial neural networks inclusive of input, hidden and output layers.

Key Advantages as Applied to Biomass Milling

- The application of ANN with milling is high and has the ability to work with every independent variable and produce response output again for every dependent variable as can be seen in literature using ANN with mill circuits (Ahmadzadeh & Lundberg, 2013; Miguel Gil et al., 2013; Pani & Mohanta, 2013; Shuiping et al., 2002; V. Singh, Banerjee, Tripathy, Saxena, & Venugopal, 2013; H. Wang et al., 2010).

- There are many methods, strategies and algorithms for solution of ANN's, therefore accuracy could be improved if the problem requires a more compatible technique (Miguel Gil et al., 2013; Graupe, 2007; H. Wang et al., 2010).
- Processing times for ANN's are short and does not required large computational resources. Furthermore, the implementation can be achieved through software packages like MatLabTM's Neural Network Toolbox or through PyPR, a free Python based pattern recognition program.

Key Disadvantages as Applied to Biomass Milling

- Optimisation of the functions that are designed to help train the ANN have the potential to optimise to local minima values that cause error in the results.
- ANN requires a substantial amount of experimental data on which to train a good performing model; furthermore, data needs to be widely distributed to cover the range of variable values to be accurate in the extremes of the ranges.
- Too many layers in the ANN can result in overtraining. The network learns the patterns of the data set; this results in a lack of generality due to a model developed so precisely for the training data, that when presented with a blind test, would fail (Gardner & Dorling, 1998).

Scorecard Assessment Conclusions

Using the assessment method as outlined in section 3.2 with the comments already made the following scorecard has been produced and scores allocated for the ANN method. Further justification for the scores attributed to the method are as follows:

1. Validation of the simulation is easily achieved with blind test data however inference of secondary variables of interest may not be possible due to the simulation being highly dependent on the training data which may not be available in some cases.
2. Upscaling and simulation changes will require significant changes and potentially redesign with each new application, whether that be mill, fuel or scale.

Table 3.8 displays the scorecard for the Artificial Neural Network method.

<i>Ranking Category</i>	<i>Score</i>
Modelling the Scenario	3
Computational Requirements	5
Software and Coding	5
Data dependency	1
Model validation	3
Industrial scale-up	3

3.3.2 Population Balance Equation Method

General Theory

The PBE technique is built on a foundation of conservation. These quantities generally are for mass and volume where milling practices are employed. The breakage (specifically) PBE equation can be seen in 3.2; this describes the rate of change of a distribution ($f(x)$). The first term on the right hand side of equation 3.2 describes the death rate of the quantity out of size x , whilst the second describes the birth rate of size x from all greater sizes, y .

$$\frac{df(x, t)}{dt} = -s(x)f(x, t) + \int_x^\infty b(x, y)s(y)f(y, t)dy \quad (3.2)$$

The birth and death rates are governed by a selection function, $s(x)$, that describes the probability of breakage in any given time interval and a breakage function, $b(x)$, that describes the distribution of the progeny from a quantity y .

Key Advantages as Applied to Biomass Milling

- There many different methods of solution of the partial and ordinary differential equation forms of the PBE that have different degrees of accuracy dependent on the application (Mantzaris, Daoutidis, & Srienc, 2001a; Mantzaris et al., 2001b; Mantzaris, Daoutidis, & Srienc, 2001c; Daniele L Marchisio & Fox, 2005; Daniele L. Marchisio, Vigil, & Fox, 2003; Nicmanis & Hounslow, 1996, 1998; Ramkrishna, 2000).
- For particle assemblies, the PBE's can be discretised conveniently into a set of n coupled ODE's governing each particle size class (Herbst & Fuerstenau, 1980); this is analogous of standard mass oversize sieve analysis that is used in the measure particle assemblies.
- Computational times for simulations, subject to the method employed to find the solution, is below the defined requirement in section 3.2 (Klimpel & Austin, 1977).
- Whilst there are software packages that can provide a base for a PBE simulation, such as ANSYS® Fluent's PBE module, development of self-developed code would be straightforward in any programming language.

Key Disadvantages as Applied to Biomass Milling

- Use of PBE's in literature has often relied on optimisation of the selection and breakage functions against experimental data which optimises based on the fuel, mill type and mill operating parameters. Thus, limiting the use of a simulation to a specific application; advances in material characterisation experiments are attempting to mitigate this (Miguel Gil, Luciano, & Arauzo, 2015a; Koka & Trass, 1987).

- Computational resource requirement and time is proportional to the discretisation of the spatial domain and seeking a more accurate solution on high resolution grids could lead to increases.
- PBE's whilst applicable to many aspects of milling, PSDs, air flow, mass transport, etc. the output is of an empirical nature and will not provide information on fundamental concepts of grinding.

Scorecard Assessment Conclusions

In conjunction with the assessment of the technique made above the justification for the scorecard results are:

1. It is expected that the scale up for industrial purposes will be based on volume, mass throughput etc. increases and the technique should be equally applicable and require only minor amendments to the simulation.
2. Software is available through the university at a small license contribution cost however program development is applicable as well.
3. Validation of all the primary variables of concern is possible; PSDs and mass throughput are inherent in the method, energy consumption has been linked with PBE in literature (Gao, Forsberg, & Weller, 1996; Otwinowski, 2006; Stamboliadis, 2007). Coupled PBEs also have the potential to model the airflow and pressures throughout a mill, based on previous applications to fluid dynamics (Daniele L Marchisio & Fox, 2005; Daniele L. Marchisio et al., 2003).

Table 3.9 displays the scorecard results for PBE methods.

Ranking Category	Score
Modelling the Scenario	3
Computational Requirements	5
Software and Coding	4
Data dependency	2
Model validation	4
Industrial scale-up	4

3.3.3 Discrete Element Method

General Theory

Developed by Cundall and Strack (Cundall & Strack, 1979), DEM is a numerical method for determining the behaviour of granular assemblies using algorithms based on Newton's second law of motion (Mishra & Rajamani, 1992). Each body is subject to finite rotations and displacements as governed by the equations:

$$m_i \frac{d\mathbf{v}_i}{dt} = \sum_{j=1}^{k_i} (\mathbf{f}_{c,ij} + \mathbf{f}_{d,ij}) + m_i \mathbf{g} \quad (3.3)$$

And:

$$I_i \frac{d\boldsymbol{\omega}_i}{dt} = \sum_{j=1}^{k_i} (\mathbf{M}_{t,ij} + \mathbf{M}_{n,ij} + \mathbf{M}_{r,ij}) \quad (3.4)$$

Table 3.10 displays the nomenclature for equations 3.3 and 3.4.

Description of Variable	Key
The mass of particle \mathbf{i}	m_i
The moment of inertia for particle \mathbf{i}	I_i
Translational velocity of particle \mathbf{i}	\mathbf{v}_i
Rotational velocity of particle \mathbf{i}	$\boldsymbol{\omega}_i$
Gravitational force of particle \mathbf{i}	$m_i \mathbf{g}$
Number of particles interacting with a particle \mathbf{i}	k_i
Elastic force between particles \mathbf{i} and \mathbf{j}	$\mathbf{f}_{c,ij}$
Viscous damping force between particles \mathbf{i} and \mathbf{j}	$\mathbf{f}_{d,ij}$
Tangential torque acting on \mathbf{i} by \mathbf{j}	$\mathbf{M}_{t,ij}$
Normal force when the normal does not pass through the particle centre	$\mathbf{M}_{n,ij}$
Torque as a result of rolling friction between particles \mathbf{i} and \mathbf{j}	$\mathbf{M}_{r,ij}$

Movement of the elements results in the need to resolve collisions between elements and boundaries of the domain. The two steps to achieve this requires contact detection and collision resolution algorithms. Once resolved the vector forces and particle movement can then be applied before the next pass through the process.

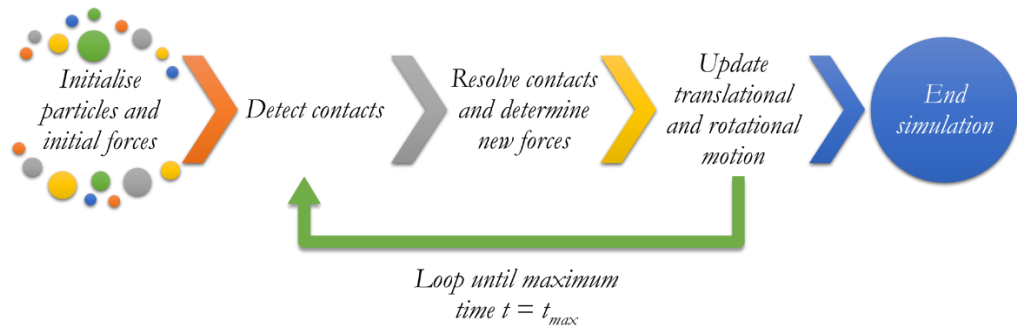


Figure 3.7 displays the process flow algorithm of DEM.

In the interests of modelling grinding processes various strategies have been employed to model the physical phenomenon. Two such approaches are shown in figure 3.8, a particle package and replacement method (Delaney et al., 2010), and particle bonded method (Abe & Mair, 2005).

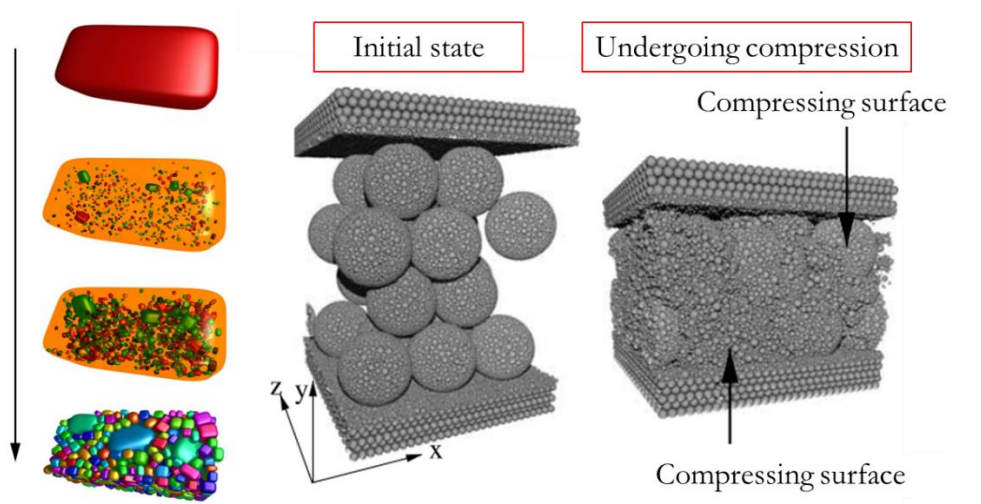


Figure 3.8 displays the 2 stated methods of breakage modelling in DEM, particle packing and replacement (left), and the bonded particle method (right).

Key Advantages as Applied to Biomass Milling

- DEM has the capability to produce results for many of the variables of interest, particle size, mass throughput; the exceptions to which are the system and gas phase physical properties (da Cunha, de Carvalho, & Tavares, 2013; Iwasaki et al., 2010; Lee et al., 2010; Naik et al., 2013; Rosenkranz, Breitung-Faes, & Kwade, 2011; A. Sato, Kano, & Saito, 2010); this increases the usefulness to develop understanding as to the fundamental physics of grinding processes.
- Due to the physical modelling nature many of the independent variables can be directly modelled (Alizadeh, Bertrand, & Chaouki, 2014; da Cunha et al., 2013; Iwasaki et al., 2010; Lee et al., 2010; S. D. Liu, Zhou, Zou, Pinson, & Yu, 2014; Mishra, 2003; Naik et al., 2013; Rosenkranz et al., 2011; A. Sato et al., 2010; J. Wang et al., 2011).
- Domain geometry can be constructed with elements from the DEM regime set with defined laws (Naik et al., 2013). Alternatively many software packages have the ability to import directly from computer aided design (CAD) software files or devised within the software itself, e.g. PFC v5 (Itasca Consulting Group, 2017).
- Numerous strategies are available to improve contact detection; common plane, fast common plane, neighbour search and more (Dawei, Erfan, Youssef, & Jamshid, 2006; G Nezami, MA Hashash, Zhao, & Ghaboussi, 2006; S. D. Liu et al., 2014; Nezami, Hashash, Zhao, & Ghaboussi, 2004; Tijskens, Ramon, & Baerdemaeker, 2003). Additionally multiple techniques for collision resolution are available (da Cunha et al., 2013; Dabeet, Wijewickreme, & Byrne, 2014) all of which can be trialled to achieve accuracy and improve computational time.

Key Disadvantages as Applied to Biomass Milling

- Modelling non-spherical shapes in DEM increases complexity of contact detection, collision resolution and rotational translation algorithms that all contribute to increased processing time (Favier, Abbaspour-Fard, Kremmer, & Raji, 1999).
- Whilst various strategies have been implemented to decrease processing time, e.g. reduced order modelling (Boukouvala, Gao, Muzzio, & Ierapetritou, 2013) and GPU execution (Ono, Nakashima, Shimizu, Miyasaka, & Ohdoi, 2013), execution time can be far beyond the modelled time (H. Li, McDowell, & Lowndes, 2014; Ono et al., 2013).

Scorecard Assessment Conclusions

Further to the advantages and disadvantages listed earlier in the chapter, the following statements about DEM should be made:

1. There are several DEM software packages available, such as EDEM™ (EDEM Simulation, 2017) and PFC (Itasca Consulting Group, 2017). The cost for academic licenses is approximately £6k to £12k depending on the type of license available.
2. Upscaling to industrial size milling simulations would most likely be unfeasible given the time taken for simulations to run completely however small subsections could be modelled as a snapshot of what is happening in a full-scale mill.
3. Most methods of validation for DEM simulations are replicating the circumstances with observational experiments (Fraige, Langston, & Chen, 2008; Höhner, Wirtz, & Scherer, 2014). Due to the volatility in grinding the ability to directly observe the experiments is unlikely and validation would be by inference from the output particle size distributions.

Table 3.11 displays the scorecard results for DEM.

Ranking Category	Score
Modelling the Scenario	4
Computational Requirements	2
Software and Coding	2
Data dependency	3
Model validation	4
Industrial scale-up	2

3.3.4 Finite Element Method

General Theory

The finite element method uses the variational (or weak) form of a partial differential equation to solve boundary value problem over a finite domain (Ω). The transformation is a consequence of applying Green's Theorem and application of boundary conditions for the problem. Equation 3.5 shows the variational form of a reaction diffusion equation. Ω is discretised into elements consisting of nodes and edges of various geometries (see figure x.9), defined on a functional space, $H^1(\Omega)$.

$$\int_{\Omega} \nabla u \cdot \nabla v + c \int_{\Omega} uv = \int_{\Omega} fv + \int_{\Gamma_N} g_1 v, \quad \forall v \in H_{\Gamma_D}^1(\Omega) \quad (3.5)$$

To determine the scalar functions, u , at each node of the elements a simple weighting function, v , is trialled to approximate the complex function of the actual solution. Boundary values, Γ , provide the conditions at the boundaries of the domain; various types of boundaries exist in numerical analysis of which Neumann, N , and Dirichlet, D , are represented in equation 3.5. These specify the derivative of the solution on the boundary and the value on the boundary itself respectively.

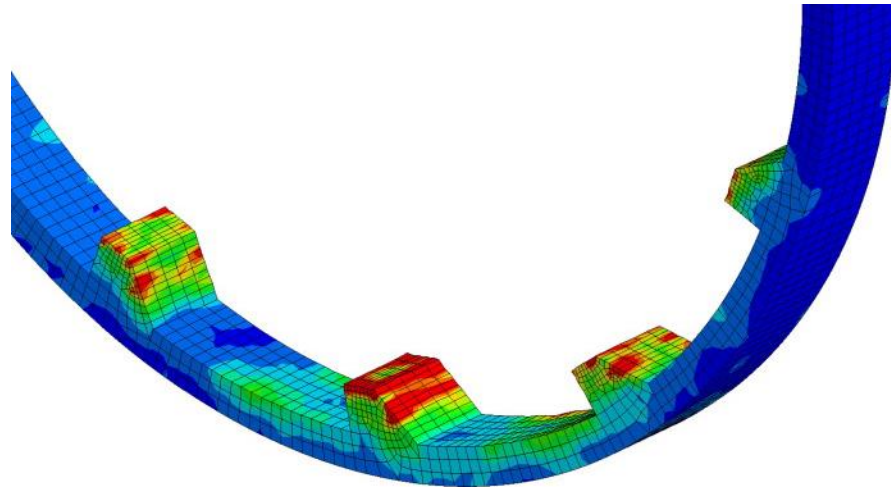


Figure 3.9 displays how domains are discretised in finite element simulations, here the stresses on a tumbling ball and tube type mill liner are simulated (Jonsén, Pålsson, & Häggblad, 2012).

Key Advantages as Applied to Biomass Milling

- Finite element modelling could provide insight into many secondary variables of interest in milling; these include the air flow and pressures in the mills (F. Liu et al., 2015), stresses on mill components and material (Khennane, Khelifa, Bleron, & Viguier, 2014; Munjiza & John, 2002; Özcan et al., 2009; Rousseau, Frangin, Marin, & Daudeville, 2009; Zhou, Liu, Tang, Cao, & Chi, 2014) and wear on mill components (Forsström, Lindbäck, & Jonsén, 2014; Jonsén¹ et al., 2014; Jonsén et al., 2012; Jonsén, Pålsson, Stener, & Häggblad, 2014; Jonsén et al., 2011; Jonsén, Stener, Pålsson, & Häggblad, 2015; Zhou et al., 2014).
- Complex geometries can be easily defined as well as different material conditions (Khennane et al., 2014), so flexibility in the simulations is possible.
- As a numerical approach the accuracy in the simulation can be increased by refined grids and multigrid techniques. (Ralston & Rabinowitz, 2001).
- There are many different software packages available for FEM and FEA (finite element analysis) available through the university such

as COMSOL Multiphysics®, ANSYS® Structural, SIMULIA Abaqus, and open source packages like KRATOS Multiphysics.

Key Disadvantages as Applied to Biomass Milling

- FEM is highly developed for structural analysis problems and is widely used for such purposes. However for the problems of fracture and crack propagation it can be cumbersome (Dolbow & Belytschko, 1999). This is due to the necessity to re-mesh the domain following a crack or fracture.
- As FEM is a Eulerian numerical method it solves PDE's in the continuous phase space, hence the method, whilst good for modelling the stress and fracture of objects, each object is its own self-contained domain, for grinding processes application to each particle would be impractical and the technique does not model one of the primary variables of concern, the PSD or energy consumption in grinding.

Scorecard Assessment Conclusions

Justification for the scores in the assessment of FEM, alongside those already discussed are:

1. Computational requirements are high in FEM and proportional to the resolution in the grid, however some of the software available is able to run on the university HPC and optimised for local parallel execution on a high specification machine.
2. Validation of simulations, which would be for secondary variables since FEM is not of use for primary, would be based on collecting much more experimental data that has not formed the basis of much of the experimental work collected by the sister project.

3. Scaling up simulations for industrial application would require complete overhaul of geometries for industrial scale mills; this task could prove to be difficult to adequately represent and validate. Additionally, this would be time consuming to branch out to more than one type of mill.

Table 3.12 displays the scorecard for the FEM.

<i>Ranking Category</i>	<i>Score</i>
Modelling the Scenario	2
Computational Requirements	3
Software and Coding	3
Data dependency	3
Model validation	1
Industrial scale-up	2

3.3.5 Finite Volume Method

General Theory

The finite volume method is often used for the basis of computational fluid dynamics modelling and again uses the weak integral form of partial differential equations on which to formulate a discrete representation of the domain for a problem. Again, these discretisations are represented by polyhedral elements (called cells), in many problems. Where as in FEM the line segments of the polyhedral discretisation are the target of the solutions, in FVM the volume contained within the cell is the focus of the solution. Three approximations are made for the discretisations:

- An approximation of the function $u \approx u_h$.
- An approximation for the domain $\Omega \approx \{b_i \in \mathcal{B}, i = 1: M\}$ where M is the number of cells of the domain and b_i is a volume element.
- An approximation for the flux through a boundary of a cell, ∂b_i , in the normal direction, \mathbf{n} , from the boundary

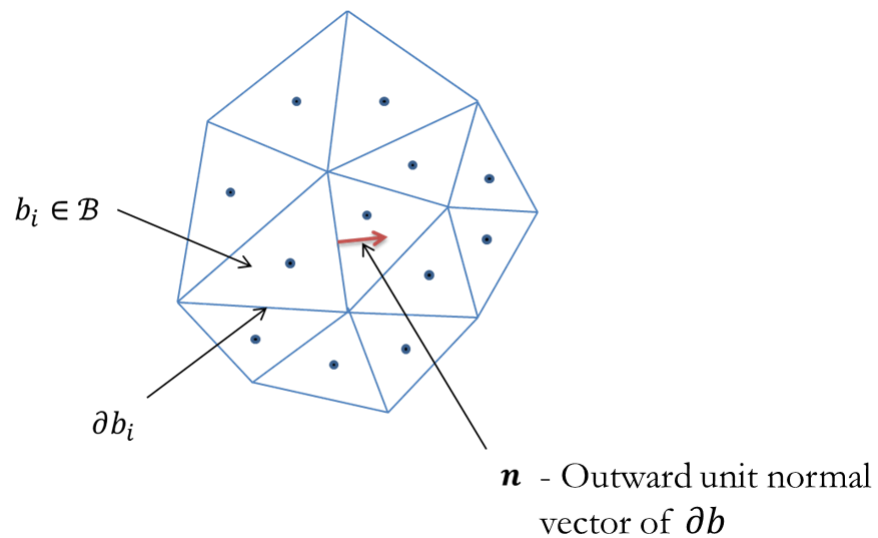


Figure 3.10 displays the concept of the finite volume method.

Key Advantages as Applied to Biomass Milling

- As with FEM, pressure, gas, temperature, and fluids can be modelled in mills with FVM (Blecher, Kwade, & Schwedes, 1996; Graeme, 1999a; Liying & Chundong, 2011; Takeuchi, Nakamura, Iwasaki, & Watano, 2012).
- Complex geometries can be modelled adequately with the suitable discretisation of the domain. Accuracy of the simulation can be increased with changes in number of control volumes and shapes of the volumes (Maire & Breil, 2012; Takeuchi et al., 2012).
- Again, there is a mature and robust selection of software available for the implementation of FVM, some available through the university and some externally, e.g. MatLab™ PDE Toolbox, ANSYS® Fluent and KRATOS Multiphysics.

Key Disadvantages as Applied to Biomass Milling

- As with FVM the scope of the main variables of interest are not represented well by FVM and implementation of the scheme would

be on the continuous phase variables (air flow, pressure, heat transport) only.

- Implementing FVM for secondary variables again has the complexity that for a mill, the geometry can be very complex that would require refined grid, hence increasing processing time.

Scorecard Assessment Conclusions

As detailed above and with the same justifications for the scores as in section 3.3.4 for the FEM method, the following scores are awarded.

Table 3.13 displays the scorecard for FVM.

<i>Ranking Category</i>	<i>Score</i>
Modelling the Scenario	2
Computational Requirements	3
Software and Coding	3
Data dependency	3
Model validation	2
Industrial scale-up	3

3.3.6 Particle Finite Element Method

General Theory

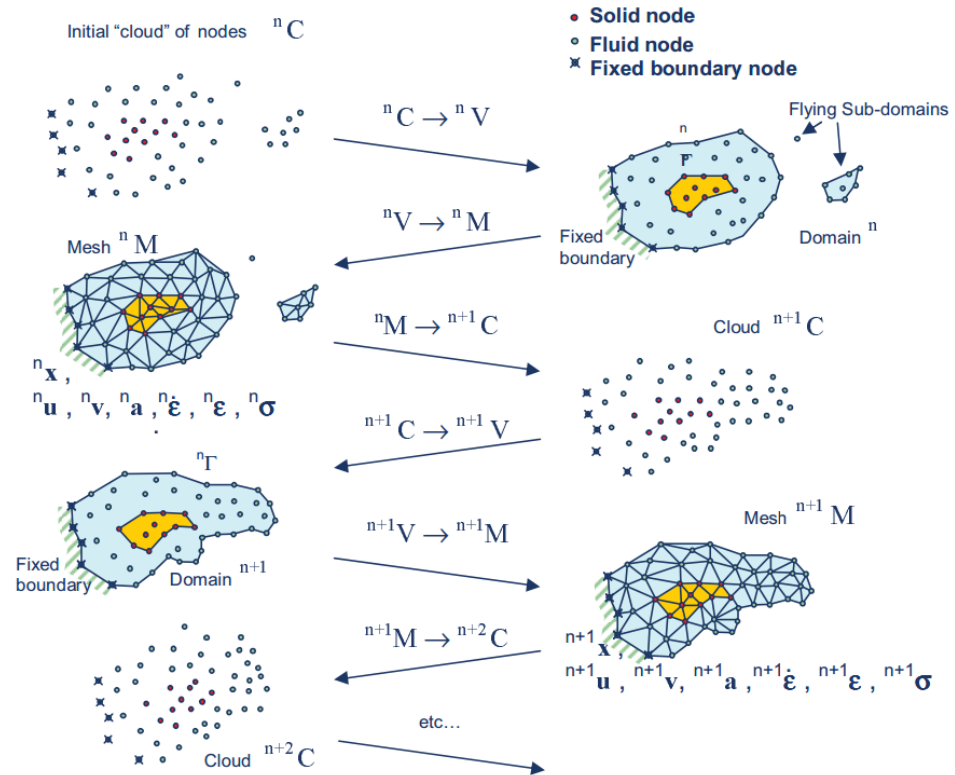


Figure 3.11 displays a representation as how PFEM works, detailing the meshing, solution, and updating of nodal position in the process (E. Oñate et al., 2011).

PFEM uses a set of particles to represent an assembly, at each time step the particles act as nodes in a finite element grid and it solves the domain using FEM. As figure 3.11 suggests after the finite element solution in that time step has been solved the particle points are adjusted based on the physics of the system and translated accordingly. The mesh for the finite element solution is then recreated. This provides a key advantage over a normal FEM simulation, as the domain for solution can change shape, and/or split into 2 or more separate domains for solution (Carey, Mason, Barbosa, & Scott, 2014; Kakuda, Hayashi, & Toyotani, 2014; Zhu, 2014; Zhu & Scott, 2014). Additionally, non-linear problems can be solved with a large time step and still obtain stable accurate and fast solutions (Idelsohn, Marti, Becker, & Oñate, 2014).

Key Advantages as Applied to Biomass Milling

- Using multi-phase flow abilities of PFEM various aspects of milling can be modelling concurrently, such as the air flow, pressure and temperature changes as well as the bulk flow of particles in the mill (Cante et al., 2014).
- There are a few software packages on offer for the technique, Marc by MSC Software, an advanced nonlinear simulation solution and Kratos Multiphysics.

Key Disadvantages as Applied to Biomass Milling

- Elements of milling such as fracture and grinding of a particulate assembly would not be possible as PFEM still operates with an Eulerian continuum numerical method for the solution, and would be more applicable to the bulk flow within a mill (Cante et al., 2014). This limits the simulation to only 1 of the key variables of interest despite the ability to model a few of the secondary variables.
- Due to the need to update and translate each particle at each time step the computational requirements becomes more expensive in general than for a FEM simulation.

Scorecard Assessment Conclusions

In conjunction with the advantages and disadvantages given for PFEM the following statements also contribute to the final scores for the technique:

1. Computational requirements could be considerable, subject to how refined a mesh might be and how many particles would be required to adequately represent the system.
2. Validation of the modelling may not be possible on the bulk flow in some milling systems due to batch processing requirements and

closed systems. On mills where throughput is measurable this would be possible but may require additional monitoring systems.

3. Upscaling to industrial processes would be based on a scaling of geometry to compensate for the size of mills in industry. The numerical technique may require additional nodes and grid refinement that would increase computational time.

Table 3.14 displays the scorecard for PFEM.

<i>Ranking Category</i>	<i>Score</i>
Modelling the Scenario	2
Computational Requirements	2
Software and Coding	2
Data dependency	3
Model validation	1
Industrial scale-up	1

3.3.7 Smoothed Particle Hydrodynamics Method

General Theory

SPH is a method that has an association with finite elements whereby a scalar function $F(\mathbf{r})$ is smoothly interpolated with the function, $W(\mathbf{r}, h)$, where \mathbf{r} is a positional vector and h a characteristic width of the system. Through this interpolation, the system can be represented by the average value of the neighbouring particles and is described in its discrete form by equation 3.6, s represents the smoothed interpolant function. A representation of the scheme is given in figure 3.12.

$$F_s(\mathbf{r}) \simeq \sum_j \frac{m_j}{\rho_j} F_j W(\mathbf{r} - \mathbf{r}_j, h) \quad (3.6)$$

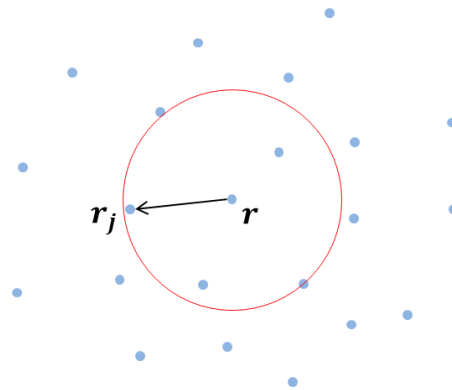


Figure 3.12 displays a representation of the smoothed particle hydrodynamics method.

Key Advantages as Applied to Biomass Milling

- Again the technique has been and can be applied to many aspects of milling, such as the fluid phases, air flow, pressures, heat transfer; in addition to that, breakage has also been modelled in SPH (Paul W. Cleary, 2015; Das & Cleary, 2010; Deng, Liu, Wang, Ge, & Li, 2013; Ganzenmüller, 2015; Harrison, Cleary, Eyres, Sinnott, & Lundin, 2014; Simon M. Harrison et al., 2014; Jonsén et al., 2012; Jonsén et al., 2015; Pramanik & Deb, 2015; Schörghenhuber, Gruber, & Gerstmayr, 2013; Zhou et al., 2014).
- A few mature software packages are available commercially, ANSYS® Fluent, and LS-Dyna both available at cost.
- Whilst unable to simulate the geometries with the method itself, the software packages have the ability to import and use CAD generated boundaries of the control domain and hence replicate the milling environments.

Key Disadvantages as Applied to Biomass Milling

- The operational conditions under which SPH has to be constrained can have considerable effect on the accuracy of the simulation, such as the smoothing length to particle spacing ratio and if the particles have an uneven distribution (Deng et al., 2013).

- To adequately model the scenario of comminution in a simulation, as in other works that considers similar mechanisms (Simon M. Harrison et al., 2014), many particles would be necessary for each and every biomass pellet, hence the computational time for increased particles could be extensive (Schörghener et al., 2013). This would be further exacerbated by upscaling to industrial simulations.

Scorecard Assessment Conclusions

Additional justification for the conclusions of the scorecard include the following:

1. It is expected that significant computational resources would be required for SPH, however restriction on the use of HPC's in the software could prohibit use to just a single high specification computer.
2. Again, model validation for SPH would be based on post milling study of the PSD and throughput. Energy calculations, like with DEM can be collected and compared to energy consumption.

Table 3.15 displays the scorecard for SPH.

<i>Ranking Category</i>	<i>Score</i>
Modelling the Scenario	2
Computational Requirements	2
Software and Coding	2
Data dependency	3
Model validation	1
Industrial scale-up	1

3.3.8 Hybrid Modelling Techniques in Literature

The list of hybrid models in relation to milling are extensive and summarised in table 3.16. The general strategy of coupling techniques is to alleviate the challenges of the computationally heavier technique. The combined score for each hybrid system is evaluated in appendix F.

Table 3.16 displays examples in literature of hybrid modelling techniques.

<i>Purpose of technique coupling</i>	<i>Reference</i>
Micro DEM simulations are used to determine the selection and breakage parameter values for a PBE simulation.	(M. Capece et al., 2014; M. Capece, E. Bilgili, & R. N. Davé, 2014; M. Capece, Davé, & Bilgili, 2015)
Even smaller DEM simulations are used, and an ANN technique is used to learn the appropriate parameters for selection and breakage functions of PBE.	(Barrasso, Tamrakar, & Ramachandran, 2014)
FEM is used to examine the stresses on the individual DEM particles in a simulation.	(Munjiza & John, 2002; E. Oñate & Rojek, 2004)
DEM particles are used and when impacting a containment vessel, the stresses on the vessel are evaluated.	(Forsström et al., 2014; Jonsén ¹ et al., 2014; Jonsén et al., 2012; Jonsén et al., 2014; Jonsén et al., 2011; Jonsén et al., 2015)
DEM is used to model the particle flow and FVM is used to model the fluid phase of the simulations.	(Schmidt & Nikrityuk, 2011; Takeuchi et al., 2012).
SPH is used to simulation fluid phases in wet milling and coupled with DEM for the solid phases.	(Paul W. Cleary, 2015; Jonsén et al., 2014; Jonsén et al., 2015)
DEM is used to model the rock fragments and SPH is used to model a pressurised gas injected into the rock to facilitate explosion.	(Fakhimi & Lanari, 2014)

3.4 Model Ranking Results

Following the implementation of the modelling technique evaluation and ranking, the following course of action has been taken:

- Implementation of a PBE simulation to provide quick answers to industrial partner questions regarding the performance of biomass fuels in mills.
- Implementation of DEM with a view for coupling the technique with PBE to overcome computational requirements for a full DEM simulation whilst still allowing study into the fundamentals of grinding using DEM.

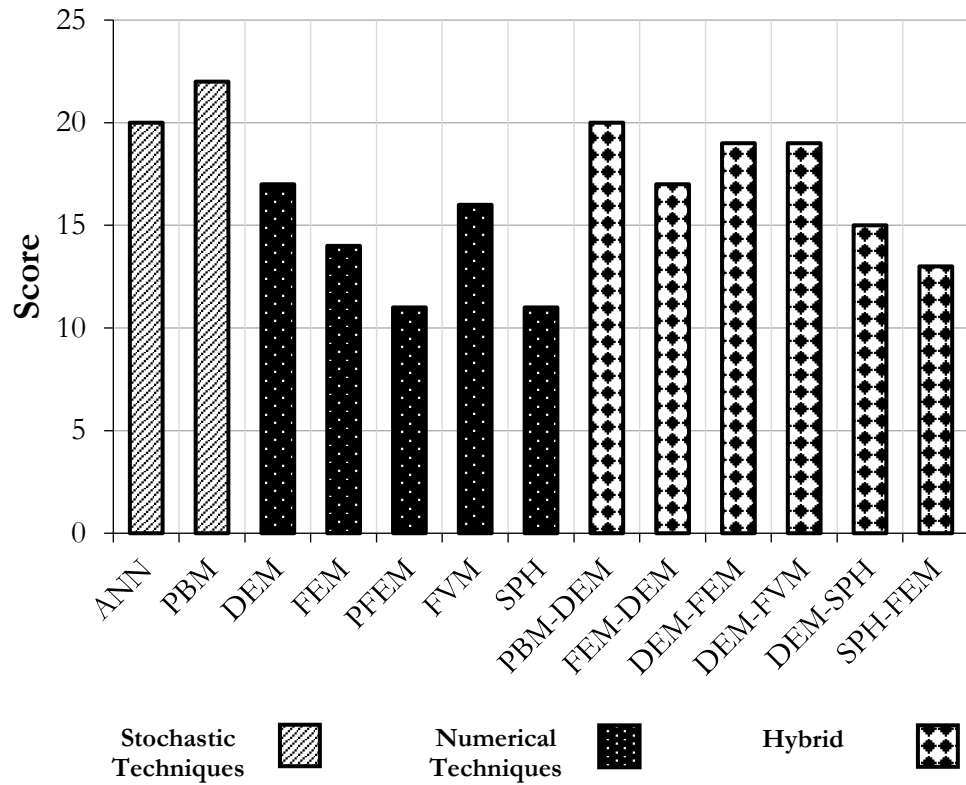


Figure 3.13 displays the final total scores from the model technique evaluation process.

Based on the scores in figure 3.13 a few comments can be made about the different techniques; for a graphical presentation of the results in all areas please see appendix E – Model Ranking Scores.

Scores for the techniques of ANN and PBE are high in comparison to the other techniques. The ability of the two techniques in modelling the scenario coupled with the minimal computational requirements and processing times makes both techniques competitive. PBE scores higher in that to decouple the need for extensive milling experiments, progress has been made which means there would be an expected lower dependency on data to formulate the simulation.

For the numerical simulation techniques, whilst all are reduced in the category of computational requirements, all can simulate different aspects of the milling process. Except for DEM, none model the key variables of interest completely; hence why DEM was selected. Additionally, model validation is difficult as the mills are not viewable from the inside, many implementations would require additional experimentation other than those considered under the sister project.

Hybrid models are ranked high in modelling the scenario category and marginally higher in computational requirements. As discussed previously this is based on the ability to model some other aspect of the milling process or speed up the execution of a simulation in general. The strongest contender is the PBE-DEM hybrid as it still encapsulates all the variables of interest and helps develop understanding of the fundamentals whilst offsetting the main detractor from DEM somewhat. Therefore, long term goals for the project should be to develop a PBE-DEM linked simulation.

Chapter 4 - The Population Balance Equation Method

4.1 General Theory

4.1.1 Background

The population balance method is focused on describing the evolution of particulate systems. As in general particulate systems contain significant numbers of particles, it is often more convenient to simulate the behaviour of the population rather than the individual.

In the scope of applications of PBE systems, the evolution of the population's characteristics can focus on a broad range of properties. The framework of the PBE method properties of the particulate system can focus on the external location of particles in a domain, as well as the 'internal' state; the latter can be any properties that can be quantified (S. Kumar & Ramkrishna, 1996a). In the context of the project the primary focus is associated with the internal state of the particles.

The internal state of PBE simulation often focuses on density quantities, namely, number, volume, or mass; literature about grinding and fuel preparation focuses on the relevant quantities of mass and volume. The foundation of the method is as in equation (4.1) whereby as individual particle sizes can take an infinite number of differences the entire population at any time can be captured through the integration over a domain, Ω .

$$N(x, t) = \int_{\Omega} n(x, t) dx \quad (4.1)$$

If $n(x, t)$ is considered the actual number of particles in each unit volume, V , of space, an average number density $f(x, t)$ in a unit volume such that integration over infinitesimally small volumes (equation 4.2) can recover the number of particles so long as $f(x, t)$ is a sufficiently smooth function.

$$n(\mathbf{x}, t) = \int_V dV f(\mathbf{x}, t) \quad (4.2)$$

The number density becomes of more use, as through the moments of a distributions, other characteristics can be determined based on what the quantity \mathbf{x} represents. For example, using \mathbf{x} as a representative of volume size within a distribution, then the actual volume can be calculated with the first moment of a distribution, the volume class size multiplied by the density, i.e. $\mathbf{x} f(\mathbf{x}, t)$.

Consider now that \mathbf{x} , is a vector that represents a range of different regions, then transport through the regions is a description of our particulate system with time. The regions have flux through their respective boundaries and the number density of each region changes based on equation 4.3.

$$\frac{d}{dt} \int_a^b f(\mathbf{x}, t) dx = \dot{X}(a, t)f(a, t) - \dot{X}(b, t)f(b, t) \quad (4.3)$$

By transposing equation 4.3 so that the right hand side is equal to 0 and absorbing the flux term into the integral, as as long as all functions are sufficiently smooth, the solution of the integral is trivial and therefore the integrand must equal 0 which leads to equation 4.4 (S. Kumar & Ramkrishna, 1996a).

$$\frac{\partial}{\partial t} f(\mathbf{x}, t) + \frac{\partial}{\partial \mathbf{x}} (\dot{X}(\mathbf{x}, t)f(\mathbf{x}, t)) = 0 \quad (4.4)$$

4.1.2 The Breakage Population Balance Method

From equation 4.4, population balance equation methods can be applied to many different areas of research. The equation describes the rate of change of the density of a quantity, the first term on the left is the progression with time, and the second is the progression because of growth processes, such as nucleation. In the process of modelling breakage events, this term is redundant, as no such process occurs in particle breakage phenomenon. We do however have different events, a source term from which particles can be born into the specific \mathbf{x} class from other classes and a sink term whereby particles can leave a class; therefore, another term, $H(\mathbf{x}, t)$, which encompasses sink and sources terms is added to equation 4.4. These

can include, birth by agglomeration from smaller particles, and breakage from larger particles, additionally death from agglomeration, particles moving out of the region to larger ones and from breakage to smaller particle regions. At the sizes considered for biomass fuel preparation, agglomeration does not need to be considered for the simulation as the effects would be minimal.

Taking this into account the population balance equation, 4.4 is appended to accommodate birth and death processes (see equations 4.5-4.6).

$$\frac{\partial}{\partial t} f(\mathbf{x}, t) = H(\mathbf{x}, t) \quad (4.5)$$

Where:

$$H(\mathbf{x}, t) = \int_x^{\infty} s(y)b(\mathbf{x}, y)f(y, t)dy - s(\mathbf{x})f(\mathbf{x}, t) \quad (4.6)$$

The first term on the right-hand side encompasses the entrance into the size class of \mathbf{x} from all classes, where the size is larger than that under evaluations, i.e. $y > \mathbf{x}$. And the second term is the sink term from the current size, \mathbf{x} . When applying the breakage population balance equation (BPBE), to problems where conservation of, for example, mass and volume are present, this leads to 2 important concepts given in equation 4.7, 4.8 and 4.9.

$$\int_0^y b(\mathbf{x}, y)dx = 1 \quad (4.7)$$

$$b(\mathbf{x}, y) = 0, \quad \mathbf{x} > y \quad (4.8)$$

$$\int_0^y \mathbf{x}b(\mathbf{x}, y)dx = y \quad (4.9)$$

From these constraints and the integration of 4.6 into 4.5 gives the final form of the continuous BPBE. This can be solved in a several different ways that are discussed in chapter 4.1.3 where an overview was provided.

4.1.3 Method of Solution

In various literature there are a few techniques have been used that would suit the purposes of the problem. The differences of the schemes are in how the problem is posed. In some of the works developed over the last 20 years, investigations of breakage have included solution via Monte Carlo techniques (Kostoglou, Dovas, & Karabelas, 1997; Mishra, 2000), direct quadrature methods of moments (Daniele L. Marchisio et al., 2003), a range of different fixed pivots and cell averaged techniques (J. Kumar et al., 2006; S. Kumar & Ramkrishna, 1996a, 1996b). Most of the techniques revolve around dividing the domain of interest into sections and solving over that section for an amount of time. These fit grinding processes well as analysis of the resultant progeny is usually analysed through discrete measure, e.g. sieving, and represented as a discrete cumulative distribution. To this end a discretised method, using matrices can be employed (Bilgili & Scarlett, 2005a, 2005b; Bilgili et al., 2006; Maxx Capece, Bilgili, & Dave, 2011; Miguel Gil et al., 2015b; Herbst & Fuerstenau, 1980), where each row and column represent the different size classes. In such a case the integrals in the population balance equation can be replaced with summations over the range (equation 4.9), a change in notation is implemented here, i and j represent size classes, s , b , f and t represent the selection function at size i , breakage function of size class j in to i , the quantity at size i and time respectively.

$$\frac{df_i}{dt} = \sum_{j=i}^l s_j b_{i,j} f_j - s_i f_i \quad (4.9)$$

From 4.9, enacting a forward difference scheme in the time domain leads to equation 4.10.

$$f_i(t + \Delta t) = (1 - \Delta t s_i) f_i(t) + \Delta t \sum_{j=i}^{i-1} s_j b_{ij} f_j(t) \quad (4.10)$$

From here, calculation of the whole system can be represented as matrices. To do so requires that each the of selection and breakage functions take the form of a $n \times n$ matrix where n is the number of size classes. The selection matrix

becomes a diagonal matrix, and the breakage matrix either an upper or lower triangular matrix, subject to the order of the size classes in the simulation.

$$\text{Selection function: } \begin{pmatrix} s_{1,1} & \dots & 0 \\ \vdots & \ddots & \vdots \\ 0 & \dots & s_{n,n} \end{pmatrix} \quad (4.11)$$

$$\text{Breakage function: } \begin{pmatrix} b_{1,1} & \dots & b_{1,n} \\ \vdots & \ddots & \vdots \\ 0 & \dots & b_{n,n} \end{pmatrix} \quad (4.12)$$

This leads to the convenient construction of a matrix form of the BPBE as in equation 4.13.

$$\mathbf{F}^{(t+\Delta t)} = (\mathbf{I} - \Delta t \mathbf{S} + \Delta t \mathbf{B} \mathbf{S}) \mathbf{F}^{(t)} \quad (4.13)$$

With successive multiplication at each interval Δt the progression at any time can be calculated. And based on the value of Δt , the matrix form can be evaluated as equation 4.14, where k is the number of steps given by $t_{max}/\Delta t$.

$$\mathbf{F}^{(t)} = (\mathbf{I} - \Delta t \mathbf{S} + \Delta t \mathbf{B} \mathbf{S})^k \mathbf{F}^{(0)} \quad (4.14)$$

Under batch conditions this method has been used to calculate the solution. Additionally, as has been completed in other literature, the solution to the series of ordinary differential equations as in equation 4.10 can be computed, and in literature most frequently with MatLab™ ODE45 or ODE115 functions. Using the matrix method though seems to give as high an accuracy as any ODE solved solution (Petrakis & Komnitsas, 2017).

4.2 Selection and Breakage Functions

The selection and breakage functions of the simulation have a key role in defining the how evolution of the particle size distribution progress with time. Each plays a specific role in the equation. The selection function, provides a rate of change based on a condition of x ; in the context of the project, this is a rate of breakage for particles of size x . The breakage function describes the distribution of the quantity that is broken down. Subject to how the PBE simulation is targeted as mentioned in 4.1.1, the constraints on the breakage function for conserved quantities are as in equations 4.7 through to 4.9. Again, in the context of the project, the selection function also has a constraint whereby the rate of breakage at each time interval cannot exceed 1, i.e. $s(x) \leq 1$. Generally, in the case of comminution the rate of breakage is to reduce as the size of x decreases. As part of the study in chapter 3, a set of breakage and selection functions were collected that form part of the study completed in this research. Chapter 7, tables 7.1 and 7.2 provide details of the selection and breakage functions used within this project. Within the matrix PBE model the breakage function is expressed as a cumulative distribution, $B_{i,j}$, which when calculated requires the transformation into a discrete fraction, hence equation 4.15.

$$b_{i,j} = B_{i,j} - B_{i-1,j} \quad (4.15)$$

Here i and j represent the size the particle is going to, i , and the particle coming from, j .

4.3 Simulation Implementation

4.3.1 Method Validation

Initial development of the population balance for batch processes was developed that satisfies the numerical scheme outlined. As a test case to ensure the developed simulation is providing accurate solutions to problems the data from (Petrakis & Komnitsas, 2017) will be used due to the similarity of the simulation. As the achieved accuracy is to within 99.9% of the experimental data in that

literature, should the model constructed here achieve the same level it can be taking as achieving appropriate solutions to the problem and valid for use in the research.

4.3.2 Parameter Back Calculation Method

It will become necessary to alter the individual parameters of the breakage and selection functions during the research so that the parameters can be correlated with the output of the mills and identify how the operational and material characteristics influence the simulation. Optimisation to back calculate these parameters was completed using the ‘fmincon’ routine in MatLab™. This process completes non-linear optimisation of the parameters when there are constraints with the parameters. ‘fmincon’ comes with several different settings. For this research, after initial tests higher accuracy was found using an ‘interior-point’ algorithm as detailed (Byrd, Hribar, & Nocedal, 1999). As an objective function to minimise, the overlapping coefficient, OVL, has been employed in favour of measures of accuracy, such as linearising the particle distributions through log-log plots of the Rosin-Rammler distribution, whereby to ensure fits, data must be trimmed from either end to ensure calculation for the log-log axis before R^2 , or employing other tests which are not suited to the non-linear nature of a PSD. The optimisation routine has several parameters that are set to terminate optimisation when specific conditions are met. In this work the tolerances are set to the standards of the MatLab™ fmincon function except for changes in the objective function, ‘TolFun’, which was set to halt when the change was less than 10^{-4} ; trials with smaller tolerances, e.g. 10^{-6} proved more time consuming, yet provided little or no gain in accuracy.

4.4 The Overlapping Coefficient

As mentioned 4.3.2, various measures of accuracy can be used in evaluating the model, however standard measures, such as R^2 , are unsuitable for non-linear systems. In other literature, the researchers have linearised the particle size distributions with logarithmic transforms in order to compare distributions which often omits the top and bottom of a distribution in order to fulfil the transformation. As an alternative, the Overlapping Coefficient, OVL, is used to assess particle size distributions and variance between them. The basis of the theory

is that for two distinct probability density functions, $g(x)$ and $h(x)$, the OVL coefficient is 1 if and only if $g(x) = h(x)$, otherwise the value is in the interval $[0, 1]$ where the value gives an indication as to how close the distributions are to one another; this is calculated as in equation 4.16 whereby with discrete data the integral can be replaced with a summation over the range. Figure 4.1 displays the concept of the OVL principle. When used as an objective function for the ‘fmincon’ MatLab™ optimisation routine, the actual target function to minimise is 1-OVL .

$$OVL = \int_0^{\infty} \min\{g(x), h(x)\} dx \quad (4.16)$$

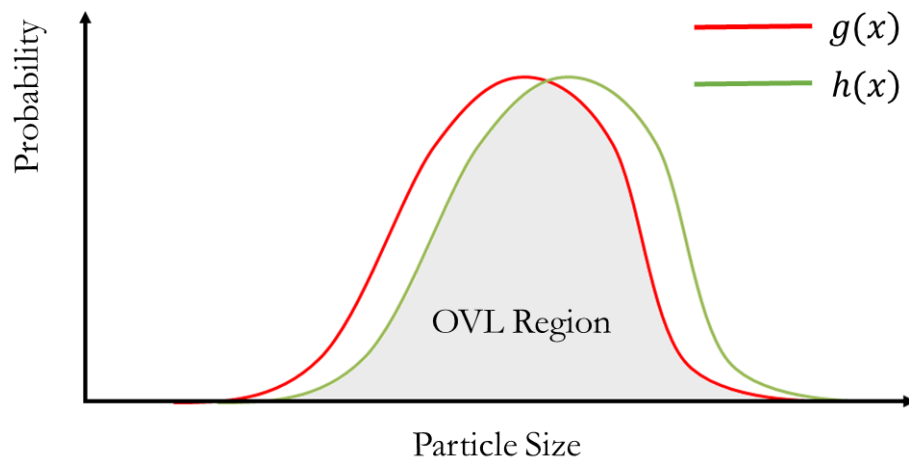


Figure 4.1 displays the concept of the overlapping coefficient, which is used in comparing distributions and as an objective function for optimisation.

4.5 Steady-State Simulations

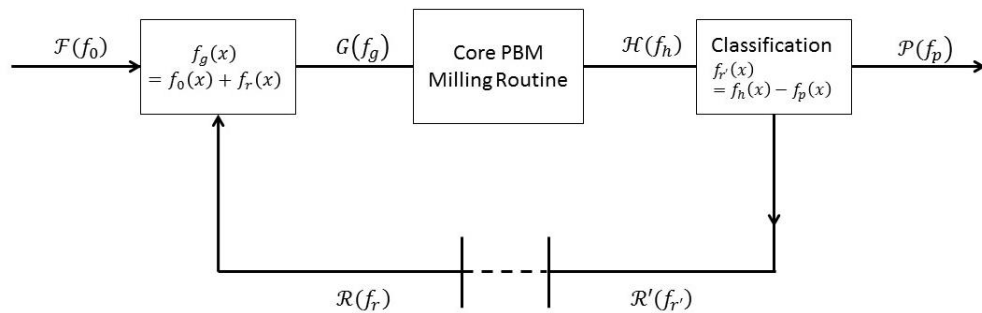


Figure 4.2 displays the concept of the steady state PBE model.

Steady state simulations are used as representations of the continuous throughput mills more applicable to an industry milling setting. The application of the PBE can be implemented through iterations of the scheme until the input flow rate matches the output as symbolised in equation 4.17 and represented in figure 4.2. At steady state there would be no change in the PSD within the mill and product flow rate out should match the flow rate into the mill. A residence time parameter θ is an unknown within the model.

$$\frac{1}{\theta} (f_{in} - f_{out}) + \sum_{j=i}^I s_j b_{i,j} f_j - s_i f_i = 0 \quad (4.17)$$

Due to the unknown residence time the simulation is iterated to a steady state, whereby the residence time is encapsulated into an input and exit rate of the mill. Therefore 4.17 becomes as in 4.18.

$$\mathcal{F}_i f_0 - C_i f_h + \sum_{j=i}^I s_j b_{i,j} f_j - s_i f_i = 0 \quad (4.18)$$

Where \mathcal{F}_i is the input or feed rate and C_i the output rate, in to and out of the mill respectively at each size interval i . C_i is governed by a classification function a probabilistic function that gives the likelihood of a particle of size i passing the classifier.

Steady state conditions are considered to have been reached when a recycle rate, \mathcal{R} , in the previous iteration matches the current recycle rate, \mathcal{R}' to within a certain tolerance as shown in figure 4.2. Using the back-calculation method described in 4.3.2 the resultant PSD can be optimised to meet experimental conditions.

4.6 Simulation Experimental Process

The following method explains the process of numerical simulations and process used to extract the factors that affect how a mill responds when the operational conditions are changed and the changes in material.

4.6.1 Domain Separation

As mentioned previously, as grinding experiments are naturally analysed through discrete size intervals, the domain of results is already separated out. The separation is often coarse due to the practicalities of particle size analysis through physical separation methods, such as sieving which usually uses intervals where the next size is a multiple of $\sqrt{2}$ to the previous. In general, more accurate numerical calculations can be achieved through increasing the number of intervals in the size domain so that $\Delta x \rightarrow 0$. However, when using a numerical scheme that has many more intervals than those of experimental results, information is lost in the reconstitution of a coarser grid. A number of works have stated that it is possible to achieve highly accurate solutions using coarser separations and non-linear grid separation is seemingly handled well by PBE methods subject to the method of solution (S. Kumar & Ramkrishna, 1996b; Petrakis & Komnitsas, 2017). Therefore, in the following research the particle size domain over which calculation of the discrete size intervals takes place is set to match that of the experimental work to which it is attempting to optimise too and predict.

4.6.2 Feed generation

Input material generation is created where possible to match that of the different materials used in this project. Several species of biomass pellets are used and material properties have been recorded, specifically the mean pellet diameter and length along with their respective standard deviations. In each simulation feed is generated using MatLabTM's 'normrnd' function to generate 10^6 individual elements with normally distributed minimum chord diameters, d_{c_min} , using the information of the mean and standard deviation information. Once generated the particles are used to create a probability distribution to be used as the initial distribution of each simulation.

4.6.3 Optimised Selection and Refinement

The process by which the back calculation of parameter values and zoning in on the optimal model conditions would take the following steps:

- Selection and Breakage Function
 - Optimise each experimental run against each combination of selection and breakage function, (20 combinations), to maximise OVL (*note: the optimisation function will look to minimise 1-OVL*)
 - Frequency plot the occurrence of each selection and breakage model combination, determine the most popular; where results are close determine 2nd and 3rd preferential models and include in the frequency plot.
- Optimise selected selection and breakage function combination against training data.
 - Evaluate the parameter data to look for trends related to changes in the experiment conditions.
 - If no relations seem present, alter the initial starting parameter values and run the optimisation again.
 - If still no relation moves to the next most frequent SB combination.
- Where possible relationship with each parameter, constrain others where no relation seems to exist.
 - When so doing ensure that the possible relationships are maintained.
 - Ensure that overall accuracy of the simulation can be maintained within significant levels.

- If relationships fail, or accuracy drops below acceptable levels consider alternative amendments, or multi-independent variable reliance.
- If relationships between parameter values and independent variables materialise develop model and blind test.
 - Use data unused in the training of the model to evaluate the accuracy.
 - If accuracy is too low, review and repeat process.

By using this process, the objective is that the model can be quantified against the material and operating conditions. If successful it may lead to the possibility of establishing a more predictable PBE simulation that may reduce the need for extensive experimental runs. As material characteristics would be easier to analyse and quantify the effects they have on set milling conditions they will be analysed first.

Chapter 5 - Experimental Methodology

This chapter discusses the experimental methods used throughout the research. It covers areas from the analysis methods used for the particle analysis, energy analysis and mass throughput. Additionally, for the Lopulco mill how the air flow through the mill was measured and collected to obtain data for some of the secondary variables of interest as highlighted in chapter 3.1.4. The chapter also includes a section on the experimental results taken from the sister project “On Biomass Milling for Power Generation” (Williams, 2016).

5.1 General Analysis Methods

5.1.1 Particle Analysis

Particle analysis on the product of milling experiments and material characterisation experiments has been carried out in 2 ways. The first has been via mass-based sieve analysis to give mass fractions of the particle size distributions. The second is through dynamic image analysis. Figure 5.1 displays the effective range of several particle analysis techniques.

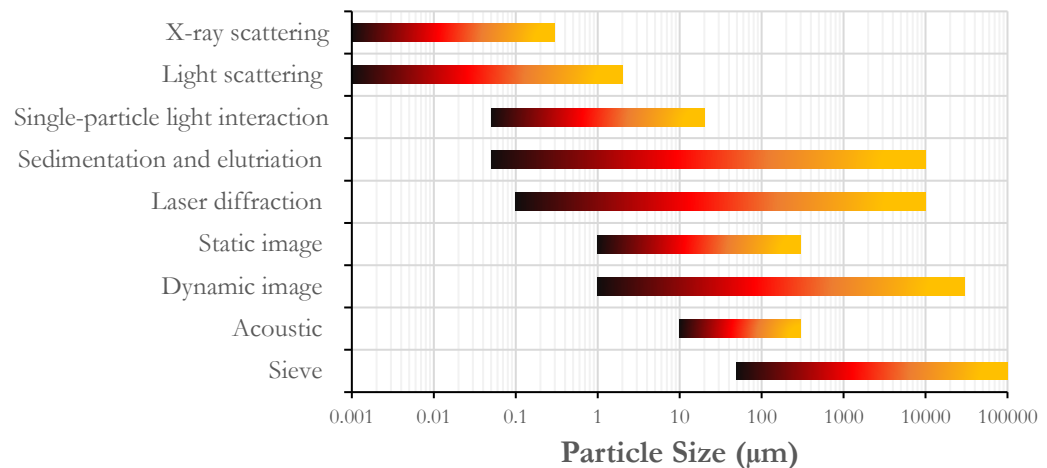


Figure 5.1 displays the particle size ranges for which various particle analysis techniques are effective.

5.1.2 Mass Fraction Oversize Sieve Analysis

Mass fraction over size analysis is completed with 20 cm diameter sieves from by Retsch Technology following the BS EN ISO 17827-2:2016 standard.

Following trials on milled biomass material it was found that 15 minutes was sufficient time to fulfil the standard guideline of achieve below 0.3% change per minute between sequential sieves for all biomass pellet species. Analysis is carried out using sieve sizes: (3350 μm , 2360 μm , 1700 μm , 1180 μm , 1000 μm , 850 μm , 600 μm , 300 μm , 150 μm). The sieves are stacked in descending order on a Retsch Technology AS200 sieve shaker, set to intermittent pulsed sieving, each pulse occurring for 10 seconds before a 3 second settling break; this method was used on the recommendation of Retsch Technology. The masses are measured using an Ohaus Pioneer balance measured to nearest 0.01g representing a $\pm 0.005\text{g}$ potential error.

5.1.3 Volume Fraction Undersize Dynamic Analysis

Dynamic image analysis is achieved using a Retsch Technology Camsizer® P4 that conforms to the BS ISO 13322-2:2006 standard. The technology uses two 30 frames per second cameras, with a resolution 1.3 megapixel each, one of the cameras is zoomed in on a region at the top centre of the viewable area. Particles traverse along a vibratory feeder and allowed to drop between the cameras and a back lit screen into a collection receptacle. The cameras capture images are analysed for size and shape parameters (see appendix F for definitions used as part of this thesis), producing distributions on a volume basis. The range of particle recognition is from 30 μm through to 30 mm. Both cameras analyse all particles captured in each image. The zoom camera is used to give a statistically based likely number of the smallest particles that are not captured by the basic camera. The CAMSIZER reports particle sizes to the nearest μm down to the minimum of its capability, representing a margin of error of $\pm 0.5 \mu\text{m}$ with every reading. The shape parameters are subject to this margin of error, additionally shape characteristics are calculated by the CAMSIZER to 8 decimal places; they are reported to 2 within this work.

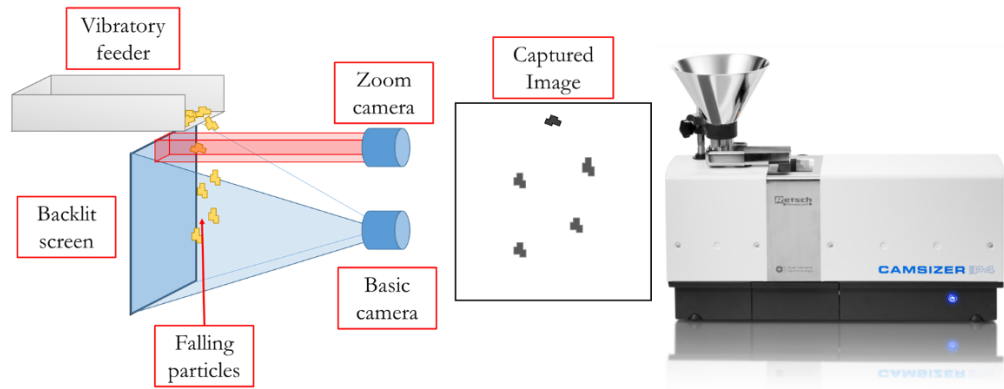


Figure 5.2 displays the concept of the CAMSIZER P4 and how it captures and analyses particle information.

5.1.4 Energy Consumption Data Logging

Energy consumption was recorded whilst the mills were in use by an ElComponent SPC Pro data logger by ElComponent Ltd. The data collected includes the current, voltage and phase angle at 1 second intervals to calculate total power, P . Data is processed with accompanying software. Specific effective energy (E_e), i.e. energy consumption per unit mass relative to the idle energy consumption (idle power, P_I), is calculated using equation 5.1 (V. S. R. Bitra et al., 2009; Gravelsins & Trass, 2013). Further information is contained in (Williams, 2016) on the technical aspects of how the energy meter works. The data logger reports the power consumption to the nearest Watt. Potential error is therefore ± 0.5 W.

$$E_e = \int_0^t \frac{P}{m} dt - \int_0^t \frac{P_I}{m} dt \quad (5.1)$$

5.1.5 Mass Output Analysis

Output Rate

Tracking the output of mass from a mill has been achieved using an Ohaus PA4202C, self-calibrating top pan balance, with a maximum capacity of 4kg and precision to 0.01g. The balance was connected to a laptop running the Ohaus DAS (data acquisition software). Through this, mass can be recorded at set time intervals greater than 1 second. The balance was used to track output from several mills during experimentation (figure 5.4). The potential error in the measurements is ± 0.005 g.

Residence Time

Using the information about the feed rates and output rates, a residence time for each experimental run will be calculated based on difference in time from when 50% of the feed load has been fed into the mill and when 50% of the feed has exited the mill.

5.2 Lopulco E1.6 Mill

5.2.1 Mill

The E1.6 Lopulco Mill is a laboratory scale ring and roller mill (see figure 5.3). Table 5.1 displays the dependent and independent variables for the experiment. The objective of the experiments was to create a set of results on a mill similar in operation to those used in industrial milling and investigate how the independent variables (mill settings) effect the dependent variables. These experiments are to be used in conjunction with the material study carried out in the sister project, (Williams, 2016).

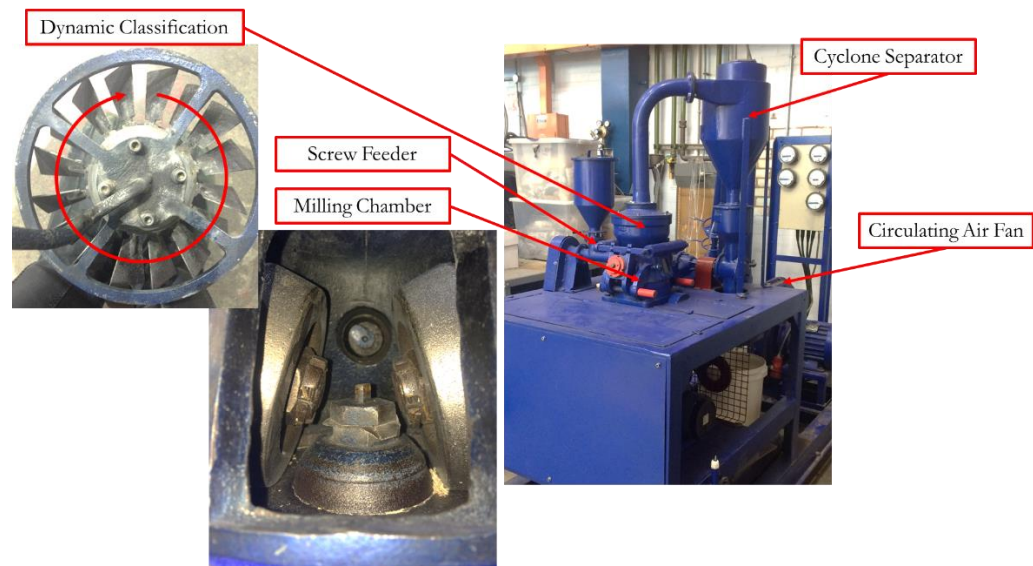


Figure 5.3 displays pictures of the Lopulco E1.6 mill used in the project and based at the University of Nottingham.

The mill and monitoring equipment was set up as in figure 5.4 and include the pressure and temperature information tapping points (see table 5.2 for equipment details). Figure 5.5 provides a close-up schematic of a pressure tap with transducer arrangement used to collect pressure and to calculate airflow through the mill via the differential pressure transducer at the venture tube.

Table 5.1 displays the independent and dependent variables for the Lopulco mill experiments.

Independent Variables	Dependent Variables
Feed Rate	Product PSD
Mill Table Speed	Mass output rate
Classifier Vane Angle	Air flow
Product Input (1 kg)	Calculated residence time
	Mill energy consumption
	Milling chamber differential pressure
	Inlet air temperature
	Outlet air temperature
	Ambient temperature
	Ambient humidity

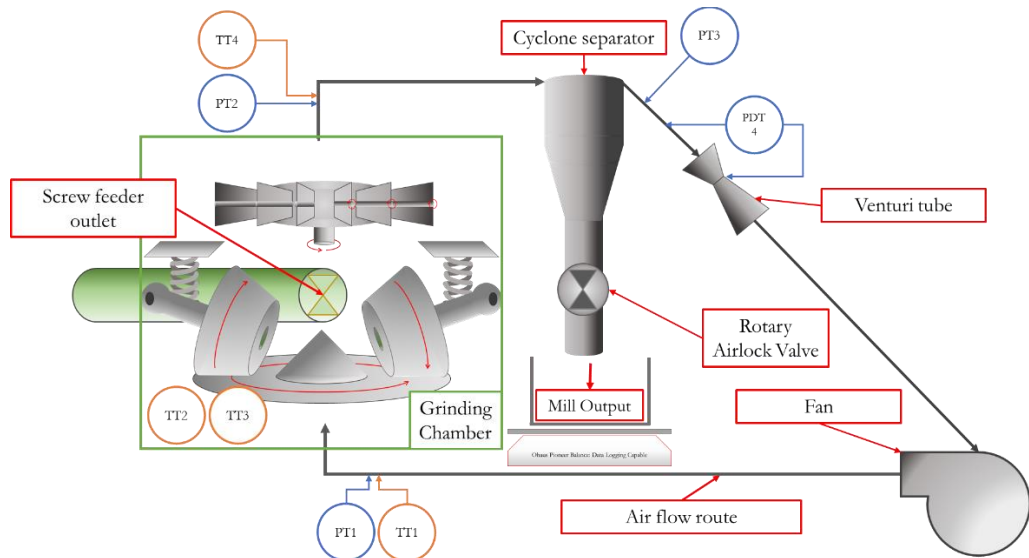


Figure 5.4 displays the set up for the Lopulco mill experiments including, mass output, temperature and pressure tapping points.

The mill has several adjustable parameters; these are digital controls for the mill table speed, mill screw feeder speed and manual adjustment of 16 classifier vanes. In the experiments these were set by measurement with a protractor as

closely to the desired angle as possible, using an upward angle measure from the horizontal plane (see figure 5.6). The classifier unit is itself fixed to the mill table and rotates at the same speed as the mill table.

Table 5.2 displays the sensors used for the Lopulco milling experiments.

Label	Manufacturer/Model	Use
PT1, PT2, PT3	OMRON MEMS 2SMPP	Gauge Pressure Transducer
PDT4	Freescale Semiconductor MPX10DP	Differential Pressure Transducer
TT1, TT2, TT3, TT4	T-type	Temperature thermocouple
Data Logger ¹	Campbell Scientific CR23X Micrologger	Transducer and thermocouple signal detection and logging
Ambient Data Logger ¹	Lascar Electronics UK EL-USB-1	Ambient temperature and humidity
Energy data logger ¹	ElComponent SPC Pro	Energy consumption
At mill output	Ohaus Pioneer PA4202C balance	Mass output

¹ Devices not shown on the diagram

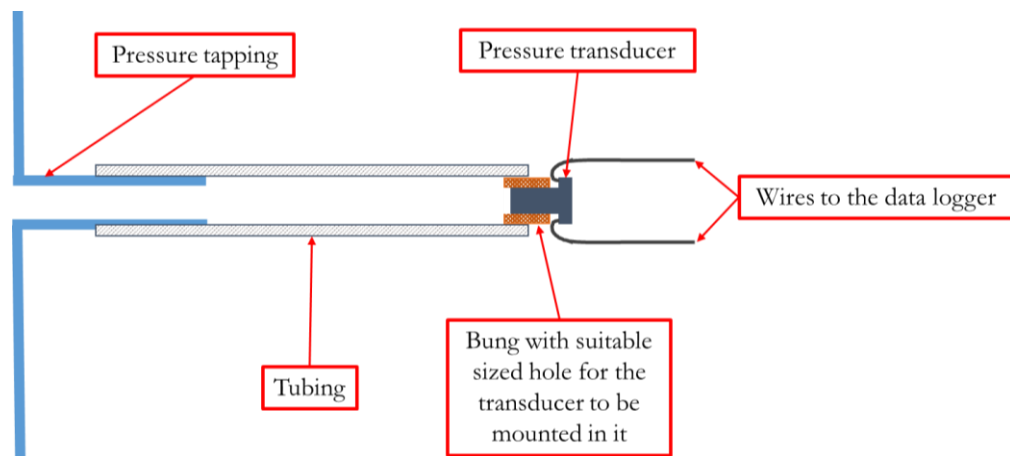


Figure 5.5 displays the close-up schematic of the pressure transducer mounting on the Lopulco mill.

5.2.2 Air Flow Rates

To measure the mass airflow rates through the mill, a differential pressure transducer was set up to span the inlet and constrictionappings of a Venturi tube, PDT4 on figure 5.4, built in to the air recycling pipe of the Lopulco mill. As the air flow rates were a secondary objective of the project and because of the limitation of the CR23X data logger allowing only mean, maximum and minimum readings from the transducers every minute, the results of the air flow rates are not focused on too much in this research. Inclusion is for illustrative purposes only, therefore adherence to the standard BS ISO 5167-3,4 was not observed. Gauge pressure transducers were also utilised for monitoring the mill to ensure problem free running during experiments only; figure 5.5 provides an illustration as to set up of the pressure transducers. Air flow rates were calculated using the pressure differential value at PDT4 of figure 5.4 and converted by using the Bernoulli equation (5.2) of constant streamlines. Table 5.3 gives the internal diameters and heights of the respective pressure tapings of the Venturi tube. The differential pressure transducer used has a measurement error of approximately ± 0.3 kPa which equates to about ± 0.002 ms⁻¹.

$$I = P + \frac{1}{2}\rho v^2 + \rho gh \quad (5.2)$$

$$Q = v_i A_i \quad (5.3)$$

$$Q = \sqrt{\frac{2\Delta P}{\rho} + 2g\Delta h} / \left(\frac{1}{A_2} - \frac{1}{A_1}\right) \quad (5.4)$$

Table 5.3 displays the Venturi tube specification from the Lopulco E1.6 mill

<i>PDT4 Venturi Tube Tap Point</i>	<i>Height (m)</i>	<i>Inner Diameter (m)</i>
Inlet	1.185	0.05625
Neck	1.055	0.03125

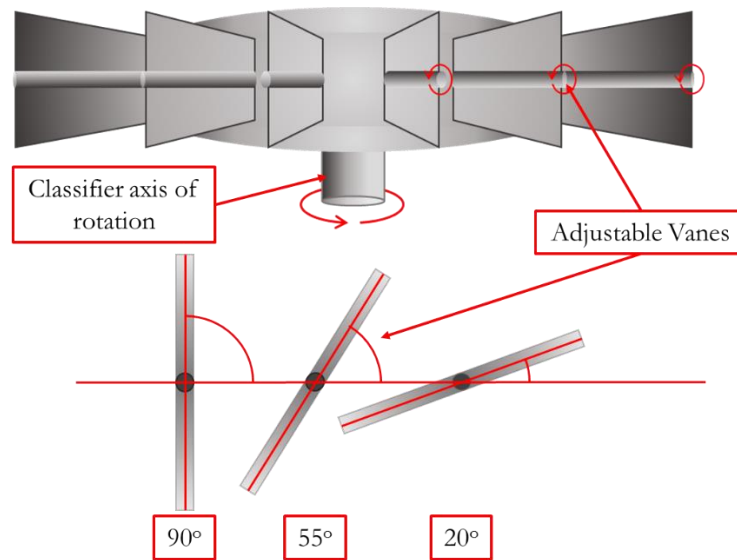


Figure 5.6 displays a representation of the adjustable vanes on the Lopulco mill classifier system; (upper) the rotating core, (lower) individual vanes.

5.2.3 Experimental Design

Due to the expected curvature in the response of the mills dependent variables a full factorial experimental design with at least 3 levels of the independent variables would have been preferred however constraints existed within the project. To complete the experiments an appropriate experimental design was required that satisfied the constraints of:

1. Limited time with the Lopulco mill.
2. Limited time for the assistance in completing the experiments.
3. Limited quantities of the raw biomass pellets that were initially supplied to the sister project.
4. Limited research budget to purchase more biomass pellets.

To capture the expected non-linear relationship of the independent variables with the dependent variables of the mill whilst minimising the number of experimental runs required, the experimental design followed a Response Surface Central Circumscribed (CCC) design (NIST/SEMATECH, 2013); this method was selected to draw out the non-linear relationship of the independent variables with the dependent variables, the embedded factorial design that is augmented by the extreme 'star-points' set at a multiple of $\alpha = 1.682$ that of the distance between the high and low points from the centre point of the experimental conditions (see figure

5.7), and the ability of the method to provide high quality predictions in detecting curvature whilst scaling back the number of experiments required. Each experimental condition was repeated 3 times except at the centre point where more results are required in a CCC design; 18 results would be preferential however due to the limitations this was scaled back to 9 repeats. Using Minitab software an order for experimental runs was obtained so that noise from environmental variables was minimised. The mill settings for the experiments are listed in table 5.4.

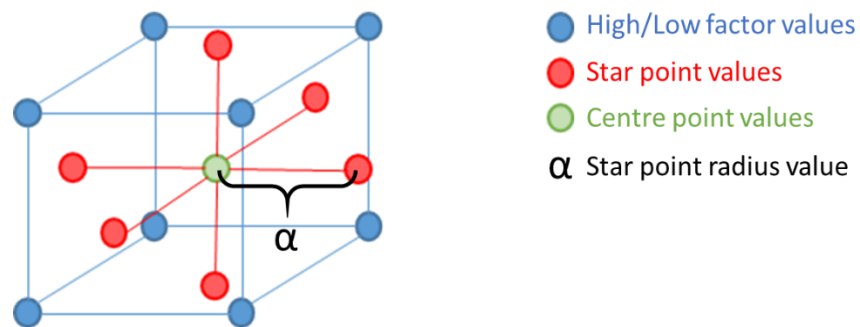


Figure 5.7 displays the central composite circumscribed experimental design philosophy.

Table 5.4 displays the experimental settings used in the Lopulco mill experiments.

Independent Variable	Low		High		Upper Star Point
	Lower Star Point	Factorial Point	Centre Point	Factorial Point	
Feeder speed (g s^{-1})	3.63	6.32	10.17	14.02	16.71
Table Speed (RPM)	175	202	242	282	309
Classifier vane angle ($^{\circ}$)	-	20	55	90	-
Target run fuel load (kg)					1.00

The mill speed is set by the mill and verified by high speed video capture using a reflective paint on the mills core and is correct to within ± 1 RPM. The feed rate has been determined by trial runs of the feeder prior to the experiments and has a potential error in the delivery rate of $\pm 1 \text{ g s}^{-1}$, however the mill feeding is sometimes variable in delivery if pellets become jammed, hence constant monitoring is required. The classifier vane angles are set manually and are dependent on both the protractor accuracy stated as accurate to $\pm 0.5^{\circ}$ but is also more susceptible to operator error than any other part of the experimental set up.

The experimental process is as follows. The pellets are loaded into the feed hopper. Once the mill fan, rotatory airlock, screw feeder and grinding table are up and running at the required setting, the trap on the hopper is release. The pellets fall into the screw feeder and are conveyed and dropped onto the grinding table. Centrifugal action and the table rotation transports the pellets to the rollers whereby friction cause them to be gripped, pulled between, and compressed by the rollers and table. Once the particles are small enough, the circulating air will pick them up and carry them to the classifier. The classifier will reject particles if they cannot pass it and are returned to the grinding table for a repeat of the process. Particles passing the classifier are carried to a cyclone separator where up they are removed from the air stream and fall to the air lock valve whilst the air circulates back to the fan.

5.3 Material Characterisation

Investigations into the material properties of different biomass pellets is to be carried out to pursue the possibility of linking the characteristics to the performance of the pellet in the mill. The objective is to correlate the performance of fuels and their measurable output (see 5.1.1, particle analysis for details) with the output of material testing. If there is a correlation, the hope is that with this information, a PBE simulation could use a material linked parameter upon which to predict how the mill may perform.

5.3.1 Sister Project Characterisation Summary

As part of the sister project, characterisation of different biomass pellets was completed also. The characterisation was performed on the fuel biomass pellets through mechanical strength testing (Williams, 2016) in an axial, diametric and flexure setup. The results are collated in chapter 7.2.2 and appendix H as a comparison to some of the characterisation completed within the experiments of this research project. The tests completed under the sister project that have been used in the analysis of this project are:

- **Quasi Mechanical Strength** (see figures 5.8, 5.9 and 5.10) tests in the axial, diametric and flexure arrangements on an Instron Mechanical 5969 testing machine: this determined the compressive resistance of each material between 2 plates, the first of which is

fixed in position beneath the test sample, and the second, a driver plate applying force until the load gives way. The samples were tested in the axial and diametric orientations and through a 3-point bending arrangement for the flexure analysis. The output of the Instron machine are stress-strain curves that are used to calculate Young's modulus and then converted to the units of MJ m^{-3} via the machines software to remain consistent with this work.

- **Particle Density** testing; a technique that takes the mass of a sample, then measures the volume displacement in deionised water. A calculation of $\rho = m/v$ is then used to collect the density. The density is reported in units of g cm^{-3} .

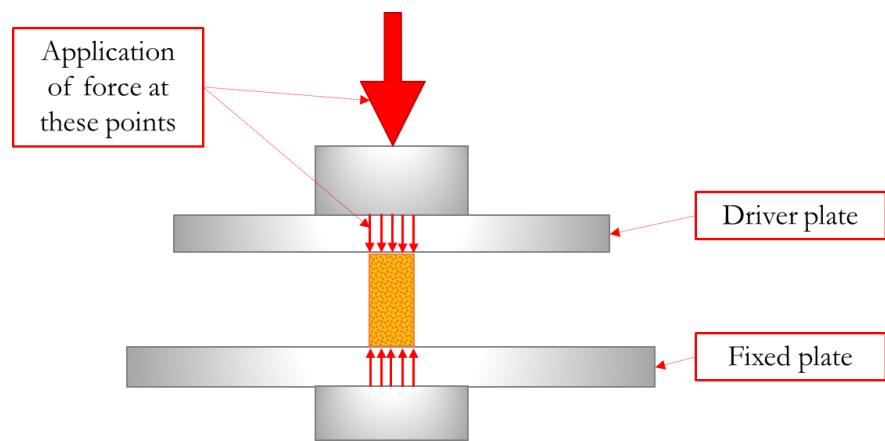


Figure 5.8 displays the axial orientation Instron mechanical testing arrangement.

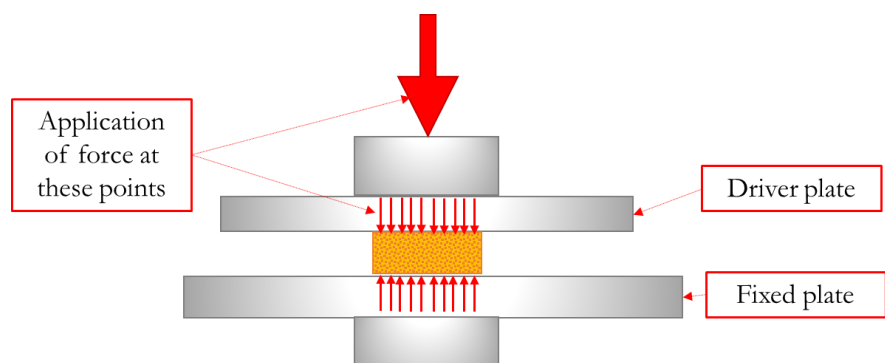


Figure 5.9 displays the diametric orientation Instron mechanical testing arrangement.

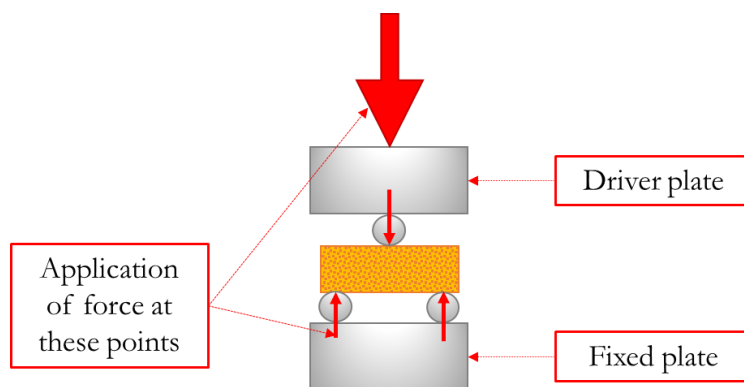


Figure 5.10 displays the flexure Instron mechanical testing arrangement.

5.3.2 Skeletal Density Measurements

Helium pycnometry is completed using an AccuPyc 1340 gas pycnometer, to determine the skeletal density of the pellets. A 10cc receptacle is loaded with biomass pellet. 20 purge cycles with He are used to measure the differences in pressure between the sample chamber and a reference chamber of known volume and pressure; He is used as the molecules are small enough to penetrate open pores in the pellet. Maintaining a constant temperature and within the sealed chamber, the ideal gas law is used to determine the volume of the sample before a density measurement is calculated with knowledge of the mass. The average of the 20 cycles is used. As moisture on the surface of the sample can influence the results a reference sample that has been dried is used for comparison and the differences were negligible in comparison the measured samples (Webb, 2001).

5.3.3 Surface Area Analysis via Kr Gas Adsorption

Using Micrometrics ASAP2420, surface area measurements were calculated based on the isotherm output from experiments using a range of biomass pellets (the Eucalyptus, Miscanthus, Sunflower, microwave torrefied and Brites wood pellets) to correlate the material mechanical testing properties and milling output with the surface area. The adsorbate used was krypton, selected to target filling the void space within the macroscale cracks and fissures in the biomass pellets, which are because of the pellet manufacturing process rather than penetrating the pores contained in the natural growth structures of biomass. The hypothesis of which relates to classical breakage theory of crack exploitation. The experiments, for which each sample was completed in triplicate, followed the procedure outlined in the paper (Wood et al., 2016); samples are loaded into glass tubes and sealed before

degassing under vacuum at 80°C for 48 hours to remove moisture and other adsorbed gases. Using Kr, isotherms were collected from 0.07-0.25 relative pressure, (p/p_0), at -195.85°K. The specific Kr isotherms were then determined by fitting the Kr isotherms and application of the Brunauer-Emmett-Teller method equation for determination of surface area of each pellet.

5.4 Statistical Analysis and Error

The analysis of the experimental data consists of calculating the mean results from multiple runs where possible. In a minor number of cases some of the information was not collected due to malfunctions in the data logger or the logging software from the balance used. In such cases the mean was calculated on the data available. Further analysis includes calculation of the standard deviation of multiple results where possible. On graphical presentation of results error bars are included and represent 1 standard deviation from the mean result. Margins of error in the measurement of both the independent and dependent variables are either listed in the columns or the notes attached to the various tables of results in Appendix I; these are generally to a certain precision of significant figures or decimal places. In some instance percentage of error may be listed.

5.5 Conclusion

In this chapter the methods used to analyse the output of the experimental results has been given, this includes general methods that have been used across the entirety of the experiments, the Lopulco mill and Single Impact Testing results as details in chapters 6 and 8 respectively. The experimental process of the Lopulco mill has also been discussed, as well as the material characterisation techniques that determine density and surface area of the biomass pellets prior to grinding. A summary of the experimental data taken from the sister project has also been described.

Chapter 6 - Experimental Results

The following chapter discusses the results obtained from the Lopulco milling experiments undertaken. This includes analysis of the reaction to changes in the independent variables, mill table speed, feed rate and classifier vane angle. It focuses on the analysis of the key dependent variables of product particle size distribution, energy consumption and mass throughput. The analysis also includes the reaction of the mill to different biomass species pellets, Eucalyptus wood, Miscanthus grass and a Microwave Torrefied wood pellet. The correlations sought and presented here include the correlation of the mill output with experimental data obtained through this research and that of the sister project. The latter section of the chapter completes a material study to obtain any correlation between the deformation testing completed by the sister project and other characterisation techniques completed in this research.

6.1 Lopulco Ring and Roller Mill

Using a standard fuel, Balcas Brites wood pellets, investigations into the response of the mill and the product were assessed reviewing several key areas; particle size and shape, energy consumption, mill throughput. The summary data here can be used in conjunction with the mean run data in appendix I that lists all the mean experimental run data.

As a summary of all the experiments the following statements on particle measure can be said:

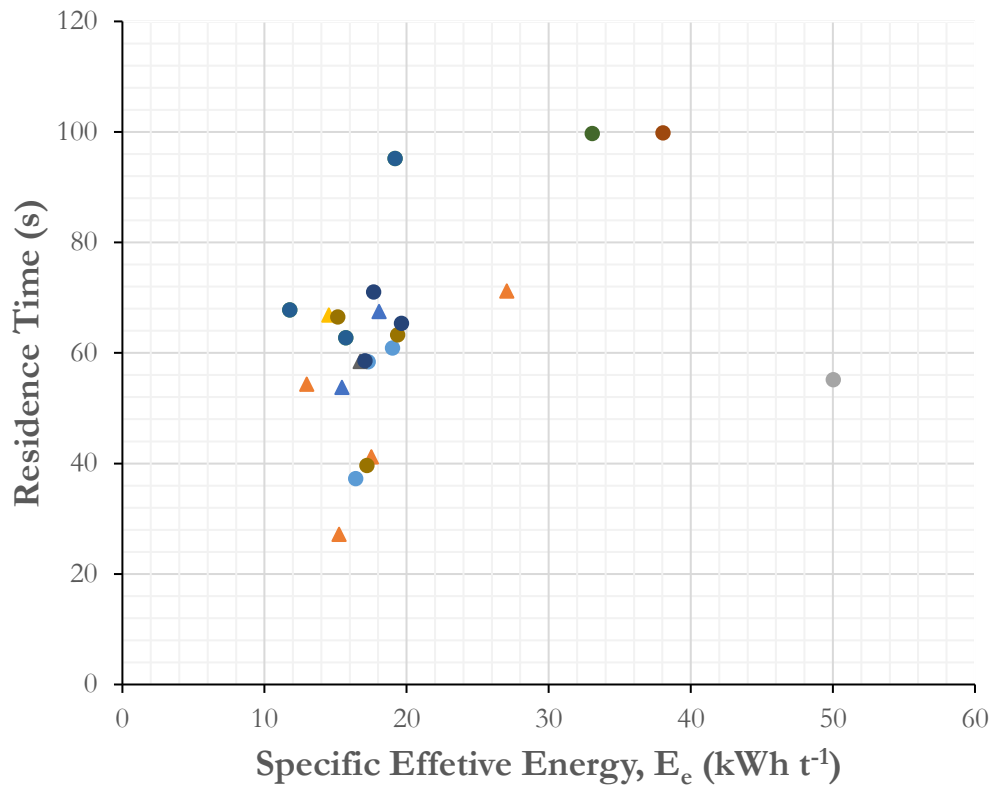
- All samples have a coefficient of gradation and coefficient of uniformity that suggest that all particle distributions through the experimental regime are well graded with a good mix of particles of all size ranges.
- The kurtosis, K_g , of all PSD's all show platykurtic tendencies.
- All PSD's have a slight left shift to the curve identified by the inclusive graphic skewness, $K_I > 0$.
- The Volumetric Relative Span of all results lies in the range of (2.0, 2.6) indicating that the PSD's are varied.

- The uniformity index, U_1 , of all PSD's are in the range of (6.0, 14.0) indicating the small particles are substantially lower than the large particles, on average there is a ratio of 10:1.

For the ensuing analysis, PSD's are evaluated at the Rosin-Rammler characteristics, d' and n , as well as at the percentiles d_{25} , d_{50} , d_{75} for variation in the trends observed at d' . To evaluate the other primary aspects for concern in the process of milling, evaluation of mass throughput by way of mass output rates and estimated residence time is conducted, and lastly there is an evaluation of the specific effective energy, E_e , for each experimental condition and material type.

Correlation fits have been assessed for linear and exponential fits to each characteristic analysis, with the best fit shown on the figures. Quadratic fits were considered however due to the fit being based on the star-points of the CCC experimental design, a quadratic fit would fit the 3 points perfectly and hence not really reveal the usefulness of the information.

6.1.1 Initial Observations



- 242 RPM, Classifier Vane Angle: 20, 0.0102 kg Feed Rate
- ▲ 242 RPM, Classifier Vane Angle: 55, 0.0102 kg Feed Rate
- 242 RPM, Classifier Vane Angle: 90, 0.0102 kg Feed Rate
- ▲ 309 RPM, Classifier Vane Angle: 55, 0.0102 kg Feed Rate
- ▲ 175 RPM, Classifier Vane Angle: 55, 0.0102 kg Feed Rate
- 282 RPM, Classifier Vane Angle: 20, 0.014 kg Feed Rate
- 282 RPM, Classifier Vane Angle: 20, 0.014 kg Feed Rate
- 202 RPM, Classifier Vane Angle: 20, 0.014 kg Feed Rate
- ▲ 242 RPM, Classifier Vane Angle: 55, 0.0036 kg Feed Rate
- 282 RPM, Classifier Vane Angle: 20, 0.0063 kg Feed Rate
- 202 RPM, Classifier Vane Angle: 20, 0.0063 kg Feed Rate
- 202 RPM, Classifier Vane Angle: 90, 0.0063 kg Feed Rate

Figure 6.1 displays the relation between the residence time and the specific effective energy. It shows that there is no relation between the two. The triangular data points represent the star points of the CCC DoE regime.

The specific effective energy is a characteristic of each fuel, it is expected that this should not vary too much beyond the attributed figure. However, if the material is held up in the mill there may be a correlation leading to increased energy consumption and therefore a higher E_e . As can be seen in figure 6.1, this does not seem to be the case and other factors are influencing the energy consumption, as in

this mill the E_e is intrinsically a product of the mill table motor and the energy draw to maintain rotational speed. Should sufficient quantities of feed material be present between the roller and mill table, friction induced by the pressure exerted in the downward force by the roller mounting spring and the material, can cause a reduction in the speed of the table. The table motor reacts and draws more power to overcome the additional friction forces and maintain the mill table speed. This is viewable in figures 6.13 and 6.14 where material is fed into the mill the instantaneous energy consumption can be seen to increase.

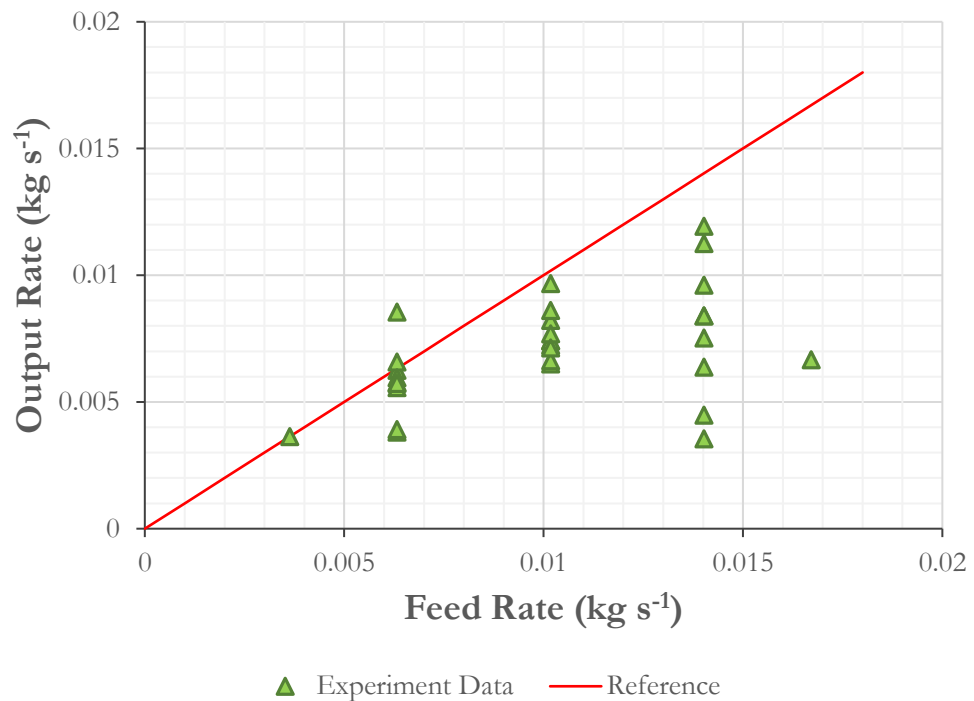


Figure 6.2 displays the feed rate against the output rate of the milling experiments to highlight that using the experimental mill, it becomes difficult to achieve a steady state experiment.

One of the aims where possible was to achieve particle size distributions from a continuous throughput mill. Ideally the results would show a steady state operation. In figure 6.2 the experimental feed rates are plotted with the mill output for the experiments where the output rates were collected and shows that a steady state was not achieved, however a reasonable data set was generated. There are several reasons why this may have been so. Given the logarithmic curve on figure 6.2 though the likely case is that the maximum grinding rate of the mill is too low

to cope sufficiently with the higher feed rate. This is likely linked to the size and volume of the Lopulco E1.6 mill. This causes the milling chamber to continue to fill up and instead of moving the material under the rollers, it moves to parts of the mill where comminution does not take place.

6.1.2 Response to Mill Table speed

This section evaluates the change in the output of the mill based on the variation of the mill table speed and all graphs here are based on variation in this. The analysis focuses on the particle size distribution, mass throughput then energy consumption.

Particle Characteristics

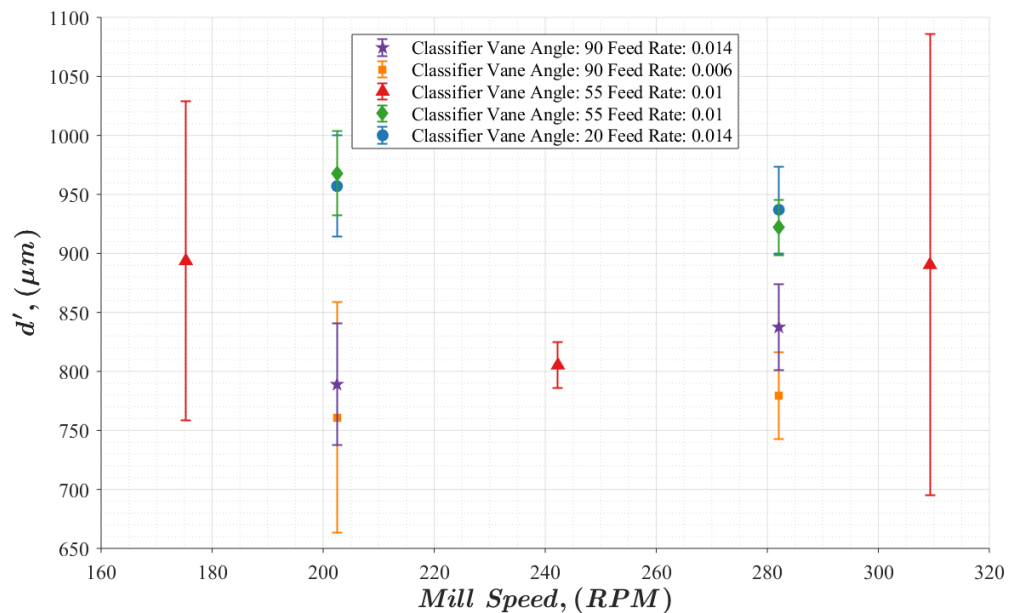


Figure 6.3 displays the Rosin-Rammler characteristic size parameter with variation in mill speed for the Lopulco milling experiments. It shows there seems to be either no or a quadratic relationship.

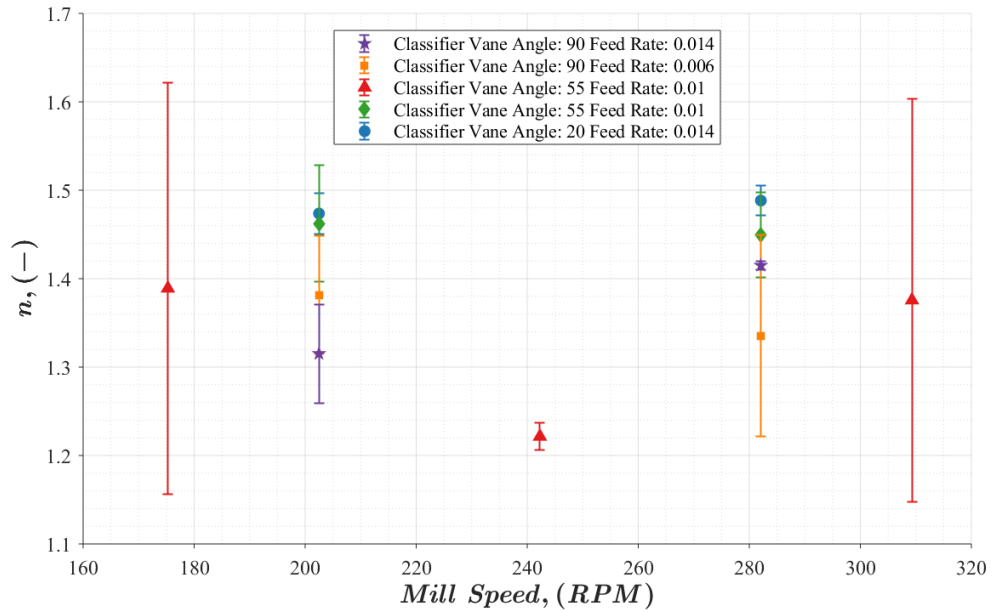


Figure 6.4 displays the Rosin-Rammler spread parameter with variation in mill table speed for the Lopulco mill experiments. Again, it shows that there is no or a possible quadratic relationship.

Figure 6.3 indicates that there is very little variation in the products d' when the mill speed is changed. There is possibly a possible quadratic relationship as can be seen with the change in mill speed at the extremes through the centre point of the experimental range. This is somewhat obscured by the large variance in the experimental results of repeated runs. The Rosin-Rammler distribution spread parameter, n , similarly suggests a possible quadratic relationship (see figure 6.4) and indicates that there is a wider spread of particles at the centre point, 242 RPM, of the experimental range. This pattern is exhibited throughout the particle size range and is not limited to only the Rosin-Rammler characteristic parameters; it was observed at particle sizes, d_{25} , d_{50} and d_{75} . A high standard deviation throughout the results is clouding the recognition of clear trends.

Mass Throughput

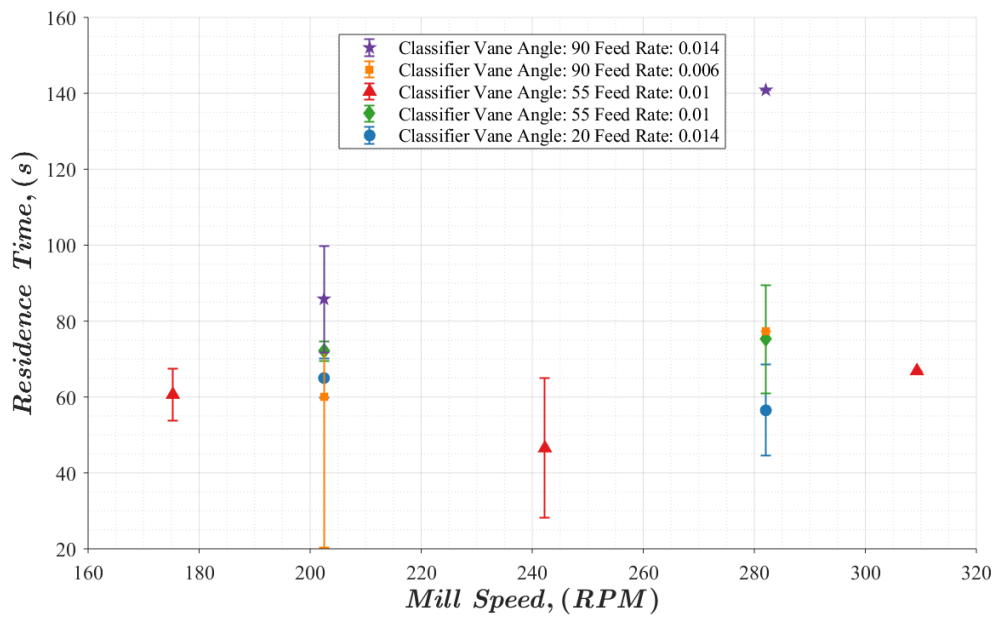


Figure 6.5 displays the variation in residence time with mill speed for the Lopulco milling experiments. It shows that there is little variation except where other parameters are factored into the argument.

Figures 6.5 and 6.6 show that potentially there is an effect on the residence time, however this is not necessarily based on mill speed. As the range seems small, except for 1 result (90° vane angle at 0.014 kg s⁻¹ and 282 RPM), evidence suggests this is more to do with the classifier vane angle in conjunction with the mill speed. Further to this the effect on the output rates with the speed, is again, seemingly affected by the classifier vane angle in conjunction with the speed.

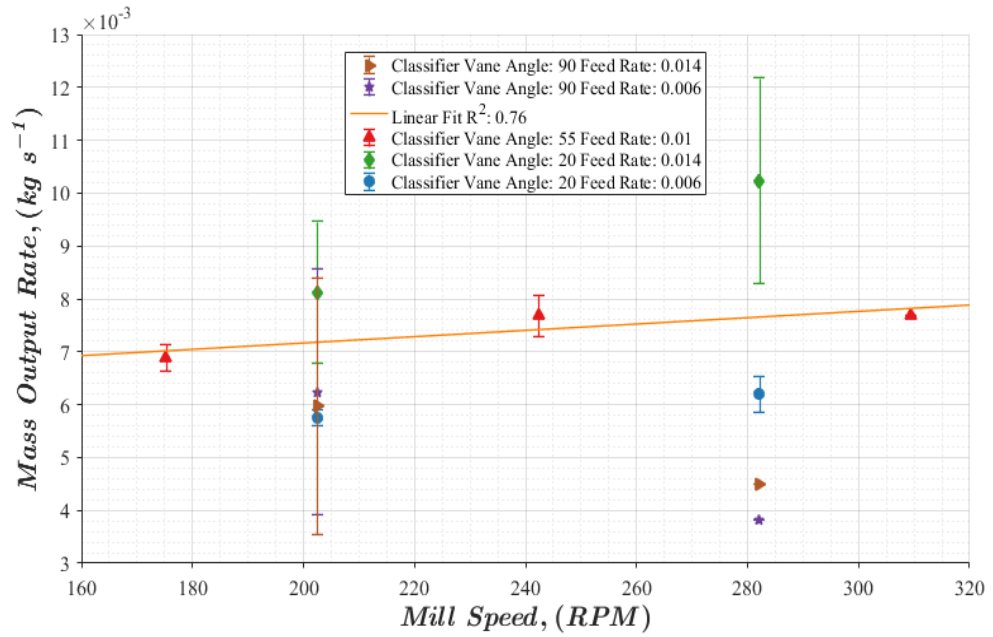


Figure 6.6 displays the variation in mass output of the Lopulco mill experiments with the mill speed. Here it shows that the mass output is likely a product of the mill speed with the classifier vane angle.

Specific Effective Energy

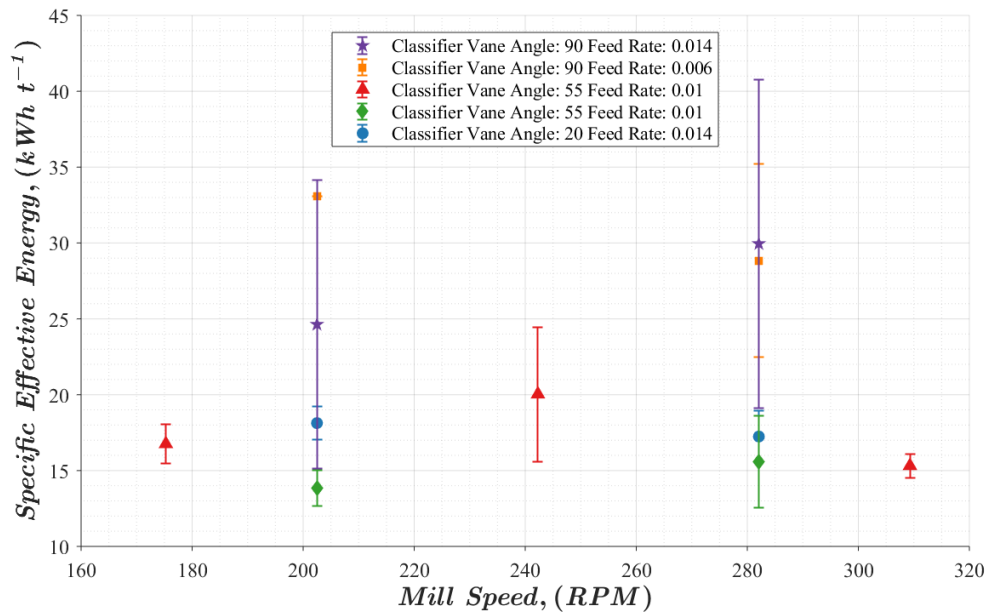


Figure 6.7 displays the Specific Effective Energy consumption attributed to the Brites wood pellets with varying mill speed. Whilst mill speed seems to have little effect on the result there is high variation in between experimental repeats.

As seems to be the case with the mill speed variable, still no clear relation between the mill speed and E_c is present. The effect of mill speed through the centre point experimental conditions, where the smallest particles seem to be generated, (see figure 6.3) and the lowest residence times are observed (see figure 6.5), also shows a peak energy consumption indicating that more of the input energy has been consumed by the mill in actual comminution as opposed frictional losses (see figure 6.7). The conditions here could be closer to ideal for the application of the energy input of the mill to the grinding of the fuel. Mill speed seems to have a higher influence on the energy consumption when the classifier vane is at 90° . At this angle, the higher speeds help to decrease energy consumption.

6.1.3 Response to Change in Feed Rate

The following section of this chapter analysis the output of the mill when the feed rate has been changed. Again, it assesses the product particle size distributions, energy consumption and mass throughput with all graphs displaying the variation of each with changes in the feed rate.

Particle Characteristics

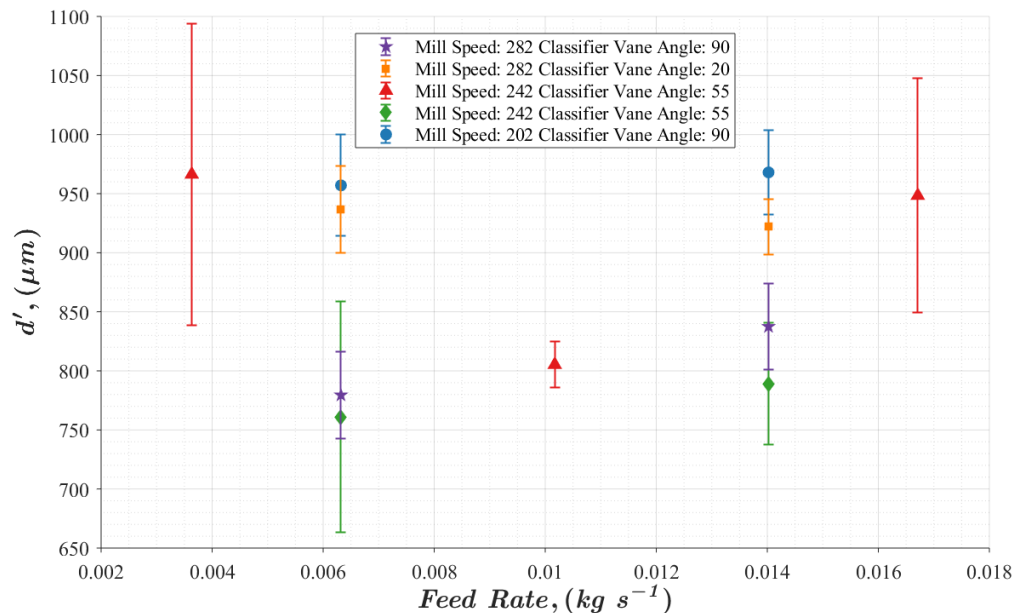


Figure 6.8 displays the Rosin-Rammler characteristic size parameter with variation in feed rate for the Lopulco milling experiments, again showing the potential quadratic relationship.

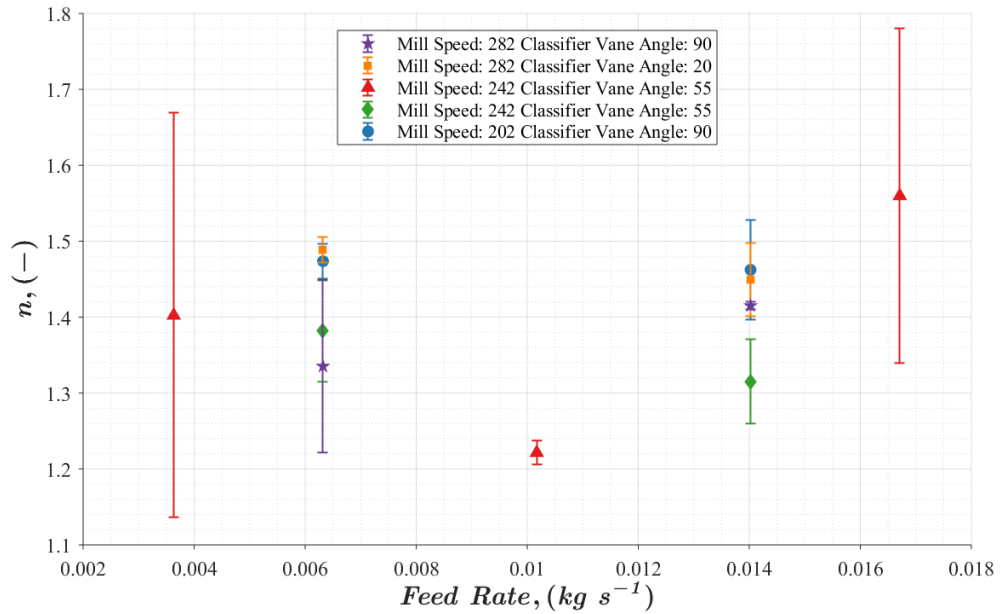


Figure 6.9 displays the variation of the Rosin-Rammler characteristic spread parameter with feed rate. It shows again a possible quadratic relationship.

Again, the effect of the feed rate does not seem to be highly influential with the particle size characteristics beyond that of general experimental error; again, though the error could be hiding the relation which could be representative of an optimal in the feeding rate midrange. Again, similar patterns occur in the d_{25} , d_{50} and d_{75} , which indicates that the PSD is affected similar throughout the particle sizes.

Mass Throughput

During the experimental process, some of the data for the mass output was lost at the extremes of the experimental range, hence why there are no error bars on the lowest and highest feed rate, due to time constraints these could not be repeated.

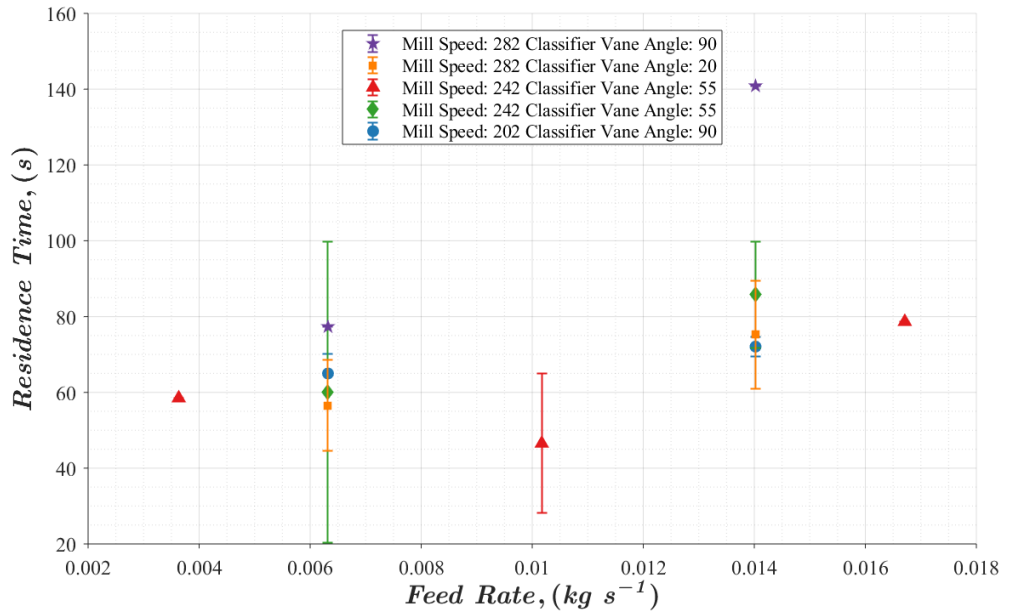


Figure 6.10 displays the residence time variation with feed rate in the Lopulco mill experiments. Only small variation is observed that could be a consequence of experimental error. Outside effects of high mill speed and a fully open classifier shows signs of a greater effect.

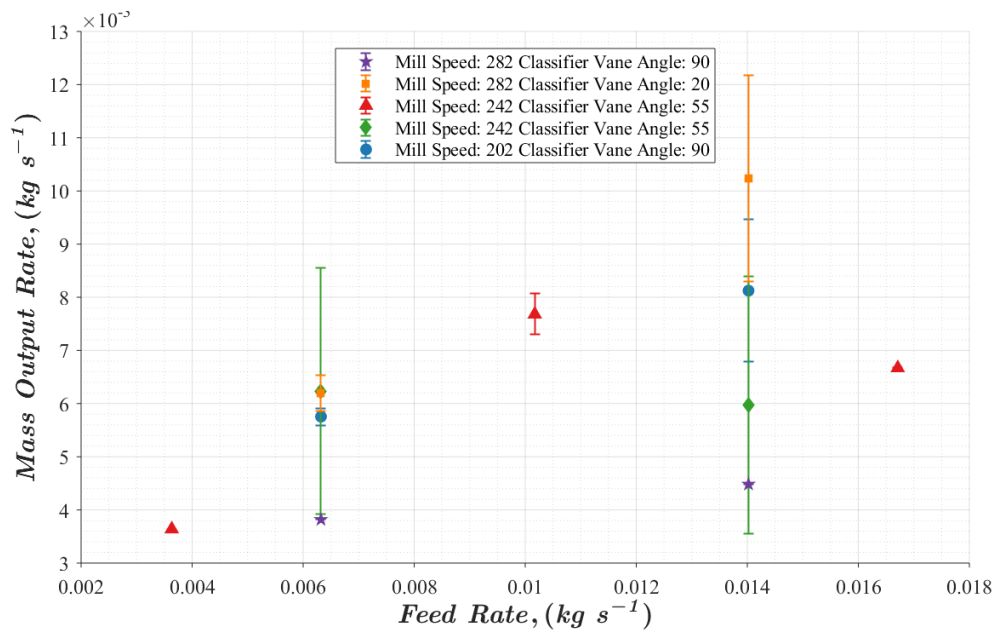


Figure 6.11 displays the variation in mass output rate with feed rate. As there was no one to one relationship, there are indications that steady-state conditions were not achieved.

Increasing the feed rate shows an upwards trend in the residence time, suggesting that the presence of more material inhibits transport through the mill.

The mass output rate increases with increasing feed rate, this however could simply be a consequence of the presence of more material and a quick throughput. However, this is also contrary to observation of marginal increase in the residence time.

Specific Effective Energy

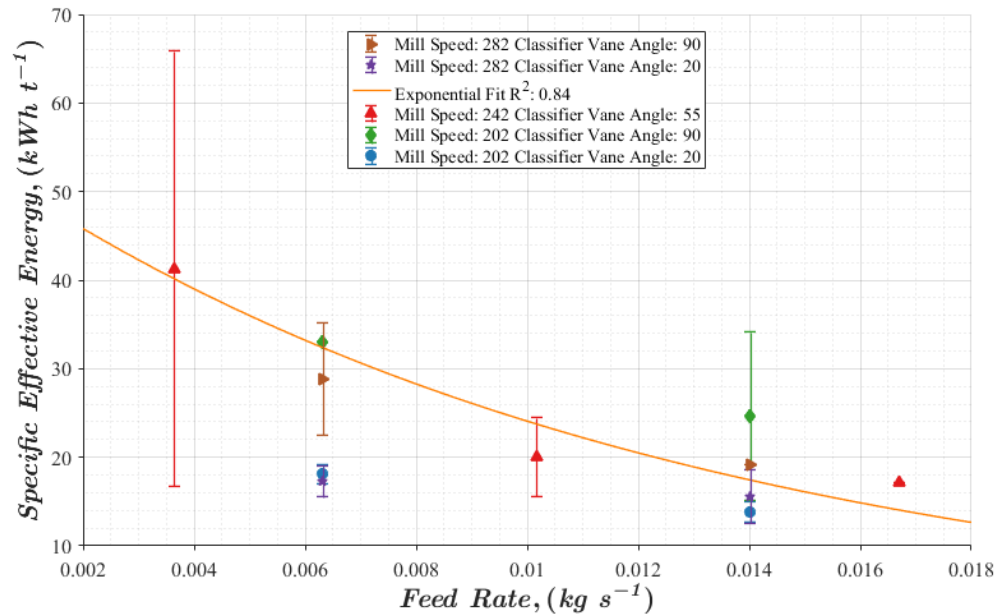


Figure 6.12 displays the Specific Effective Energy to mill the pellets at varying feed rates into the mill. A decaying exponential relationship is observed in increasing feed rates.

Energy requirements seem to be higher when the mill is fed at slower rates, this could be indicative of the action of material particle-particle interactions, friction between the materials particles may lead to a more efficient pulling apart of the material than that of the grinding elements. The rollers in the mill are made from aluminium and the table is made of steel, both surfaces are relatively smooth. As the biomass is broken down by the mill, dust is released that coats all areas of the mill but importantly the mill rollers and table, as well as smaller particles. The increased presence of the smaller particles and dust when the mill is fed at higher rates, could be helping the rollers and table grip the biomass particles and pull them into the comminutions zones, under each roller, more effectively than when there is less material present at the lower feeding rates. This suggests that different material used on covering the grinding elements could also increase the efficiency of grinding. Reviewing the running data from the mill for 2 of the experimental runs (figures 6.13, for 202 RPM, feed rate of 0.014kg s⁻¹ at a 90° vane angle, and

figure 6.14, for 202 RPM, feed rate of 0.006kg s^{-1} at a 90° vane angle) shows that there is a prolonged period of energy consumption that accounts for the higher consumption when the feed rate is low, approximately 65 more seconds of low energy consumption above the base line (marked as ‘Observed end of grinding:’ on figures 6.13 and 6.14). Air flow rates are not as consistent, as shown by the larger variation from the mean at each minute interval (the red lines on figures 6.13 and 6.14). This could all be explained by the lack of the extra material being there to provide the abrasive grinding mechanism between particles, which are then rejected by the classifier and returned to the table for further grinding. The slower dissipation of temperatures in figure 6.14 in comparison to the quick rise and fall in figure 6.13 (the yellow line), suggest that grinding is taking place even at the latter time periods of figure 6.14 which also suggests the presence of continued recycle.

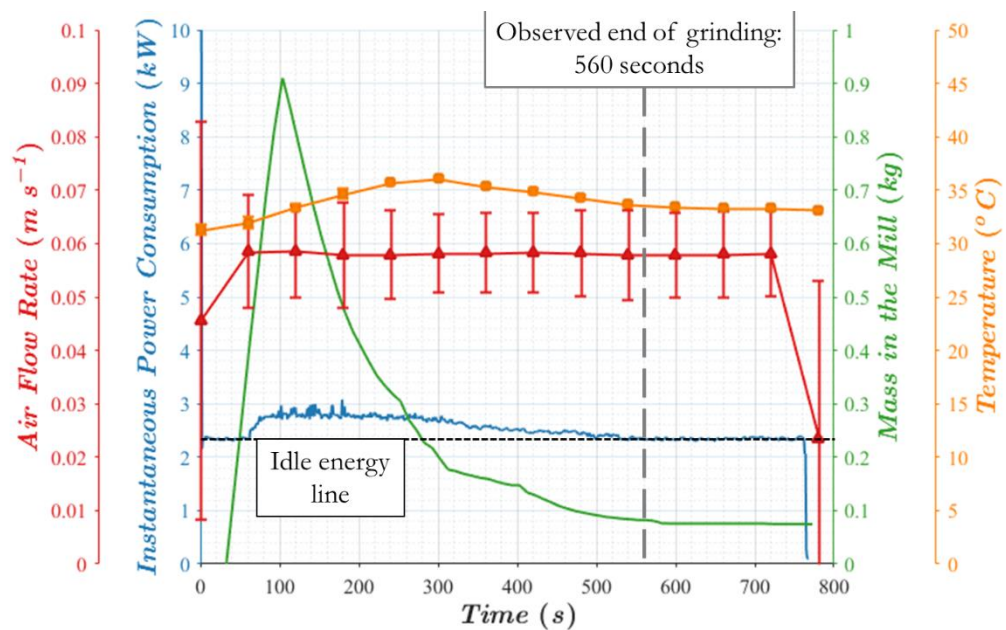


Figure 6.13 displays the running energy consumption, mass throughput, air flow and temperature for the 3rd experimental run of conditions whereby, feed rate: 0.014 kg s^{-1} , mills speed: 202 RPM and the classifier vane is 90° .

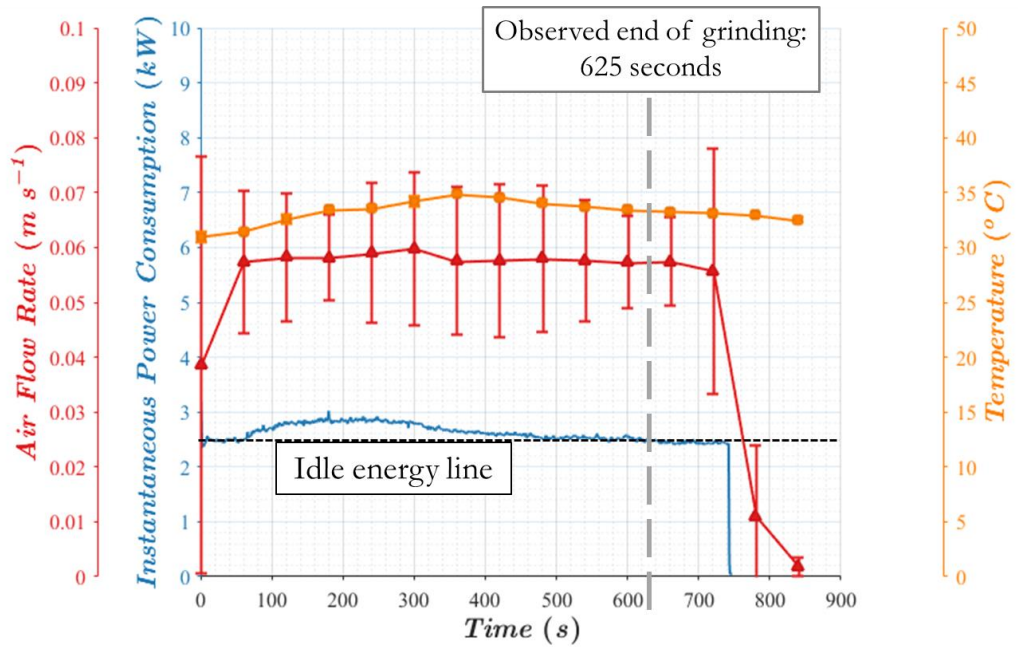


Figure 6.14 displays the 1st experimental run energy consumption, air flow and mill outlet air temperature for the running conditions of feed rate: 0.006 kg s^{-1} , mill speed: 202 RPM and classifier vane angle: 90° .

6.1.4 Response to Change in Classifier Vane Angle

Particle Characteristics

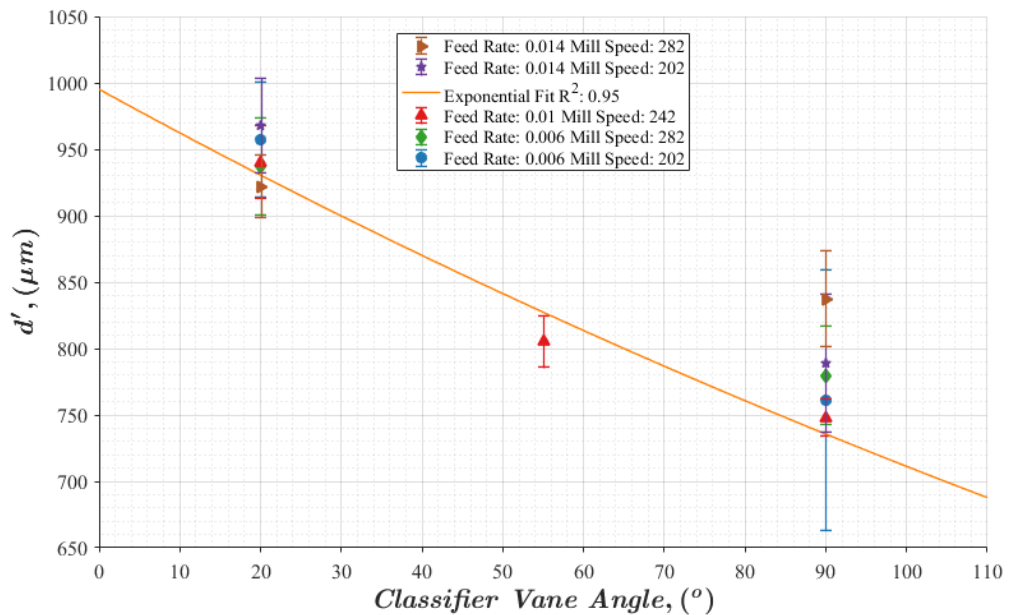


Figure 6.15 displays the variation in the Rosin-Rammler characteristic size variation with the classifier vane. The correlation seems strong as expected however it seems to be in a contrary relation to that which was expected.

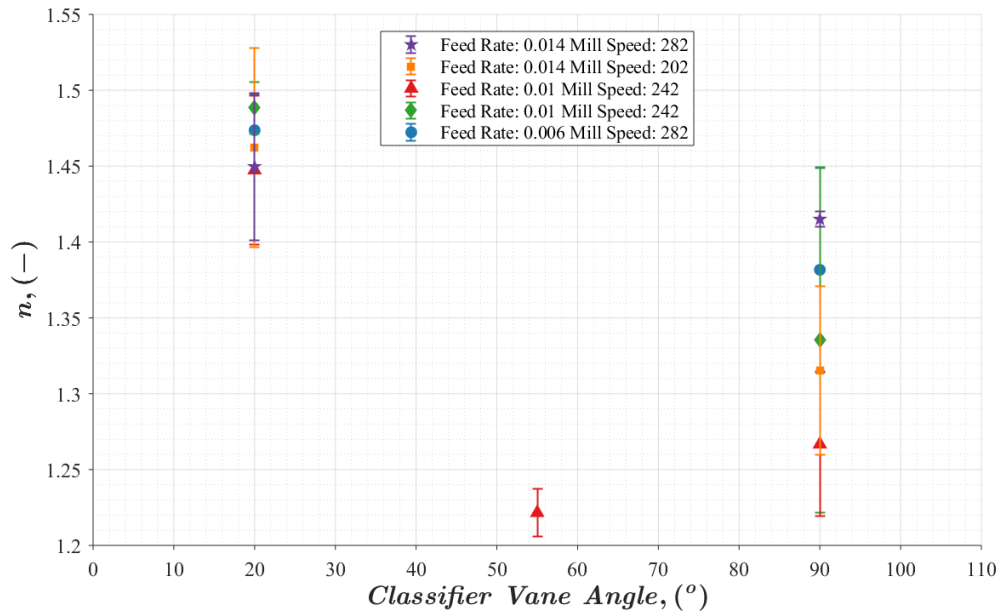


Figure 6.16 displays the variation in the Rosin-Rammler characteristic spread parameter with the classifier vane. The graph shows a narrower spread at smaller angles as expected, yet there is much higher spread of results with a fully open classifier vane.

The classifier vane angle seems to have a significant effect on the particle size, as expected. The effect seems to be directly in contrast to that expectation with lower particle sizes observed throughout the PSD achieved when the classifier vanes are fully open and higher when at only a 20° angle. A narrow spread (n) of particle sizes is observed at a narrower angle, this is following the expectation. The 90° angle however shows non-linear trends and could be dependent on other factors. One such possibility could be due to the concept outlined in figure 6.17.

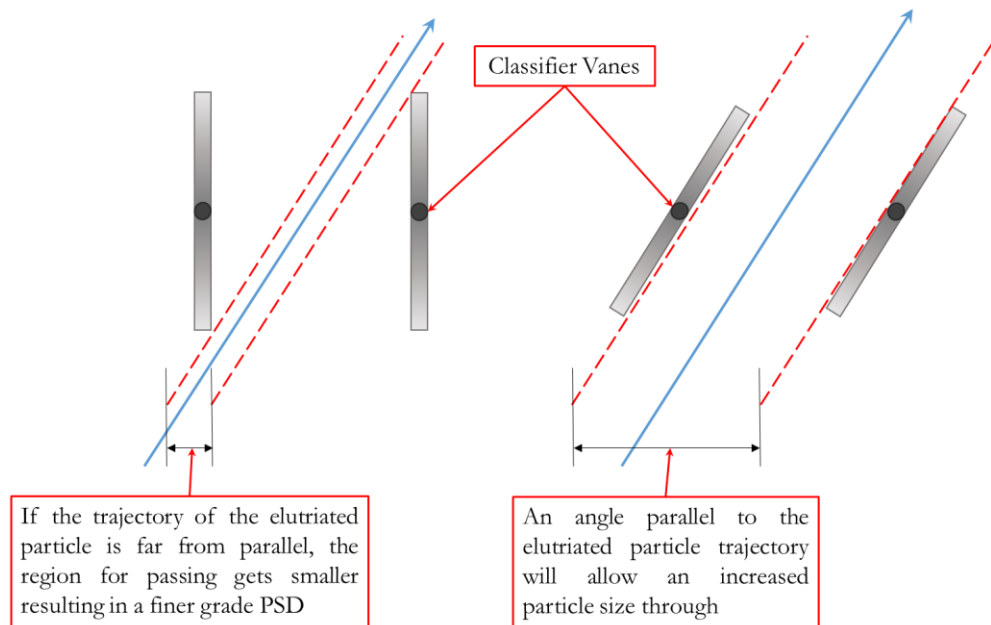


Figure 6.17 displays the concept of how the fully open classifier vane in the Lopulco mill might allow larger particles through when at narrow angles and reject them when fully open.

Streamline of the air flow through the mill are likely not to be vertical from the base of the mill chamber to the exit. This hypothesis of what is happening supports the CFD experiments completed in the research by Bhambare et. al. whose CFD simulations of a ring-roller mill at an industrial scale shows an acute angled streamline of the air flow (Bhambare, Ma, & Lu, 2010). With all the elements in the mill and the friction on the air flow caused by the mill table, the streamlines may be at angles that are better suited by the shallower angle of the vane (right of figure 6.17). Larger particles may have a greater chance of being knocked out of the air stream in the wider vane angle (figure 6.17, left). This does highlight that custom-made functions may be more appropriate for modelling rather than a general, one model fits all; this also leads to the conclusion that experiments with the classifier would be required to create a system model.

Mass Throughput

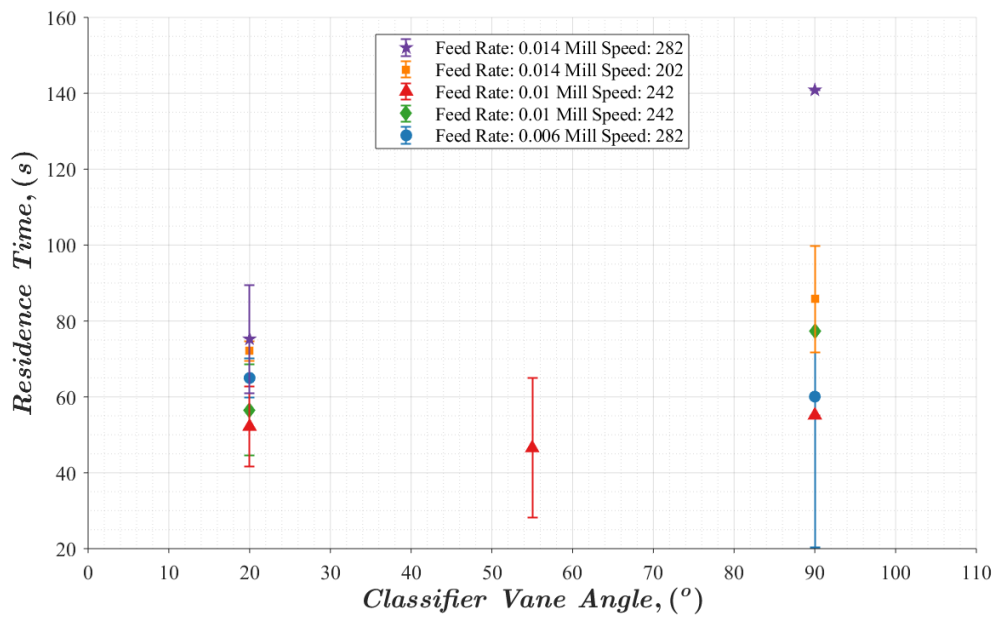


Figure 6.18 displays the variation in the residence time with classifier vane angle. It shows a consistent time except when the classifier is fully open, and a vast elongation when coupled with a fast mill speed.

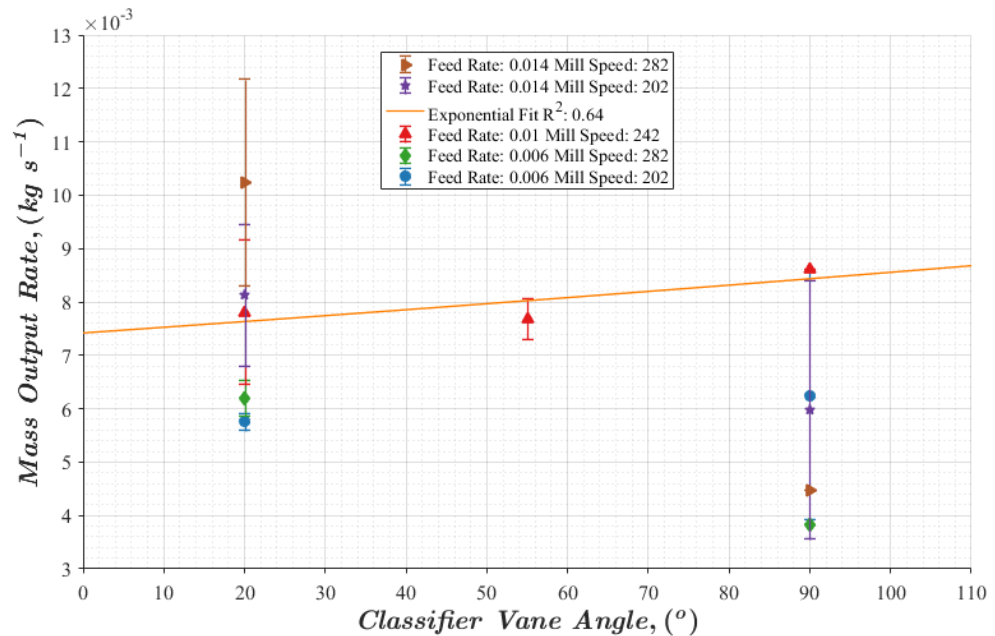


Figure 6.19 displays the variation in the mass output rate with classifier vane angle. It displays the only small variation until the vane angle is fully open at which point it seems to significantly slow the output when the speeds are high.

The effect of the classifier on residence time seems constant when the mill speed and feed rate are held constant, see figure 6.18, and variation looks to be dependent on other factors; feed rate shows to be more influential in these results which supports the conclusion of figures 6.5 and 6.10. At 90°, the combination of angle and mill speed significantly affects the residence time (again supporting figure 6.5 and 6.10). This is reflected by a much lower mass throughput when the speed is also high signifying the classifier is impeding mass output, see figure 6.19. This supports the theory that the classifier, with the 90° angle, is an inhibitor to particle passing.

Specific Effective Energy

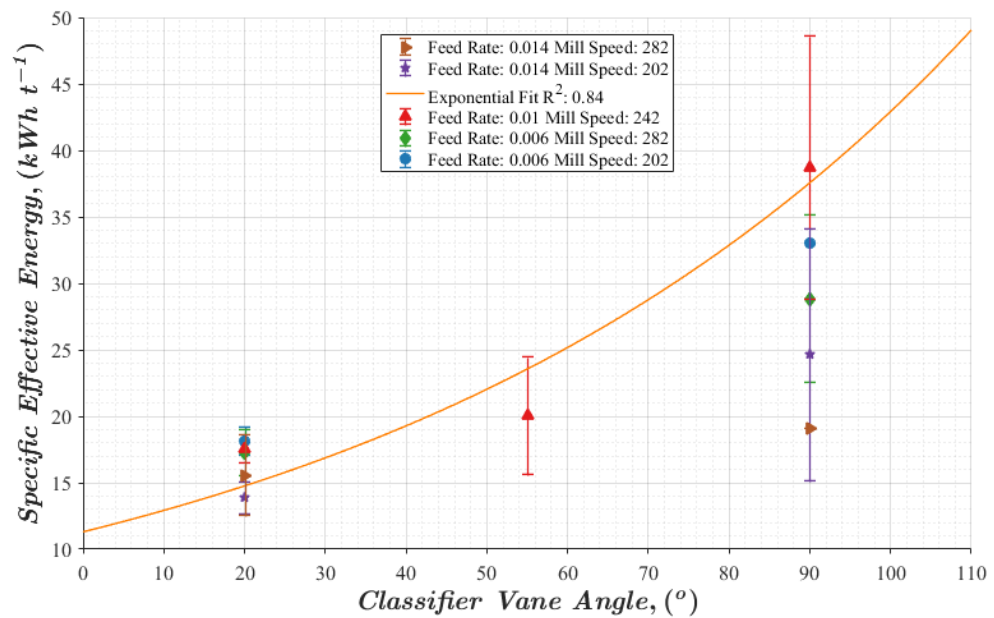


Figure 6.20 displays the variation in the specific effective energy with the classifier vane angle. It reinforces the evidence that material is staying in the mill longer with the fully open classifier and subsequently being milled for longer.

The response on the energy consumption shows that there is an upward trend as the classifier vane opens from the 20° to the 90°. This reinforces some of the other observations of elongated residence time and lower mass output at the 90° vane angle and provides reasons why there is a smaller output product size as the material has more energy focused on size reduction because of higher rejection rates from the classifier than at narrower angles.

6.1.5 Response to Fuel Type

Material variation in the mill is studied to see if there is a correlation between the material characteristics of the biomass fuel and the measures by which we are assessing the performance of the mill in grinding the fuel to the required product grade. This section looks to correlate the deformation energies, axial, diametric and flexure, taken from the sister project (detailed in table 6.1) with the product size, energy consumed in the transport of the material through the mill. Only 3 of the fuels, Eucalyptus, Microwave Torrefied and Miscanthus were available for the Lopulco experiments and were used in the deformation testing by the sister project.

Table 6.1 displays the deformation energies in the various orientations taken from the sister project for the biomass pellets used in the material variation Lopulco experiments.

Material	Diametric (MJ m ³)	Axial (MJ m ³)	Flexure (MJ m ³)
Eucalyptus	74.70	30.10	0.24
Microwave Torrefied	46.00	13.90	0.17
Miscanthus	47.80	28.30	0.21

Particle Characteristics

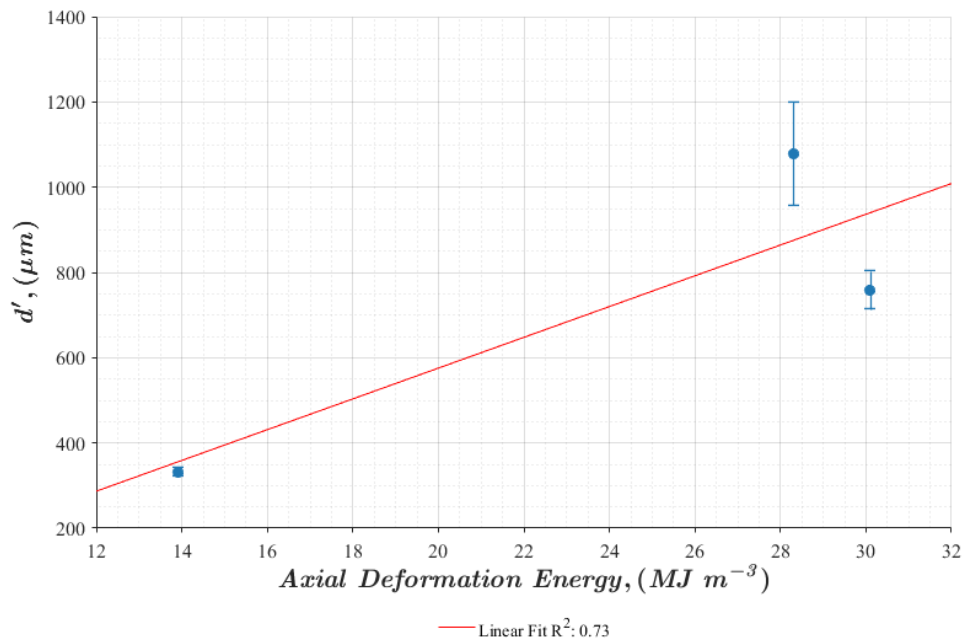


Figure 6.21 displays the variation in the Rosin-Rammler characteristic size with material axial deformation energy. The figure alludes to a possible relation.

Unexpectedly a relationship seems to exist between axial deformation energy requirements and the Rosin-Rammler spread parameter (n) as seen in figure 6.23, this could be due to how the rollers grip and crush the pellets, and the roller's load being applied inconsistently across the pellet, as opposed to diametric deformation energy requirements, that has the load in the test applied evenly along the length (see figure 6.24). A similar but less clear correlation can be seen in the Rosin-Rammler characteristic particle size (figures 6.21 and 6.23). Additionally, more abrasion may occur rather than compression on the pellets with a higher resistance to deformation. This could cause more intra-particle friction which is also an abrasion mechanisms, creating smaller more consistent progeny particles at later phases of breakage. Furthermore, if the axial deformation energy is high this suggests a tighter packing of the pellet when formed that leads to the higher mass of particles in the pellet that when released, increase the probability of this action. Understandably, flexure energy also seems to have some correlation with the particle spread parameter, n (see figure 6.24, in terms of the particle size though, it shows little correlation (figure 6.22).

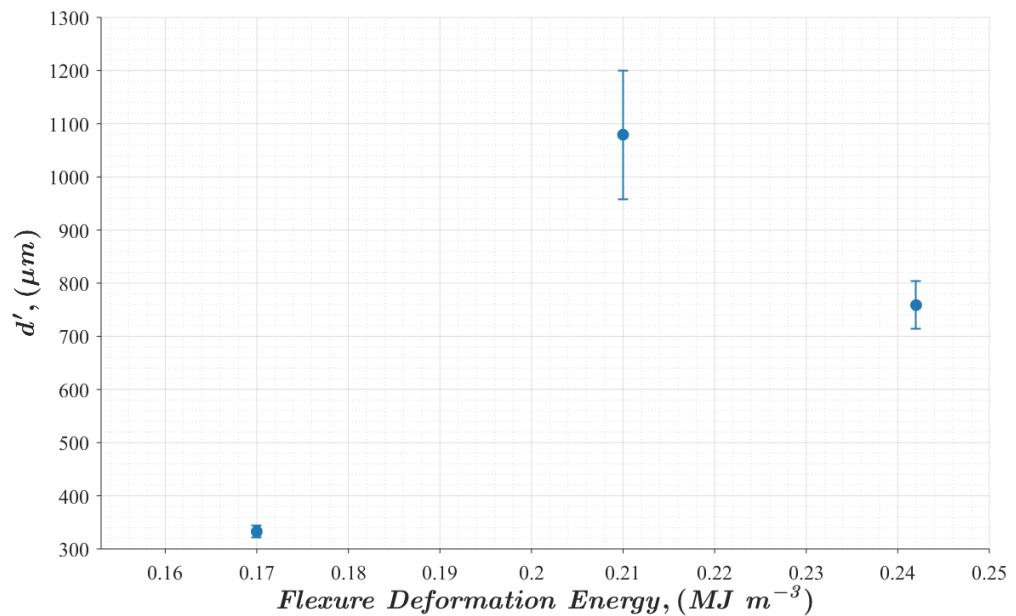


Figure 6.22 displays the variation in Rosin-Rammler characteristic size with flexure deformation energy. Here the relation seems to have far less relevance on the output.

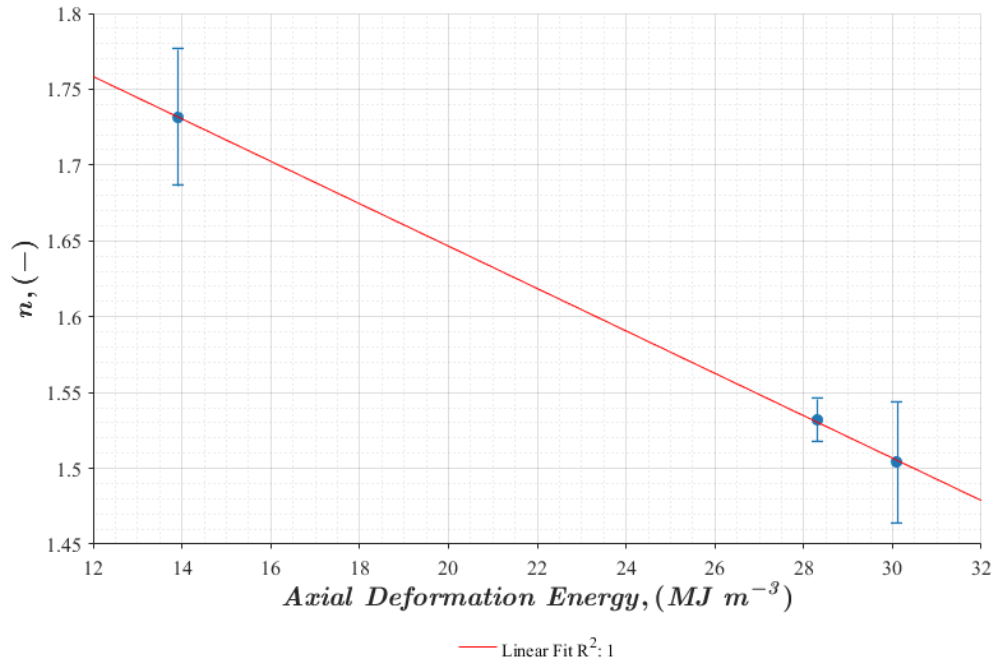


Figure 6.23 displays the variation in the Rosin-Rammler characteristic spread parameter with axial deformation. Here a strong correlation seems to exist.

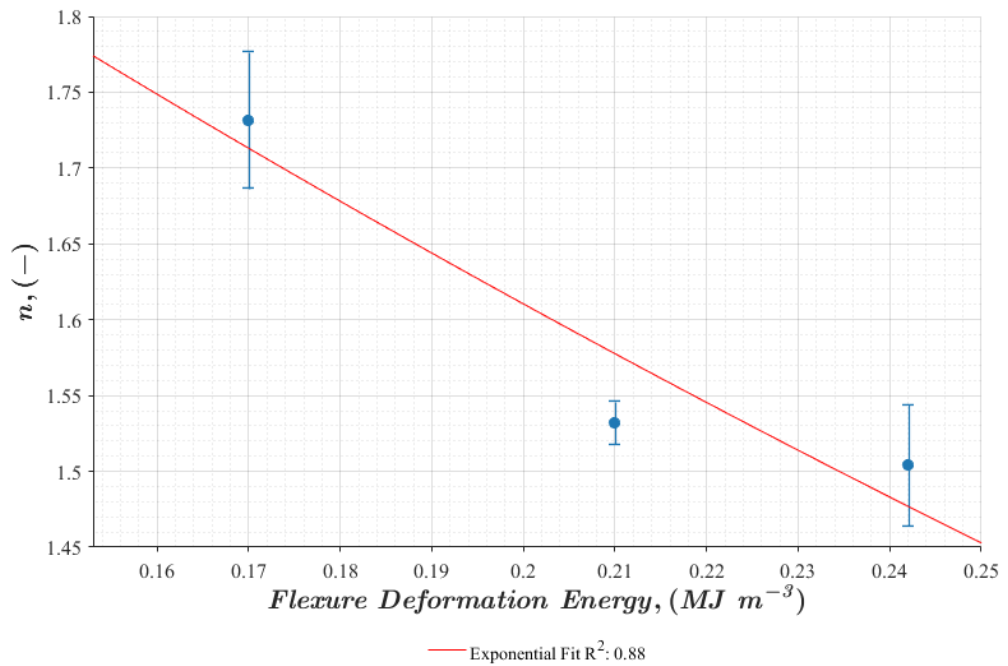


Figure 6.24 displays the variation in the Rosin-Rammler characteristic spread parameter with flexure deformation. Here again strong correlation seems to exist however it is not as strong as in figure 5.23.

Mass Throughput

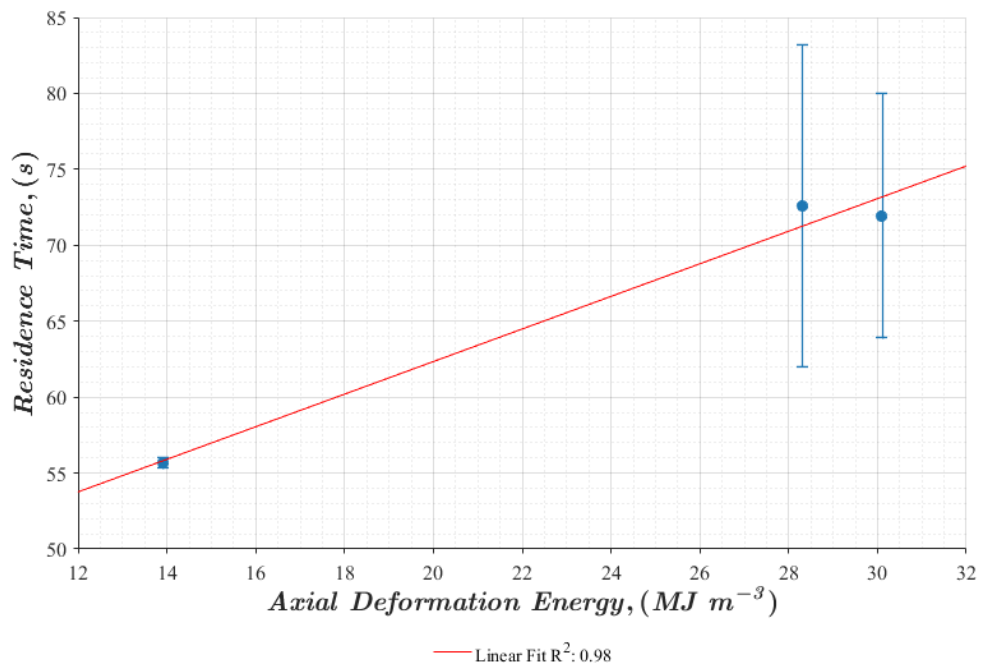


Figure 6.25 displays the residence time variation with axial deformation energy. A strong relationship seems present with this.

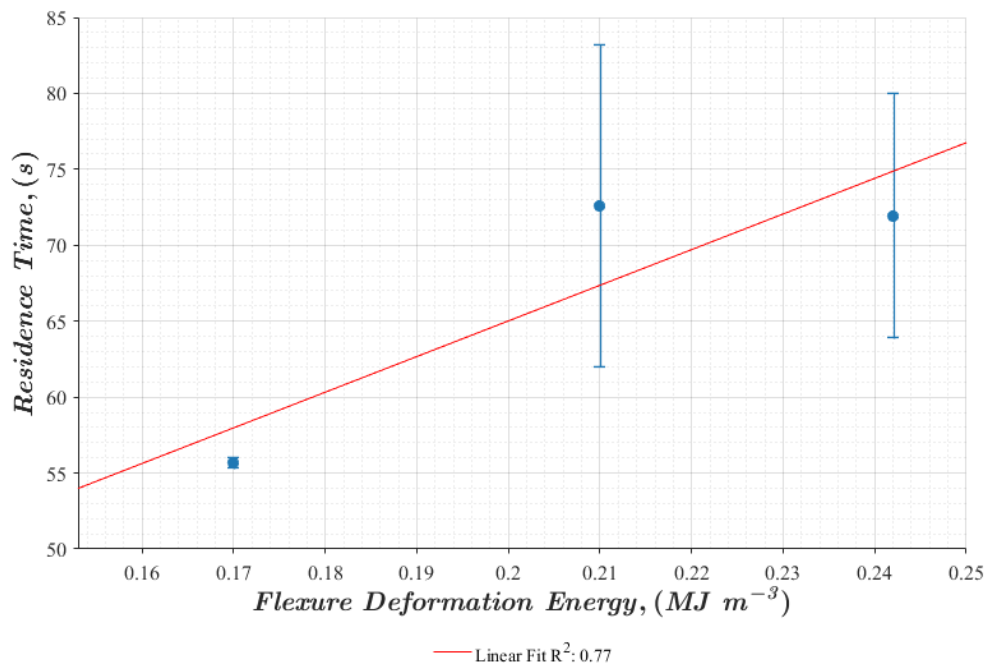


Figure 6.26 displays the variation in residence time with flexure deformation energy. Here again the relationship looks likely but not as strong as the axial deformation.

Figure 6.27 displays a conceptual diagram that explain how the axial deformation energy may correlate more to the product of milling with a ring and roller type mill than the other orientations from the material deformation testing.

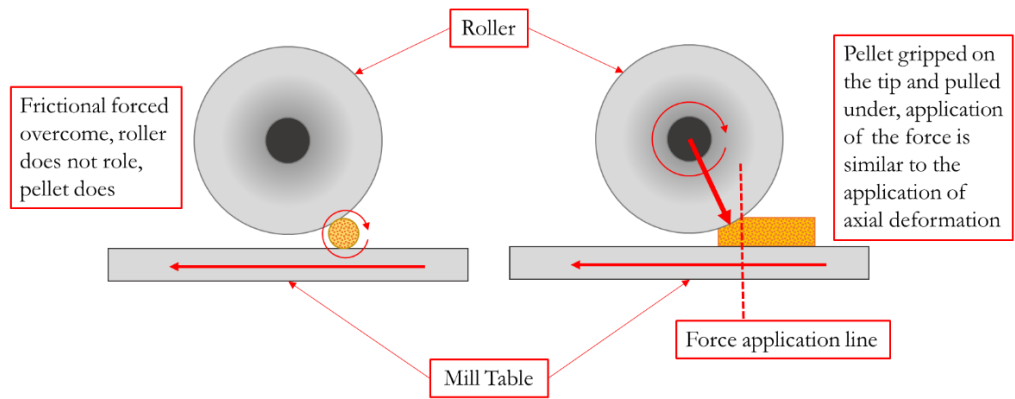


Figure 6.27 displays a conceptual diagram showing how axial deformation energy may provide better correlations with the product of milling over diametric deformation energy.

Evidence suggests that there is a correlation between the flexure deformation energy and residence time. In the other logical measure of deformation energy, diametric, which would seemingly be the way in which pellets would align with the grinding media in the mill, however no correlation seems present. Mass throughput is unaffected by the change in material.

Specific Effective Energy

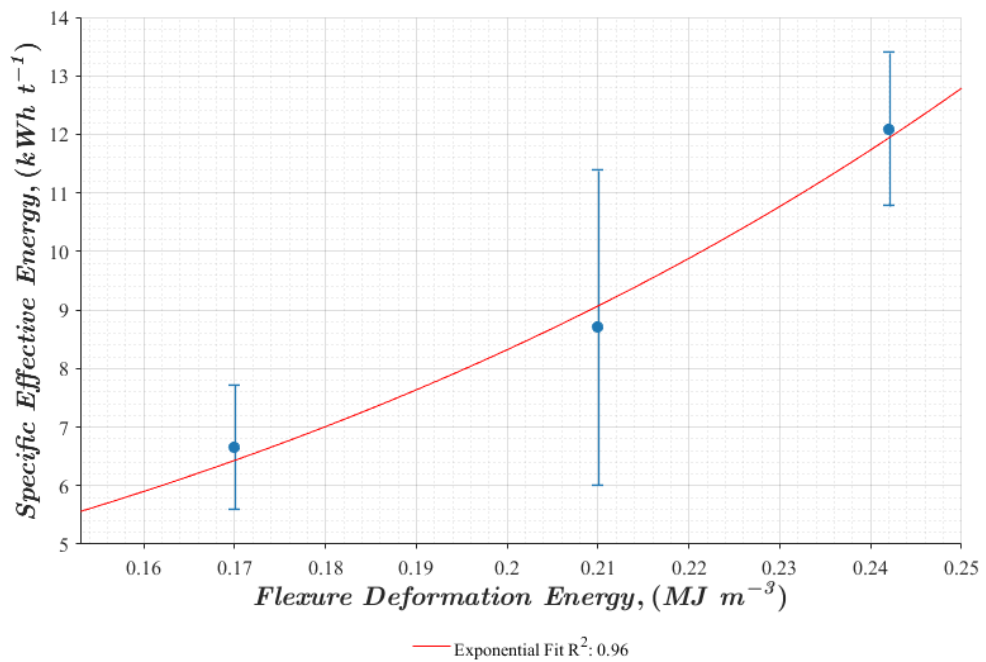


Figure 6.28 displays the flexure deformation energy variation with the specific effective energy. The results suggest that flexure energy provides good correlation in this regard.

All the deformation energy measures seem to have a reasonable relation with E_c , however the strongest is observed with flexure deformation energy. This is not unexpected given that all measures are resistance to compression, the mill operates in much the same way. In relation to the other observations here flexure has proved to also provide a reasonable correlation with the products of mill however axial seems more appropriate. The flexure test requires 3 points of application of forces. In the mill, it is assumed 2 from the mill table and roller however flexure energy could show that the interaction of other particles provides a pivot upon which flexure deformation could ensue.

6.2 Material Characterisation

As possible relationships seem to exist between the deformation energies and that of the performance in the Lopulco mill, further characterisation with even more fundamental tests were also completed. The deformation energy test, whilst looking to be useful may be only a small reduction in the experimental work required to complete milling trials and therefore may not be an advantage, relating the materials to less time consuming and more repeatable methods could alleviate

the experimental trials even further. Hence relationship was investigated between the deformation energies and the various other tests completed either in the sister project or through this one, see table 6.1 for details of the sources of the experiments.

Table 6.2 displays which tests were carried out as part of which project; this one, “Modelling of Biomass Milling” or the sister project, “On Biomass Milling for Power Generation”.

<i>Modelling of Biomass Milling</i>	<i>On Biomass Milling for Power Generation</i>
Skeletal Density	Particle Density
Surface Area	Deformation Energy

Several cross correlations have been observed to establish if this can be completed. Initial review shows that there may be some evidence of relation to the measured surface area and the axial deformation that builds upon the research already completed.

It is estimated that a lower surface area would indicate a more densely packed pellet and as it is expected that the lignin bonds of the pellets is where any deformation is focused, lower surface area would be correlated with a stronger pellet. This does not necessarily seem to be the case. Tested against the axial and diametric orientations shows that these differ. This could be due to the structure within the pellets; if particles are layered and packed in with the fibres orientated to span the diameter, axial compression would initially only close the volumes, somewhat like a spring. In contrast, application of the diametric compression would exploit those free space voids to squeeze them apart. This could be an explanation as to why the pellets increase in axial deformation when the surface area increases and reduces in the diametric orientation. The effect of skeletal density seems to be consistent with expectations that the pellet requires more energy in the axial orientation, however not in the diametric, which shows, albeit unconvincingly with the variation in the deformation testing results, that density seems to decrease the deformation energy required. This could be explained by increased lamination like formation of the pellet which shows anisotropic fracture mechanisms; somewhat like that of raw biomass yet in the alternative orientation. Further tests with micro-computerised tomography or something similar would show this.

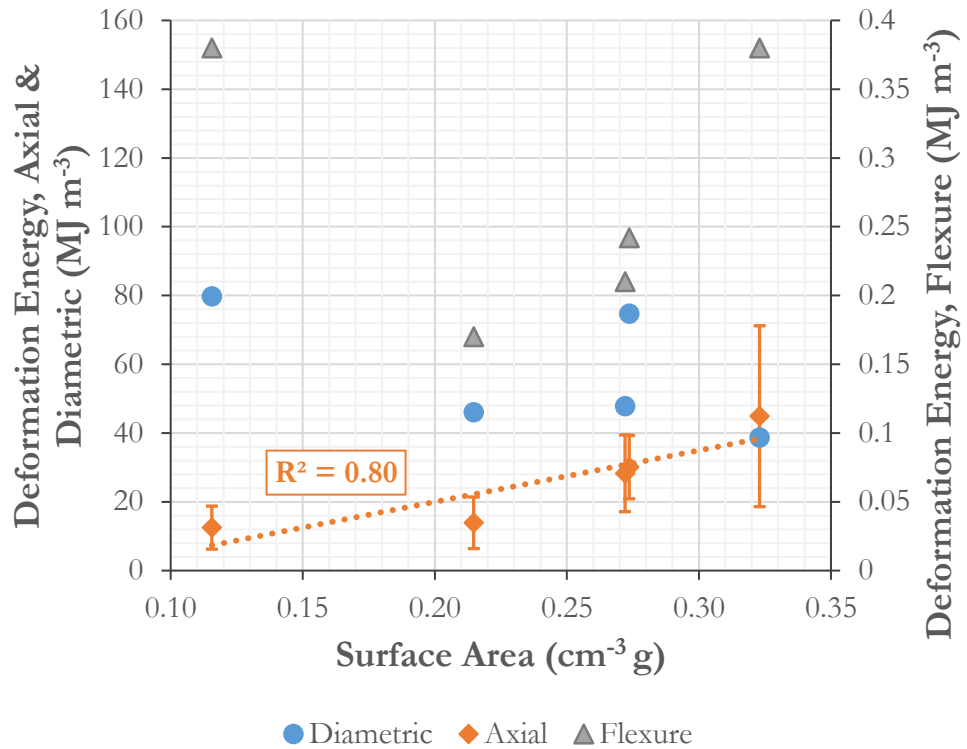


Figure 6.29 displays the variation in the deformation energies with surface area. As no relation with flexure is observed the error bars have been omitted. A reasonable correlation between the surface area and axial deformation energy is present.

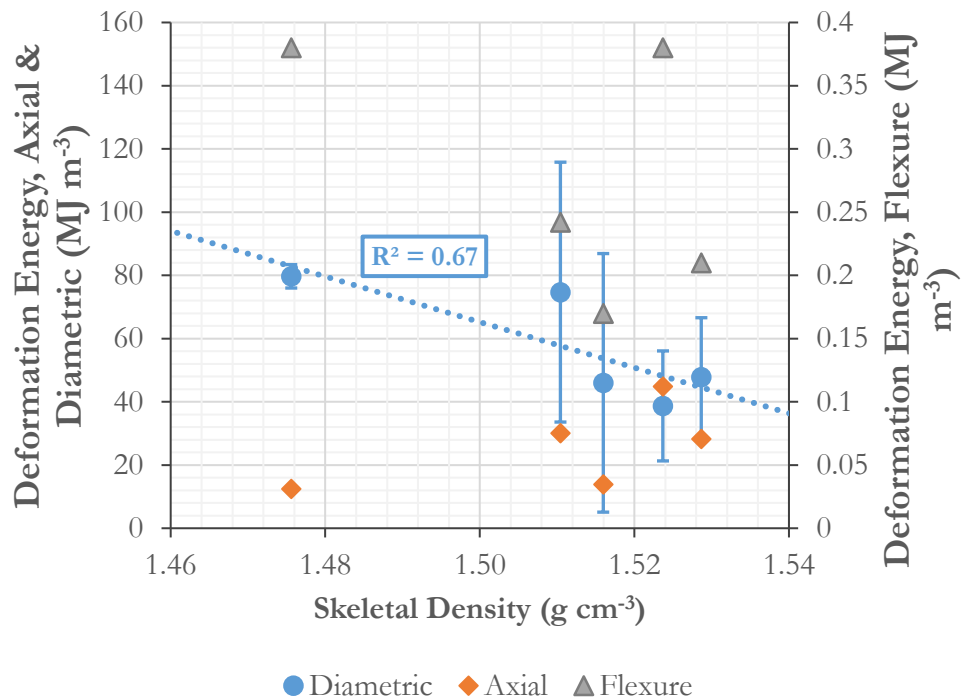


Figure 6.30 displays the deformation energy variation with skeletal density. Here potential relationships may exist with the diametric and axial deformation energies.

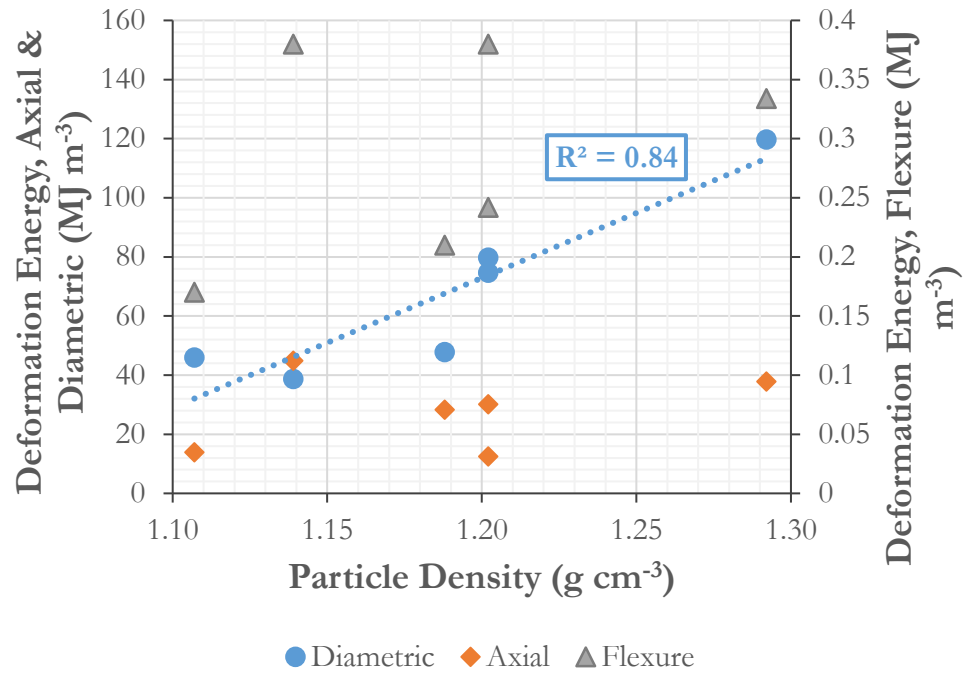


Figure 6.31 displays the variation in deformation energy with the variation in the particle density.

Despite some of the analysis showing potential correlation to the three measures investigated, the data does not look enough to draw definitive conclusions. So, the data will not be used in modelling efforts however it could be potential lines of investigation in any future work.

6.3 Conclusions

The first concluding note is that, despite attempts to do so, a steady state in the milling experiments could not be achieved. This is believed to be a problem with the hopper size of the mill and the lack of ability to continuously feed in material. Further to this it may be that the range on the mill table speeds may also not be sufficient to grind the material quantity at rates that support a steady input-output flow rate. The consequence is that data is not available upon which to model exact steady state data and allowance in any model prediction should include this as any error analysis.

The variation in E_e cannot be attributed to the residence time of the experimental run and must relate to some other factor. With this mill, the vane angle in conjunction with the mill speed affects the residence time and the E_e of

each run. Mill speed does, when in conjunction with a large classifier aperture, appear to affect the mass throughput and residence time. This is likely to be largely due to the classifiers rotation being fixed to the table speed along with the relation depicted in figure 6.17.

Mill speed seems to have little influence on the final particle size. This could be due to the pellet phenomenon, whereby the pellets are broken into the pre-pelletised state, coupled with the inability of this mill to adequately grinding the pellets further. There is subtle evidence to suggest that the interaction of mill speed and feed rate together is influencing the output product size through a complex relation based on both. As opposed to each affecting it individually. There may be evidence to suggest with this type of mill, that mill load may help increase the efficiency of grinding through improved comminution between material interactions as opposed to grinding element-material interaction. This could mean that the selection of the material for the lining of grinding media play a strong role in efficiency. An in-depth study of classifiers may be required for a greater in depth understanding as to how they work and what their optimal conditions are. This is concluded based on the seemingly counter intuitive behaviour of the classifier in these experiments. This is likely to be classifier type dependent. Due to this, for modelling efforts, a specific classification function, dependent on mill speed and counter to the expected behaviour should be developed; additionally, for each type of classifier study and development of its behaviour may be necessary before accurate models can be produced.

Basing modelling efforts on deformation energy looks as though it may have potential. Strong correlations to the axial deformation seems as though there may be a basis by which small scale material testing could provide insight into the performance of the mill. The data from the deformation testing has a large standard deviation, hence a large degree of error in a model could be present however if a more consistent material testing procedure is found this could be improved. In the meantime, though the axial deformation energy, where potential application has been explained, may prove suitable for modelling purposes.

It should be noted that an issue with the results is the high level of variation in results of the same conditions. Despite efforts to limit this, it is still large. The limitations placed on the design of experiment made increasing the number of

experimental runs impossible. The range of the experiment independent variables was a practical limitation of the mill; trial runs of the mill showed that if mill speed was too low or the combinations of conditions contributed to the mill chamber becoming too full, the mill would grind to a halt. Setting the range took several trials. The significance of this is that it shows that there is a balance to be found between the independent variables. Post experimental analysis suggests that a full factorial experiment would significantly improve the quality of the conclusions, and possibly at 4 levels rather than 3 to ensure the non-linear results of the dependent variables. Furthermore, the number of repeats for each experiment should be increased to reduce the variance in the experimental results; the higher number at the centre point shows that the results do become more consistent with more repeats. The variation could be due to a few reasons. The scale of the mill for which, in comparison to industrial scale mills, the grinding media to material ratio is low. This means the ability of the material to counter the objective of the mills is quite high, e.g. jam between roller and mounting arm, fall of the table before ground. Therefore, it is believed that modelling efforts of the future should be focused on industrial data, whereby the capacity and experimental run data would be much more consistent. In an industrial setting, the full-scale mills are less susceptible to issues with the size of the pellets in comparison to the feeding mechanisms or grinding media as they are much larger relative to the pellets. Additionally, the mills operate for hours if not days or months at a time with continuous feeding. This means that with little disruption to the process, the product sample can be collected from the mill outlet air stream and continuous energy samplings can be taken. By increasing the number of readings, the variance that is exhibited in the lab scale could be significantly reduced, leading to improved models.

Chapter 7 - Population Balance

Modelling Results

7.1 Model Validation

7.1.1 Discretised Matrix PBE

A simulation using the scheme outlined in chapter 4 has been created. Validation of the technique has been completed against results from literature using the same scheme as in (Petrakis & Komnitsas, 2017) along with the results for grinding experiments published in this paper. The BPBE simulation is validated using selection function 4, and breakage function 5 in table 7.1 and 7.2 respectively.

The exact parameter values obtained in the validating paper could not be matched, however the parameters were still optimised to within a high level of accuracy; details are given table 7.1. This could be a result of unspecified settings in the optimisation routine in MatLab™ or to the objective function, however they advise an R^2 correlation of 0.999 to linearised Rosin-Rammler distributions; using the OVL method similar accuracy is reported here (see figure 7.1 and table 7.2). The ability to optimise to the experimental results proves the scheme is capable of optimising to a PSD and is therefore determined as suitable for use.

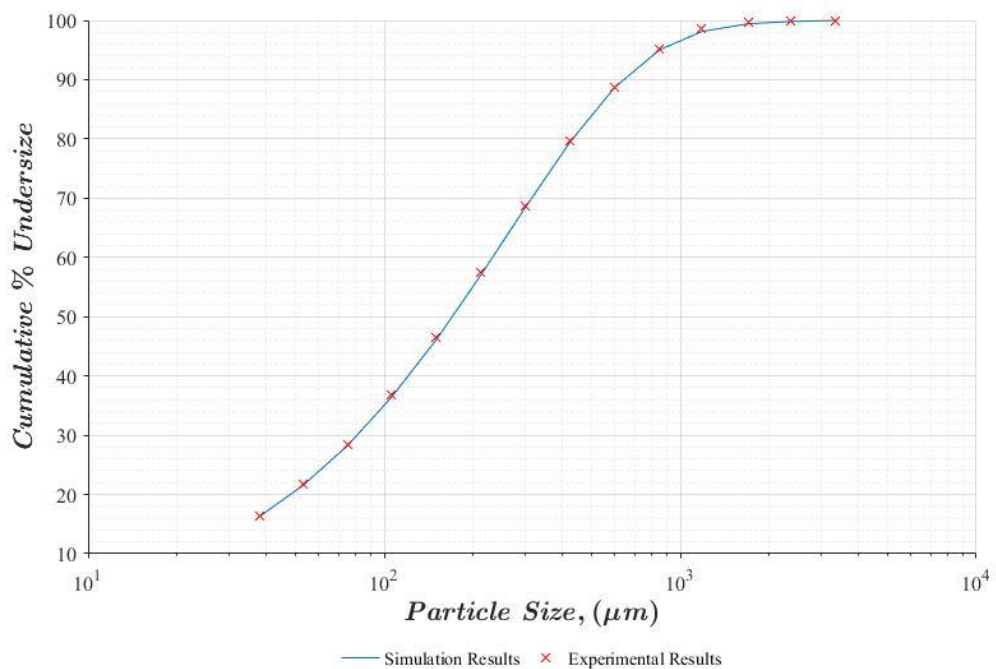


Figure 7.1 displays the validation of the Matrix BPBE model against publicised results for the same scheme.

Table 7.1 displays the selection functions used in the population balance equation simulations.

Selection Function	Function Code	Reference	Notes on parameters
$S_i = \left(\frac{x_i}{\mu}\right)^\alpha$	S1	Function designed by the researcher.	μ, α – fitted parameters
$S_i = 1 - e^{-\left(\frac{x_i}{\mu}\right)^\alpha}$	S2	Function designed by the researcher.	μ, α – fitted parameters
$S_i = A \left(\frac{x_i}{x_0}\right)^\alpha$	S3	(Bilgili & Scarlett, 2005b; Maxx Capece et al., 2011; Klimpel & Austin, 1977; Kumar Akkisetty, Lee, Reklaitis, & Venkatasubramanian, 2010; Petrakis & Komnitsas, 2017)	x_0 - largest size class A – Fitted parameter in the interval [0,1] α - Fitted parameter in the interval
$S_i = A \left(\frac{x_i}{x_0}\right)^\alpha \frac{1}{1 + \left(\frac{x_i}{\mu}\right)^\Lambda}$	S4	(L. Austin et al., 1976; Klimpel & Austin, 1977; Petrakis & Komnitsas, 2017)	x_0 - largest size class A, Λ, μ, α – fitted parameters

Table 7.2 displays the breakage functions used in the population balance equation simulations.

Breakage Function	Function Code	Reference	Notes on parameters	Notes on use
$B_{i,j} = 1 - e^{-\left(\frac{d_i}{\beta d_j}\right)^\gamma}$	B1		γ, β – fitted parameters	Defined by the researcher based on Rosin-Rammler distribution for particle breakage. Note: this is a cumulative distribution, for the implementation of the model a difference discrete integration is used in the form of: $B_{i,j} = b_{i,j} - b_{i+1,j}$
$b_{ij} = \phi \left(\frac{d_i}{d_j}\right)^\gamma + (1 - \phi) \left(\frac{d_i}{d_j}\right)^\beta$	B2	(Bilgili & Scarlett, 2005b; Maxx Capece et al., 2011; Klimpel & Austin, 1977; Kumar Akkisetty et al., 2010; Lee, Klima, & Saylor, 2012; Mazzinghy,	ϕ - a constant for normalised breakage systems and a value between [0,1]; $\gamma \geq \beta \geq 0$ – fitted parameters with a relation of	Note: this is a cumulative distribution, for the implementation of the model a difference discrete integration is used in the form of: $B_{i,j} = b_{i,j} - b_{i+1,j}$

		Schneider, Alves, & Galéry, 2015; Verkoeijen, A. Pouw, M. H. Meesters, & Scarlett, 2002)		
$b_{i,j} = \frac{1}{2} \left(1 + \tanh \frac{d_i - d_n}{d_n} \right) \left(\frac{d_j}{d_i} \right)^\beta$	B3	(Miguel Gil et al., 2015b; Vogel & Peukert, 2005)	d_n – is a minimum size class considered. β – fitted parameter	In literature β is lined to material minimum breakage energy and mill speed where used. Note: this is a cumulative distribution, for the implementation of the model a difference discrete integration is used in the form of: $B_{i,j} = b_{i,j} - b_{i+1,j}$
$\left(\frac{d_i}{d_j} \right)^\beta$	B4	(Frances & Liné, 2014)	β – experimentally fitted to the data	Note: this is a cumulative distribution, for the implementation of the model a difference discrete integration is used in the form of: $B_{i,j} = b_{i,j} - b_{i+1,j}$

$$b_{ij} = \frac{1 - e^{-\frac{d_j}{d_i}}}{1 - e^{-1}}$$

B5

(Broadbent & Callcott, 1956; Petrakis & Komnitsas, 2017)

Broadbent and Calcott model requires no fitting of parameters for the breakage however assumes that no variation in how the material breaks.

Note: this is a cumulative distribution, for the implementation of the model a difference discrete integration is used in the form of:

$$B_{i,j} = b_{i,j} - b_{i+1,j}$$

Table 7.3 displays the optimisation values to which the optimisation process back calculated the parameter values to. Included is a measure of the time taken to complete the back calculation and for providing a solution when handed a set of values.

OVL	A	α	μ (mm)	Λ	Time for Optimisation (seconds)	Time for Solution (seconds)
0.992	0.839	0.818	3000	2.143	8.534	0.168

7.2 Batch Process Model

Experimental results from the sister project using a Retsch PM100 are used to compare a simulation with experimental results for a batch process. The results are from an experiment whereby 100ml of biomass material was placed in a 500ml steel bowl along with 8, 30mm diameter steel balls and. The mill was then set going for 3 minutes at a speed of 300 RPM before the load was extracted and the particle size assessed. Five different biomass species selected from those described in appendix H were used: Eucalyptus, Microwave Torrefied, Miscanthus, Mixed Wood and Sunflower pellet. Figure 7.2 displays a top down view of how a planetary ball mill grinding mechanism works.

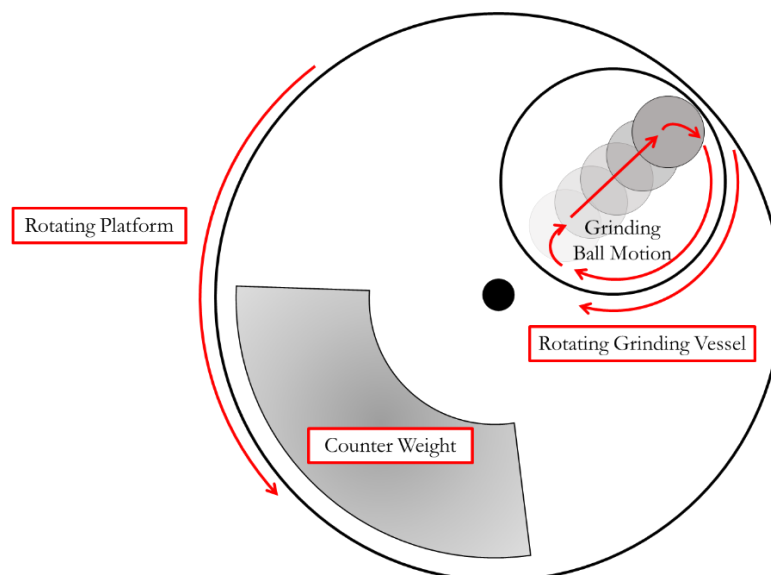


Figure 7.2 displays a top down conceptual diagram of the motion of a PM100 planetary ball mill. Material is only loaded into a grinding vessel with 8 stainless steel grinding balls that follow similar motion to that indicated. Loaded material is ground between the balls and the grinding vessel walls as well as through interactions with other material in there.

7.2.1 Determining Appropriate Selection and Breakage Functions, Batch Processing

Following the process outlined in chapter 4.7.3, initial optimisation to determine the optimal combination of selection and breakage function to use determined which of the functions was most appropriate to use in the simulations for the Batch system model. In figure 7.3 an example of the results of initial optimisation is shown for Eucalyptus pellet experimental runs and highlights the optimal model for this species. Such surveys were carried out for all biomass pellet species as listed above.

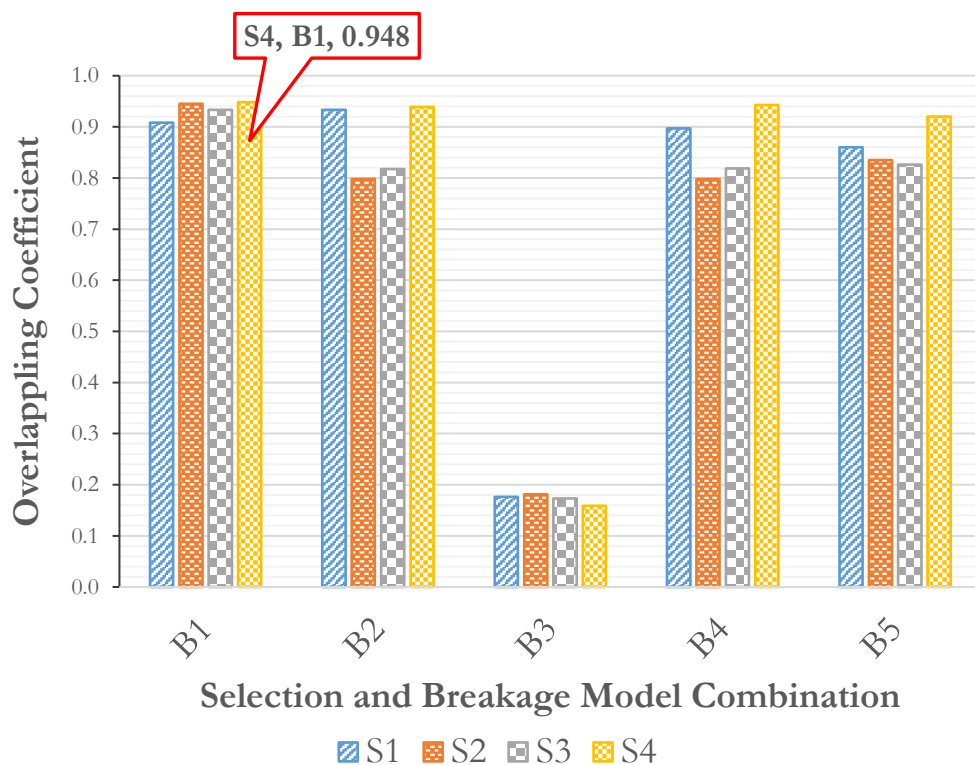


Figure 7.3 displays the OVL values for the initial back calculation of the parameter values for all the selection and breakage functions when trained against experimental runs for Eucalyptus wood pellets.

As table 7.1 shows, selection function 3 with breakage function 1 (S3, B1) appears in the top 3 performing models for 4 of the biomass species. Any model involving breakage function 3 performed poorly; this is believed to be a result of the constraints imposed on the parameter of the breakage function that are used to make the option a viable breakage function. Table 7.2 shows the output of the first optimisation run.

Table 7.4 displays the initial optimisation optimal models, along with the second and third ranked model for each biomass species.

<i>Biomass Pellet Species</i>	<i>Optimal Model</i>	<i>OVL</i>	<i>2nd Best</i>	<i>OVL</i>	<i>3rd Best</i>	<i>OVL</i>
Eucalyptus	S4, B1	0.948	S2, B1	0.945	S4, B4	0.942
Microwave Torrefied	S4, B1	0.964	S1, B1	0.931	S3, B1	0.920
Miscanthus	S3, B1	0.964	S4, B1	0.938	S4, B2	0.930
Mixed Wood	S2, B5	0.911	S4, B5	0.911	S3, B1	0.910
Sunflower	S3, B1	0.937	S4, B4	0.932	S4, B2	0.931

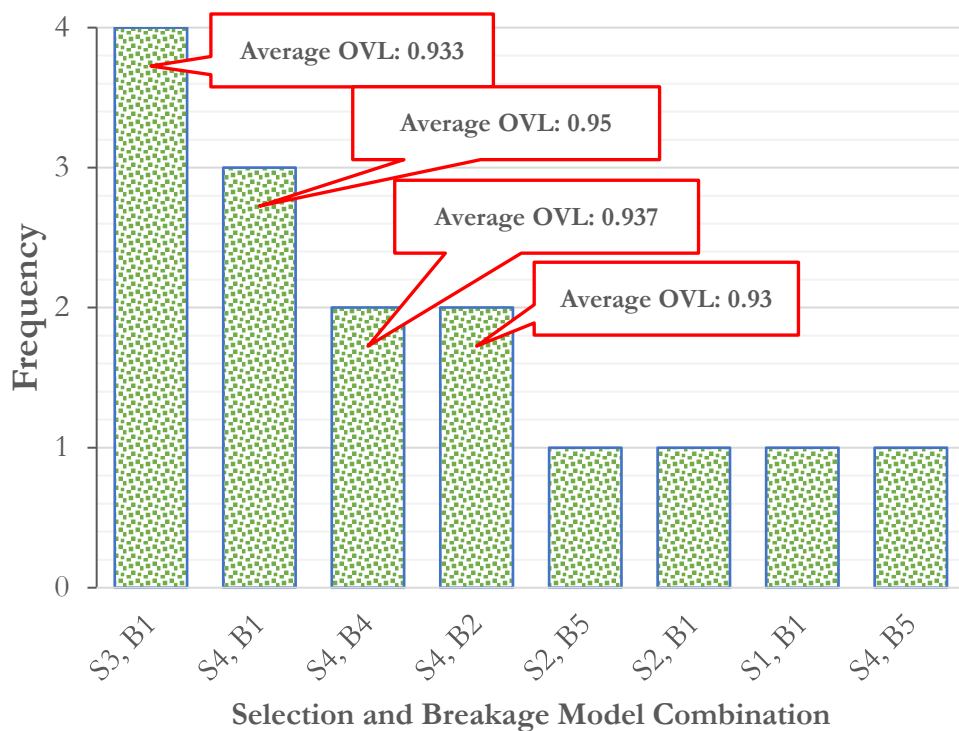


Figure 7.4 displays the frequency chart for the selection and breakage function combinations when optimised against the PM100 planetary ball mill experiments for raw biomass species. Included are the average OVL scores for the combinations of high frequency.

As the model S3, B1 performs the best and the average OVL is still reasonable in comparison to the best performing model combination (S4, B1) on an individual basis, this combination was chosen to proceed with the modelling efforts to determine the effect of material on the modelling parameters.

7.2.2 Extracting Material Differences, Batch Simulations

Continuing with the process of back calculation, the initial optimisation against all materials with the selected combination (S3, B1, see tables 7.1 and 7.2), produced reasonable OVL scores in the interval (0.91, 0.97). The ensuing study into the variation in the four parameters showed low standard deviations in parameters A and β . Hence an assumption was created that these, as they show low variation when the machine parameters are unchanged and only the material has changed, may be parameter values linked to the mill; constraint narrowing should then focus on reducing these parameters to constants.

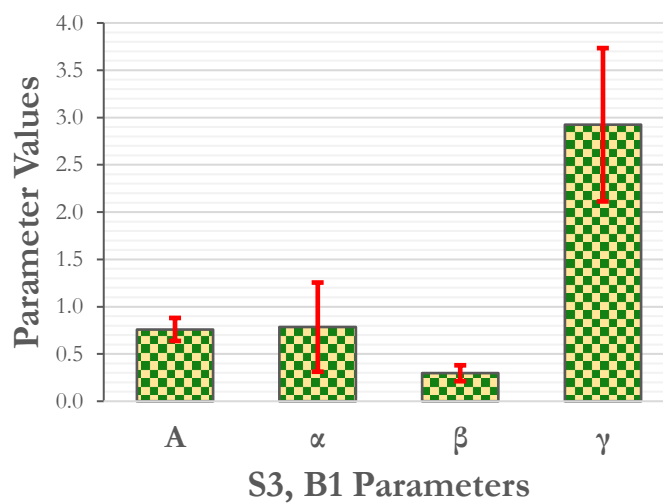


Figure 7.5 displays the parameter values for the 4 parameters of the selection and breakage combination S3, B1 to indicate the variance and why when studying the material difference effect on the parameters it was concluded to peruse parameters α and γ as material parameters.

Trials of fixed values for these two were completed to establish relations between α and γ based entirely on the material. Using deformation energy test results completed under the sister project, a basis of comparison was used to develop a relation between material characteristics and the values of the selection and breakage function parameters α and γ . Table 7.3 lists the values extracted from the sister project for the different mechanical deformation testing which have been used in this analysis to investigate the link of the material characterisation and the product of the mill.

Table 7.5 displays the deformation energies in the different axis for each of the biomasses used in the PM100 batch milling trials.

<i>Material</i>	<i>Diametric (MJ m⁻³)</i>	<i>Axial (MJ m⁻³)</i>	<i>Flexure (MJ m⁻³)</i>
Eucalyptus	74.70	30.10	0.24
Microwave Torrefied	46.00	13.90	0.17
Miscanthus	47.80	28.30	0.21
Mixed Wood	79.70	12.50	0.38
Sunflower	38.70	44.90	0.38
Steam Exploded	50.2	31.0	0.5

In the paper (Petrakis & Komnitsas, 2017) it suggested that parameter A in selection function S4, which is very similar in form to S3, is machine dependent and in the context of S3, the rate of breakage for the largest size class as opposed to a selected size, which this research adds evidence to. β did not follow the anticipated trend and influenced the optimisation of α and γ ; this suggests that β is linked to the material, and as a relation could not be attained for all 5 it must be concluded that β is linked to both the material and the mill. As it seems that β is linked to both the material and mill, constraints on its value were still imposed to limit its effect on the optimisation process and imposed to a range considered reasonable and in line with the other materials from the material variation experiments. The objective was still to provide a linear link to α and γ , whilst maintaining a reasonable degree of accuracy. A linear relationship was sought to create a simple model if possible that links the material deformation energy required to break the pellets with the parameters of the selection and breakage functions. Figure 7.6 displays the OVL scores through the steps of altering the constraints on β to achieve a linear relation in α and γ .

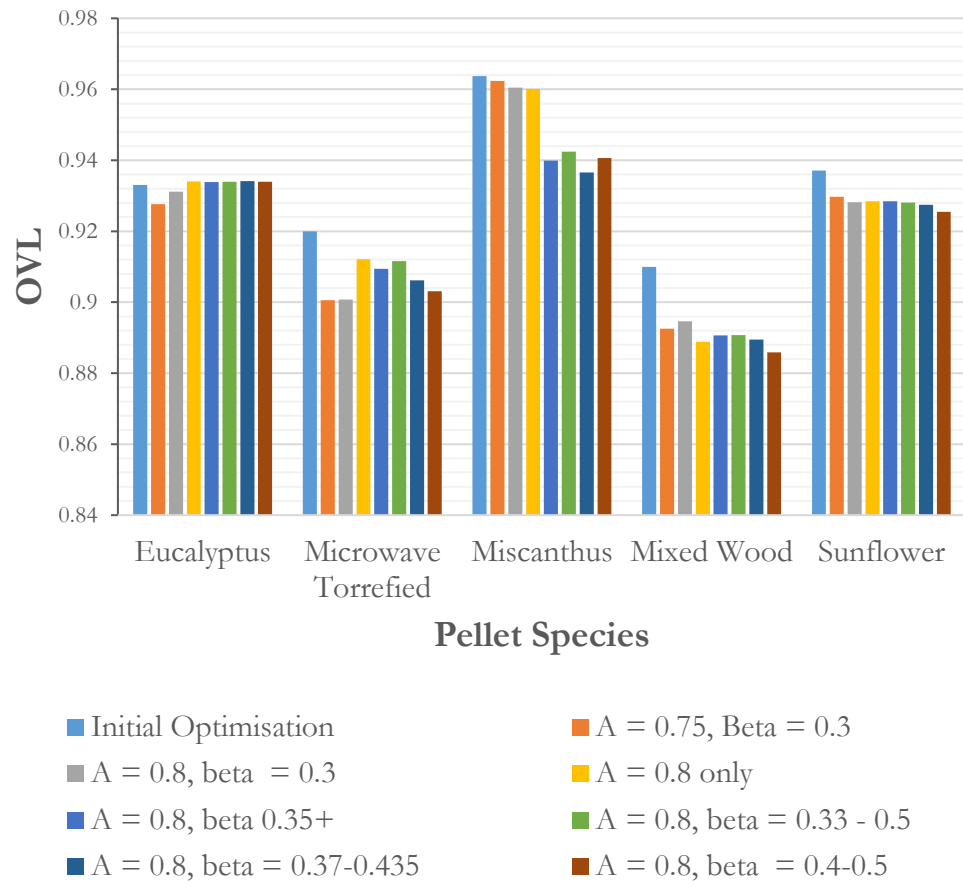


Figure 7.6 displays the evolution of the average OVL scores as changes to the optimisation constraints were imposed. It displays how independent OVL accuracy is sacrificed for the ability to improve the model for all species.

Analysis into the material variation assessment of α , β and γ provides evidence to the possibility of a linear relationship between α and γ with the deformation energy required to break the pellets through a 3-point flexure test (see chapter 5.3.1). Variation in how the model optimises suggests that although the simulations can find a link there may be other effects that may need to be considered that would require additional experimentation now.

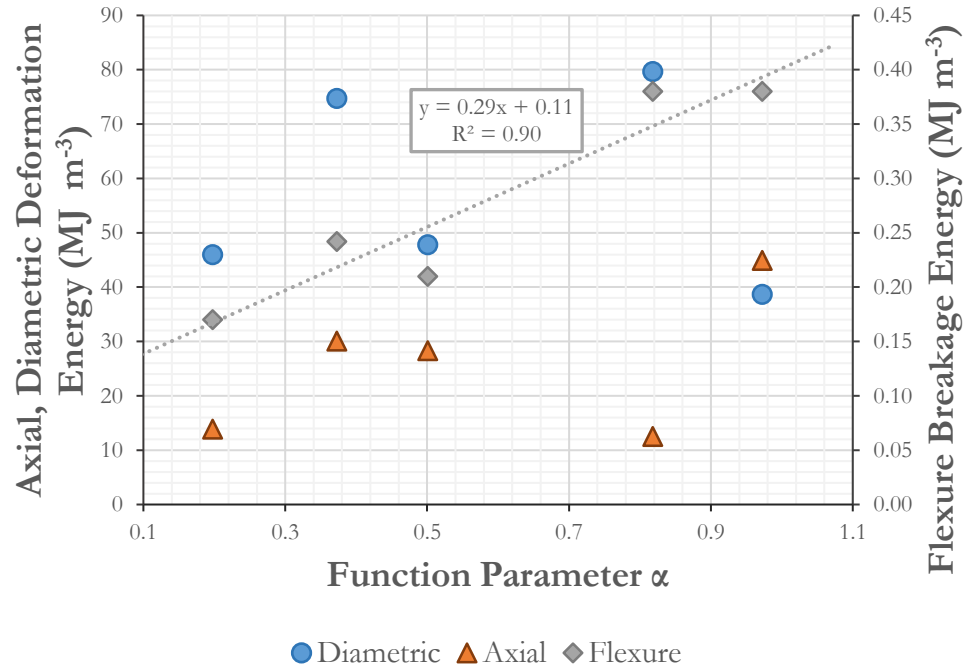


Figure 7.7 displays the study of the relation between the parameter α and the material deformation energy tests completed within the sister project regime. The final observations suggest a relation to the flexure deformation energy for this mill. Due to the strong relationship, it was hypothesised that that α may be material linked.

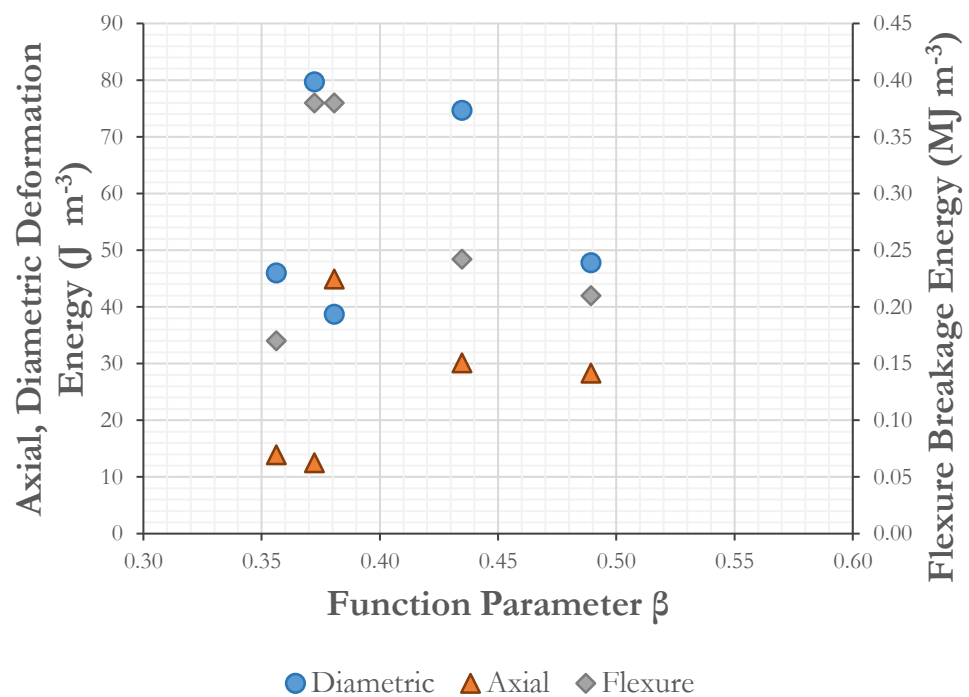


Figure 7.8 displays the final relationship observations between the deformation energies for each material with the initial optimised β parameter. It shows that there is not clear relation and why the decision to suggest β might be a machine linked parameter.

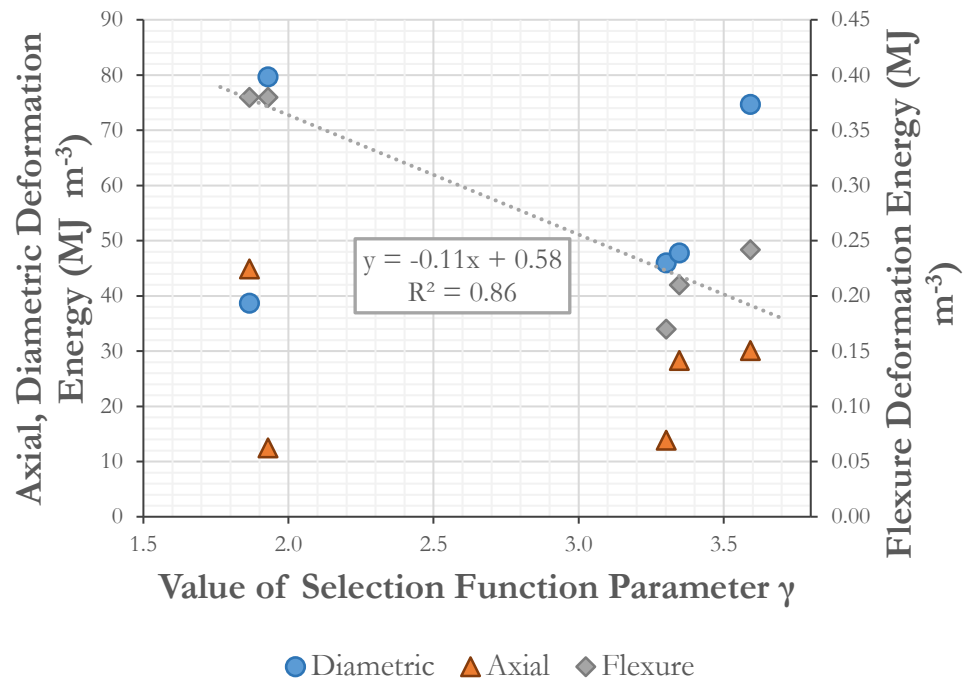


Figure 7.9 displays the final relationship between γ and the material deformation energies. Again, it shows a link between it and the flexure energy and reason to suggest that it is material linked.

Figures 7.7 through 7.9 show the relationships between α , β and γ and the 3 variations of deformation testing energies. It shows that the parameters α and γ seem to have strong correlations with flexure deformation energy requirements. Alignment as in figure 7.10 or similar between grinding balls and material load could be the cause of why the perceived relationship exists.

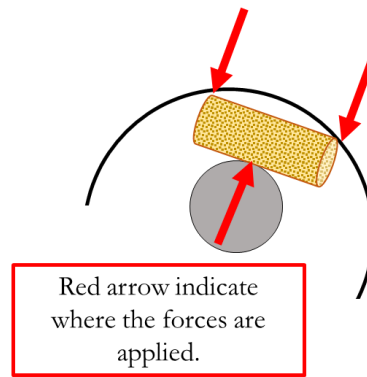


Figure 7.10 displays the concept of how the flexure deformation may be linked to the grinding mechanism in a planetary ball mill.

The schematic in figure 7.10 is a partial representation of a top down view for the grinding vessel of the PM100 with a grinding ball and biomass pellet. The application of the forces replicating those of a 3-point flexure deformation test (see figure 5.10) are also shown to highlight the similar breakage mechanism that could exist with this mill and the flexure deformation testing. From the analysis of figures 7.7 and 7.9 a relationship for calculating a value for α and γ linked to the flexure deformation energy requirements have been determined as in equations 7.1 and 7.2.

$$\alpha = \frac{E_f - 0.11}{0.29} \quad (7.1)$$

$$\gamma = \frac{0.58 - E_f}{0.11} \quad (7.2)$$

Having extracted relationships between the flexure deformation energy and the parameter values as calculated in equations 7.1 and 7.2 and inserting them into B1, an attempt at blind testing was made with a steam exploded pellet which proved unsuccessful. The use of the relationship for γ displayed a limitation in the theory. As $\gamma \rightarrow 1$, the exponential term in the breakage model begins to move towards $\exp(-1) = 0.63$. The breakage function then resolves to a value less than 1 which causes the simulation to calculate the mass output lower than the mass input. In most cases this is not a problem as when $\gamma \rightarrow \infty$, the term $\exp[-(1/\beta^\gamma)] \rightarrow 0$ and the losses become negligible. However, where flexure deformation energy requirements are in the extreme, such as with the steam exploded pellet, the model may be inappropriate as it displays this mass losing behaviour. Unfortunately, no

other data using another material was available with sufficient results to attempt a 2nd blind test.

7.3 Lopulco Milling Modelling

7.3.1 Classifier Function

The Lopulco mill as described in chapter 5.2 is a continuous throughput closed circuit mill, comprising of automated feeding through the screw feeder, grinding and classification of product and product output. To this end a routine that allows product to be removed is required and needs to provide of the true classification process.

For development of a classification function that recreates what is happening with the mill, the following conclusions must be considered:

1. The mill classifier behaves inversely to what is expected, i.e. a smaller particle size is seen with wider open vanes; a decaying exponential relationship is observed.
2. As expected, a narrower particle size distribution is created with narrower vane angles; again, a decaying exponential relationship is observed.
3. The effect of mill speed, which is linked to the rotational speed of the classifier, lessens the rate of decay in the exponential governing particle size.

To achieve this a simple model was created that fits the form of equation (7.3) designed to give a probability of passing based on particle size. The experimental results for the Rosin-Rammler d' and n parameters against classifier vane angle, ν , where variation with mill speed, ω , is also indicated, results were used to create an empirical relation for κ and Γ . Using Microsoft Excel's solver add-in, a basic optimisation for functions to govern them both was created and is given in equations 7.4 through 7.6.

$$C_i = \exp \left[- \left(\frac{x_i}{\Gamma} \right)^\kappa \right] \quad (7.3)$$

$$\kappa = 1.6 \exp(-0.002567v) \quad (7.4)$$

$$\Gamma = 1000 \exp(-0.003346v\xi) \quad (7.5)$$

$$\xi = -0.0002\omega^2 + 0.94\omega - 10.61 \quad (7.6)$$

It should be noted, that this empirical fit is proprietary to the mill in question and suggests that further study in to how classifiers of each type effect the product of mill. Additionally, there is an order of error in the function that requires further research. With the model used in this study a Chi-squared goodness of fit test was completed that provided a p-value of 0.071 determining the model is statistically significance at the 0.1 level which represents a 10% error rate in the model prediction.

7.3.2 Material Differences

In the first instance, the evaluation of the model as applied to the different biomass species has been conducted. The initial investigations followed the same principle as those for the batch testing and an analysis of different fuels as applied to different combinations of selection and breakage functions. Following initial optimisation S4, B1 proved to be the optimal model with 7 of 9 test cases achieving a higher OVL score with this combination. The only other model selected as the primary model was S3, B1. In the initial run of all biomasses optimised to S4, B1, whilst OVL scores were generally high, there seemed to be no clear start point for evaluating how the material affected the model parameters. Additionally, the optimisation of 6 parameters when many aspects are uncontrolled, coupled with a reasonably performing alternative model, a decision to not proceed with model S4, B1 was made. Tests were completed with S3, B1 which has already shown potential to extract the differences.

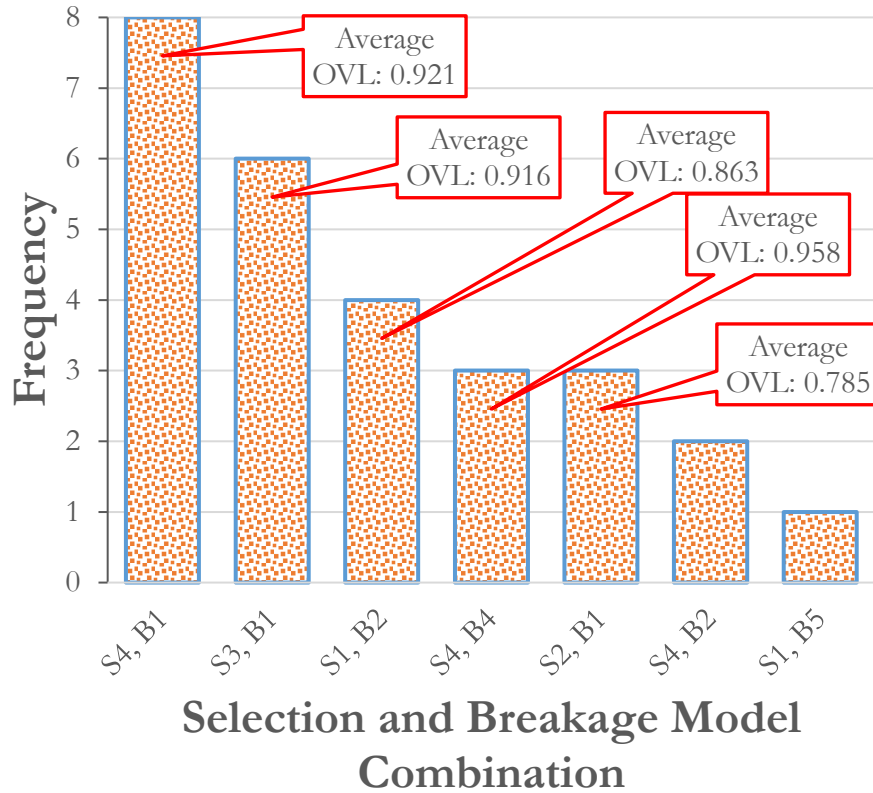


Figure 7.11 displays the frequency of the optimum selection and breakage models across the different biomass species when used under the material study for the steady state simulation.

Figure 7.13 and figure 7.14, the initial optimisation results with S3, B1. Even at the initial step several possible relationships emerged. These were between β and γ , and the axial and flexure deformation energies, which is consistent with some of the experimental results presented in chapter 6. No relationship was clear in parameters A and α .

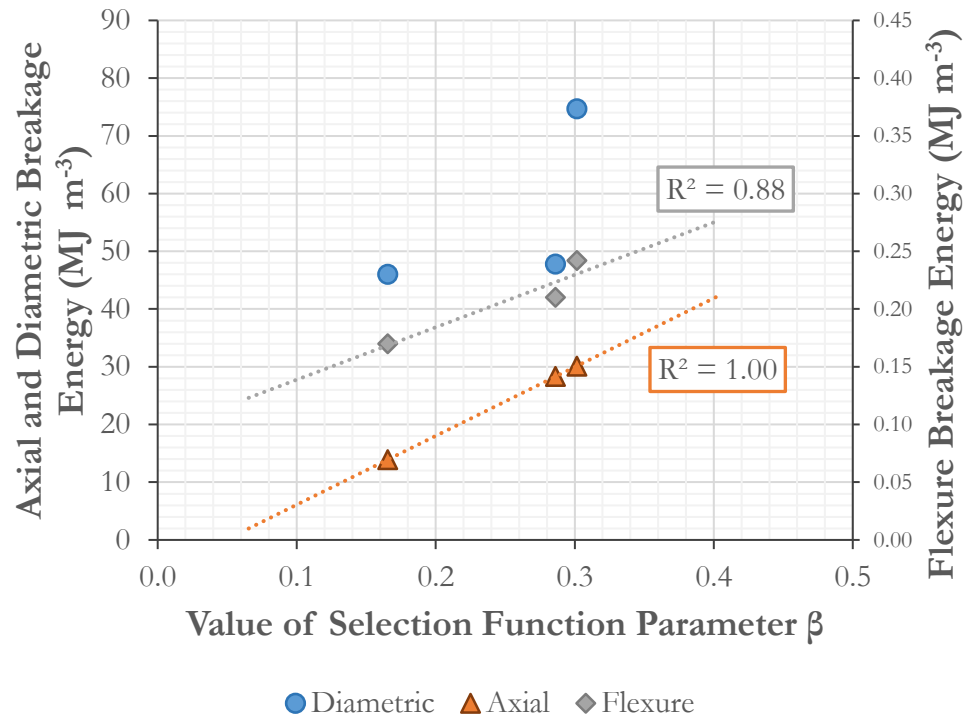


Figure 7.12 displays the relationship observations between β and the various deformation energies. Here a strong relation was initially observed between the axial and parameter β .

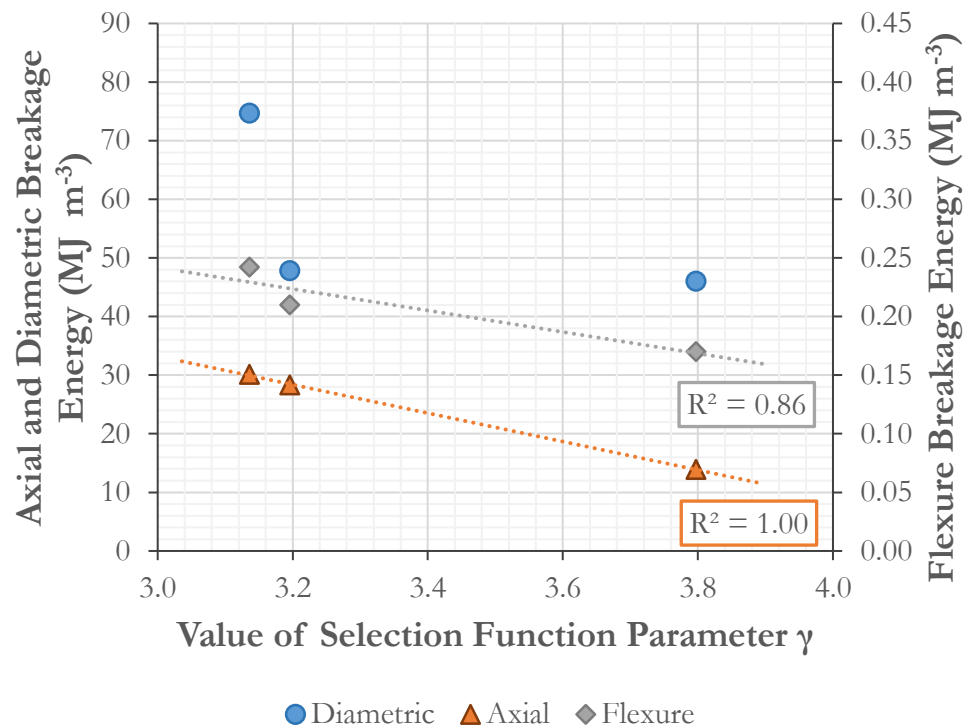


Figure 7.13 displays the initial relations between the parameter γ and the various deformation energies. Here a strong correlation was observed between γ and both the axial and flexure energies.

7 successive step changes to the constraints imposed on the model, designed to maintain these relationships whilst constraining A and α were taken. Provided the OVL scores stayed reasonably high, the change was accepted. The step changes can be seen in figure 7.14 along with new constraints that were applied at the various steps.

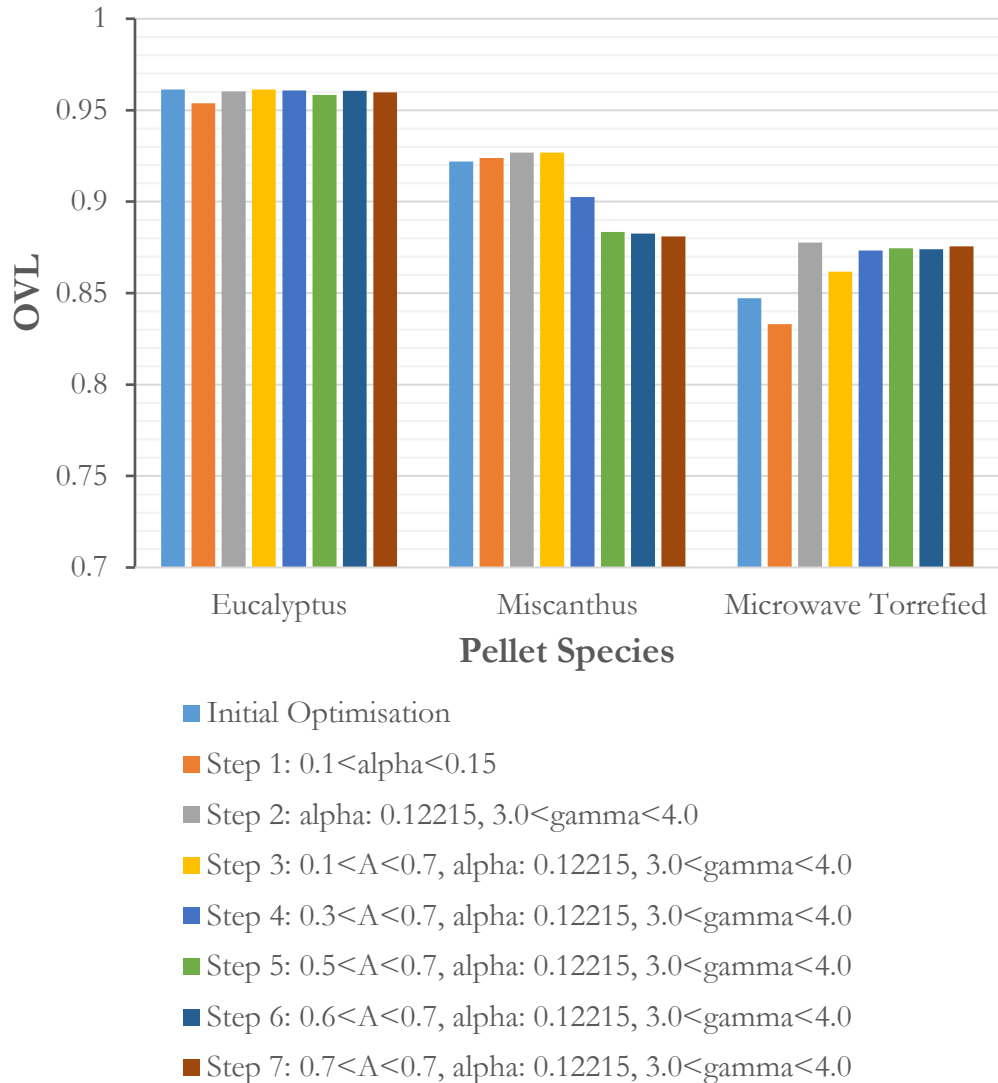


Figure 7.14 displays the progression of the OVL scores as constraints on the modelling parameters increased. It shows that the reduction in the model accuracy was manageable.

Whilst there is a reduction in the Miscanthus OVL accuracy, there is an overall gain in the Microwave Torrefied accuracy and the Eucalyptus stays constant throughout. Despite the loss in the Miscanthus simulations, the OVL still remains in relation to the overall OVL scores for which, all lie in the range of 0.87 to 0.96 by the end of the parameter setting process.

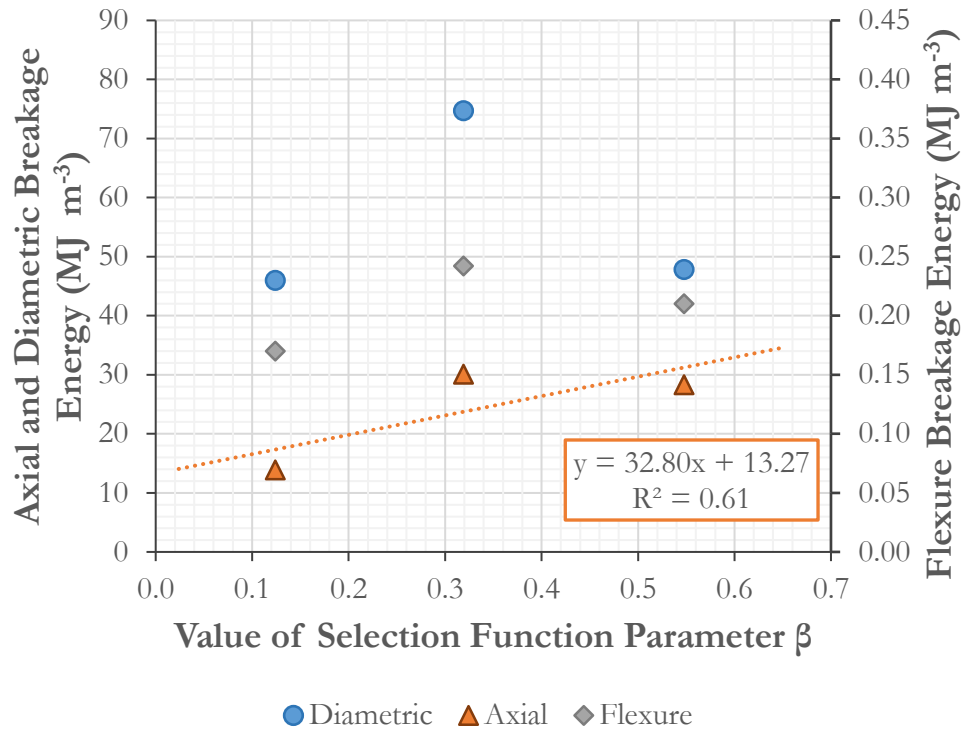


Figure 7.15 displays the relationships between β and the deformation energies after the 7 steps of optimisation, whilst the relationship is not as strong as it was initially there is still good evidence to use it as a potential model.

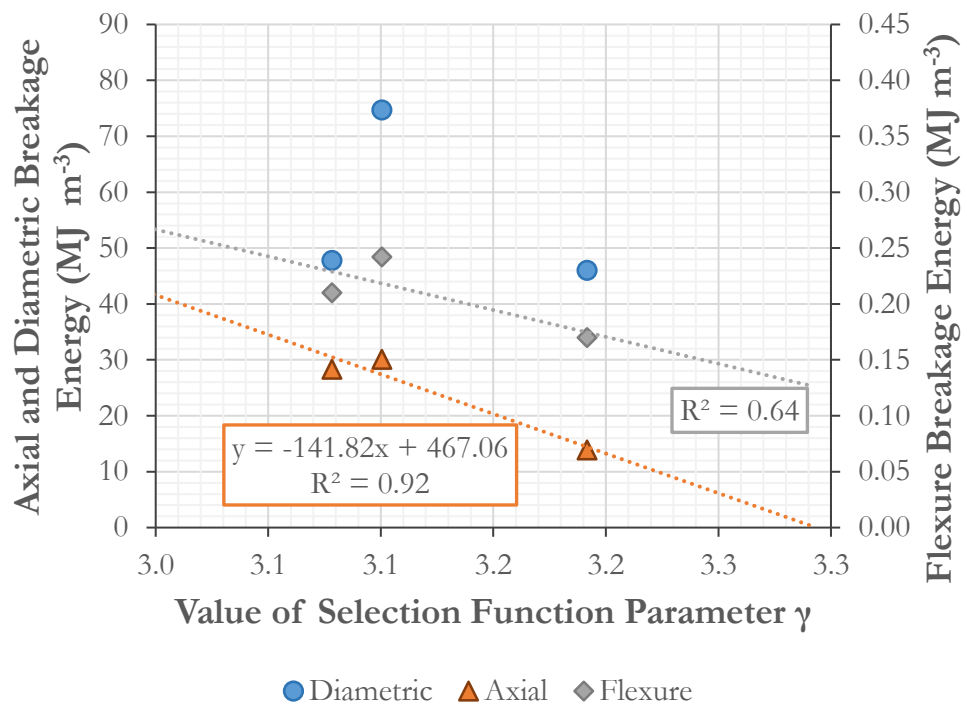


Figure 7.16 displays the relationship between the parameter γ and the deformation energies after 7 steps in optimising.

Progressing in such a manner to the final step, provided models based on material constants for β (see figure 7.16) and γ (see figure 7.17). The former has potentially more error (circa 39% as interpreted by the R^2 correlation) and as with the experiments at the batch process could indicate a small link with the machine characteristics. Table 7.4 summarises the data and models obtained for from the study.

Table 7.6 displays the values of the selection and breakage model parameters established after the optimisation programme for material differences has been completed. x indicates the axial deformation energy.

A	α	β	γ
0.7	0.12215	$\beta = 0.0305x - 0.405$	$\gamma = 3.293 - 0.007x$

7.3.3 Operational Difference

Using a standard pellet, Brites wood pellets, operational effects of the mill were studied. Brites pellets have an axial deformation energy of 37.8 MJ m^{-3} which was tested in the sister project, with a standard deviation of 16.5 MJ m^{-3} and implemented using the models for β and γ as given in table 7.5. The data used to train the model included the data from extreme points and centre point from the experimental process as outlined in chapter 5.2. Where some of the repeat experimental runs showed high deviation from the other 2 runs at the same conditions, the data was excluded from the model training process. By excluding these results, overall accuracy was improved when blind tested against the corner point experimental conditions from the CCC DoE.

Table 7.7 displays the initial optimisation values for the operational differences study into the parameters for the selection and breakage model S3, B1 as was as the initial constraints on them.

	A	α	β	γ
Initial Parameter Values	0.7	0.12215	0.7479	3.0265
Initial Parameter Limits	0.1 – 1.0	0.01 – 5.0	0.7479	3.2065

Using the same S3, B1 model, simulation output is evaluated against the runs from the operational condition experimental results. Using the values from table 7.5 for A and α as initial parameter values, and the models for β and γ , the initial optimisation of back calculated parameters for A and α began.

Initial optimisation over A and α only to see variation in the model due to milling operational conditions provided immediate potential relations in both A and α (figure 7.18). Whilst the initial results showed promise in identifying some relationships, the average OVL was below 0.70, therefore a relaxation on the constraints of β , where potential errors in the material modelling were identified, was made.

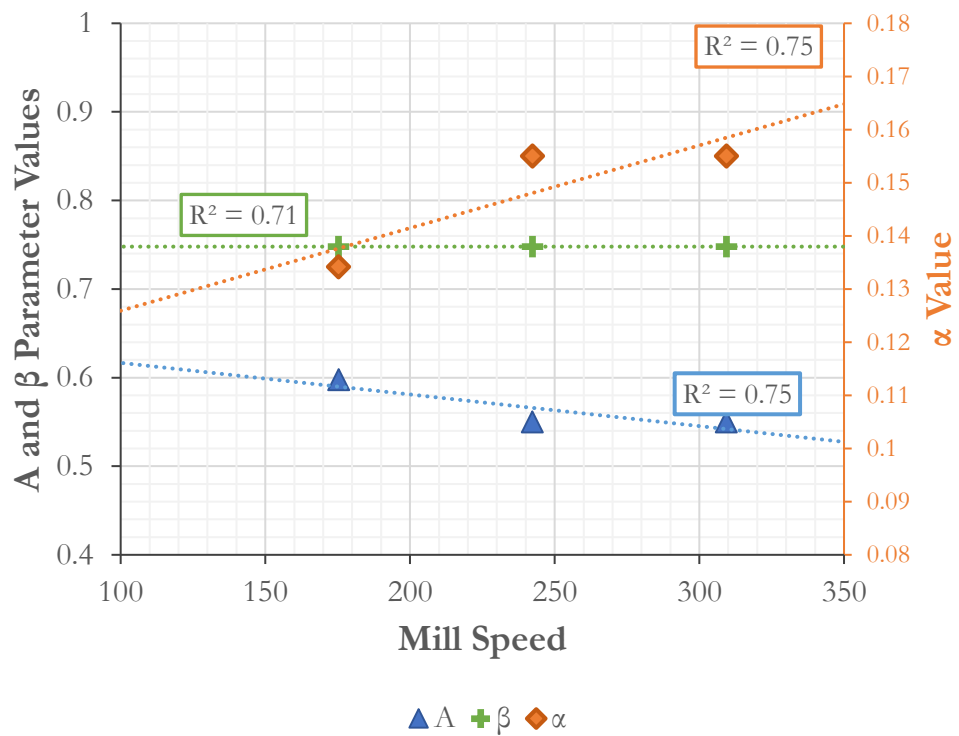


Figure 7.17 displays the relationships of the mill speed to the S3, B1 PBE model parameters after initial optimisation over A and α .

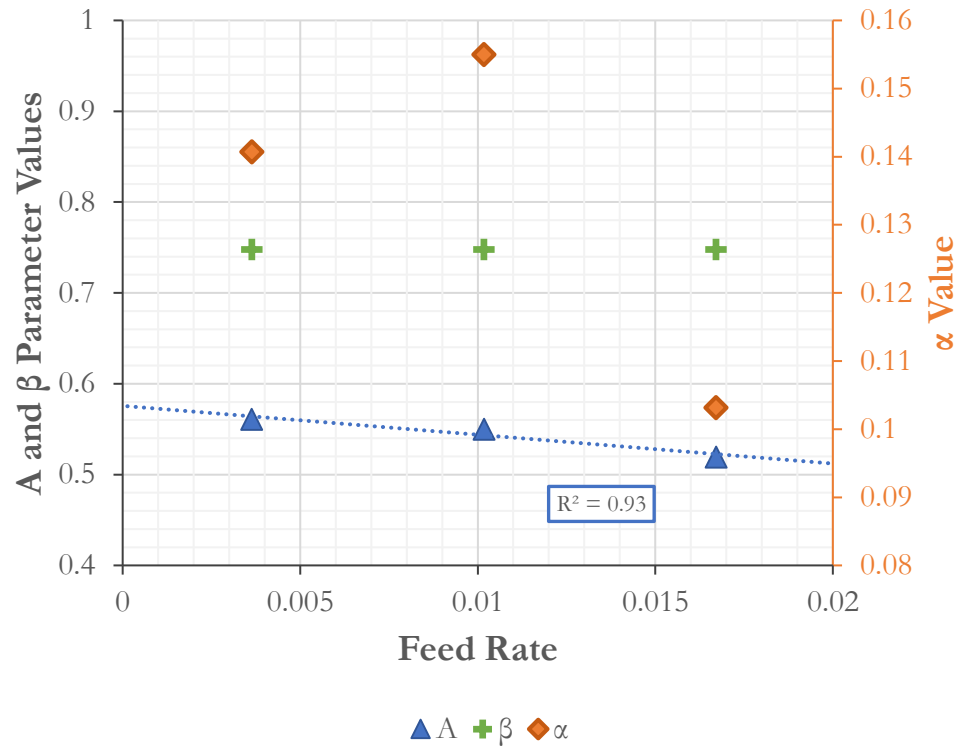


Figure 7.18 displays the relationships between the feed rate and the S3, B1 model after the initial optimisation over A and α .

The relaxation on the β due to the potential error in the materials effect study of 39% from the model value improved overall OVL scores to between 0.87 and 0.93. A relationship was still maintained between A and feed rate, as well as between α and the mill speed. In the process, no further relationships between the parameters were observed. While β stays almost constant ($\beta = 0.5277$) throughout the runs, this is lower than the expected value given in table 7.5 with a 29.4% reduction in the value; it is however within the 39% error estimate in the model that was determined from chapter 7.3.2 figure 7.16. Further optimisation steps were in attempts to negate the relaxation on the constraints in β at step 1, yet this only resulted in significantly reduced accuracy (See figure 7.21).

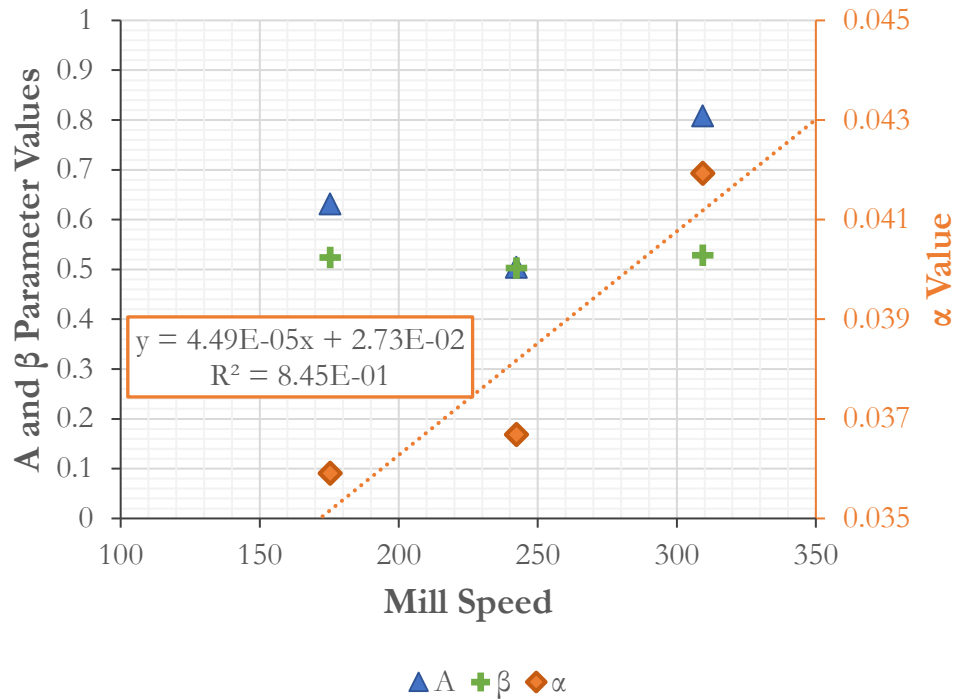


Figure 7.19 displays the relationships between the mill speed and the S3, B1 parameter values after the first step in optimisation over A and a. There is still a strong relationship between a and the mill speed. Beta remains at a constant value but lower than predicted.

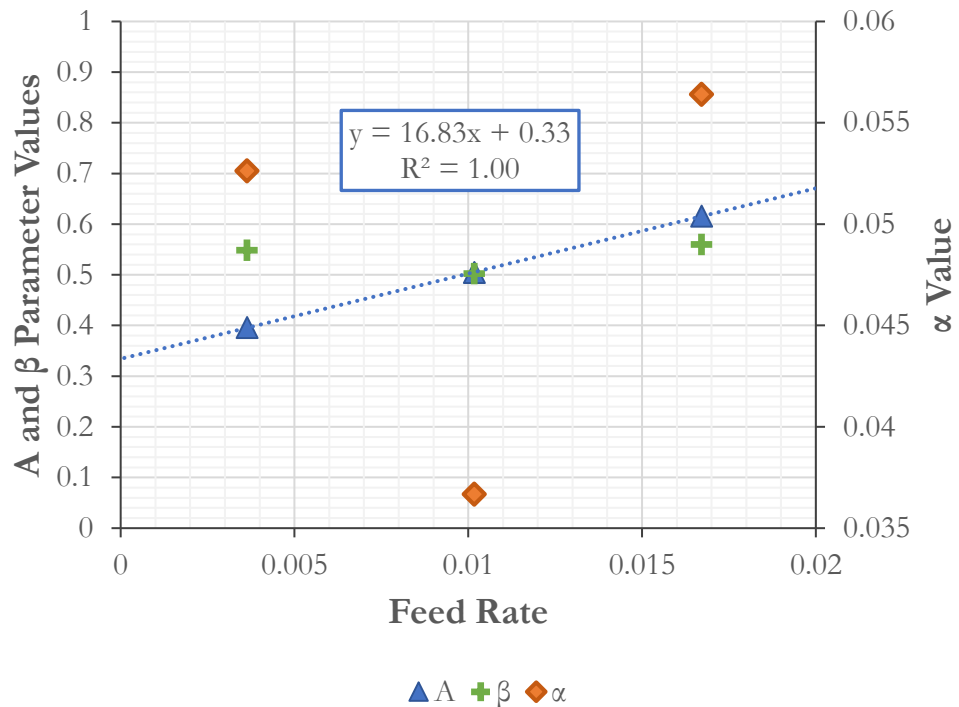


Figure 7.20 displays the relationships between the feed rate and the S3, B1 parameter values after the first step in optimisation over A and a. Here the relationship with feed rate and A persists. Beta remains constant as before.

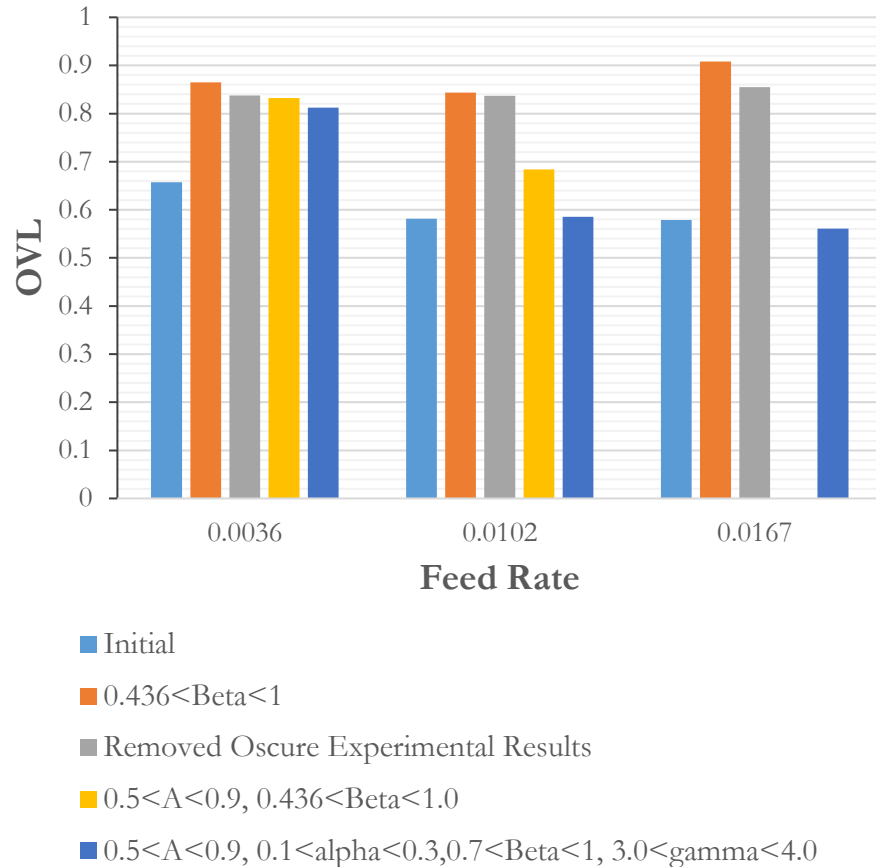


Figure 7.21 displays the OVL values as optimisation progression pushed beyond 1st step, OVL's significantly reduce as optimisation is squeezed beyond the 1st step, hence why the 1st step was used as the model.

From completion of the material and operational studies a potential semi-empirical model has been developed that accounts for the operational conditions of the Lopulco E1.6 mill and material characteristics of the pellets in question. The relationships are outlined in table 7.6. The next section will discuss blind testing of the model and assess its performance.

Table 7.8 displays the various model relationships that have been found for the S3, B1 population balance model.

Parameter Model	Independent Variable (x)
$A = 16.83x + 0.33$	Feed Rate (7.5)
$\alpha = 4.49 \times 10^{-5}x + 0.0273$	Mill Table Speed (7.6)
$\beta = (0.0305x - 0.405), \pm 29.6\%$	Axial Deformation Energy (7.7)
$\gamma = 3.293 - 0.007x$	Axial Deformation Energy (7.8)

7.4 Blind Testing of the Steady State Model

7.4.1 Blind Testing Operational Conditions

In the experimental analysis of the Lopulco E1.6 mill, 7 experimental settings out of 15 have been used to train the model, (23 runs including repeats). In the experimental regime there are a remaining 24 runs at the ‘corner points’ of the CCC experimental design that have been used as blind tests for the developed model. Using the model as given in table 1.6 for the S3, B1 combination, specifically with the 29.6% reduction in β as per the optimisation for operational conditions, blind testing was complete on the corner point experimental runs. Table 7.7 displays the statistics of the blind test results. It shows that the model is accurate to within a large margin of error however considering the factors of the variance in the axial deformation tests and the experimental results, this was to be expected. What it does show, is that the concept of using the axial deformation testing for this style of mill, an abrasive, compressive breakage mechanism seems to be suitable to base simulations on.

Table 7.9 displays the overall statistics of the operational conditions blind tests.

<i>Statistical Measure</i>	<i>OVL Score</i>
Mean	0.883
Standard Deviation	0.024
Max	0.919
Min	0.822

Upon review of the simulations where the OVL scores were lowest, there did not seem to be a specific set of conditions where the model produced low accuracy results. This suggests that the model used is sufficient and where OVL scores are low, this can be attributed to the individual experimental results being highly variable.

Table 7.10 displays the accuracy of the simulation because of the operational conditional settings. The model is unaffected by operational conditions.

<i>Operational Condition</i>	<i>Setting</i>	<i>Average OVL</i>
Feed Rate	0.006	0.884
Feed Rate	0.014	0.883
Mill Speed	282	0.883
Mill Speed	202	0.883
Classifier Vane Angle	20	0.879
Classifier Vane Angle	90	0.889

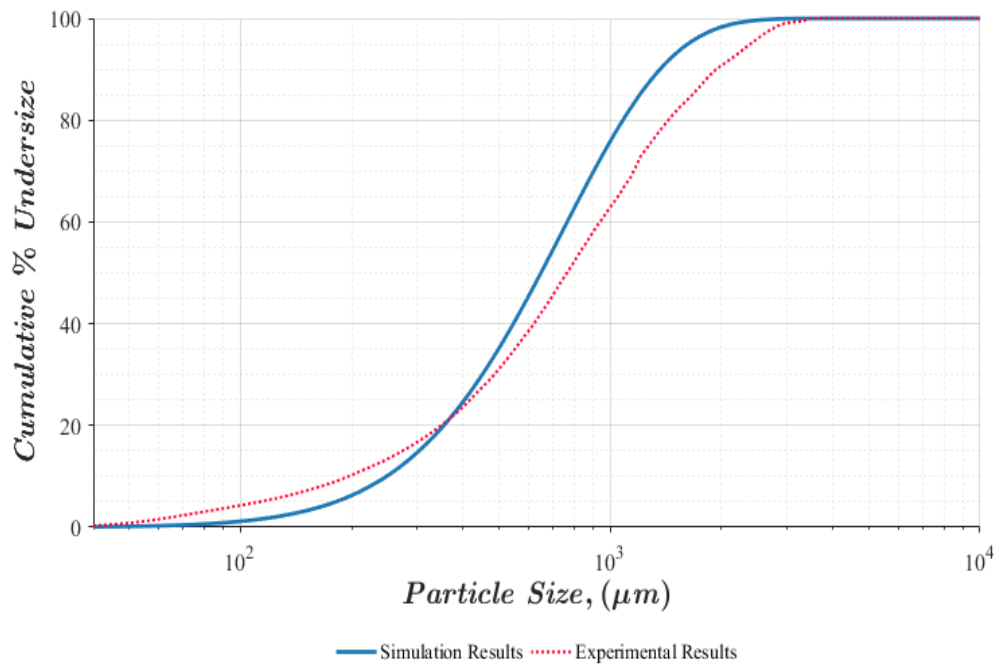


Figure 7.22 displays the worst case fit to the experimental results in the blind test, feed rate: 0.014 kg s^{-1} , mill speed, 202 RPM and the classifier vane angle of 20° . The OVL on the blind test was 0.82.

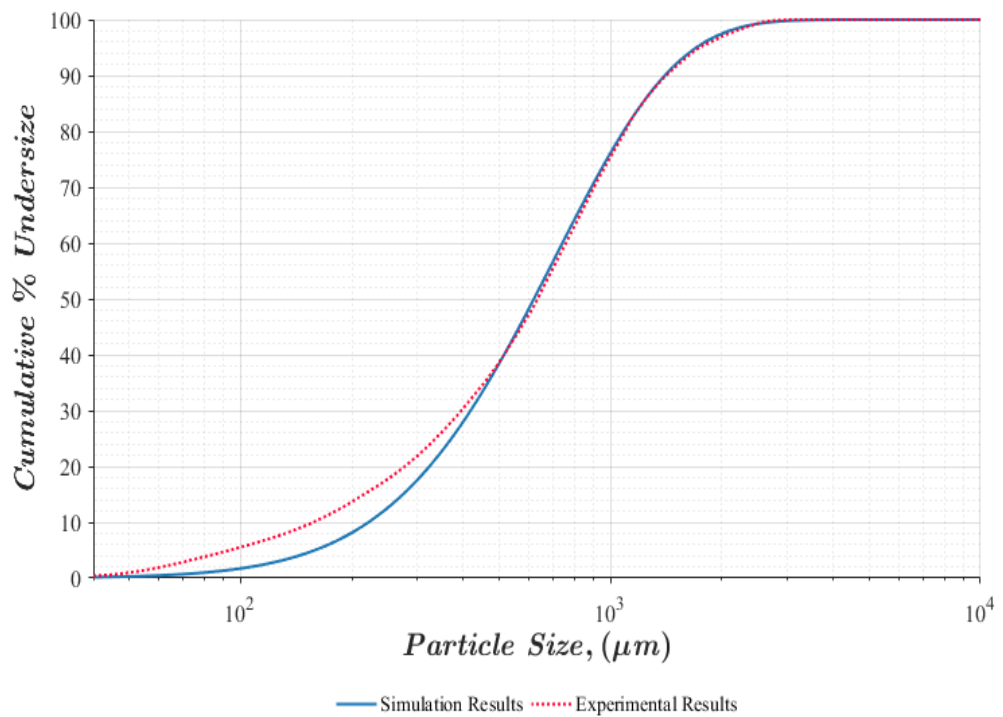


Figure 7.23 displays the best case fit to the experimental results in the blind test, feed rate: 0.014 kg s^{-1} , mill speed, 282 RPM and the classifier vane angle of 90° . The OVL on the blind test was 0.92.

As a general comment on the model, there is a trend to the results that slightly over predicts the large particle product and under predicts the fine particles as can be seen in figure 7.23. The only exception is when the feed rate and the mill speed high, at which point the production of fines only is under estimated figure 7.24. This could be a consequence of the classification function producing too tight a distribution and would need to be investigated further. As this is a proprietary function, it would require a separate study for every classifier.

7.4.2 Blind Testing Materials

As the conditions of β were altered because of the model development to account for the operational conditions show a last test was made to review the accuracy against a different biomass species, Eucalyptus pellet was chosen. The statistics of the simulations against the 3 repeats of the experiment are provided in table 7.9. Similar observations can be seen in the material study, whereby there is an under prediction in fines.

Table 7.11 displays the overall statistics of the blind test on Eucalyptus after reconfiguring the model to account for operational conditions.

<i>Statistical Measure</i>	<i>OVL Score</i>
Mean	0.897
Standard Deviation	0.019
Max	0.923
Min	0.878

7.5 Conclusions

Correlations with material characteristics were observed for both the batch processing model on the PM100 planetary ball mill, in this case with the flexure deformation energy, and the steady-state Lopulco mill model with axial deformation energy requirements. The correlations with the different deformation energy testing results is likely due to the different breakage mechanisms that occur in each mill type.

Accuracy levels are not high; however, they are still optimistic with an average blind test accuracy of 88%. The most likely reasons for this are the accuracy in experimental results for the Lopulco mill, and the mechanical testing. Any BPBE

model will require to be tailored to the individual mill as highlighted in the experimental section with the development of the classification process however other methods could be implemented to study other elements, such as a Hardgrove grindability testing machine apparatus could be employed to study breakage rates under different volumes, or residence times.

A process which is quick to implement, requires relatively small number of experiments, and low computational resources has been developed that could be applied to any type of mill. The primary selection and breakage functions, S3 and B1, seem reasonable to be used in completing modelling simulations. B1, which was developed and tested by the researcher, has limitations to its use highlighted by the batch case when parameters exceed constraints with the equation, however if the parameter γ is set to greater than 3, which is reasonable; issues arise when $\gamma \rightarrow 1$.

Chapter 8 - Single Impact Testing and a Master Curve Population

Balance Model

8.1 Background

Vogel and Peukert (Vogel & Peukert, 2003) began with the problem that the machine used in grinding and the materials interact in a complex way subject to the mill operational conditions and the material properties. In their paper, they develop a theory that could help to understand and model the process intuitively. By traversing several fields, starting with similarity of the breakage patterns in progressive breakage events, through fracture mechanics and on to evaluation of grinding performance, they arrive at a theory of a master curve for breakage probability, equation 8.1. The equation looks to associate kinetic impact energy, $W_{m,kin}$, applied by an impact mill to the particle size of d , and evaluate the resulting probability of breakage, $s(d)$, should the particle in question have a minimum threshold energy, $W_{m,min}$, required to break it.

$$s(d) = 1 - \exp[-f_{mat}kd(W_{m,kin} - W_{m,min})] \quad (8.1)$$

The parameter f_{mat} , is interpreted as a material property that is independent of particle shape and k represents the weakening of particles based on successive impacts. Within the theory, f_{mat} with $dW_{m,min}$, which is product of the particle size with the minimum threshold energy, should encompass all aspects of the material characteristic.

The work has been received well in many notable publications (Miguel Gil et al., 2015a, 2015b; Karinkanta, Illikainen, & Niinimäki, 2013; Vogel & Peukert, 2005). Specifically, these publications have been focused on impact mills. The application of this breakage rate function to compression and abrasion mills has not been tested. In this research the model was applied on the assumption that the breakage event by the rollers of the Lopulco mill is treated as a short compression

event. Additionally, and primarily why the investigation took place was due to the need to establish a more consistent material testing results to drive a developed PBE model. Since the output of the master curve experimentation is a probability of breakage, the results can be used directly as a selection function in a PBE simulation.

8.1.1 Experimental Process

The Breakage Rate (Selection) Function

The objective of the experimental procedure is to determine $W_{m,min}$ and f_{mat} for each material. 30g of biomass pellet is fed into an impact mill, 1 particle at a time. The mill was set up in a simple way to allow 1 impact event only. This is verified audially as the particles are passed through the mill during the experiment. After the sample passed through the mill, the progeny particles were collected, and particle analysis completed. This experiment used a Retsch ZM200 as seen in figure 8.1. The mill has a diameter of 9.8 cm rotor beater with 12 triangular teeth; these are where the impact with the biomass pellets will occur. The mill has varying rotational speeds between 6,000 rpm and 16,000 rpm.



Figure 8.1 displays a Retsch ZM200 mill, set up with no screen so that particles when passed through experience only 1 impact before size analysis is completed.

The mill was set up with no screen to ensure that the particles only experienced 1 impact each time they are passed through the mill, hence the experiment is known as Single Impact Testing (SIT). Breakage analysis compared with energy input is correlated by passing particles through the mill multiple times, represented by k . As the rpm of the mill is known, the input energy, $W_{m,kin}$, could be calculated as in equation 8.2, however in the literature (Miguel Gil et al., 2015a;

Vogel & Peukert, 2003) the mass parameter is taken as 1 kg hence a reduction to equation 8.3.

$$W_{m,kin} = \frac{1}{2}mv^2 \quad (8.2)$$

$$W_{m,kin} = \frac{1}{2}v^2 \quad (8.3)$$

Analysis of the progeny particles was completed by sieve analysis for a mass basis result consistent with the experiments completed by other literature. The particle size distributions were collected as per the sieve size ranges given in chapter 5. As the theory states $W_{m,min}$ is independent of size a top size is used as the target size in the experiments, this is a 4750 μ m sieve. Additionally, the CAMSIZER P4 results were collected to test the assumption of no shape influence. Due to the nature of biomass having anisotropic structure, one theory that this experimental setup can test is the potential for different energy requirements in different axis of the biomass particles. This was tested by comparing the output of the CAMSIZER P4 PSD evaluation at maximum, d_{Fe_max} , and minimum chord diameters, d_{xc_min} , which are only obtainable with such dynamic particle analysis methods.

f_{mat} and $W_{m,min}$ were then determined by non-linear least squares fitting of equation 8.1 to the data collected; this was completed using MatLabTM's 'lsqnonlin' function. For $W_{m,min}$ the plot is of the unbroken mass proportion of the material feed with each experiment against the particle size (d), with input energy, $kdW_{m,kin}$, k is included in order to compound the energy under which a particle has been exposed for multiple impacts. By plotting these results and fitting an equation of the form $E = 1 - \exp[kdW_{m,kin}]$ to the data, the intercept of the abscissa with the model provides the minimum energy threshold, $W_{m,min}$. Once the threshold value has been determined the results breakage probability can be plotted against $kx(W_{m,kin} - W_{m,min})$, where k , the number of impacts, is the number of times the sample is passed through the ZM200 mill. Again, fitting the curve of equation 8.1 with the data provides the value of f_{mat} .

The Breakage (Distribution) Function

The breakage mechanism used with the SIT experimental process is fundamentally different from that with the Lopulco E1.6 mill, however an investigation will be completed to confirm how the material test compares with others. If a relation can be observed with the leading material test, the axial deformation as observed in chapter 5 a relation could be extrapolated and tested against the Lopulco mill data. If successful implementation of the relation can be substituted into breakage function 1 (repeated in equation 8.4) in the PBE simulation.

$$b_{i,j} = 1 - \exp \left[- \left(\frac{d_i}{\beta d_j} \right)^{\nu} \right] \quad (8.4)$$

The SIT PBE Method

The modelling method proposed is similar the matrix BPBE as outlined in chapter 4.6 for the steady state model. The key difference the way the SIT model works is in tracking the number of breakage events that each volume quantity at each size class undergoes. For this reason, the particle size distribution, $f(d)$, becomes a $m \times k$ matrix where m is the size class, and k the number of impacts the particle size distribution in that column has undergone. The output of the mill is a summation over the rows of the product matrix.

With the Lopulco mill, the baseline energy input provided into the mill is not necessarily the energy transferred to the pellet in the breakage event of the compression between the mill table and mill rollers due to the potential energy in the springs holding the mill roller in place. Unfortunately, this was unknown and dismantling of the mill to determine this was not possible. To extrapolate a value for this, optimisation over a multiplier on the minimum mill table speed kinetic input energy, as calculated via equation 8.3, added to the kinetic energy operated at the mill speed as defined in each experiment. The optimisation, would again take place over the 30 of the experimental regime and tested, should it be successful, against the remaining 17 runs of the experiments. An input multiplier will be allowed to range between 1 and 15.

Materials

In these experiments, 3 different biomass species were trialed, all of which were used for the Lopulco mill experiments, these are the Brites wood pellets, the Miscanthus grass pellet and the Microwave Torrefied pellets. These were selected to test the theory and provide a basis of comparison the modelling already completed with three very different biomass species. To minimise variation, pellets of approximately 15 mm in length were selected however the other features of the biomass pellets are as previously specified in the research.

8.2 Experimental Results

8.2.1 Master Curve

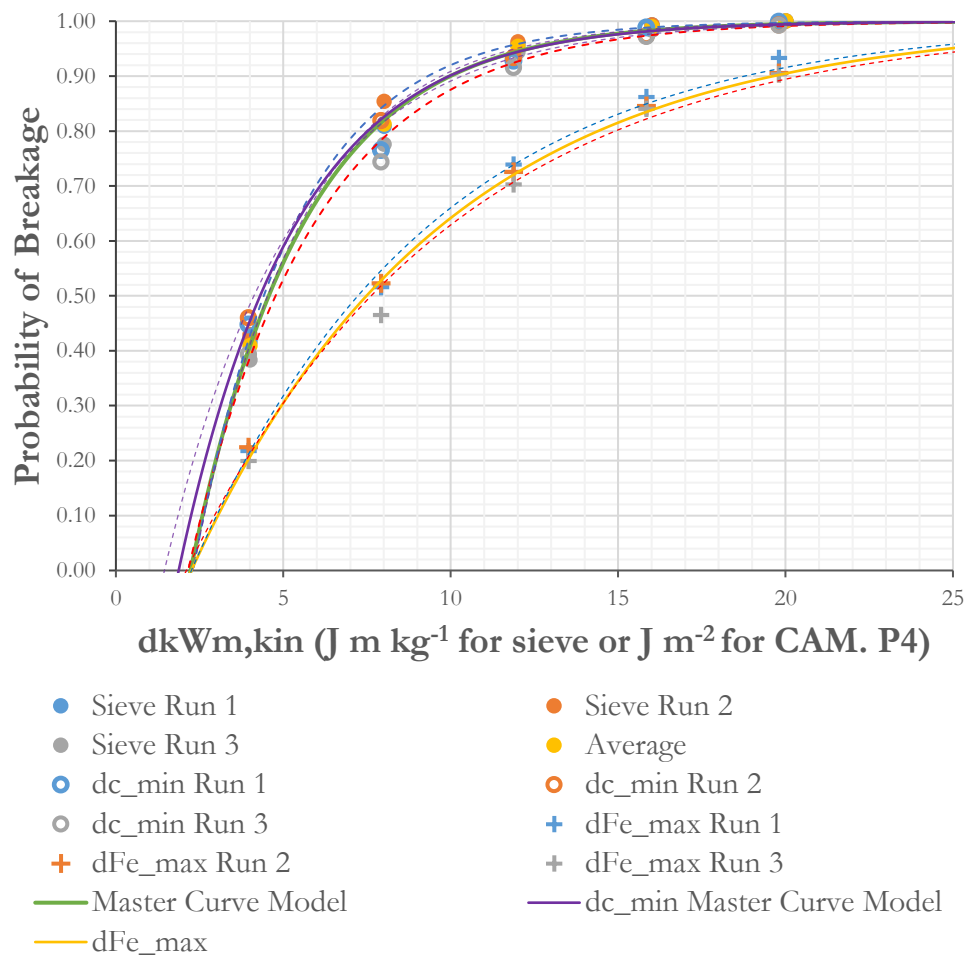


Figure 8.2 displays the single impact testing results for Brites wood pellets, shown are the results from sieve analysis, CAMSIZER P4 analysis for minimum and maximum chord, along with the fitted master curve models; standard deviations in the models signified by the dotted lines.

Following the implementation of the Master Curve technique to the 3 biomass pellet species several observations can be drawn out. As in figure 8.2, the dynamic particle analysis seems to provide results that are like the sieving technique using the d_{c_min} characteristic. This is to be expected due to its close relation to the principles of sieving. The f_{mat} parameter seems to be affected by the brittleness of the material, this is shown in literature and as in this research as can be seen with the Microwave Torrefied pellet results. In this case the f_{mat} parameter increases, and the master curve has a steeper gradient. With the d_{Fe_max} measure, the curve is shallower, this is most likely the effect of the aspect ratio of the material however this does raise a question as to the validity of the independence from size and shape of f_{mat} . The experiments do show though that there is very little difference, regardless as to which measure is used between the $W_{m,min}$ parameters. For all 3 measures, the values are consistent within the order of 1 standard deviation from the mean. The only pellet to deviate from this is the Microwave Torrefied pellet that showed a considerable difference when based on d_{Fe_max} , figure 8.3 summarises the results.

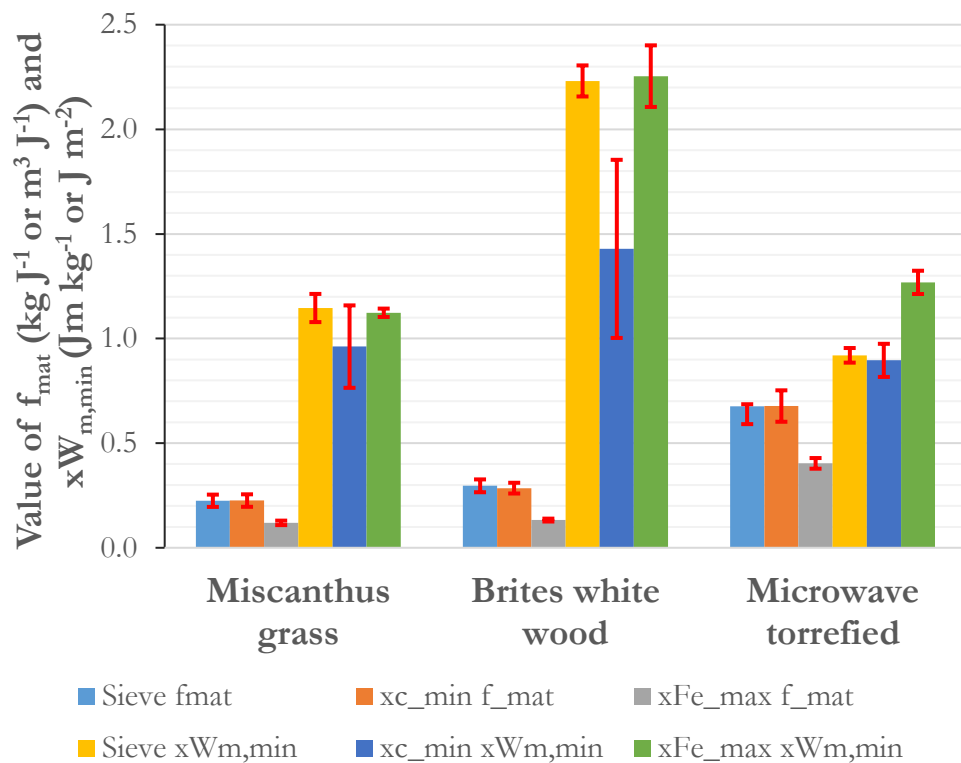


Figure 8.3 displays the f_{mat} and $xW_{m,min}$ results for the single impact tests completed on 3 different biomass pellet species. The assessment shows the results from the mass based sieve analysis and the volume based CAMSIZER P4 dynamic particle analysis.

To judge the result, a comparison has been completed with the results in the literature from which the theory came. The results seem reasonable with similar materials. This can be seen in figure 8.4 where the sieve related f_{mat} and $W_{m,min}$ collected in this research are compared. This comparison also corroborates the observation that more brittle materials have a higher f_{mat} value.

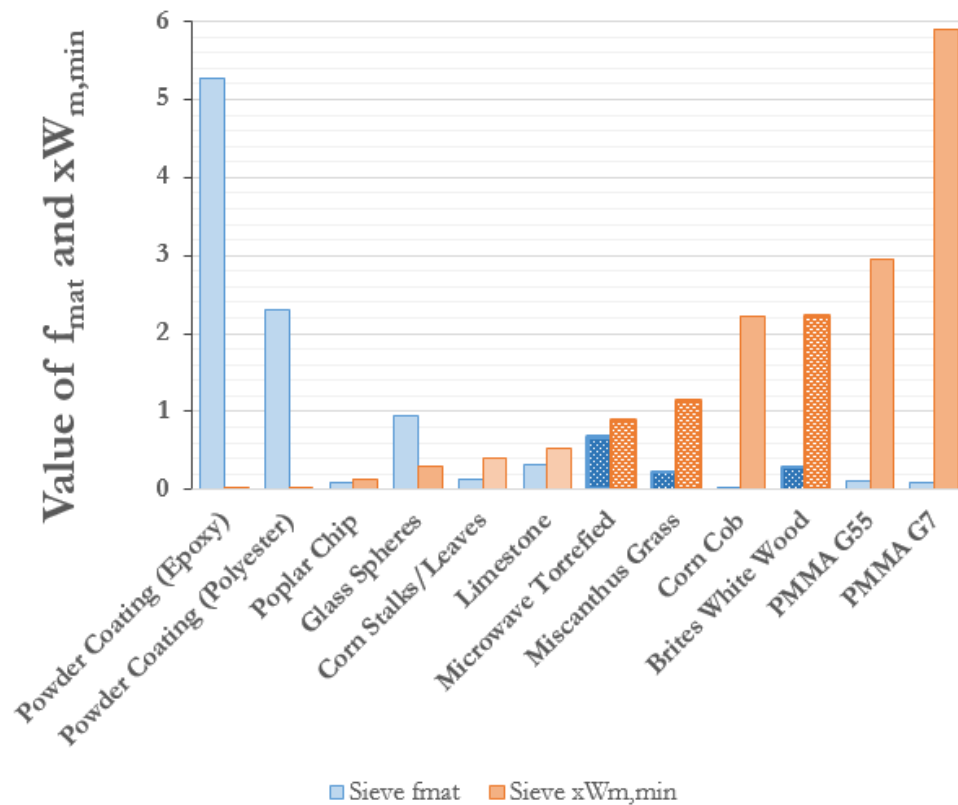


Figure 8.4 displays the materials used in this research in context with the literature from (Vogel & Peukert, 2003) and (Miguel Gil et al., 2015b). The patterned bars are the results from this research. All results here are presented on mass basis from sieve analysis.

8.2.2 Comparison with Material Characterisation Tests

Several comparisons with the deformation energy analysis completed under the sister project shows how f_{mat} and $W_{m,min}$ relate with them. Figures 8.5 and 8.6 show the correlations. $W_{m,min}$, shows reasonable correlation with all orientations of deformation testing, much more strongly in the flexure test. This could be due to the high-speed impact on the pellet under the SIT resisted only with localised

resistance in the region of the impact, which is like the flexure test and has an almost 1:1 correlation with it. The axial and diametric tests resist through the structure of the pellet. f_{mat} shows some correlation with the axial orientation deformation testing, stronger than that with the $W_{m,min}$; the other 2 deformation tests showed no such correlation.

Using the information from figure 8.5, equation 7.8 can be redefined in terms of the $W_{m,min}$, so that the details can be used in a simulation (see equation 8.6).

$$\gamma = 3.293 - \left(0.827/W_{m,min}\right) \quad (8.6)$$

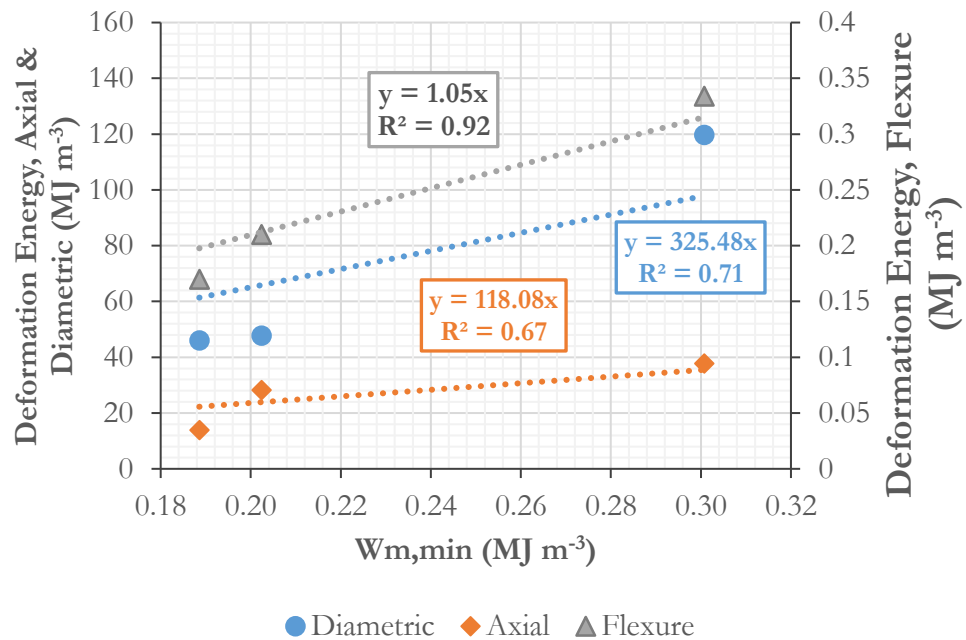


Figure 8.5 displays the correlation of the minimum breakage energy $W_{m,min}$ from the single impact testing correlated to the deformation energy results from the sister project for the 3 materials tested in the SIT regime.

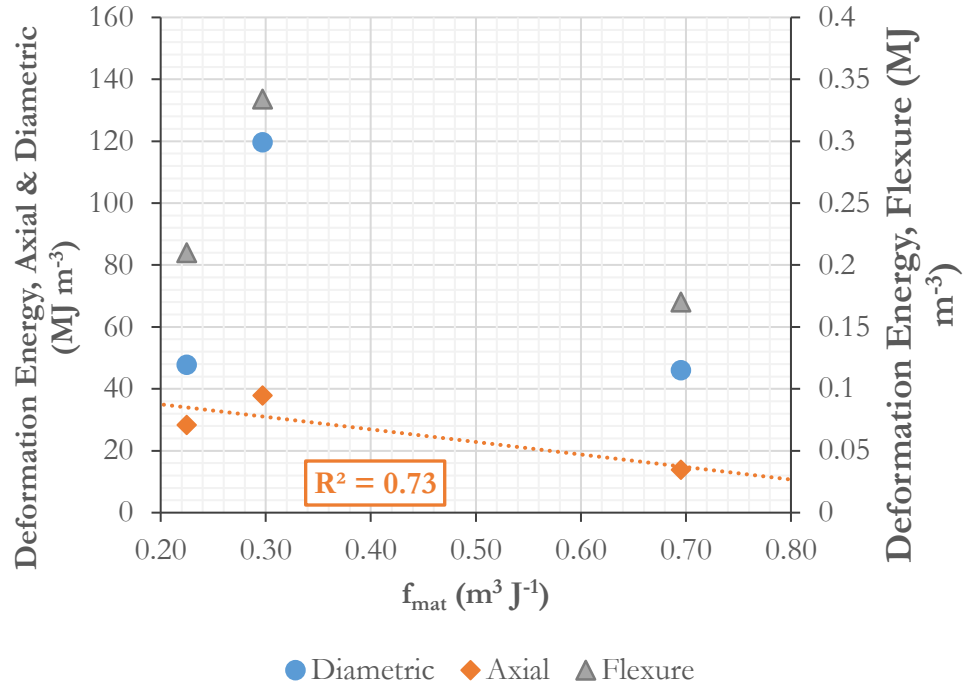


Figure 8.6 displays the correlation of f_{mat} to the deformation energies in the various orientations.

8.3 Simulation Results

The application of the PBE simulation using the results of the SIT experiments provided an initial OVL accuracy of 0.514, significantly less accurate than those of the PBE simulations discussed in chapter 7. In order to improve accuracy several iterations of the simulation were completed, each time reducing the iteration calculation step in order to increase accuracy. After two successive iterations in reducing this the simulation results increased to a maximum OVL of 0.66. The steps taken can be seen in table 8.1. Examples of the simulation PSD prediction against the experimental results can be seen in figure 8.7 and a summary of the simulation results is given in table 8.2. As this method seemed to be less accurate than those in chapter 7 the SIT method PBE simulation was discontinued.

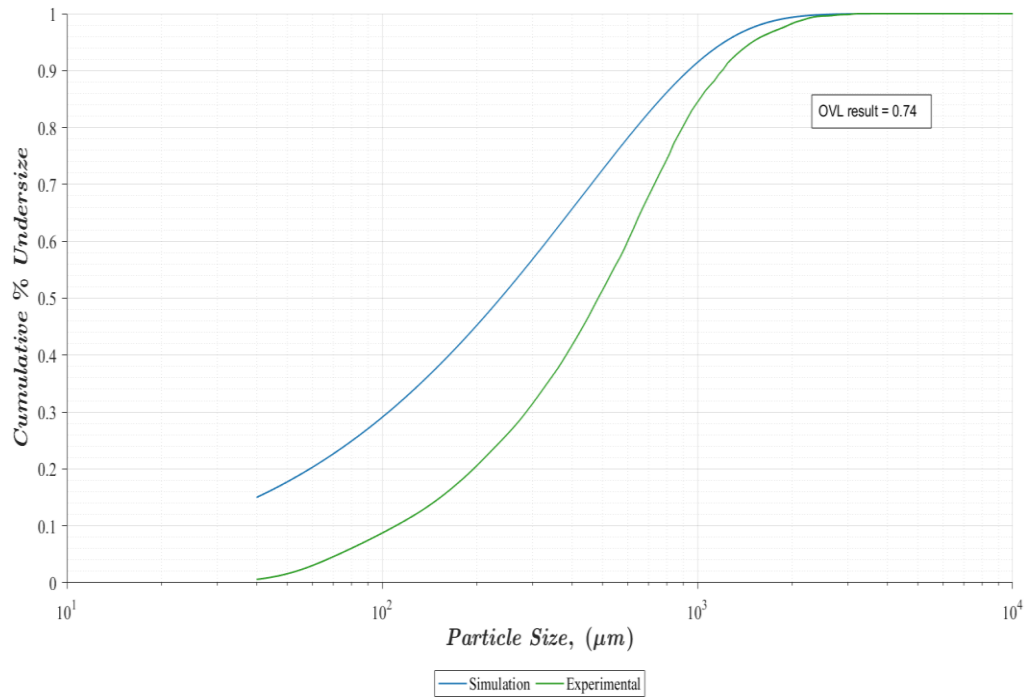


Figure 8.7 displays the Single Impact Testing PBE based simulations against the experimental results for a Lopulco E1.6 mill experiment results, 0.006 kg s^{-1} , 202 RPM, 90° vane angle.

Table 8.1 displays the improvements in accuracy of the Single Impact Testing based Population Balance Equation simulation with reductions in the iteration step size.

<i>Iteration Step Size</i>	<i>Average OVL</i>	<i>Optimal Multiplier</i>
1.0	0.514	2.59
0.2	0.647	1.57
0.1	0.659	1.57

Table 8.2 displays the statistics of the OVL results for the SIT PBE simulation training.

<i>Average</i>	<i>Minimum</i>	<i>Maximum</i>
0.66	0.48	0.74

Overall the results significantly overpredict the finer size production of the biomass particles. This is due to the high rates of breakage created by selection function base equation and the required base energy to overcome limits of the function. Together this causes an over estimation of the degree of breakage at each step.

8.4 Conclusions

As a material characterisation method, the SIT experiments provide significantly less variation than the deformation testing, therefore application to milling in general is encouraged. This does have limitation. Application to mills of similar input energy magnitude and breakage mechanisms would be consistent with the theory yet mills with vastly different mechanisms show that it cannot be implemented directly.

Observations show that a link between SIT minimum threshold energy with flexure energy consumption, and possibly with the axial deformation seems likely however this requires further comparison to more pellets to be confirmed. This can be explained by the application of breakage mechanism acting on a small area of the pellet, such as the flexure point on the flexure deformation energy test or on the smaller area of the pellet top in the axial deformation testing.

Application of the SIT technique is currently not feasible for the Lopulco mill type. With the potential to verify the relationships between the axial and flexure deformation tests, and the single impacting testing, there may be options for use subject to a deeper investigation to characterise the relationships between them; implementation of which could be achieved as the axial deformation has been in chapter 7. This could help to reduce the error in the simulation.

Chapter 9 - Conclusions and Future Work

9.1 Objectives

The objective of the project was to build a simulation for the grinding of biomass pellets using where possible the data from the experimental work completed by the research of the sister project, “On Biomass Milling for Power Generation” (Williams, 2016). If optimisation of the biomass pellet milling proves successful, power generators may choose to adopt biomass as a potential fuel through efficiency savings and gains that can be made through producing electricity with renewable and carbon neutral fuel sources. The simulation was to focus on the key areas of concern in order of replicating a product particle size distribution, ensuring a mass throughput (where appropriate) and simulating energy consumption. Furthermore, the model should be developed to be as intuitive as possible and be driven with as little experimental data as possible.

9.2 Modelling Review

The conclusions here build upon the literature already published and other research completed by the sister project. The first of such conclusions is that the population balance equation, PBE, method, has proven to be a versatile method for prediction of particulate assemblies and their evolution. The technical review in chapter 3 provides analysis of other techniques, yet with this approach simulations can be generated for the entire scenario of comminution. The advantages of PBE methods over interpolation of experimental results is the ability to extract the contribution of the mill and materials in question. This research has also shown that the PBE method can be trained based on relatively small amounts of experimental data that provides very good representations of what is happening.

A second modelling approach was identified, the discrete element method, DEM, that has the potential to develop understanding of the fundamentals of milling. The computational resources and time are where DEM has the disadvantage over the PBE simulation method. As experimentation became necessary for the research and application of the PBE method, the project was unable to incorporate a DEM model.

9.3 The Population Balance Equation Method

This project has implemented a PBE method, tested and reviewed a catalogue of selection and breakage functions; it has, within known limits, developed and implemented a function designed by the researcher based on the Rosin-Rammler equation (breakage function 1) that has proven to fit the distributions with greater accuracy than others for this application. The breakage function shows consistent accuracy with different types of mills which enables a similar PBE structure to be applied across the variation of mill types. It has shown, that when applied to different mill types the parameters may not vary based on the same condition. For example, batch milling with a planetary ball mill, parameter β in the S3, B1 model was dependent on the machine and the material whereas in the Lopulco ring and roller mill, it varied with material only.

The PBE method was implemented and a simulation developed that predicted the experimental particle size distribution in blind tests to within a minimum accuracy of 82% and on average to 88%. Given the error in the material deformation project and the variation which seemed inherent in the Lopulco mill results this seems reasonable. Increases in the material testing result accuracy would aid this as more experimental results could help reduce the variation and consequently improve the model. Extraction of machine and material contributions were successfully identified for the Lopulco mill. This shows that the process of back calculation was applicable and useful in determining the contributions of each component for the ring and roller type mill. Attempts for a planetary ball mill were taken as far as the experimental study results allowed and showed that it too was possible however different parameters were dependent on different components.

The application of material characterisation to drive the PBE method simulation has been shown to be possible for the Lopulco and Planetary ball style mills. High variation in the test used, deformation testing, limits the current scope of the research to certify this conclusion. Other potential tests, such as the single impact testing in chapter 8 show that material testing can be improved however application to certain mil types may not be directly possible.

9.4 Experimental

From the experimental research here, results have shown that to develop a simulation biomass grinding intricate details need to be available on the functioning of the classifier specific to the mill. As shown in the project, the classifier unit on the Lopulco mill behaved contrary to expectations and required a custom classification function be developed based on the experimental data.

The research has shown a correlation to axial deformation energy and the product, throughput, and energy consumption of the Lopulco mill. Initial expectations for this were correlations to diametric energy, however it is theorised that axial may be more appropriate due to the alignment of the pellets with the rollers, and how the rollers function in gripping the pellets. Application of the deformation energy is not across the full length of the pellet, rather a section of the length, more consistent with axial deformation energy levels.

Further to this, there is an observed efficiency gain by increasing feed rate into the mill. This is possibly due to the frictional forces present between the pellet and the grinding elements not being sufficient to cause movement under the grinding roller. Presence of more material encourages appropriate alignment and coatings on the grinding media increase frictional forces. Non-linear grinding kinetics would suggest this is limited to a maximum capacity which was undetermined in this research.

The single impact testing also showed that material characterisation for biomass pellets can be completed with a lower variance in the results. The limitation is that this cannot be directly applied to Lopulco style mills, presumably ball and tube mills and possibly other types that are not based on an impact grinding mechanism. However, there may be correlations to other characterisation tests as shown in chapter 8 that imply application of the SIT experimental $W_{m,min}$ parameter can be used to drive other style mill simulations.

9.5 Recommendations for Future work

Initial recommendations for future work would be to work on increasing the accuracy of the experimental results. Limitations on the project were linked to the quantity and scale of the experimental operations, additionally the variation in material testing. Finding alternative material characterisation tests would be one

such improvement. As with the SIT experiments a similar, more controlled experiment for ring and roller type mills would make a characterisation test more applicable to the Lopulco mill and other vertical spindle mills. Understanding of the breakage kinetics of the biomass pellets would significantly improve a PBE simulation.

Additionally, the size of the pellets relative to the lab-scale mills could also influence the accuracy of the experimental results. Recommendations would be to take the experiments and base the model on results from industrial scale mills; longer running times and quantity of mass throughput would aid in producing consistent experimental results.

Energy consumption is expected to be related to the degree of comminution, energy coupling modelling would be the next focus of future work. As a model that showed reasonable predictability was not developed until late on, this could not be completed. Furthermore, the accuracy of the model would influence the results of any energy coupled routine.

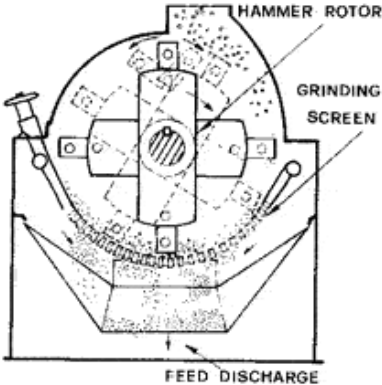
Non-linear grinding effects should also be considered in the model. These however would be hard to test with the Lopulco milling experiments. Initial development of such a model would be better suited to batch processes to understand the interaction of mill volume with grinding mechanism in a controlled way before implementation on steady state simulations, or even unsteady state. Specifically, for Lopulco style mills, use of such equipment as a HGI testing mill could help improve understanding of material properties and interaction with this style of grinding media, additionally build upon the knowledge required to facilitate non-linear grinding effects.

Further research into the classifier systems is possibly the most important research required; it has been shown to be important in this research and believed to be a necessary component for a rigorous development of a PBE simulation. Unexpected behaviour observed displays a need for greater understanding of classifier dynamics. For elutriated air classification, the majority of which is found in industry the study of biomass particles in the air stream and with the component of a classification system should also be investigated.

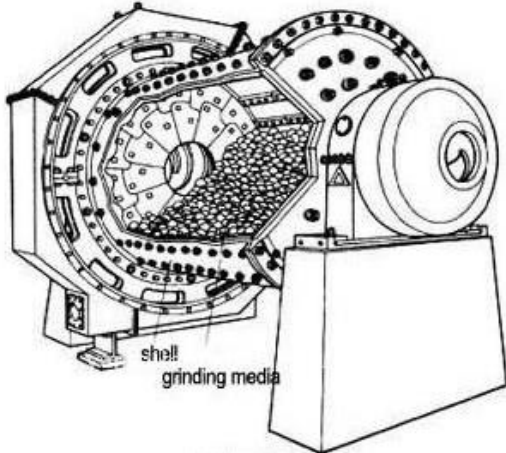
With computers becoming more powerful and some impressive developments in software, DEM modelling of biomass would also aid in developing selection and breakage function parameters and driving the PBE simulation. Additionally, some of the observations in relation to the pellet and grinding media interactions that are hypothesised as the reasons why certain material characteristics seem to correlate with the output of milling, could be verified with small scale DEM simulations. Implementation of anisotropic biomass characteristics, and non-spherical shapes could be approximated in a bonded particle method DEM simulation until better non-spherical element modelling can be achieved.

Appendix A: Mill Types

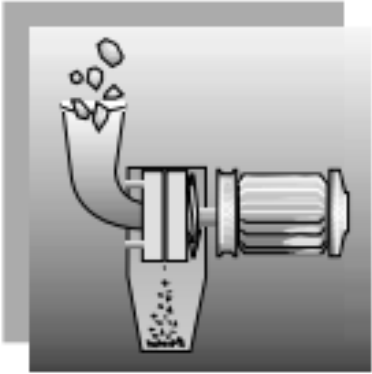
The following appendix provides an overview of some of the mills that are in operation within the current coal pulverising structure as well as some other designs used in the industries identified for investigation due to possible application to biomass milling. It is by no means a complete itinerary of milling equipment.

	<i>Breakage Modes</i>	<i>Parameters</i>	<i>Specification notes</i>	<i>Product grading</i>
<i>Hammer</i>				
	<ul style="list-style-type: none"> • Impact • Shearing/abrasion • Attrition 	<ul style="list-style-type: none"> • RPM • Screen Size • Feed rate • Hammer shape • Free swinging or fixed hammer options • Hammer mounting angle (fixed hammers) • Hammer-screen clearance 	<ul style="list-style-type: none"> • Hammer mills have internal classification as standard so no need to include closed circuit operation • Gravity loaded operation via hopper and/or gravity shoot. • Feed discharge into pneumatic conveyance streams for industrial application. 	<p>>125 μm</p> <p>achievable depending on the screen aperture.</p>
<p>Grinding Principle:</p> <p>Feed material is fed under gravity into the milling chamber. The rotating shaft rotates the hammers in the mill. The hammers provide the impacting force on the feed material through contact with the arms or the hammer head. Shearing Forces apply to material trapped between the head and the screen.</p>				

Manufacturers	<ul style="list-style-type: none"> • West Salem: http://westsalem.com/machines/wsm-hammermills/ • Andritz: http://www.andritz.com/fb-215-gb-hammermill.pdf • Retsch: http://www.retsch.com/api/?action=product_pdf&productId=87&id=2296508&L=0&userId=&site=retsch&print_language=0&print_info=1&print_image=1&print_images=1&print_examples=1&print_advantages=1&print_features=1&print_video=1&print_principle=1&print_orderinfo=1 • Bühler: http://www.buhlergroup.com/global/en/products/hammer-mill-dfzc.htm#.VE7a8PldWwt • Christy Turner: http://www.christy-turner.com/products/hammer-mills/ • CPM: http://www.cpm.net/index.php?option=com_product&task=view&id=1&Itemid=26
References	(L. G. Austin et al., 1979; Miguel Gil & Arauzo, 2014; Temmerman et al., 2013; G. Wang, Zhao, Li, Li, & Wang, 2012)

	<i>Breakage Modes</i>	<i>Parameters</i>	<i>Specification notes</i>	<i>Product grading</i>
<i>Ball and Tube (Rod and Tube)</i>				
	<ul style="list-style-type: none"> • Impact • Compression 	<ul style="list-style-type: none"> • RPM • Ball charge • Ball size • Feed rate • Lifters (optional) • Liner Friction • Alternative grinding media can be rods 	<ul style="list-style-type: none"> • Batch or circuit operation • Closed or Open Cycle Circuits • Circuit operation can be used with air sweeping or internal classification on one end of the mill • Air sweeping often has dual use of heating the fuel to reduce moisture content • Lifters on the interior of the mill is optional, in coal comminution these are not often used • Mixtures of ball sizes is optional 	>20 μm
<p>Grinding Principle: The rotation of the containment tube causes the lifting of the grinding media and feed material; the RPM and liner friction defines the height reached. At a point the material and grinding media will lose contact and fall back in on itself.</p>				

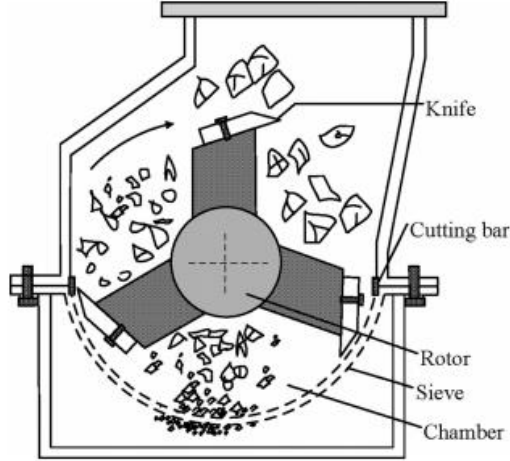
Manufacturers	<ul style="list-style-type: none">• Metso<ul style="list-style-type: none">○ http://www.metso.com/miningandconstruction/mm_grin.nsf/WebWID/WTB-041124-2256F-8A711?OpenDocument#.U_31D_ldX_E• Alstom Power<ul style="list-style-type: none">○ http://www.alstom.com/power/coal-oil/mills-pulverisers/tube/• Babcock Power Services Group<ul style="list-style-type: none">○ http://www.babcockpower.com/pdf/RPI-TO-0010.pdf
References:	(Coulson, 1999; Erdem & Ergün, 2009; Green, 2008; Jankovic & Valery, 2013; Kalala, Breetzke, & Moys, 2008; Powell, Weerasekara, Cole, LaRoche, & Favier, 2011)

	<i>Breakage Modes</i>	<i>Parameters</i>	<i>Specification notes</i>	<i>Product grading</i>
<i>Disc Mill</i>				
	<ul style="list-style-type: none"> • Compression • Shearing 	<ul style="list-style-type: none"> • Disk separation • RPM • Feed rate 	<ul style="list-style-type: none"> • Batch or continuous cycles • Open or closed cycle operation • Integration of classification through use of pneumatic conveyance system is possible 	< 100 μm
<p>Grinding Principle: Compression and shearing forces acting between two rotating disks, rotation causes feed material to be centrifugally transferred to the disk periphery where grinding disks set with a gap depending on the product requirement. The grinding disks can come with radial tothing.</p>				

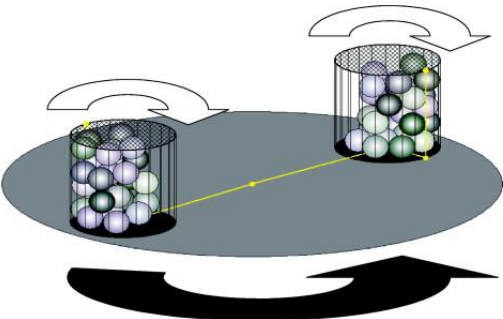
Manufacturers:

- Fritsch
 - <http://www.asi-team.com/asi%20team/fritsch/Fritsch%20data/pulverisette13.pdf>
- Neue Herbold
 - <http://www.directindustry.com/prod/neue-herbold-maschinen-u-anlagenbau-gmbh/disc-mills-50063-396385.html>
- Pallmann
 - http://www.pallmann.eu/language/upload/pdf/PMM_Masterbatch_EN.pdf
- Retsch
 - <http://www.retsch.com/products/milling/disc-mills/dm-200/function-features/>

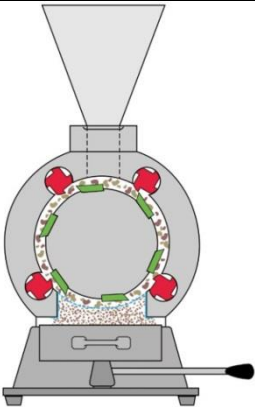
References:

	<i>Breakage Modes</i>	<i>Parameters</i>	<i>Specification notes</i>	<i>Product grading</i>
<i>Knife Mill</i>				
 <p>The diagram illustrates the internal components of a knife mill. A central rotor with three blades is shown rotating within a chamber. A cutting bar is positioned opposite the rotor. Material is fed into the chamber and is cut by the blades. A sieve is located at the bottom of the chamber to separate the product. Labels include: Knife, Cutting bar, Rotor, Sieve, and Chamber.</p>	<ul style="list-style-type: none"> • Cutting • Shearing 	<ul style="list-style-type: none"> • Blade separation • RPM • Feed rate • Internal classification • Variable screen sizes • Blade clearance 	<ul style="list-style-type: none"> • Batch processes available • More regularly applied to circuit operation • Closed circuit operation based on the use of internal classification 	> 250 μm
Source: (M. Zhang et al., 2012)				
<p>Grinding Principle: When the material gets trapped between the knives and the cutting bar the material is cut. Material that has is now small enough to pass through the sieve does so; any product larger than the sieve size is recirculated and milled further.</p>				

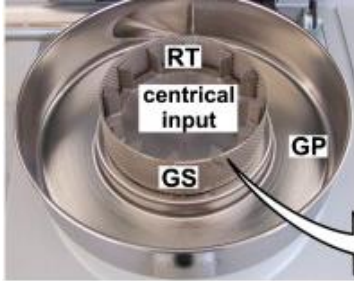
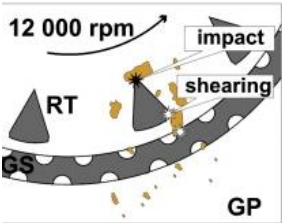
Manufacturers:	<ul style="list-style-type: none">• Retsch<ul style="list-style-type: none">○ http://www.retsch.com/products/milling/cutting-mills/sm-100/function-features/• <u>Thomas Scientific</u><ul style="list-style-type: none">○ http://www.thomasci.com/wileymill
References:	(V. S. P. Bitra et al., 2009; Miao et al., 2011; F. Nasaruddin et al., 2012; M. Zhang et al., 2012)

	<i>Breakage Modes</i>	<i>Parameters</i>	<i>Specification notes</i>	<i>Product grading</i>
<i>Planetary Ball Mill</i>				
	<ul style="list-style-type: none"> • Impact • Compression 	<ul style="list-style-type: none"> • RPM • Grinding Ball size • Grinding ball charge • Ball-Fill ratio • Grinding chamber diameter and volume. 	<ul style="list-style-type: none"> • Batch operation • Limited number of continuous open cycle systems in operation • Machinery can often contain multiple vials • Mainly used in laboratory testing 	> 1 μm
<p>Source: (A. Sato et al., 2010)</p> <p>Grinding Principle: The mill consists of a rotating plate attached to which are cylindrical vials that are fixed to the plate in a manner that allows them to rotate. As the main plate rotates the vials rotate themselves in a direction opposite to that of the main plate. Grinding media and charge in the vials are subjected to centrifugal forces that alternate in relative directions as to the main plate rotates. Charge that is caught between the grinding media and vial is subject impacting forces.</p>				

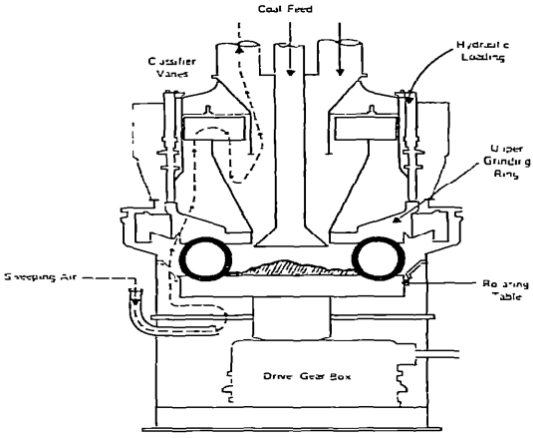
Manufacturers:	<ul style="list-style-type: none">• Leotec<ul style="list-style-type: none">○ http://leotecld.com/upload/medialibrary/8a3/8a3564a0d224b1bf6759d642509d18d7.pdf• Retsch<ul style="list-style-type: none">○ http://www.retsch.com/products/milling/ball-mills/
References:	(Mandal et al., 2014; Rosenkranz et al., 2011; A. Sato et al., 2010)

	<i>Breakage Modes</i>	<i>Parameters</i>	<i>Specification notes</i>	<i>Product grading</i>
<i>Rotary Mill</i>				
	<ul style="list-style-type: none"> • Cutting 	<ul style="list-style-type: none"> • Feed rate • RPM • Internal classification • Sieve screen size • Variable knife protrusion 	<ul style="list-style-type: none"> • Hopper fed or gravity loaded • Batch operation • Could be adapted to open cycle continuous operation • Mainly used in laboratory operations 	<ul style="list-style-type: none"> • > 500 μm achievable depending on the screen aperture.
<p>Source: http://www.brabender.com/english/food/products/sample-preparation/grinding/rotary-mill.html</p> <p>Grinding Principle: The material is fed through the top of the mill and cut between knife blades on the mill shell and blades at the tips of the impellers on the rotor. Product milled to the required size will pass the sieve; larger particles will be recirculated for further milling.</p>				

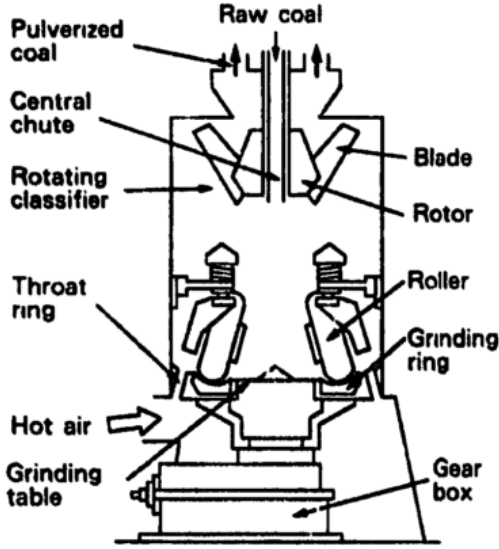
Manufacturers:	<ul style="list-style-type: none">• Brabender<ul style="list-style-type: none">○ http://www.brabender.com/english/food/products/sample-preparation/grinding/rotary-mill.html
References:	

<i>Breakage Modes</i>	<i>Parameters</i>	<i>Specification notes</i>	<i>Product grading</i>
<i>Centrifugal Mill</i>			
  <p>RT: rotor teeth GS: grinding screen GP: ground</p> <p>Source: (Silva & Xavier, 2011)</p>	<ul style="list-style-type: none"> • Impact • Shearing 	<ul style="list-style-type: none"> • Rotor teeth number • Rotor teeth size • Sieve aperture size • Feed rate 	<ul style="list-style-type: none"> • Batch operation • Open cycle operation via hopper and feed system and • More situated to lab scale milling with small samples. • Various designs may have different grinding media.
<p>Grinding Principle:</p> <p>Centrifugal acceleration throws the material outwards with high energy impacting the wedge-shaped rotor teeth that is moving at high speed. The shearing of particles then occurs between the rotor and the fixed ring sieve.</p>			

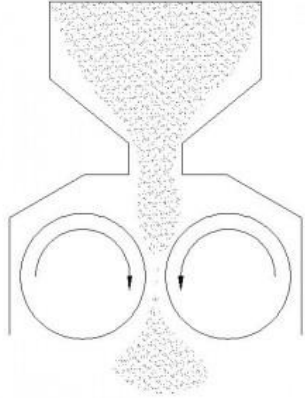
Manufacturers:	<ul style="list-style-type: none">• Retsch<ul style="list-style-type: none">○ http://www.retsch.com/api/?action=product_pdf&productId=5&id=2296508&L=0&userId=&site=retsch&print_language=0&print_info=1&print_image=1&print_images=1&print_examples=1&print_advantages=1&print_features=1&print_video_link=1&print_principle=1&print_orderinfo=1
References	(Silva & Xavier, 2011)

	<i>Breakage Modes</i>	<i>Parameters</i>	<i>Specification notes</i>	<i>Product grading</i>
<i>Ball and Race Mill</i>	 <ul style="list-style-type: none"> • Compression 	<ul style="list-style-type: none"> • Number of grinding balls • Size of the grinding media • RPM • Feed rate 	<ul style="list-style-type: none"> • Small scale batch processing units available • Continuous open cycle and closed cycle operations via air classification • Mills are fed via gravity chute • A variant on this mill is used to Hardgrove Grindability Indexing • Some variation in design whereby compression is generated via centrifugal action on the balls instead of being held and rotated by the upper race ring. 	>76 μm
<p>Grinding Principle: The fuel is fed through the centre on to a rotating table. Centrifugal action throws the fuel out to race where the grinding media, large grinding balls, grinds the fuel. The ground material passes over the rim of the table where it is swept by air flowing at high velocity carrying it to the classifying unit, oversized particles are returned to the rotating table for further comminution.</p>				

Manufacturers:	<ul style="list-style-type: none"> • Williams Patent Crusher and Pulveriser Co. <ul style="list-style-type: none"> ○ http://www.retsch.com/api/?action=product_pdf&productId=5&id=2296508&L=0&userId=&site=retsch&print_language=0&print_info=1&print_image=1&print_images=1&print_examples=1&print_advantages=1&print_features=1&print_videolink=1&print_principle=1&print_orderinfo=1 • Alstom India Ltd. <ul style="list-style-type: none"> ○ http://www.alstom.org/Global/Power/Resources/Documents/Brochures/mills-ball-race-mill.pdf
References:	(L. G. Austin et al., 1982; L. G. Austin et al., 1981)

<i>Breakage Modes</i>	<i>Parameters</i>	<i>Specification notes</i>	<i>Product grading</i>
<i>Ring and Roller</i>			
	<ul style="list-style-type: none"> • Compression 	<ul style="list-style-type: none"> • Number of grinding rollers • RPM • Feed rate 	<ul style="list-style-type: none"> • Continuous open cycle and closed cycle operations via air classification • Mills are fed via gravity chute • Variation in the design is a bowl mill where the ring is shaped like a bowl
Source: (Shoji et al., 1998)			
<p>Grinding Principle: The fuel is fed through the centre on to a rotating table. Centrifugal action throws the fuel out to race where the grinding media, large grinding rollers, grinds the fuel. The ground material passes over the rim of the table where it is swept by air flowing at high velocity carrying it to the classifying unit, oversized particles are returned to the rotating table for further comminution.</p>			

Manufacturers:	<ul style="list-style-type: none">• Alstom Power Steam Auxiliary Components Mills Group<ul style="list-style-type: none">○ http://www.alstom.com/power/coal-oil/mills-pulverisers/bowl/• Loesche<ul style="list-style-type: none">○ http://www.loesche.com/en/products/dry-grinding-plants/technology/modul-concept/
References:	(K. Sato et al., 1996; Shoji et al., 1998)

	<i>Breakage Modes</i>	<i>Parameters</i>	<i>Specification notes</i>	<i>Product grading</i>
Roller				
	<ul style="list-style-type: none"> • Compression • Shearing 	<ul style="list-style-type: none"> • Roller separation distance • Feed rates • Roller diameter and length • Rollers may have teeth • Teeth may be aligned in synchronous rotation or opposing rotation • RPM 	<ul style="list-style-type: none"> • Mainly open cycle operation • Not often used on coal more for the food processing industry • Gravity chute and hopper fed • Roller separation is a method of internal classification • They are not great for fine grinding or consistent particle distributions 	>250 μm
<p>Source: http://blog.insta-pro.com/tag/roller-mills/</p>				
<p>Grinding Principle:</p> <p>The raw material is fed between two or more motor driven rollers. As they material passes between them it is compressed and the stress propagation causes cracking and breakage of the material. This continues until the product is fine enough to pass between the roller separation distances.</p>				

Manufacturers:	<ul style="list-style-type: none">• Alvan Blanch<ul style="list-style-type: none">○ http://www.alvanblanchgroup.com/roller-mills-rv-range• Renn Mill Center Inc.<ul style="list-style-type: none">○ http://www.renncenter.com/grain-processing/rollermills/standard/
References:	(G. M. Campbell, Bunn, Webb, & Hook, 2001; Grant M. Campbell et al., 2012; G. M. Campbell & Webb, 2001)

Appendix B: Modelling Technique Evaluation and Ranking Analysis Paper Summary

The following appendix provides a table for papers listed that contributed to the analysis of literature used in chapter 3. These papers aided in development of the model ranking evaluation and scorecard. This included determining the appropriate variables to focus on, highlight key conclusions that did not need to be investigated more, and highlight where the gaps in the literature were.

<i>No.</i>	<i>Reference</i>	<i>Mills</i>	<i>Manufacturer</i>	<i>Scale</i>	<i>Independent Variables</i>	<i>Materials</i>	<i>Dependent Variables</i>	<i>Objective of Paper</i>
1	(Oyedeji & Fasina, 2017)	Hammer	Bell Co. 10HBLPK	Pilot	<ul style="list-style-type: none"> • Drying – grinding sequence 	<ul style="list-style-type: none"> • Loblolly pine chips 	<ul style="list-style-type: none"> • Moisture Content • Drying energy consumption • Specific grinding energy • PSD • Aspect Ratio • Bulk Density • Tap Density • Flow index • Compressibility Index 	Determine an optimal drying-grinding sequence for grinding of wood pine for combustion.
2	(Bitra et al., 2011)	Cutting	H.C. Davis Sons Mfg. Co., Inc.:	Medium	<ul style="list-style-type: none"> • Screen Size 	<ul style="list-style-type: none"> • Wheat straw 	<ul style="list-style-type: none"> • PSD • Rosin-Rammer Char • Geometric mean & SD • Percentiles: 10,50,90 	Determine the effect of different mill operating conditions on cut size of wheat straw

							<ul style="list-style-type: none"> • Mass relative span 	
3	(V. S. R. Bitra et al., 2009)	Hammer	Schuttle Buffalo	Lab	<ul style="list-style-type: none"> • Angular velocity • Hammer mounting angle 	<ul style="list-style-type: none"> • Switch grass • Wheat straw • Corn Stover 	<ul style="list-style-type: none"> • PSD • Specific grinding energy • Rosin-Rammler Char • Uniformity index ($D_5:D_{95}$) • Size guide: Median x100 • Geometric mean & SD 	Study the effect of mill settings on cut size and energy consumption
4	(Doroodchi, Zulfiqar, & Moghtaderi, 2013)	Ball	Bico-Braun	Lab	<ul style="list-style-type: none"> • Time • Blend ratio 	<ul style="list-style-type: none"> • Lithgow coal • Eucalyptus chip 	<ul style="list-style-type: none"> • PSD: sieve and malvern • Aspect ratio • Circularity • Roundness • Sphericity 	Study into coal/biomass blends in lab and pilot scale mills
5	(Miao et al., 2011)	Hammer Cutting Hammer	David Bradley (hammer mill 1) Retsch SM2000	Industry Lab Lab	<ul style="list-style-type: none"> • Type • Screen size 	<ul style="list-style-type: none"> • Miscanthus grass • Switchgrass • Willow chips • Energy cane 	<ul style="list-style-type: none"> • PSD • Geometric mean & SD • Absolute density • Particle surface area 	Investigate relationships between comminution energy consumption and

			Retsch SK100				<ul style="list-style-type: none"> • Ratio of comminution • Specific grinding energy 	resulting particle physical properties
6	(Mani, Tabil, & Sokhansanj, 2004)	Hammer	N/A	Pilot	<ul style="list-style-type: none"> • Screen size 	<ul style="list-style-type: none"> • Wheat straw • Barley straw • Corn stover • Switchgrass 	<ul style="list-style-type: none"> • PSD • Moisture content • Bulk density • Absolute density • Heating value • Ash content • Geometric mean & SD • Specific grinding energy 	Measure and compare handling related physical properties of biomass with respect to grinding and particle size.
7	(Tamura et al., 2014)	Ball Vertical Roller Vibratory	N/A	Lab Lab Lab	<ul style="list-style-type: none"> • Type • Grinding media • Speed • Time 	<ul style="list-style-type: none"> • Cedar chip • Pinus bark • Wood pellet 	<ul style="list-style-type: none"> • PSD • Specific grinding energy 	Study three different pulverisation methods, understand the continuous grinding phenomenon
8	(Womac et al., 2007)	Cutting Hammer	N/A	Lab Lab	<ul style="list-style-type: none"> • Speed • Screen size 	<ul style="list-style-type: none"> • Switchgrass • Corn stover • Wheat straw 	<ul style="list-style-type: none"> • PSD • Specific grinding energy 	To develop a common-platform

		Disk		Lab			<ul style="list-style-type: none"> • Geometric mean & SD 	instrument system for determining product and energy efficiency of rotary mills
9	(M Gil et al., 2008)	Duplex (hammers and strikers) Hammer	N/A		<ul style="list-style-type: none"> • Screen size • Type • Batch or continuous cycle • Process variation 	<ul style="list-style-type: none"> • Corn stover • Pine chips 	<ul style="list-style-type: none"> • PSD • Specific grinding energy • Bulk density 	Evaluation of milling energy requirements for biomass residues in a pilot plant for co-firing
10	(V. S. P. Bitra et al., 2009)	Cutting	H.C. Davis Sons Mfg. Co., Inc	Lab	<ul style="list-style-type: none"> • Speed • Feed rate • Screen size 	• Switchgrass	<ul style="list-style-type: none"> • PSD • Rosin-Rammer Char • Geometric mean & SD • Percentiles: 10,50,90 • Mass relative span • Skewness • Kurtosis 	Study to the product of knife milled switchgrass with different mill operating conditions

							<ul style="list-style-type: none"> • Uniformity index (D₅:D₉₅) • Size guide: Median x100 • Coefficient of uniformity (D₆₀/D₁₀) • Coefficient of gradation: (D₃₀²/D₁₀xD₆₀) 	
11	(Esteban & Carrasco, 2006)	Hammer		Lab	<ul style="list-style-type: none"> • Screen size • Process 	<ul style="list-style-type: none"> • Poplar chip • Pine chip • Pine bark 	<ul style="list-style-type: none"> • Moisture • Bulk density • PSD • Arithmetic mean • Ratio of comminution • Specific grinding energy 	Finding the optimal for obtaining the desired PSD and minimal energy from the milling of 3 biomass species
12	(Kobayashi et al., 2008)	Vibratory Cutting		Lab Lab	<ul style="list-style-type: none"> • Time • Media • Moisture content 	<ul style="list-style-type: none"> • Spruce shavings 	<ul style="list-style-type: none"> • PSD • Aspect ratio • Crystallinity 	Study pulverisation methods in for wood powder creation
14	(J. S. Tumuluru et al., 2014)	Hammer Chopper	Glen Mills Inc.	Lab	<ul style="list-style-type: none"> • Screen size 	<ul style="list-style-type: none"> • Barley straw • Wheat straw • Oat straw 	<ul style="list-style-type: none"> • Specific grinding energy • Moisture content 	Focuses on the relation between

						<ul style="list-style-type: none"> • Canola straw 	<ul style="list-style-type: none"> • Bulk density • Tapped density • Absolute density • Geometric mean & SD • Porosity • Hausner Ratio • Carr index 	grinding energy and physical properties of biomass
15	(Adapa, Tabil, & Schoenau, 2011)	Chopper Hammer		Lab	<ul style="list-style-type: none"> • Screen size • Feed rate 	<ul style="list-style-type: none"> • Barley straw • Wheat straw • Oat straw • Canola straw 	<ul style="list-style-type: none"> • PSD • Geometric mean & SD • Specific grinding energy • Moisture content • Bulk density • Absolute density 	Evaluation of the difference in non-treated and steam exploded biomass straws is investigated
16	(Too et al., 2012)	Cutting	Dickson DFT-150	Lab	<ul style="list-style-type: none"> • Time • Load 	<ul style="list-style-type: none"> • Star anise • Cinnamon • Coriander 	<ul style="list-style-type: none"> • PSD • Moisture • Absolute density • Arithmetic mean • Throughput efficiency • Ratio of comminution 	Study the effect of load and time on grinding statistics

							<ul style="list-style-type: none"> • Rate of comminution 	
17	(Miguel Gil & Arauzo, 2014)	Hammer		Lab	<ul style="list-style-type: none"> • Moisture content • Feed size • Target size • Angular velocity 	<ul style="list-style-type: none"> • Poplar • Corn stover 	<ul style="list-style-type: none"> • PSD • Geometric mean & SD • Skewness • Kurtosis • Rosin-Rammler Char • Mass relative span • Coefficient of uniformity (D_{60}/D_{10}) • Coefficient of gradation: ($D_{30}^2/D_{10} \times D_{60}$) • Uniformity index ($D_5:D_{95}$) • Percentiles: 10,50,90 	Determine the influence of biomass conditions and mill operating condition on the final product size
18	(Z. Ghorbani, Masoumi, & Hemmat, 2010)	Hammer		Lab	<ul style="list-style-type: none"> • Screen size 	<ul style="list-style-type: none"> • Alfalfa 	<ul style="list-style-type: none"> • Specific grinding energy • PSD • Geometric mean & SD 	Investigate grinding energy and with screen sizes and

							<ul style="list-style-type: none"> Moisture content 	relation to Kick, von Rittenger and Bond
19	(Goswami & Singh, 2003)	Disk	Ukani	Lab	<ul style="list-style-type: none"> Feed rate Temperature 	<ul style="list-style-type: none"> Cumin seeds 	<ul style="list-style-type: none"> PSD Ratio of comminution Specific grinding energy 	Investigate feed rates and feed temperatures of cumin grinding
20	(F Nasaruddin et al., 2012)	Cutting	Dickson DFT-150	Lab	<ul style="list-style-type: none"> Load Time 	<ul style="list-style-type: none"> Cardamom seed Clove seed Cumin seed 	<ul style="list-style-type: none"> PSD Rate of comminution Size reduction efficiency 	Investigation in to the effect of grinding time and load on particle product
21	(Zahra Ghorbani, Masoumi, Hemmat, & Seifi, 2013)	Hammer			<ul style="list-style-type: none"> Feed size Screen size 	<ul style="list-style-type: none"> Alfalfa 	<ul style="list-style-type: none"> PSD Specific grinding energy Geometric mean & SD Bulk density 	Determining the correlation coefficient between physical and mechanical properties of grinding

Appendix C: Modelling Technique

Evaluation and Ranking Industrial Partner Survey

This appendix is a copy of the survey issued to the BF2RA members and documents their response to the survey questions. The survey was designed to determine how the members put into action the key findings of the literature review and helped to shape the model ranking evaluation and scorecard.

1. I would like to compile a list of mills in use by the members of the BF2RA to include details such as type, use, location and size (defined by throughput); the objective of which is to know where to focus the modelling efforts going into the model development stage.
 - a. Could the members provide me with that?
 - b. When do you think that would be available?

“Coal Plant at Ratcliffe uses Babcock 10E mills (vertical spindle mill, ball and ring). Throughput of each mill is approx. 35 tonnes/hour. 8 mills per unit installed, of which 6 required in service at full load (2 spare).

Ball mills are installed at Cottam and Eggborough (Foster Wheeler D 9 pressurised, horizontal ball mills).

Mills at West Burton, Fiddlers Ferry have Lopulco mills installed which are vertical spindle.

Other mills which have been used in the power industry include the Raymond roller mills.

For biomass firing hammer mills are generally used which can be of the horizontal or vertical type, with number of manufacturers in the market place. In addition, Losche mills have been used at Avedoere and Amager plants for milling biomass which are of the vertical roller type. Throughputs for the mills vary considerable

with fuel type and generally trials are undertaken before mills are selected for a particular application.

Biomass hammer mills installed at Fiddlers Ferry (two DFZK2 vertical hammer mills are installed) and Drax are of the Buhler vertical spindle design.

Amer 8 has horizontal hammer mills (Christy, Briton 960).

For the Ironbridge biomass conversion project 10 hammer mills installed per unit, approx. 23 tonnes per hour each.

Companies that produce mills for biomass, but not limited to, include Christy Turner, Andritz, Losche and CPM. Further details of the biomass mills can be obtained from the manufacturer's web sites."

2. Likewise, for the different source fuels used by the members, I appreciate this is likely to change often though. Again:
 - a. Could the members provide a list¹?
 - b. When would this be available?
 - c. How often do these changes and what determines the change in fuel? The following is a list of assumptions in this matter.
 - i. Seasonal growth patterns, for example, olives are harvested for about 4 months of the year from late October through to Jan.
 - ii. Storage capability – enhanced by initial pre-treatment; pelletisation, torrefaction, etc.
 - iii. Crop yield.
 - iv. Susceptibility to environmental conditions.
 - v. Cost.

¹ It is recognised that members may not want to share details of the materials used and strategies in place to protect their own interest, whilst the information would be useful for determining key focuses of the modelling project, the project will not be detrimentally affected by the absence of this information.

“Coal Plant: Ratcliffe fires both indigenous and import coals.

Typical biomass fuels that have been available in large quantities include wood pellet, palm kernels, olive pellets and olive cake. However, a number of other fuels such as willow, Miscanthus and straw have been tested in a number of power plants. A list of fuels of interest to the BF2RA members was sent 10th February 2014.

Biomass Plant: Ironbridge fires wood pellets. Different product specifications are available known as I1, I2 and I3.”

3. To establish what practices are used in industry already I would like to compile a database of what is used.
 - a. Can the members provide me with a list of techniques, methodologies, or processes by which they are determining milling parameters within their operations already?
 - i. Info on this is also requested on the practices for coal if possible.

Coal Plant: Coal throughput is controlled by flow rate of primary air (higher flow means more coal is carried out of the mill). The level of coal in the mill is monitored by mill differential pressure and is controlled by adjusting the feeder speed, which delivers coal from the bunker to the mill table. In a vertical spindle mill, coal is recirculated around the mill via a classifier: undersize material is carried out of the mill while oversize material is recirculated for further grinding.

The coal mill also has to dry raw coal. Typically, around 2/3rds of the coal moisture is evaporated and carried out of the mill with the PA/PF stream. Outlet temperature is typically 70-85oC, and inlet temperature is typically 180 – 250oC (depending on coal moisture and throughput).

The PA/PF ratio is maintained under a fuel-rich condition during steady-state operation, (typically the PA/PF ratio is 1.3 to 2 on a mass basis and depends on the mill type). This reduces the risk of fires/explosions. However, during start-up and shut-down the PA/PF ratio passes through the explosive range.

The Coal Quality Impact models that are used include the calculation of the following parameters:

- *Mill throughput and number of mills required in service. This is dependent on coal NCV, moisture content and HGI.*
- *Pulverised fuel (PF) grind quality (relative to a baseline value) – there is a trade-off between mill throughput and grind quality.*
- *Mill power demand.*
- *Mill heat balance, i.e. whether there is sufficient hot primary air from the air heaters to dry the coal (the lowest acceptable PA/PF outlet temperature is ~60-65°C)*
- *Mill wear rates and mill maintenance demands (i.e. component replacement costs).*

Biomass Plant: biomass throughput in some cases is controlled by mill feeder speed, which takes fuel from an intermediate hopper. This hopper is replenished from the main fuel bunker via another feeder. There is no fuel recirculation within the hammer mill, but only undersize material passes through the screens and onwards to the boiler (via being fed into the primary air stream).

The most important parameters regarding mill performance monitoring are:

- *Biomass throughput and grind quality (particle size distribution). The hammer mills primarily break-up the pellets into the original particles, but there is some additional comminution.*
- *Mill wear rate: hammers wear out relatively quickly and require replacement.*
- *Mill power demand. Mill power is known to change depending on level of hammer wear, as well as due to mill throughput, moisture content and inlet particle size.*

In general, full scale milling trials are undertaken with the design biomass fuel in order to be able to select a mill and screen size, for the correct throughput, whilst

giving the required fuel grading. As for coal, the fuel properties such as NCV determine the throughput required from the mill with the moisture content and inlet particle size/properties affecting the mill performance. Most hammer mill applications utilise ambient air for transport of the milled fuel to the boiler.”

Appendix D: Modelling Technique Evaluation and Ranking Scorecard

This appendix documents the scorecard applied to the evaluation of the modelling techniques that were considered for review in chapter 3 of this thesis. The scorecard describes the sections under which each was evaluated and the scoring criteria for each score.

		<i>Score</i>	<i>Definition for rank in the corresponding Category</i>
Modelling the Scenario	Application to the modelling variables is assessed. Priority is given to the techniques ability to model the primary variables of investigation with further bonus points for the capability to account for secondary variables.	1	The technique is capable of modelling just a few secondary interest variables and no primary interest variables.
		2	The technique is capable of modelling a few primary variables, potential application for some secondary interest variables.
		3	The technique is capable of modelling all primary interest variables
		4	The technique is capable of modelling all primary interest variables, potential application for some secondary interest variables
		5	The technique is capable of modelling all primary interest variables, application to several secondary interest variables available
Computational Requirements	The expected computational requirement for implementation of the modelling technique s assessed and a score awarded based on the deviation from the desired implementation: desired is defined as able to run on a standard desktop computer with computational time of less than 7 hours.	1	Requires more than 7 hours real time processing with parallel processing on high end resources, i.e. UoN's High Performance Cluster.
		2	Requires more than 7 hours real time processing on a high specification computer.
		3	Requires a less than 7 hours real time processing on a high specification computer
		4	Requires more than 7 hours real time processing on a standard desktop computer
		5	Requires less than 7 hours real time processing on a standard desktop computer

Software and Coding	The desirable trait is that suitable software for implementing the technique is available from within the university with no associated cost or obtainable with little or no cost externally. Deviation from this is considered in the direction of availability and increase in price. Program development is considered less preferable due to the time it takes to develop the core code and user interface.	1	No software is available and would require program development.
		2	Software is available at significant cost and the university has no appropriate software already.
		3	Software is available at significant cost; the university already has suitable software that requires contribution.
		4	Software is available at little or no cost or the university already has access to appropriate software that requires a contribution.
		5	Software is available with minimal or no cost or the university has software available for use already.
Data dependency	The ideal scenario is one whereby the physical aspects of milling are modelled directly and a simulation of the milling practices can be used to generate results and optimisation. Reductions from the ideal increase the reliance on data to determine the model parameters, therefore making the simulation less predictive.	1	The technique relies wholly on direct milling experimental results to determine the model
		2	The technique requires some direct milling experiments to determine the model however further elements can be determined from material characterisation.
		3	The technique can be driven from physical principals and data provided from material characterisation
Model validation	In general validation will come from comparison with	1	There is no way to validate the results of the simulation without significant design and implementation of experiments.

	<p>experimental results however given the nature of the a mill environment, experimental result may not be available, requiring extra work to obtain or they may not be obtainable based on the facilities at hand. 'significant redesign' is defined as, for validation, experimental results would require extensive planning and research into how to validate the variables, additionally access to the appropriate apparatus for the required period is an unknown factor.</p>	2	The model can be validated against key variables with the aid of some additional experimentation
		3	The model can be validated against key variables with results readily available, secondary interest variables requires extensive design and implementation of experiments.
		4	The model can be validated against key variables with results readily available, secondary interest variables requires some additional experimentation
		5	The model can be validated against key and secondary variables with results readily available
Industrial scale-up	<p>This category relates to the adaptability of the modelling technique when industrial scale-up becomes necessary to advance the project. Considerations that are required are whether the modelling technique is appropriate to facilitate the modelling of industrial scale millings measurable dependent variables. Furthermore an</p>	1	The application of the modelling technique is inappropriate to industrial scale milling. Use of alternative modelling techniques would be required.
		2	The modelling technique has application potential to industrial scale milling however significant overhaul of the model program would be required to accommodate the measurable industrial dependent variables.
		3	The modelling technique is directly applicable to industrial scale modelling however adaptation to accommodate the industrial variables would require significant model changes.

	assessment as to scale of work necessary to alter the program in order to facilitate this is made.	4	The modelling technique is directly applicable to industrial scale milling covering all the measurable independent variables with minor modification of the program to accommodate this.
		5	The technique is directly transferable and applicable to industry scale modelling of mills (minor alterations based on the industrial independent variables are tolerated).

Appendix E: Modelling Technique Evaluation and Ranking Results

This appendix provides the results of the modelling technique evaluation and scoring process. Here you will find the tables that allocate each score to the technique in a fashion outlined in appendix D. The table of scores lists the techniques in isolation and scores for hybrid implementations of the technique.

	<i>ANN</i>	<i>PBM</i>	<i>DEM</i>	<i>FEM</i>	<i>PFEM</i>	<i>FVM</i>	<i>SPH</i>	<i>PBM-DEM</i>	<i>FEM-DEM</i>	<i>DEM-FEM</i>	<i>DEM-FVM</i>	<i>DEM-SPH</i>	<i>SPH-FEM</i>
Modelling the Scenario	3	3	4	2	2	2	2	4	5	5	5	4	2
Computational Requirements	5	5	2	3	2	3	2	3	2	2	2	2	3
Software and Coding	5	4	2	3	2	3	2	3	2	2	2	2	3
Data dependency	1	2	3	3	3	3	3	3	3	3	3	3	3
Model validation	3	4	4	1	1	2	1	4	4	4	4	3	1
Industrial scale-up	3	4	2	2	1	3	1	3	1	3	3	1	1
Totals	20	22	17	14	11	16	11	20	17	19	19	15	13

Appendix F: Particle Characteristics

This appendix lists the different methods of partial characterisation and their governing equations/methods of analysis. In practice most of these are calculated directly by the CAMSIZER as detailed in chapter 5.1.3. The tables are split into 3 section, particle size distribution analysis, measures of particle size and measures of particle shape.

<i>Measure of particle size distribution dispersion</i>	<i>Definition</i>
<p>Coefficient of gradation, used in conjunction with C_u to determine if all size classes in a particle size distribution are suitably represented.</p>	$C_g = \frac{d_{30}^2}{d_{10}d_{60}}$
<p>Coefficient of uniformity, values less than 4 are considered uniformly graded and the particle sizes are similar.</p>	$C_u = \frac{d_{60}}{d_{10}}$
<p>Inclusive graphic skewness, shows the deviation of the distribution from a normal bell curve, $K_I = 0$ indicates a normal curve, $K_I > 0$ indicates a left shift in the curve, $K_I < 0$</p>	$K_I = \left(\frac{d_{16} + d_{84} - 2d_{50}}{2(d_{84} - d_{16})} \right) + \left(\frac{d_5 + d_{95} - 2d_{50}}{2(d_{95} - d_5)} \right)$

indicates a right shift in the distribution curve.

Kurtosis, is a measure of the peakedness of a distribution, $K_g = 3$ indicates 'normal' mesokurtic, $K_g < 3$ indicates a wider, platykurtic distribution, $K_g > 3$, indicates narrower, leptokurtic distribution.

$$K_g = \frac{d_{95} - d_5}{2.44(d_{75} - d_{25})}$$

Relative span, (mass, m or volume, v), is a measure of how varied a PSD is, the smaller the number the less varied the distribution is: CAMSIZER P4 obtained for volume measure

$$RS_v = \frac{d_{90} - d_{10}}{d_{50}}$$

Uniformity Index, is the ratio of the extreme sizes in the PSD, 100 indicates particles are the same size, 50 indicates the small particles are half the size of the large: CAMSIZER P4 obtained

$$U_I = 100 \frac{d_5}{d_{90}}$$

Coefficient of variation, is the standard deviation of the size distribution divided by the median size: Not currently used.

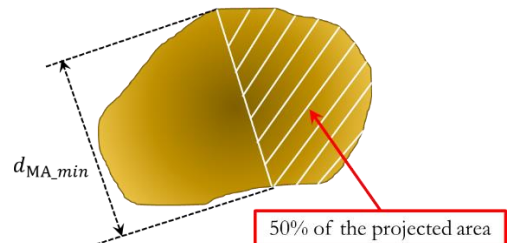
$$C_v = 50 \frac{d_{84} - d_{16}}{d_{50}}$$

<i>Measure of particle size</i>	<i>Definition</i>
p^{th} % passing size – PSD: CAMSIZER P4 obtained	d_p , determined by interpolation between PSD points from a measured distribution.
p^{th} % passing size - calculated: CAMSIZER P4 obtained	$d_p = d' \left[-\ln \left(1 - \frac{F(d)}{100} \right) \right]^{1/n}$
Geometric mean diameter , between size classes, used as a precursor for determining the geometric mean for the particle size distribution.	$\bar{D}_i = \sqrt{d_i \cdot d_{i-1}}$
Geometric mean diameter , distribution where M_i indicates the % fraction at size class i (mass, m or volume, v)	$D_{gm} = \exp \left[\frac{\sum M_i \ln(\bar{D}_i)}{\sum M_i} \right]$
Geometric standard deviation alternative to the whole system, calculated from the ratio of high to low particle size fractions	$S_{gm_p} = \sqrt{\frac{d_{84}}{d_{16}}}$
Geometric standard deviation of the high regions of the particle size distribution	$S_{gm_h} = \frac{d_{84}}{d_{50}}$
Geometric standard deviation of the low region of the particle size distribution	$S_{gm_l} = \frac{d_{50}}{d_{16}}$

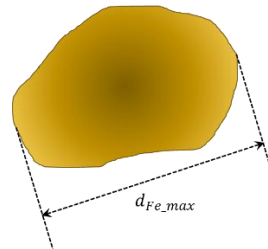
Geometric standard deviation, calculated based on the geometric mean diameter between size classes.

$$S_{gm_w} = \exp \left[\frac{\sum (M_i (\ln d_i - \ln \bar{D}_i))^2}{\sum M_i} \right]$$

Martin diameter, d_{Ma} is the minimum bisecting diameter separating 50% of the projection area: CAMSIZER P4 obtained



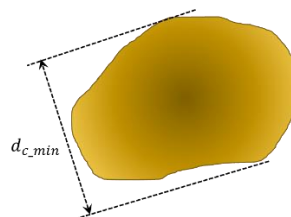
Maximum Feret diameter, d_{Fe} , is the longest diameter through a particle projection: CAMSIZER P4 obtained



Maximum Stretched Length, $d_{Stretch}$ is a measure of the length of the projection when stretched out to eliminate curvature: CAMSIZER P4 obtained

$$d_{stretch} = \frac{A}{d_{Ma_min}}$$

Minimum chord diameter, d_c . analogous to sieve analysis, minimum size passing, is the minimum of the maximum diameters in each orientation of the particle: CAMSIZER P4 obtained



Rosin-Rammler

cumulative distribution
function: CAMSIZER P4
obtained

$$R(d) = 100 \left[1 - \exp \left[- \left(\frac{d}{d'} \right)^n \right] \right]$$

Rosin-Rammler

distribution function

$$r(d) = \left(\frac{n}{d'} \right) \left(\frac{x}{d'} \right)^{n-1} \exp \left[- \left(\frac{d}{d'} \right)^n \right]$$

Size Guide Number, is the
diameter of the median particle
size, (note: **d_{50}** is expressed in
mm): CAMSIZER P4 obtained

$$C_{SGN} = 100d_{50}$$

Measure of Particle Shape

Definition

Aspect ratio, the ratio of
the length to the breadth
of a particle: CAMSIZER
P4 obtained

$$\psi_{AR} = \frac{d_{c_min}}{d_{Fe_max}}$$

Circularity, ratio of area
equivalent diameter to
perimeter equivalent
diameter: CAMSIZER P4
obtained

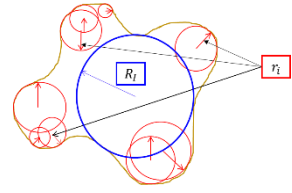
$$\psi_c = \frac{4\pi A}{p^2} = \frac{d_{ev}}{p^2}$$

Operational sphericity,
ratio of a volume
equivalent diameter, to
the circumscribed
diameter of the particle:
CAMSIZER P4 obtained

$$\psi_{op} = \frac{\pi^{-\frac{1}{3}}(6V)^{\frac{1}{3}}}{d_{Fe_max}} = \frac{d_{ev}}{d_{Fe_max}}$$

Roundness, measure of the radii of 'corners' in the particle to an inscribed maximum circle within the particle:
CAMSizer P4 obtained

$$\psi_R = \frac{\sum_{i=1}^n r_i}{nR_I}$$



Sphericity, volume based surface area calculation/area of particle projection: Not currently used.

$$\psi_s = \frac{\pi^{\frac{1}{3}}(6V_p)^{\frac{2}{3}}}{A_p}$$

Appendix G: Overlapping Coefficient Calculation MatLab™ Script

This script was created and used in the research for calculating the Overlapping Coefficient between two probability distribution functions. The script is implemented in the MatLab™ and uses several built in MatLab™ functions for interpolating distributions where the size classes are not the same and the maximum and minimum function.

```
function OVL = ovlfit(ExpPSD, SimPSD, eSize, sSize)

% OVL provides a measure of assessment for
% probability frequency
% distributions that is separate from the
% other methods in that comparison
% of non-linear data can be easily
% achieved.

uMax    = max(max(eSize), max(sSize));
uMin    = min(min(eSize), min(sSize));
nGrd    = uMin:1:uMax;

exIn    = interp1(eSize, ExpPSD, nGrd, 'pchip');
siIn    = interp1(sSize, SimPSD, nGrd, 'pchip');

exIn    = exIn./sum(exIn);
siIn    = siIn./sum(siIn);

OVLdiff = min(exIn, siIn);
OVL     = sum(OVLdiff);

end
```

Appendix H: Biomass Materials Used in the Research

This appendix provides data relating to the different biomass fuel pellets used in this research. The first table lists the characteristics determined through this research whilst the second table displays the information collected from the sister project. Each provides a different way to characterise the biomass pellets.

<i>Material</i>	<i>Mean Surface Area (cm² g⁻¹)</i>	σ_{SA}	<i>Particle Density (g cm³)</i>	<i>Mean Skeletal Density (g cm³)</i>	σ_{skel}	Single Impact Testing (Sieve Results)				TGA Moisture Content (%), SIT Samples	
						f_{mat} (J m kg ⁻¹)	σ_{mat}	$W_{m,min}$	$\sigma_{W_{m,min}}$	<i>Mean Moisture Content (%)</i>	σ_{mc}
<i>Uncertainty in Measurement</i>	± 0.00005	-	± 0.00005	± 0.00005	-	± 0.0005	-	± 0.0005	-	± 0.005	-
Brites Wood	0.1334	0.0117	1.2920	1.5001	0.0073	0.297	0.031	0.301	0.016	7.26	0.21
Eucalyptus	0.2736	0.0098	1.202	1.5104	0.0090	-	-	-	-	-	-
Miscanthus	0.2720	0.0182	1.188	1.5287	0.0094	0.225	0.029	0.202	0.014	6.71	0.27
Mixed Wood	0.1156	0.0187	1.202	1.4756	0.0056	-	-	-	-	-	-
Microwave Torrefied	0.2148	0.0090	1.107	1.5160	0.0192	0.695	0.080	0.189	0.006	3.85	0.1
Sunflower	0.3230	0.0658	1.139	1.5237	0.0364	-	-	-	-	-	-

Mechanical Testing Deformation energy									
<i>Material</i>	<i>Diametric (MJ m⁻³)</i>	<i>σ_{dia}</i>	<i>Axial (MJ m⁻³)</i>	<i>σ_{axl}</i>	<i>Flexure (MJ m⁻³)</i>	<i>σ_{flx}</i>	<i>Bulk Density (kg m⁻³)</i>	<i>Pellet Length (mm)</i>	<i>Pellet Diameter (mm)</i>
<i>Uncertainty in Measure</i>	± 0.05	-	± 0.05		± 0.0005		± 0.5	± 0.005	± 0.005
Brites Wood	119.7	17.6	37.8	16.5	0.334	0.18	626	19.05	6.10
Eucalyptus	74.7	41.1	30.1	9.2	0.242	0.118	667	17.42	8.39
Miscanthus	47.8	18.8	28.3	11.16	0.210	0.114	667	19.73	6.29
Mixed Wood	79.7	3.7	12.5	6.26	0.380	0.191	667	21.07	8.40
Microwave Torrefied	46	40.9	13.9	7.5	0.170	0.109	667	18.22	5.76
Sunflower	38.7	17.4	44.9	26.3	0.380	0.329	500	14.16	8.62

Appendix I: Lopulco Experiment Mean Results

This appendix provides the mean result tables for the Lopulco experiments. The analysis includes the general running experiment details, mass output, energy consumption etc. Additionally, all the particle characterisation characteristics, calculated from the CAMSIZER analysis are given, with results for the particle measure techniques listed in appendix F. The results are split between the operational condition variation experiments completed with Brites wood pellets and the Material Variation experiments completed with Eucalyptus wood pellets, Miscanthus grass pellets and a Microwave Torrefied wood pellet.

Operational Variation Experiments

<i>Feed Rate (kg s⁻¹)</i>	<i>Mill Speed (rpm)</i>	<i>Classifier Vane Angle (°)</i>	<i>Input mass (kg to 1 d.p)</i>	<i>Output mass (kg to 1 d.p)</i>	<i>Specific Effective Energy (kWh t⁻¹ to 2 d.p)</i>	<i>Output Rate (kg s⁻¹ to 4 d.p)</i>	<i>Residence Time (s to 1 d.p)</i>
<i>Uncertainty in Measure</i>							
± 0.00001	± 1	± 0.5	± 0.00005	± 0.00005	± 0.005	± 0.000005	± 0.005
0.0102	242	20	1000.3	977.5	24.23	0.0096	69.0
0.0102	242	55	1000.1	978.7	22.29	0.0080	72.2
0.0102	242	90	1000.1	967.6	13.85	0.0081	72.1
0.0102	309	55	1000.0	955.2	15.37	0.0074	73.6
0.0102	175	55	1000.2	948.8	17.11	0.0084	71.8
0.0140	282	20	1000.4	933.1	17.93	0.0084	71.8
0.0140	282	90	1000.5	949.7	28.28	0.0060	85.8
0.0140	202	20	1000.4	953.8	27.60	0.0062	83.4
0.0140	202	90	1000.3	970.1	27.60	0.0051	89.2
0.0167	242	55	1000.2	967.6	17.17	0.0067	78.6
0.0036	242	55	1000.3	985.1	16.72	0.0036	58.5
0.0063	282	20	1000.4	974.0	41.28	0.0036	58.5
0.0063	282	90	1000.4	974.0	41.28	0.0036	58.5
0.0063	202	20	1000.3	993.4	42.60	0.0062	63.3
0.0063	202	90	1000.3	1061.1	18.29	0.0060	51.5

<i>Feed Rate (kg s⁻¹)</i>	<i>Mill Speed (rpm)</i>	<i>Classifier Vane Angle (°)</i>	<i>D bar (μm)</i>	<i>Sigma D bar (μm)</i>	<i>d' (μm)</i>	<i>n (- to 2 d.p)</i>	<i>SGN (- to 0 d.p)</i>	<i>D_{gm} (μm)</i>	<i>S_{gmv} (μm to 2 d.p)</i>	<i>S_{gml} (μm to 2 d.p)</i>	<i>S_{gmb} (μm to 2 d.p)</i>	<i>S_{gmp} (μm to 2 d.p)</i>
<i>Uncertainty in Measure</i>												
<i>±0.00001</i>	<i>±1</i>	<i>±0.5</i>	<i>±0.5</i>	<i>±0.5</i>	<i>±0.5</i>	<i>±0.00005</i>	<i>-</i>	<i>±0.5</i>	<i>-</i>	<i>-</i>	<i>-</i>	<i>-</i>
0.0102	242	20	832	604	910	1.39	70	602	2.36	2.71	1.99	2.32
0.0102	242	55	911	678	983	1.43	75	660	2.30	2.54	2.06	2.29
0.0102	242	90	895	655	968	1.46	75	657	2.22	2.49	2.02	2.24
0.0102	309	55	830	612	897	1.45	70	610	2.22	2.59	1.98	2.26
0.0102	175	55	787	598	846	1.39	66	567	2.36	2.73	2.02	2.35
0.0140	282	20	724	583	769	1.29	59	503	2.58	2.94	2.11	2.49
0.0140	282	90	747	621	784	1.31	59	518	2.55	2.86	2.14	2.47
0.0140	202	20	752	621	791	1.29	60	519	2.59	2.94	2.14	2.50
0.0140	202	90	827	636	879	1.45	68	604	2.26	2.64	2.02	2.30
0.0167	242	55	881	626	948	1.56	74	671	2.04	2.46	1.96	2.19
0.0036	242	55	877	615	949	1.55	74	667	2.08	2.53	1.96	2.21
0.0063	282	20	864	628	942	1.38	73	628	2.42	2.91	2.02	2.42
0.0063	282	90	883	631	966	1.40	75	648	2.41	2.90	2.01	2.40
0.0063	202	20	903	627	990	1.49	77	679	2.17	2.63	1.96	2.26
0.0063	202	90	917	626	1001	1.59	79	705	1.97	2.34	1.92	2.12

<i>Feed Rate (kg s⁻¹)</i>	<i>Mill Speed (rpm)</i>	<i>Classifier Vane Angle (°)</i>	<i>d₅ (μm)</i>	<i>d₁₀ (μm)</i>	<i>d₁₆ (μm)</i>	<i>d₂₅ (μm)</i>	<i>d₃₀ (μm)</i>	<i>d₅₀ (μm)</i>	<i>d₆₀ (μm)</i>	<i>d₇₅ (μm)</i>	<i>d₈₄ (μm)</i>	<i>d₉₀ (μm)</i>	<i>d₉₅ (μm)</i>	<i>d₉₉ (μm)</i>
± 0.00001	± 1	± 0.5	± 0.5	± 0.5	± 0.5	± 0.5	± 0.5	± 0.5	± 0.5	± 0.5	± 0.5	± 0.5	± 0.5	± 0.5
0.0102	242	20	104	177	259	377	441	700	848	1131	1402	1675	2068	2695
0.0102	242	55	122	201	292	413	479	742	905	1215	1532	1864	2372	2979
0.0102	242	90	127	205	296	417	481	737	895	1191	1492	1804	2277	2971
0.0102	309	55	119	189	271	384	444	691	835	1105	1370	1658	2100	2846
0.0102	175	55	105	169	242	349	407	651	793	1058	1310	1569	1982	2876
0.0140	282	20	87	139	198	291	345	583	722	989	1227	1482	1897	2763
0.0140	282	90	93	147	207	301	354	588	729	1004	1256	1538	1989	3060
0.0140	202	20	91	144	204	299	354	595	736	1014	1267	1566	2010	3011
0.0140	202	90	130	196	266	371	430	675	814	1088	1355	1660	2111	3156
0.0167	242	55	165	239	315	422	484	734	879	1166	1428	1716	2154	3037
0.0036	242	55	163	235	312	420	481	737	882	1163	1434	1711	2123	2917
0.0063	282	20	126	191	266	383	450	724	879	1177	1457	1739	2139	2830
0.0063	282	90	133	202	279	401	472	746	902	1207	1483	1762	2166	2869
0.0063	202	20	149	225	307	432	502	767	920	1227	1496	1773	2170	2885
0.0063	202	90	165	249	338	460	524	779	925	1229	1494	1769	2166	3003

<i>Feed Rate (kg s⁻¹)</i>	<i>Mill Speed (rpm)</i>	<i>Classifier Vane Angle (°)</i>	<i>RS_V (- to 2 d.p)</i>	<i>U_I (- to 2 d.p)</i>	<i>C_U (- to 2 d.p)</i>	<i>C_g (- to 2 d.p)</i>	<i>K_I (- to 2 d.p)</i>	<i>K_g (- to 2 d.p)</i>	<i>psi c (- to 2 d.p)</i>	<i>psi AR (- to 2 d.p)</i>	<i>psi op (- to 2 d.p)</i>	<i>psi R (- to 2 d.p)</i>	<i>psi symm (- to 2 d.p)</i>
<i>Uncertainty in Measure</i>													
± 0.00001	± 1	± 0.5	-	-	-	-	-	-	-	-	-	-	-
0.0102	242	20	2.13	5.95	4.80	1.30	0.30	1.06	0.39	0.51	0.59	0.04	0.73
0.0102	242	55	2.24	6.35	4.52	1.27	0.36	1.15	0.43	0.50	0.56	0.06	0.75
0.0102	242	90	2.17	6.93	4.38	1.26	0.35	1.14	0.43	0.50	0.56	0.06	0.75
0.0102	309	55	2.13	7.00	4.47	1.25	0.33	1.12	0.42	0.50	0.56	0.05	0.74
0.0102	175	55	2.16	6.47	4.78	1.24	0.33	1.09	0.41	0.50	0.56	0.05	0.74
0.0140	282	20	2.31	5.63	5.19	1.18	0.35	1.06	0.40	0.49	0.52	0.04	0.73
0.0140	282	90	2.37	5.83	5.00	1.17	0.38	1.10	0.39	0.49	0.52	0.04	0.72
0.0140	202	20	2.39	5.70	5.16	1.18	0.37	1.10	0.39	0.50	0.53	0.03	0.72
0.0140	202	90	2.19	7.67	4.46	1.19	0.35	1.13	0.41	0.50	0.53	0.04	0.73
0.0167	242	55	2.04	9.27	4.03	1.15	0.34	1.10	0.44	0.49	0.47	0.04	0.75
0.0036	242	55	2.03	9.17	4.21	1.16	0.33	1.08	0.44	0.49	0.47	0.04	0.75
0.0063	282	20	2.16	6.93	5.17	1.27	0.32	1.04	0.43	0.50	0.52	0.05	0.75
0.0063	282	90	2.13	7.07	5.13	1.29	0.31	1.03	0.44	0.50	0.53	0.05	0.75
0.0063	202	20	2.04	7.97	4.49	1.27	0.31	1.04	0.45	0.50	0.52	0.06	0.76
0.0063	202	90	1.97	8.87	3.83	1.21	0.31	1.07	0.44	0.49	0.51	0.06	0.76

Material Variation Experiments

<i>Material</i>	<i>Input mass (kg to 1 d.p)</i>	<i>Output mass (kg to 1 d.p)</i>	<i>Specific Effective Energy (kW/h t⁻¹ to 2 d.p)</i>	<i>Output Rate (kg s⁻¹ to 4 d.p)</i>	<i>Residence Time (s to 1 d.p)</i>
<i>Uncertainty in Measure</i>					
	± 0.00005	± 0.00005	± 0.005	± 0.000005	± 0.005
Eucalyptus	1001	970	12.09	0.007	72
Microwave Torrefied	1000	1003	6.66	0.008	56
Miscanthus	1000	995	8.70	0.011	73

<i>Material</i>	<i>D bar (μm)</i>	<i>Sigma D bar (μm)</i>	<i>d' (μm)</i>	<i>n (- to 2 d.p)</i>	<i>SGN (- to 0 d.p)</i>	<i>D_{gm} (μm)</i>	<i>S_{gmw} (μm to 2 d.p)</i>	<i>S_{gml} (μm to 2 d.p)</i>	<i>S_{gmb} (μm to 2 d.p)</i>	<i>S_{gmp} (μm to 2 d.p)</i>		
<i>Uncertainty in Measure</i>												
	± 0.5	± 0.5	± 0.5	± 0.00005	-	± 0.5	-	-	-	-		
Eucalyptus	706	517	759	1.50	58	528	2.06	2.40	2.02	2.21		
Microwave Torrefied	310	215	333	1.73	26	243	1.91	2.11	1.86	1.98		
Miscanthus	989	689	1079	1.53	83	753	1.95	2.34	2.01	2.17		
<i>Material</i>	<i>d₅ (μm)</i>	<i>d₁₀ (μm)</i>	<i>d₁₆ (μm)</i>	<i>d₂₅ (μm)</i>	<i>d₃₀ (μm)</i>	<i>d₅₀ (μm)</i>	<i>d₆₀ (μm)</i>	<i>d₇₅ (μm)</i>	<i>d₈₄ (μm)</i>	<i>d₉₀ (μm)</i>	<i>d₉₅ (μm)</i>	<i>d₉₉ (μm)</i>
<i>Uncertainty in Measure</i>												

	-	-	-	-	-	-	-	-	-	-	-	-
Eucalyptus	121	180	241	327	377	578	698	943	1169	1403	1755	2455
Microwave Torrefied	72	97	124	160	179	261	309	403	486	576	709	1069
Miscanthus	174	260	350	474	539	822	995	1350	1653	1955	2356	3197

<i>Material</i>	$RS_V (-)$	$U_I (-)$	$C_U (-)$	$C_g (-)$	$K_I (-)$	$K_g (-)$	$psi_c (-)$	$psi_{AR} (-)$	$psi_{op} (-)$	$psi_R (-)$	$psi_{symm} (-)$
<i>Uncertainty in Measure</i>											
Eucalyptus	2.12	8.27	3.88	1.13	0.36	1.09	0.50	0.49	0.42	0.04	0.77
Microwave Torrefied	1.84	12.33	3.18	1.07	0.33	1.07	0.64	0.50	0.42	0.11	0.81
Miscanthus	2.07	8.67	3.82	1.12	0.34	1.02	0.42	0.42	0.36	0.05	0.73

References

- Abbasi, T., & Abbasi, S. A. (2007). Dust explosions—Cases, causes, consequences, and control. *Journal of Hazardous Materials*, 140(1–2), 7–44. doi:<http://dx.doi.org/10.1016/j.jhazmat.2006.11.007>
- Abe, S., & Mair, K. (2005). Grain fracture in 3D numerical simulations of granular shear. *Geophysical Research Letters*, 32(5), L05305. doi:10.1029/2004GL022123
- Adapa, P., Tabil, L., & Schoenau, G. (2011). Grinding performance and physical properties of non-treated and steam exploded barley, canola, oat and wheat straw. *Biomass and Bioenergy*, 35(1), 549–561. doi:<https://doi.org/10.1016/j.biombioe.2010.10.004>
- Ahmadzadeh, F., & Lundberg, J. (2013). Application of multi regressive linear model and neural network for wear prediction of grinding mill liners. *International Journal of Advanced Computer Science and Applications (IJACSA)*, 4(5).
- Alakangas, E. (2010). New European Pellets Standard—EN 14961-1: Jyväskylä, Finland: EuroBioNet.
- Alizadeh, E., Bertrand, F., & Chaouki, J. (2014). Comparison of DEM results and Lagrangian experimental data for the flow and mixing of granules in a rotating drum. *Aiche Journal*, 60(1), 60–75. doi:10.1002/aic.14259
- Allen, M. R., Barros, V. R., Broome, J., Cramer, W., Christ, R., Church, J. A., . . . Dubash, N. K. (2014). IPCC fifth assessment synthesis report—climate change 2014 synthesis report.
- Austin, L., Shoji, K., Bhatia, V., Jindal, V., Savage, K., & Klimpel, R. (1976). Some Results on the Description of Size Reduction as a Rate Process in Various Mills. *Industrial & Engineering Chemistry Process Design and Development*, 15(1), 187–196. doi:10.1021/i260057a032
- Austin, L. G. (1973). A commentary on the Kick, Bond and Rittinger laws of grinding. *Powder Technology*, 7(6), 315–317. doi:[http://dx.doi.org/10.1016/0032-5910\(73\)80042-7](http://dx.doi.org/10.1016/0032-5910(73)80042-7)
- Austin, L. G., Jindal, V. K., & Gotsis, C. (1979). A model for continuous grinding in a laboratory hammer mill. *Powder Technology*, 22(2), 199–204. doi:[http://dx.doi.org/10.1016/0032-5910\(79\)80027-3](http://dx.doi.org/10.1016/0032-5910(79)80027-3)
- Austin, L. G., Luckie, P. T., & Shoji, K. (1982). An analysis of ball-and-race milling part II. The babcock E 1.7 mill. *Powder Technology*, 33(1), 113–125. doi:[http://dx.doi.org/10.1016/0032-5910\(82\)85045-6](http://dx.doi.org/10.1016/0032-5910(82)85045-6)
- Austin, L. G., Shah, J., Wang, J., Gallagher, E., & Luckie, P. T. (1981). An analysis of ball-and-race milling. Part I. The hardgrove mill. *Powder Technology*, 29(2), 263–275. doi:[http://dx.doi.org/10.1016/0032-5910\(81\)87029-5](http://dx.doi.org/10.1016/0032-5910(81)87029-5)
- Avellar, B. K., & Glasser, W. G. (1998). Steam-assisted biomass fractionation. I. Process considerations and economic evaluation. *Biomass and Bioenergy*, 14(3), 205–218. doi:[http://dx.doi.org/10.1016/S0961-9534\(97\)10043-5](http://dx.doi.org/10.1016/S0961-9534(97)10043-5)
- Bailey, A. J. (1936). Lignin in douglas fir: Composition of the middle lamella. *Industrial & Engineering Chemistry Analytical Edition*, 8(1), 52–55. doi:10.1021/ac50099a024
- Barrasso, D., Tamrakar, A., & Ramachandran, R. (2014). A reduced order PBM—ANN model of a multi-scale PBM—DEM description of a wet granulation

- process. *Chemical Engineering Science*, 119(0), 319-329. doi:<http://dx.doi.org/10.1016/j.ces.2014.08.005>
- Barrett, J., Haigh, I., & Lovegrove, J. (1981). Fracture Mechanics and the Design of Wood Structures [and Discussion]. *Philosophical Transactions of the Royal Society of London. Series A, Mathematical and Physical Sciences*, 299(1446), 217-226.
- Bhambare, K. S., Ma, Z., & Lu, P. (2010). CFD modeling of MPS coal mill with moisture evaporation. *Fuel Processing Technology*, 91(5), 566-571. doi:<https://doi.org/10.1016/j.fuproc.2010.01.002>
- Bhandari, B., Bansal, N., Zhang, M., & Schuck, P. (2013). *Handbook of food powders: Processes and properties*. Elsevier.
- Bhasker, C. S. C., Tushar, W; Biswas, S; Chandrakar, AL. (1999). *CFD Modelling Of Bowl Mill*. Paper presented at the Proceedings of the 26th National Conference on Fluid Mechanics and Fluid Power:(December 15-17, 1999).
- Bilgili, E., & Scarlett, B. (2005a). Numerical simulation of open-circuit continuous mills using a non-linear population balance framework: Incorporation of non-first-order effects. *Chemical Engineering & Technology*, 28(2), 153-159. doi:10.1002/ceat.200407110
- Bilgili, E., & Scarlett, B. (2005b). Population balance modeling of non-linear effects in milling processes. *Powder Technology*, 153(1), 59-71. doi:10.1016/j.powtec.2005.02.005
- Bilgili, E., Yepes, J., & Scarlett, B. (2006). Formulation of a non-linear framework for population balance modeling of batch grinding: Beyond first-order kinetics. *Chemical Engineering Science*, 61(1), 33-44. doi:10.1016/j.ces.2004.11.060
- Bioenarea. (2012). BISIPLAN web-based handbook.
- Biomass Energy Centre. (2013). *UK Biomass Power Stations*. <http://www.biomassenergycentre.org.uk> Retrieved from http://www.biomassenergycentre.org.uk/pls/portal/docs/PAGE/BEC_TECHNICAL/REF_LIB_TECH/EXISTING%20INSTALLATIONS/UK%20BIOMASS%20POWER%20STATIONS%20V1.4%20MARCH%202013.PDF.
- Biswas, A. K., Yang, W., & Blasiak, W. (2011). Steam pretreatment of Salix to upgrade biomass fuel for wood pellet production. *Fuel Processing Technology*, 92(9), 1711-1717. doi:<http://dx.doi.org/10.1016/j.fuproc.2011.04.017>
- Bitra, V. S. P., Womac, A. R., Yang, Y. T., Igathinathane, C., Miu, P. I., Chevanan, N., & Sokhansanj, S. (2009). Knife mill operating factors effect on switchgrass particle size distributions. *Bioresource Technology*, 100(21), 5176-5188. doi:10.1016/j.biortech.2009.02.072
- Bitra, V. S. P., Womac, A. R., Yang, Y. T., Miu, P. I., Igathinathane, C., Chevanan, N., & Sokhansanj, S. (2011). Characterization of wheat straw particle size distributions as affected by knife mill operating factors. *Biomass & Bioenergy*, 35(8), 3674-3686. doi:10.1016/j.biombioe.2011.05.026
- Bitra, V. S. R., Womac, A. R., Chevanan, N., Miu, P. I., Igathinathane, C., Sokhansanj, S., & Smith, D. R. (2009). Direct mechanical energy measures of hammer mill comminution of switchgrass, wheat straw, and corn stover and analysis of their particle size distributions. *Powder Technology*, 193(1), 32-45. doi:10.1016/j.powtec.2009.02.010
- Blecher, L., Kwade, A., & Schwedes, J. (1996). Motion and stress intensity of grinding beads in a stirred media mill. Part 1: Energy density distribution and motion of single grinding beads. *Powder Technology*, 86(1), 59-68. doi:[http://dx.doi.org/10.1016/0032-5910\(95\)03038-7](http://dx.doi.org/10.1016/0032-5910(95)03038-7)

- Bond, F. C. (1954). Crushing and Grinding Calculation. *The Canada. Min. Metall. Bull.*, 47, 466-472.
- Boukouvala, F., Gao, Y., Muzzio, F., & Ierapetritou, M. G. (2013). Reduced-order discrete element method modeling. *Chemical Engineering Science*, 95(0), 12-26. doi:<http://dx.doi.org/10.1016/j.ces.2013.01.053>
- Brezani, I., & Zelenak, F. (2010). Improving the effectivity of work with Rosin-Rammler diagram by using MATLAB (R) GUI tool. *Acta Montanistica Slovaca*, 15(2), 152-157.
- Bridgeman, T. G., Jones, J. M., Williams, A., & Waldron, D. J. (2010). An investigation of the grindability of two torrefied energy crops. *Fuel*, 89(12), 3911-3918. doi:10.1016/j.fuel.2010.06.043
- Broadbent, S., & Callcott, T. (1956). A matrix analysis of processes involving particle assemblies. *Philosophical Transactions of the Royal Society of London A: Mathematical, Physical and Engineering Sciences*, 249(960), 99-123.
- Bushnell, D. J., Haluzok, C., & Dadkhah-Nikoo, A. (1989). *Biomass Fuel Characterization: Testing and Evaluating the Combustion Characteristics of Selected Biomass Fuels*. Retrieved from Corvallis:
- Byrd, R. H., Hribar, M. E., & Nocedal, J. (1999). An Interior Point Algorithm for Large-Scale Nonlinear Programming. *SIAM Journal on optimization*, 9(4), 877-900. doi:10.1137/s1052623497325107
- Campbell, G. M., Bunn, P. J., Webb, C., & Hook, S. C. W. (2001). On predicting roller milling performance Part II. The breakage function. *Powder Technology*, 115(3), 243-255. doi:10.1016/s0032-5910(00)00349-1
- Campbell, G. M., Sharp, C., Wall, K., Mateos-Salvador, F., Gubatz, S., Huttly, A., & Shewry, P. (2012). Modelling wheat breakage during roller milling using the Double Normalised Kumaraswamy Breakage Function: Effects of kernel shape and hardness. *Journal of Cereal Science*, 55(3), 415-425. doi:10.1016/j.jcs.2012.02.002
- Campbell, G. M., & Webb, C. (2001). On predicting roller milling performance Part I: the breakage equation. *Powder Technology*, 115(3), 234-242. doi:10.1016/s0032-5910(00)00348-x
- Cante, J., Dávalos, C., Hernández, J. A., Oliver, J., Jonsén, P., Gustafsson, G., & Häggblad, H. Å. (2014). PFEM-based modeling of industrial granular flows. *Computational Particle Mechanics*, 1(1), 47-70. doi:10.1007/s40571-014-0004-9
- Capece, M., Bilgili, E., & Dave, R. (2011). Identification of the breakage rate and distribution parameters in a non-linear population balance model for batch milling. *Powder Technology*, 208(1), 195-204. doi:<http://dx.doi.org/10.1016/j.powtec.2010.12.019>
- Capece, M., Bilgili, E., & Davé, R. (2014). Insight into first-order breakage kinetics using a particle-scale breakage rate constant. *Chemical Engineering Science*, 117(0), 318-330. doi:<http://dx.doi.org/10.1016/j.ces.2014.06.019>
- Capece, M., Bilgili, E., & Davé, R. N. (2014). Formulation of a physically motivated specific breakage rate parameter for ball milling via the discrete element method. *Aiche Journal*, 60(7), 2404-2415. doi:10.1002/aic.14451
- Capece, M., Davé, R. N., & Bilgili, E. (2015). On the origin of non-linear breakage kinetics in dry milling. *Powder Technology*, 272(0), 189-203. doi:<http://dx.doi.org/10.1016/j.powtec.2014.11.040>
- Cardoso, C., Oliveira, T., Junior, J. S., & Ataíde, C. (2013). Physical characterization of sweet sorghum bagasse, tobacco residue, soy hull and fiber sorghum bagasse particles: density, particle size and shape distributions. *Powder Technology*, 245, 105-114.

- Carey, T., Mason, H. B., Barbosa, A. R., & Scott, M. H. (2014). *Modeling framework for soil-bridge system response during sequential earthquake and tsunami loading*. Paper presented at the 10th US National Conference on Earthquake Engineering.
- Chabannes, M., Ruel, K., Yoshinaga, A., Chabbert, B., Jauneau, A., Joseleau, J. P., & Boudet, A. M. (2001). In situ analysis of lignins in transgenic tobacco reveals a differential impact of individual transformations on the spatial patterns of lignin deposition at the cellular and subcellular levels. *The Plant Journal*, 28(3), 271-282.
- Channiwala, S. A., & Parikh, P. P. (2002). A unified correlation for estimating HHV of solid, liquid and gaseous fuels. *Fuel*, 81(8), 1051-1063. doi:[http://dx.doi.org/10.1016/S0016-2361\(01\)00131-4](http://dx.doi.org/10.1016/S0016-2361(01)00131-4)
- Chelgani, S. C., Hower, J. C., Jorjani, E., Mesroghli, S., & Bagherieh, A. (2008). Prediction of coal grindability based on petrography, proximate and ultimate analysis using multiple regression and artificial neural network models. *Fuel Processing Technology*, 89(1), 13-20.
- Chen, W.-H., Cheng, W.-Y., Lu, K.-M., & Huang, Y.-P. (2011). An evaluation on improvement of pulverized biomass property for solid fuel through torrefaction. *Applied Energy*, 88(11), 3636-3644. doi:<http://dx.doi.org/10.1016/j.apenergy.2011.03.040>
- Cleary, P. (2001). Modelling comminution devices using DEM. *International Journal for Numerical and Analytical Methods in Geomechanics*, 25(1), 83-105. doi:10.1002/1096-9853(200101)25:1<83::aid-nag120>3.0.co;2-k
- Cleary, P. W. (1998). Predicting charge motion, power draw, segregation and wear in ball mills using discrete element methods. *Minerals Engineering*, 11(11), 1061-1080. doi:[http://dx.doi.org/10.1016/S0892-6875\(98\)00093-4](http://dx.doi.org/10.1016/S0892-6875(98)00093-4)
- Cleary, P. W. (2009). Industrial particle flow modelling using discrete element method. *Engineering Computations*, 26(6), 698-743. doi:10.1108/02644400910975487
- Cleary, P. W. (2015). Prediction of coupled particle and fluid flows using DEM and SPH. *Minerals Engineering*, 73(0), 85-99. doi:<http://dx.doi.org/10.1016/j.mineng.2014.09.005>
- Cleary, P. W., & Morrison, R. D. (2012). Prediction of 3D slurry flow within the grinding chamber and discharge from a pilot scale SAG mill. *Minerals Engineering*, 39, 184-195.
- Cleary, P. W., Prakash, M., Sinnott, M. D., Rudman, M., & Das, R. (2011). Large scale simulation of industrial, engineering and geophysical flows using particle methods *Particle-Based Methods* (pp. 89-111): Springer.
- Cleary, P. W., Sinnott, M., & Morrison, R. (2006). Prediction of slurry transport in SAG mills using SPH fluid flow in a dynamic DEM based porous media. *Minerals Engineering*, 19(15), 1517-1527.
- Colechin, M., Malmgren, A., & Britain, G. (2005). *Best Practice Brochure: Co-firing of Biomass-Main Report*: Department of Trade and Industry, Cleaner Fossil Fuels Programme.
- Coulson, J. M. (1999). *Coulson & Richardson's chemical engineering* (Vol. 1): Butterworth-Heinemann.
- Cundall, P. A., & Strack, O. D. L. (1979). A discrete numerical model for granular assemblies. *Géotechnique*, 29, 47-65. Retrieved from <http://www.icvirtuallibrary.com/content/article/10.1680/geot.1979.29.1.47>
- da Cunha, E. R., de Carvalho, R. M., & Tavares, L. M. (2013). Simulation of solids flow and energy transfer in a vertical shaft impact crusher using DEM.

- Dabeet, A., Wijewickreme, D., & Byrne, P. (2014). *Application of discrete element modeling for simulation of cyclic direct simple shear response of granular materials*. Paper presented at the 10th National Conference on Earthquake Engineering. <https://datacenterhub.org/resources/12542/download/10NCEE-001194.pdf>
- Daniel, M. J., & Morrell, S. (2004). HPGR model verification and scale-up. *Minerals Engineering*, 17(11–12), 1149-1161. doi:<http://dx.doi.org/10.1016/j.mineng.2004.05.016>
- Das, R., & Cleary, P. W. (2010). Effect of rock shapes on brittle fracture using Smoothed Particle Hydrodynamics. *Theoretical and Applied Fracture Mechanics*, 53(1), 47-60. doi:<http://dx.doi.org/10.1016/j.tafmec.2009.12.004>
- Datta, S. (2011). Genetic Algorithm in MATLAB for Process Optimization Multi-objective Approach for Optimization. Retrieved from <http://chethoughts.com/?p=631>
- Dawei, Z., Erfan, G. N., Youssef, M. A. H., & Jamshid, G. (2006). Three-dimensional discrete element simulation for granular materials. *Engineering Computations*, 23(7), 749-770. doi:10.1108/02644400610689884
- Delaney, G. W., Cleary, P. W., Sinnott, M. D., & Morrison, R. D. (2010). *Novel application of DEM to modelling comminution processes*. Paper presented at the IOP Conference Series: Materials Science and Engineering.
- Demirbas, A. (2004). Combustion characteristics of different biomass fuels. *Progress in Energy and Combustion Science*, 30(2), 219-230. doi:<http://dx.doi.org/10.1016/j.peccs.2003.10.004>
- Demirbaş, A. (1997). Calculation of higher heating values of biomass fuels. *Fuel*, 76(5), 431-434. doi:[http://dx.doi.org/10.1016/S0016-2361\(97\)85520-2](http://dx.doi.org/10.1016/S0016-2361(97)85520-2)
- Deng, L., Liu, Y., Wang, W., Ge, W., & Li, J. (2013). A two-fluid smoothed particle hydrodynamics (TF-SPH) method for gas–solid fluidization. *Chemical Engineering Science*, 99(0), 89-101. doi:<http://dx.doi.org/10.1016/j.ces.2013.05.047>
- Department of Business, E. I. S. (2016). *Coal generation in Great Britain: summary of responses to consultation*. www.gov.uk Retrieved from https://www.gov.uk/government/uploads/system/uploads/attachment_data/file/650476/unabated-coal-consultation-summary-of-responses.pdf.
- Dolbow, J., & Belytschko, T. (1999). A finite element method for crack growth without remeshing. *Int. J. Numer. Meth. Engng*, 46(1), 131-150.
- Doroodchi, E., Zulficar, H., & Moghtaderi, B. (2013). A combined experimental and theoretical study on laboratory-scale comminution of coal and biomass blends. *Powder Technology*, 235(0), 412-421. doi:<http://dx.doi.org/10.1016/j.powtec.2012.10.054>
- Durman, R. W. (1988). Progress in abrasion-resistant materials for use in comminution processes. *International Journal of Mineral Processing*, 22(1–4), 381-399. doi:[http://dx.doi.org/10.1016/0301-7516\(88\)90074-9](http://dx.doi.org/10.1016/0301-7516(88)90074-9)
- Dutta, A. L., Mathias A. (n.d.). Pros and Cons of Torrefaction of Woody Biomass. Retrieved from http://www.agrireseau.qc.ca/references/32/presentations_guelph/2Torrefaction%20-%20Pros%20and%20Cons%20By%20Mathias%20Leon%20UoG.pdf

- Džiugys, A., & Peters, B. (2001). An approach to simulate the motion of spherical and non-spherical fuel particles in combustion chambers. *Granular Matter*, 3(4), 231-266. doi:10.1007/PL00010918
- EDEM Simulation. (2017). EDEM Software. Retrieved from <https://www.edemsimulation.com/software/>
- Erdem, A. S., & Ergün, Ş. L. (2009). The effect of ball size on breakage rate parameter in a pilot scale ball mill. *Minerals Engineering*, 22(7–8), 660-664. doi:<http://dx.doi.org/10.1016/j.mineng.2009.01.015>
- Esteban, L. S., & Carrasco, J. E. (2006). Evaluation of different strategies for pulverization of forest biomasses. *Powder Technology*, 166(3), 139-151. doi:<http://dx.doi.org/10.1016/j.powtec.2006.05.018>
- Fakhimi, A., & Lanari, M. (2014). DEM–SPH simulation of rock blasting. *Computers and Geotechnics*, 55(0), 158-164. doi:<http://dx.doi.org/10.1016/j.compgeo.2013.08.008>
- Farzanegan, A., & Vahidipour, S. M. (2009). Optimization of comminution circuit simulations based on genetic algorithms search method. *Minerals Engineering*, 22(7–8), 719-726. doi:<http://dx.doi.org/10.1016/j.mineng.2009.02.009>
- Favier, J., Abbaspour-Fard, M., Kremmer, M., & Raji, A. (1999). Shape representation of axi-symmetrical, non-spherical particles in discrete element simulation using multi-element model particles. *Engineering Computations*, 16(4), 467-480.
- Food and Agricultural Organization of the United Nations. (2004). Unified bioenergy terminology. Retrieved from <ftp://ftp.fao.org/docrep/fao/007/j4504e/j4504e00.pdf>
- Forsström, D., Lindbäck, T., & Jonsén, P. (2014). Prediction of wear in dumper truck body by coupling SPH-FEM. *Tribology-Materials, Surfaces & Interfaces*, 8(2), 111-115.
- Fraige, F. Y., Langston, P. A., & Chen, G. Z. (2008). Distinct element modelling of cubic particle packing and flow. *Powder Technology*, 186(3), 224-240. doi:<http://dx.doi.org/10.1016/j.powtec.2007.12.009>
- Frances, C., & Liné, A. (2014). Comminution process modeling based on the monovariate and bivariate direct quadrature method of moments. *Aiche Journal*, 60(5), 1621-1631. doi:10.1002/aic.14358
- G Nezami, E., MA Hashash, Y., Zhao, D., & Ghaboussi, J. (2006). Shortest link method for contact detection in discrete element method. *International Journal for Numerical and Analytical Methods in Geomechanics*, 30(8), 783-801.
- Ganzenmüller, G. C. (2015). An hourglass control algorithm for Lagrangian Smooth Particle Hydrodynamics. *Computer Methods in Applied Mechanics and Engineering*, 286(0), 87-106. doi:<http://dx.doi.org/10.1016/j.cma.2014.12.005>
- Gao, M. W., Forssberg, K. S. E., & Weller, K. R. (1996). Power predictions for a pilot scale stirred ball mill. *International Journal of Mineral Processing*, 44, 641-652. doi:[http://dx.doi.org/10.1016/0301-7516\(95\)00072-0](http://dx.doi.org/10.1016/0301-7516(95)00072-0)
- Gardner, M. W., & Dorling, S. R. (1998). Artificial neural networks (the multilayer perceptron)—a review of applications in the atmospheric sciences. *Atmospheric Environment*, 32(14), 2627-2636. doi:[http://dx.doi.org/10.1016/S1352-2310\(97\)00447-0](http://dx.doi.org/10.1016/S1352-2310(97)00447-0)
- Genc, O., & Benzer, A. H. (2009). Single particle impact breakage characteristics of clinkers related to mineral composition and grindability. *Minerals Engineering*, 22(13), 1160-1165. doi:10.1016/j.mineng.2009.06.001

- Ghorbani, Z., Masoumi, A. A., & Hemmat, A. (2010). Specific energy consumption for reducing the size of alfalfa chops using a hammer mill. *Biosystems Engineering*, 105(1), 34-40. doi:<http://dx.doi.org/10.1016/j.biosystemseng.2009.09.006>
- Ghorbani, Z., Masoumi, A. A., Hemmat, A., & Seifi, M. R. (2013). Prediction of specific energy consumption in milling process using some physical and mechanical properties of alfalfa grind. *Australian Journal of Crop Science*, 7(10), 1449.
- Gil, M., & Arauzo, I. (2014). Hammer mill operating and biomass physical conditions effects on particle size distribution of solid pulverized biofuels. *Fuel Processing Technology*, 127, 80-87.
- Gil, M., Arauzo, I., & Teruel, E. (2013). Influence of Input Biomass Conditions and Operational Parameters on Comminution of Short-Rotation Forestry Poplar and Corn Stover Using Neural Networks. *Energy & Fuels*, 27(5), 2649-2659. doi:10.1021/ef4000787
- Gil, M., González, A., & Gil, A. (2008). *Evaluation of milling energy requirements of biomass residues in a semi-industrial pilot plant for co-firing*. Paper presented at the 16th European Biomass Conference and Exhibition. Valencia.
- Gil, M., Luciano, E., & Arauzo, I. (2015a). Approach to the breakage behavior of comminuted poplar and corn stover under single impact. *Fuel Processing Technology*, 131, 142-149. doi:<http://dx.doi.org/10.1016/j.fuproc.2014.11.020>
- Gil, M., Luciano, E., & Arauzo, I. (2015b). Population balance model for biomass milling. *Powder Technology*, 276(0), 34-44. doi:<http://dx.doi.org/10.1016/j.powtec.2015.01.060>
- Gil, M., Teruel, E., & Arauzo, I. (2014). Analysis of standard sieving method for milled biomass through image processing. Effects of particle shape and size for poplar and corn stover. *Fuel*, 116(Supplement C), 328-340. doi:<https://doi.org/10.1016/j.fuel.2013.08.011>
- Göktepe, B., Umeki, K., & Gebart, R. (2016). Does distance among biomass particles affect soot formation in an entrained flow gasification process? *Fuel Processing Technology*, 141, 99-105.
- Goswami, T. K., & Singh, M. (2003). Role of feed rate and temperature in attrition grinding of cumin. *Journal of Food Engineering*, 59(2), 285-290. doi:[http://dx.doi.org/10.1016/S0260-8774\(02\)00469-7](http://dx.doi.org/10.1016/S0260-8774(02)00469-7)
- Graeme, L. (1999a). *CFD modelling of a stirred bead mill for fine grinding*. Paper presented at the Proceedings of the Second International Conference on CFD in the Minerals and Process Industries, Melbourne, Australia.
- Graeme, L. (1999b). *CFD Modelling of a Stirred Bead Mill for Fine Grinding*. Paper presented at the 2nd International Conference on CFD in the Minerals and Process Industries, Melbourne, Australia, 1999.
- Grammelis, P. (2010). *Solid Biofuels for Energy*: Springer.
- Graupe, D. (2007). *Principles of Artificial Neural Networks (2nd Edition)*. River Edge, NJ, USA: World Scientific.
- Gravelsins, R. J., & Trass, O. (2013). Analysis of grinding of pelletized wood waste with the Szego Mill. *Powder Technology*, 245, 189-198. doi:<http://dx.doi.org/10.1016/j.powtec.2013.04.018>
- Green, D. W. (2008). Perry's chemical engineers' handbook. *McGraw-Hill*.
- Greensmith, B. S., Jason. (2013). *Engineering the Transformation*.
- Guo, S., Wang, J., Wei, J., & Zachariades, P. (2014). A new model-based approach for power plant Tube-ball mill condition monitoring and fault detection.

- Energy Conversion and Management*, 80(0), 10-19.
doi:<http://dx.doi.org/10.1016/j.enconman.2013.12.046>
- Hanning, L., Qun, C., Xiaohui, Z., Karen, F. N., Sharifi, V. N., & Swithenbank, J. (2012). Evaluation of a biomass drying process using waste heat from process industries: A case study. *Applied Thermal Engineering*, 71-80.
- Harmsen, P., Huijgen, W., Bermudez, L., & Bakker, R. (2010). *Literature review of physical and chemical pretreatment processes for lignocellulosic biomass*: Wageningen UR, Food & Biobased Research.
- Harrison, S. M., Cleary, P. W., Eyres, G., Sinnott, M. D., & Lundin, L. (2014). Challenges in computational modelling of food breakdown and flavour release. *Food & function*.
- Harrison, S. M., Eyres, G., Cleary, P. W., Sinnott, M. D., Delahunty, C., & Lundin, L. (2014). Computational Modeling of Food Oral Breakdown Using Smoothed Particle Hydrodynamics. *Journal of Texture Studies*, 45(2), 97-109. doi:10.1111/jtxs.12062
- Herbst, J. A., & Fuerstenau, D. W. (1980). Scale-up procedure for continuous grinding mill design using population balance models. *International Journal of Mineral Processing*, 7(1), 1-31. doi:[http://dx.doi.org/10.1016/0301-7516\(80\)90034-4](http://dx.doi.org/10.1016/0301-7516(80)90034-4)
- Höhner, D., Wirtz, S., & Scherer, V. (2014). A study on the influence of particle shape and shape approximation on particle mechanics in a rotating drum using the discrete element method. *Powder Technology*, 253(0), 256-265. doi:<http://dx.doi.org/10.1016/j.powtec.2013.11.023>
- Horner, D., Peters, J., & Carrillo, A. (2001). Large Scale Discrete Element Modeling of Vehicle-Soil Interaction. *Journal of Engineering Mechanics*, 127(10), 1027-1032. doi:doi:10.1061/(ASCE)0733-9399(2001)127:10(1027)
- Hussain, U. (2015). *Assessing the impact of torrefaction on the combustion properties of biomass fuels*. (Literature review), University of Nottingham.
- Idelsohn, S. R., Marti, J., Becker, P., & Oñate, E. (2014). Analysis of multifluid flows with large time steps using the particle finite element method. *International Journal for Numerical Methods in Fluids*, 75(9), 621-644. doi:10.1002/flid.3908
- IEA. (2013). Addressing Climate Change. Retrieved from <http://www.iea.org/policiesandmeasures/climatechange/index.php>
- International Energy Agency. (2014). Pulverised Coal Combustion. Retrieved from <http://www.iea-coal.org.uk/site/2010/database-section/ccts/pulverised-coal-combustion-pcc?>
- Itasca Consulting Group, I. (2017). PFC Version 5 General Purpose Distinct-Element Modeling Framework. Retrieved from <http://www.itascacg.com/software/pfc>
- Iwasaki, T., Yabuuchi, T., Nakagawa, H., & Watano, S. (2010). Scale-up methodology for tumbling ball mill based on impact energy of grinding balls using discrete element analysis. *Advanced Powder Technology*, 21(6), 623-629. doi:<http://dx.doi.org/10.1016/j.apt.2010.04.008>
- Jankovic, A., & Valery, W. (2013). Closed circuit ball mill – Basics revisited. *Minerals Engineering*, 43-44(0), 148-153. doi:<http://dx.doi.org/10.1016/j.mineng.2012.11.006>
- Jenkinson, P. (2012). A New Classification System for Biomass and Waste Materials for their use in Combustion.
- Jianlin, W., Jihong, W., & Shen, G. (2009, 10-12 June 2009). *Mathematic modeling and condition monitoring of power station tube-ball mill systems*. Paper presented at the American Control Conference, 2009. ACC '09.

- Jindal, V. K., & Austin, L. G. (1976). The kinetics of hammer milling of maize. *Powder Technology*, 14(1), 35-39. doi:[http://dx.doi.org/10.1016/0032-5910\(76\)80005-8](http://dx.doi.org/10.1016/0032-5910(76)80005-8)
- Jonsén¹, P., Häggblad, H.-Å., & Pålsson, B. I. (2014). Modelling of fluid, particle and structure interactions in a tumbling ball mill for grinding of minerals.
- Jonsén, P., Pålsson, B. I., & Häggblad, H.-Å. (2012). A novel method for full-body modelling of grinding charges in tumbling mills. *Minerals Engineering*, 33(0), 2-12. doi:<http://dx.doi.org/10.1016/j.mineng.2012.01.017>
- Jonsén, P., Pålsson, B. I., Stener, J. F., & Häggblad, H.-Å. (2014). A novel method for modelling of interactions between pulp, charge and mill structure in tumbling mills. *Minerals Engineering*, 63, 65-72.
- Jonsén, P., Pålsson, B. I., Tano, K., & Berggren, A. (2011). Prediction of mill structure behaviour in a tumbling mill. *Minerals Engineering*, 24(3-4), 236-244. doi:<http://dx.doi.org/10.1016/j.mineng.2010.08.012>
- Jonsén, P., Stener, J. F., Pålsson, B. I., & Häggblad, H.-Å. (2015). Validation of a model for physical interactions between pulp, charge and mill structure in tumbling mills. *Minerals Engineering*, 73(0), 77-84. doi:<http://dx.doi.org/10.1016/j.mineng.2014.09.014>
- Kakuda, K., Hayashi, Y., & Toyotani, J. (2014). Particle-based Simulations of Flows with Free Surfaces Using Hyperbolic-type Weighting Functions. *CMES: Computer Modeling in Engineering & Sciences*, 103(4), 229-249.
- Kalala, J. T., Breetzke, M., & Moys, M. H. (2008). Study of the influence of liner wear on the load behaviour of an industrial dry tumbling mill using the Discrete Element Method (DEM). *International Journal of Mineral Processing*, 86(1-4), 33-39. doi:10.1016/j.minpro.2007.10.001
- Kallis, K. X. (2012). *Biomass thermal conversion. Pelletisation of lignocelluloses and the effect on the gasification process*. (PhD PhD), Cranfield University. Retrieved from <http://dspace.lib.cranfield.ac.uk/handle/1826/7456>
- Karinkanta, P., Illikainen, M., & Niinimäki, J. (2013). Impact-based pulverisation of dried and screened Norway spruce (*Picea abies*) sawdust in an oscillatory ball mill. *Powder Technology*, 233(Supplement C), 286-294. doi:<https://doi.org/10.1016/j.powtec.2012.09.011>
- Kauffman, C. (1981). *Agricultural dust explosions in grain handling facilities*. Paper presented at the Proceedings International Conference on Fuel-Air Explosions, McGill University, Montreal.
- Khanal, M., Schubert, W., & Tomas, J. (2007). Discrete element method simulation of bed comminution. *Minerals Engineering*, 20(2), 179-187. doi:10.1016/j.mineng.2006.08.011
- Khennane, A., Khelifa, M., Bleron, L., & Viguier, J. (2014). Numerical modelling of ductile damage evolution in tensile and bending tests of timber structures. *Mechanics of Materials*, 68(0), 228-236. doi:<http://dx.doi.org/10.1016/j.mechmat.2013.09.004>
- Khorshidi, Z., Ho, M. T., & Wiley, D. E. (2014). The impact of biomass quality and quantity on the performance and economics of co-firing plants with and without CO₂ capture. *International Journal of Greenhouse Gas Control*, 21(0), 191-202. doi:<http://dx.doi.org/10.1016/j.ijggc.2013.12.011>
- Klimpel, R. R., & Austin, L. G. (1977). The back-calculation of specific rates of breakage and non-normalized breakage distribution parameters from batch grinding data. *International Journal of Mineral Processing*, 4(1), 7-32. doi:[https://doi.org/10.1016/0301-7516\(77\)90028-X](https://doi.org/10.1016/0301-7516(77)90028-X)

- Kobayashi, N., Guilin, P., Kobayashi, J., Hatano, S., Itaya, Y., & Mori, S. (2008). A new pulverized biomass utilization technology. *Powder Technology*, 180(3), 272-283. doi:<http://dx.doi.org/10.1016/j.powtec.2007.02.041>
- Koka, V. R., & Trass, O. (1987). Determination of breakage parameters and modelling of coal breakage in the Szego mill. *Powder Technology*, 51(2), 201-214. doi:[http://dx.doi.org/10.1016/0032-5910\(87\)80020-7](http://dx.doi.org/10.1016/0032-5910(87)80020-7)
- Kostoglou, M., Dovas, S., & Karabelas, A. (1997). On the steady-state size distribution of dispersions in breakage processes. *Chemical Engineering Science*, 52(8), 1285-1299.
- Kratky, L., & Jirout, T. (2011). Biomass Size Reduction Machines for Enhancing Biogas Production. *Chemical Engineering & Technology*, 34(3), 391-399. doi:10.1002/ceat.201000357
- Kumar Akkisetty, P., Lee, U., Reklaitis, G., & Venkatasubramanian, V. (2010). Population Balance Model-Based Hybrid Neural Network for a Pharmaceutical Milling Process. *Journal of Pharmaceutical Innovation*, 5(4), 161-168. doi:10.1007/s12247-010-9090-2
- Kumar, J., Peglow, M., Warnecke, G., Heinrich, S., & Mörl, L. (2006). Improved accuracy and convergence of discretized population balance for aggregation: The cell average technique. *Chemical Engineering Science*, 61(10), 3327-3342. doi:<https://doi.org/10.1016/j.ces.2005.12.014>
- Kumar, S., & Ramkrishna, D. (1996a). On the solution of population balance equations by discretization—I. A fixed pivot technique. *Chemical Engineering Science*, 51(8), 1311-1332. doi:[http://dx.doi.org/10.1016/0009-2509\(96\)88489-2](http://dx.doi.org/10.1016/0009-2509(96)88489-2)
- Kumar, S., & Ramkrishna, D. (1996b). On the solution of population balance equations by discretization—II. A moving pivot technique. *Chemical Engineering Science*, 51(8), 1333-1342. doi:[https://doi.org/10.1016/0009-2509\(95\)00355-X](https://doi.org/10.1016/0009-2509(95)00355-X)
- Lavoie, J.-M., Beauchet, R., Berberi, V., & Chornet, M. (2011). Biorefining lignocellulosic biomass via the feedstock impregnation rapid and sequential steam treatment. *Biofuel's Engineering Process Technology*.
- Lee, H., Cho, H., & Kwon, J. (2010). Using the discrete element method to analyze the breakage rate in a centrifugal/vibration mill. *Powder Technology*, 198(3), 364-372. doi:<http://dx.doi.org/10.1016/j.powtec.2009.12.001>
- Lee, H., Klima, M. S., & Saylor, P. (2012). Evaluation of a laboratory rod mill when grinding bituminous coal. *Fuel*, 92(1), 116-121. doi:<http://dx.doi.org/10.1016/j.fuel.2011.08.006>
- Lester, E., Gong, M., & Thompson, A. (2007). A method for source apportionment in biomass/coal blends using thermogravimetric analysis. *Journal of Analytical and Applied Pyrolysis*, 80(1), 111-117.
- Li, H., McDowell, G., & Lowndes, I. (2014). Discrete-element modelling of rock comminution in a cone crusher using a bonded particle model. *Géotechnique Letters*, 4(April-June), 79-82.
- Li, J., Langston, P. A., Webb, C., & Dyakowski, T. (2004). Flow of sphero-disc particles in rectangular hoppers—a DEM and experimental comparison in 3D. *Chemical Engineering Science*, 59(24), 5917-5929.
- Liu, F., Zhao, L.-q., Liu, P.-l., Luo, Z.-f., Li, N.-y., & Wang, P.-s. (2015). An extended finite element model for fluid flow in fractured porous media. *Mathematical Problems in Engineering*, 2015.
- Liu, S. D., Zhou, Z. Y., Zou, R. P., Pinson, D., & Yu, A. B. (2014). Flow characteristics and discharge rate of ellipsoidal particles in a flat bottom

- hopper. *Powder Technology*, 253(0), 70-79.
doi:<http://dx.doi.org/10.1016/j.powtec.2013.11.001>
- Livingston, W. (2005). *A review of the recent experience in Britain with the co-firing of biomass with coal in large pulverized coal-fired boilers*. Paper presented at the IEA Exco Workshop on Biomass Co-firing, Copenhagen.
- Livingston, W. (2007). *Advanced biomass co-firing technologies for coal-fired boilers*. Paper presented at the International conference on coal science and technology-keynote, Nottingham.
- Livingston, W. (2012). Recent Developments in Biomass Co-firing in Large Coal-fired Utility Boilers. Retrieved from http://www.ieabcc.nl/workshops/task32_2012_Copenhagen/Livingston-1.pdf
- Livingston, W. (2013). *The firing and co-firing of biomass in large pulverised coal boilers*. Paper presented at the IEA Exco Workshop, Jeju City.
- Liyang, C., & Chundong, L. (2011, 15-17 July 2011). *Numerical simulation on air-flow field in the milling chamber of hammer mill*. Paper presented at the Mechanic Automation and Control Engineering (MACE), 2011 Second International Conference on.
- Long, C. (2013). *Finite Volume Methods*.
- Lope, T., Phani, A., & Mahdi, K. (2011). *Biomass Feedstock Pre-Processing – Part 1: Pre-Treatment*.
- Magini, M., Iasonna, A., & Padella, F. (1996). Ball milling: An experimental support to the energy transfer evaluated by the collision model. *Scripta Materialia*, 34(1), 13-19. doi:[http://dx.doi.org/10.1016/1359-6462\(95\)00465-3](http://dx.doi.org/10.1016/1359-6462(95)00465-3)
- Mair, K., & Abe, S. (2011). Breaking Up: Comminution Mechanisms in Sheared Simulated Fault Gouge. *Pure and Applied Geophysics*, 168(12), 2277-2288. doi:10.1007/s00024-011-0266-6
- Maire, P.-H., & Breil, J. (2012). A nominally second-order accurate finite volume cell-centered scheme for anisotropic diffusion on two-dimensional unstructured grids. *Journal of Computational Physics*, 231(5), 2259-2299. doi:<http://dx.doi.org/10.1016/j.jcp.2011.11.029>
- Maiti, S., Dey, S., Purakayastha, S., & Ghosh, B. (2006). Physical and thermochemical characterization of rice husk char as a potential biomass energy source. *Bioresource Technology*, 97(16), 2065-2070.
- Mandal, T., Mishra, B. K., Garg, A., & Chaira, D. (2014). Optimization of milling parameters for the mechanosynthesis of nanocrystalline hydroxyapatite. *Powder Technology*, 253(0), 650-656. doi:<http://dx.doi.org/10.1016/j.powtec.2013.12.026>
- Mani, S., Tabil, L. G., & Sokhansanj, S. (2004). Grinding performance and physical properties of wheat and barley straws, corn stover and switchgrass. *Biomass & Bioenergy*, 27(4), 339-352. doi:10.1016/j.biombioe.2004.03.007
- Mantzaris, N. V., Daoutidis, P., & Sreenc, F. (2001a). Numerical solution of multi-variable cell population balance models. II. Spectral methods. *Computers & Chemical Engineering*, 25(11-12), 1441-1462. doi:[http://dx.doi.org/10.1016/S0098-1354\(01\)00710-4](http://dx.doi.org/10.1016/S0098-1354(01)00710-4)
- Mantzaris, N. V., Daoutidis, P., & Sreenc, F. (2001b). Numerical solution of multi-variable cell population balance models. III. Finite element methods. *Computers & Chemical Engineering*, 25(11-12), 1463-1481. doi:[http://dx.doi.org/10.1016/S0098-1354\(01\)00711-6](http://dx.doi.org/10.1016/S0098-1354(01)00711-6)
- Mantzaris, N. V., Daoutidis, P., & Sreenc, F. (2001c). Numerical solution of multi-variable cell population balance models: I. Finite difference methods.

- Computers & Chemical Engineering*, 25(11–12), 1411-1440. doi:[http://dx.doi.org/10.1016/S0098-1354\(01\)00709-8](http://dx.doi.org/10.1016/S0098-1354(01)00709-8)
- Marchisio, D. L., & Fox, R. O. (2005). Solution of population balance equations using the direct quadrature method of moments. *Journal of Aerosol Science*, 36(1), 43-73.
- Marchisio, D. L., Vigil, R. D., & Fox, R. O. (2003). Quadrature method of moments for aggregation–breakage processes. *Journal of Colloid and Interface Science*, 258(2), 322-334. doi:[http://dx.doi.org/10.1016/S0021-9797\(02\)00054-1](http://dx.doi.org/10.1016/S0021-9797(02)00054-1)
- Mazzinghy, D. B., Schneider, C. L., Alves, V. K., & Galéry, R. (2015). Vertical Agitated Media Mill scale-up and simulation. *Minerals Engineering*, 73(0), 69-76. doi:<http://dx.doi.org/10.1016/j.mineng.2014.11.003>
- Meghwal, M., & Goswami, T. K. (2014). Comparative study on ambient and cryogenic grinding of fenugreek and black pepper seeds using rotor, ball, hammer and Pin mill. *Powder Technology*, 267(0), 245-255. doi:<http://dx.doi.org/10.1016/j.powtec.2014.07.025>
- Meier, M., John, E., Wieckhusen, D., Wirth, W., & Peukert, W. (2009). Influence of mechanical properties on impact fracture: Prediction of the milling behaviour of pharmaceutical powders by nanoindentation. *Powder Technology*, 188(3), 301-313. doi:<http://dx.doi.org/10.1016/j.powtec.2008.05.009>
- Miao, Z., Grift, T. E., Hansen, A. C., & Ting, K. C. (2011). Energy requirement for comminution of biomass in relation to particle physical properties. *Industrial Crops and Products*, 33(2), 504-513. doi:<http://dx.doi.org/10.1016/j.indcrop.2010.12.016>
- Mishra, B. K. (2000). Monte Carlo simulation of particle breakage process during grinding. *Powder Technology*, 110(3), 246-252. doi:[https://doi.org/10.1016/S0032-5910\(99\)00281-8](https://doi.org/10.1016/S0032-5910(99)00281-8)
- Mishra, B. K. (2003). A review of computer simulation of tumbling mills by the discrete element method: Part II—Practical applications. *International Journal of Mineral Processing*, 71(1–4), 95-112. doi:[http://dx.doi.org/10.1016/S0301-7516\(03\)00031-0](http://dx.doi.org/10.1016/S0301-7516(03)00031-0)
- Mishra, B. K., & Rajamani, R. K. (1992). The discrete element method for the simulation of ball mills. *Applied Mathematical Modelling*, 16(11), 598-604. doi:[http://dx.doi.org/10.1016/0307-904X\(92\)90035-2](http://dx.doi.org/10.1016/0307-904X(92)90035-2)
- Mitchell, M. (1998). *An introduction to genetic algorithms*: MIT press.
- Montgomery, J. (2013). Sneak Peek: Inside The Atikokan Biomass Plant Conversion. Retrieved from <http://www.renewableenergyworld.com/rea/news/article/2013/09/sneak-peek-inside-the-atikokan-biomass-plant-conversion>
- Moore, J. J., Perez, R., Gangopadhyay, A., & Eggert, J. F. (1988). Factors affecting wear in tumbling mills: Influence of composition and microstructure. *International Journal of Mineral Processing*, 22(1–4), 313-343. doi:[http://dx.doi.org/10.1016/0301-7516\(88\)90071-3](http://dx.doi.org/10.1016/0301-7516(88)90071-3)
- Morrell, S. (2004). An alternative energy–size relationship to that proposed by Bond for the design and optimisation of grinding circuits. *International Journal of Mineral Processing*, 74(1–4), 133-141. doi:<http://dx.doi.org/10.1016/j.minpro.2003.10.002>
- Morrison, R. D., & Cleary, P. W. (2008). Towards a virtual comminution machine. *Minerals Engineering*, 21(11), 770-781. doi:10.1016/j.mineng.2008.06.005
- Motte, J.-C., Delenne, J.-Y., Rouau, X., & Mayer-Laigle, C. (2015). Mineral–vegetal co-milling: An effective process to improve lignocellulosic biomass fine

- milling and to increase interweaving between mixed particles. *Bioresource Technology*, 192, 703-710.
- Munjiza, A., & John, N. W. M. (2002). Mesh size sensitivity of the combined FEM/DEM fracture and fragmentation algorithms. *Engineering Fracture Mechanics*, 69(2), 281-295. doi:[http://dx.doi.org/10.1016/S0013-7944\(01\)00090-X](http://dx.doi.org/10.1016/S0013-7944(01)00090-X)
- Naik, S., Malla, R., Shaw, M., & Chaudhuri, B. (2013). Investigation of comminution in a Wiley Mill: Experiments and DEM Simulations. *Powder Technology*, 237(0), 338-354. doi:<http://dx.doi.org/10.1016/j.powtec.2012.12.019>
- Napier-Munn, T. (2015). Is progress in energy-efficient comminution doomed? *Minerals Engineering*, 73(Supplement C), 1-6. doi:<https://doi.org/10.1016/j.mineng.2014.06.009>
- Nasaruddin, F., Yusof, Y., Chin, N., Endan, J., Amin, N. M., & Aziz, M. (2012). Effect of loading weight and grinding time on size reduction of cardamom, clove and cumin using a knife mill. *Journal of Food, Agriculture & Environment*, 10(3&4), 240-244.
- Nasaruddin, F., Yusof, Y. A., Chin, N. L., Endan, J., Mohd Amin, N. A., & Aziz, M. G. (2012). Effect of loading weight and grinding time on size reduction of cardamom, clove and cumin using a knife mill. *Journal of Food, Agriculture and Environment*, 10(3-4), 240-244.
- Nath, A. K., Jiten, C., & Singh, K. C. (2010). Influence of ball milling parameters on the particle size of barium titanate nanocrystalline powders. *Physica B: Condensed Matter*, 405(1), 430-434. doi:<http://dx.doi.org/10.1016/j.physb.2009.08.299>
- Nezami, E. G., Hashash, Y. M., Zhao, D., & Ghaboussi, J. (2004). A fast contact detection algorithm for 3-D discrete element method. *Computers and Geotechnics*, 31(7), 575-587.
- Nicmanis, M., & Hounslow, M. J. (1996). A finite element analysis of the steady state population balance equation for particulate systems: Aggregation and growth. *Computers & Chemical Engineering*, 20, Supplement 1(0), S261-S266. doi:[http://dx.doi.org/10.1016/0098-1354\(96\)00054-3](http://dx.doi.org/10.1016/0098-1354(96)00054-3)
- Nicmanis, M., & Hounslow, M. J. (1998). Finite-element methods for steady-state population balance equations. *Aiche Journal*, 44(10), 2258-2272. doi:10.1002/aic.690441015
- NIST/SEMATECH. (2013). e-Handbook of Statistical Methods. Retrieved from <http://www.itl.nist.gov/div898/handbook/>
- Nomura, S., & Tanaka, T. (2011). Analysis of energy–size reduction relationships in batch tumbling ball mills. *Powder Technology*, 208(3), 610-616. doi:<http://dx.doi.org/10.1016/j.powtec.2010.12.028>
- Ofgem. (2017). About the RO. Retrieved from <https://www.ofgem.gov.uk/environmental-programmes/ro/about-ro>
- Oñate, E., Idelsohn, S., Celigueta, M., Rossi, R., Marti, J., Carbonell, J., . . . Suárez, B. (2011). Advances in the particle finite element method (PFEM) for solving coupled problems in engineering *Particle-Based Methods* (pp. 1-49): Springer.
- Oñate, E., & Rojek, J. (2004). Combination of discrete element and finite element methods for dynamic analysis of geomechanics problems. *Computer Methods in Applied Mechanics and Engineering*, 193(27–29), 3087-3128. doi:<http://dx.doi.org/10.1016/j.cma.2003.12.056>
- Ono, I., Nakashima, H., Shimizu, H., Miyasaka, J., & Ohdoi, K. (2013). Investigation of elemental shape for 3D DEM modeling of interaction

- between soil and a narrow cutting tool. *Journal of Terramechanics*, 50(4), 265-276. doi:<http://dx.doi.org/10.1016/j.jterra.2013.09.001>
- Otwinowski, H. (2006). Energy and population balances in comminution process modelling based on the informational entropy. *Powder Technology*, 167(1), 33-44. doi:10.1016/j.powtec.2006.05.011
- Oyediji, O., & Fasina, O. (2017). Impact of drying-grinding sequence on loblolly pine chips preprocessing effectiveness. *Industrial Crops and Products*, 96, 8-15. doi:<https://doi.org/10.1016/j.indcrop.2016.11.028>
- Özcan, D. M., Bayraktar, A., Şahin, A., Haktanir, T., & Türker, T. (2009). Experimental and finite element analysis on the steel fiber-reinforced concrete (SFRC) beams ultimate behavior. *Construction and Building Materials*, 23(2), 1064-1077. doi:<http://dx.doi.org/10.1016/j.conbuildmat.2008.05.010>
- Pani, A. K., & Mohanta, H. K. (2013, 22-23 Feb. 2013). *A hybrid soft sensing approach of a cement mill using principal component analysis and artificial neural networks*. Paper presented at the Advance Computing Conference (IACC), 2013 IEEE 3rd International.
- Pelikan, M. (2005). *Hierarchical Bayesian optimization algorithm*. Springer.
- Pérez, J., Muñoz-Dorado, J., de la Rubia, T., & Martínez, J. (2002). Biodegradation and biological treatments of cellulose, hemicellulose and lignin: an overview. *International Microbiology*, 5(2), 53-63.
- Petrakis, E., & Komnitsas, K. (2017). Improved Modeling of the Grinding Process through the Combined Use of Matrix and Population Balance Models. *Minerals*, 7(5), 67.
- Powell, M. S., Govender, I., & McBride, A. T. (2008). Applying DEM outputs to the unified comminution model. *Minerals Engineering*, 21(11), 744-750. doi:10.1016/j.mineng.2008.06.010
- Powell, M. S., Weerasekara, N. S., Cole, S., LaRoche, R. D., & Favier, J. (2011). DEM modelling of liner evolution and its influence on grinding rate in ball mills. *Minerals Engineering*, 24(3-4), 341-351. doi:10.1016/j.mineng.2010.12.012
- Pramanik, R., & Deb, D. (2015). SPH procedures for modeling multiple intersecting discontinuities in geomaterial. *International Journal for Numerical and Analytical Methods in Geomechanics*, 39(4), 343-367. doi:10.1002/nag.2311
- Prasher, C. (1987). Crushing and grinding process handbook. 1987. *John Wiley & Sons, Chichester, UK*, 474.
- Ralston, A., & Rabinowitz, P. (2001). *A first course in numerical analysis*: Courier Corporation.
- Ramkrishna, D. (2000). *Population balances: Theory and applications to particulate systems in engineering*. Academic press.
- Randles, P. W., & Libersky, L. D. (1996). Smoothed Particle Hydrodynamics: Some recent improvements and applications. *Computer Methods in Applied Mechanics and Engineering*, 139(1-4), 375-408. doi:[http://dx.doi.org/10.1016/S0045-7825\(96\)01090-0](http://dx.doi.org/10.1016/S0045-7825(96)01090-0)
- Razuan, R., Finney, K. N., Chen, Q., Sharifi, V. N., & Swithenbank, J. (2011). Pelletised fuel production from palm kernel cake. *Fuel Processing Technology*, 92(3), 609-615. doi:<http://dx.doi.org/10.1016/j.fuproc.2010.11.018>
- Reddy, J. N. (1993). *An introduction to the finite element method* (Vol. 2): McGraw-Hill New York.

- Repellin, V., Govin, A., Rolland, M., & Guyonnet, R. (2010). Energy requirement for fine grinding of torrefied wood. *Biomass and Bioenergy*, 34(7), 923-930. doi:<http://dx.doi.org/10.1016/j.biombioe.2010.01.039>
- Rigoni, L. (2012). *Success Case Of Co-firing of Biomass and Coal*. Retrieved from <http://www.megaliafoundation.it/conv.maggio12/docs/Rigoni%20Alastom.pdf>
- Rosenkranz, S., Breitung-Faes, S., & Kwade, A. (2011). Experimental investigations and modelling of the ball motion in planetary ball mills. *Powder Technology*, 212(1), 224-230. doi:<http://dx.doi.org/10.1016/j.powtec.2011.05.021>
- Rousseau, J., Frangin, E., Marin, P., & Daudeville, L. (2009). Multidomain finite and discrete elements method for impact analysis of a concrete structure. *Engineering Structures*, 31(11), 2735-2743. doi:10.1016/j.engstruct.2009.07.001
- Ryu, C., Finney, K., Sharifi, V. N., & Swithenbank, J. (2008). Pelletised fuel production from coal tailings and spent mushroom compost—Part I: Identification of pelletisation parameters. *Fuel Processing Technology*, 89(3), 269-275.
- Ryu, C., Yang, Y. B., Khor, A., Yates, N. E., Sharifi, V. N., & Swithenbank, J. (2006). Effect of fuel properties on biomass combustion: Part I. Experiments—fuel type, equivalence ratio and particle size. *Fuel*, 85(7–8), 1039-1046. doi:<http://dx.doi.org/10.1016/j.fuel.2005.09.019>
- Saidur, R., Abdelaziz, E. A., Demirbas, A., Hossain, M. S., & Mekhilef, S. (2011). A review on biomass as a fuel for boilers. *Renewable and Sustainable Energy Reviews*, 15(5), 2262-2289. doi:<http://dx.doi.org/10.1016/j.rser.2011.02.015>
- Sakai, M., & Koshizuka, S. (2009). Large-scale discrete element modeling in pneumatic conveying. *Chemical Engineering Science*, 64(3), 533-539. doi:<http://dx.doi.org/10.1016/j.ces.2008.10.003>
- Salzborn, D., & Chin-Fatt, A. (1993, 23-27 May 1993). *Operational results of a vertical roller mill modified with a high efficiency classifier*. Paper presented at the Cement Industry Technical Conference, 1993. Record of Conference Papers., 35th IEEE.
- Sarris, E., & Constantinides, G. (2013). Finite element modeling of nanoindentation on C–S–H: Effect of pile-up and contact friction. *Cement and Concrete Composites*, 36(0), 78-84. doi:<http://dx.doi.org/10.1016/j.cemconcomp.2012.10.010>
- Sato, A., Kano, J., & Saito, F. (2010). Analysis of abrasion mechanism of grinding media in a planetary mill with DEM simulation. *Advanced Powder Technology*, 21(2), 212-216. doi:<http://dx.doi.org/10.1016/j.apt.2010.01.005>
- Sato, K., Meguri, N., Shoji, K., Kanemoto, H., Hasegawa, T., & Maruyama, T. (1996). Breakage of coals in ring-roller mills Part I. The breakage properties of various coals and simulation model to predict steady-state mill performance. *Powder Technology*, 86(3), 275-283. doi:[http://dx.doi.org/10.1016/0032-5910\(95\)03061-1](http://dx.doi.org/10.1016/0032-5910(95)03061-1)
- Schmidt, R., & Nikrityuk, P. A. (2011). Direct numerical simulation of particulate flows with heat transfer in a rotating cylindrical cavity. *Philosophical Transactions of the Royal Society A: Mathematical, Physical and Engineering Sciences*, 369(1945), 2574-2583. doi:10.1098/rsta.2011.0046
- Schörghener, M., Gruber, P., & Gerstmayr, J. (2013). Interaction of flexible multibody systems with fluids analyzed by means of smoothed particle

- hydrodynamics. *Multibody System Dynamics*, 30(1), 53-76. doi:10.1007/s11044-013-9359-6
- Schreurs, P. (2009). Lecture notes-course 4A780 Concept version. *Materials Technology*.
- Sen, M., Dubey, A., Singh, R., & Ramachandran, R. (2013). Mathematical Development and Comparison of a Hybrid PBM-DEM Description of a Continuous Powder Mixing Process. *Journal of Powder Technology*, 2013, 11. doi:10.1155/2013/843784
- Shoji, K., Meguri, N., Sato, K., Kanemoto, H., Hasegawa, T., & Maruyama, T. (1998). Breakage of coals in ring-roller mills Part 2. An unsteady-state simulation model. *Powder Technology*, 99(1), 46-52. doi:10.1016/S0032-5910(98)00089-8
- Shuiping, L., Hongzan, B., Zhichu, H., & Jianzhong, W. (2002). Nonlinear comminution process modeling based on GA-FNN in the computational comminution system. *Journal of Materials Processing Technology*, 120(1-3), 84-89. doi:[http://dx.doi.org/10.1016/S0924-0136\(01\)01170-0](http://dx.doi.org/10.1016/S0924-0136(01)01170-0)
- Silva, G. G. D., & Xavier, R. S. G. (2011). Successive centrifugal grinding and sieving of wheat straw. *Powder Technology*, 208(2), 266-270. doi:<http://dx.doi.org/10.1016/j.powtec.2010.08.015>
- Singh, H., Arter, R., Dodd, L., Langston, P., Lester, E., & Drury, J. (2009). Modelling subgroup behaviour in crowd dynamics DEM simulation. *Applied Mathematical Modelling*, 33(12), 4408-4423.
- Singh, V., Banerjee, P., Tripathy, S., Saxena, V., & Venugopal, R. (2013). *Artificial Neural Network Modeling of Ball Mill Grinding Process*. *J Powder Metall Min 2: 106*. doi: 10.4172/2168-9806.1000106 Page 2 of 4 Volume 2• Issue 2• 1000106 *J Powder Metall Min ISSN: 2168-9806 JPMM, an open access journal collected from the feed ore of a pelletisation plant*. These chromite ores are of friable in nature with friable and broken particles. The bond work index of ores was 6 kWh/ton. These ore contain 30, 26, 12 and 14%, Cr₂O₃, Fe, SiO₂ and Al₂O₃, respectively. Retrieved from <http://omicsgroup.org/journals/artificial-neural-network-modeling-of-ball-mill-grinding-process-2168-9806.1000106.pdf>
- Smith, A., James, C., Jones, R., Langston, P., Lester, E., & Drury, J. (2009). Modelling contra-flow in crowd dynamics DEM simulation. *Safety Science*, 47(3), 395-404. doi:<http://dx.doi.org/10.1016/j.ssci.2008.05.006>
- Sokhansanj, S., Mani, S., Bi, X., Zaini, P., & Tabil, L. (2005). *Binderless pelletization of biomass*. Paper presented at the ASAE Annual International Meeting, Tampa Convention Centre, Tampa, Florida.
- Stamboliadis, E. T. (2007). The energy distribution theory of comminution specific surface energy, mill efficiency and distribution mode. *Minerals Engineering*, 20(2), 140-145. doi:10.1016/j.mineng.2006.07.009
- Stange, W. (1993). Using artificial neural networks for the control of grinding circuits. *Minerals Engineering*, 6(5), 479-489.
- Su, Z.-g., Wang, P.-h., & Yu, X.-j. (2010). Immune genetic algorithm-based adaptive evidential model for estimating unmeasured parameter: Estimating levels of coal powder filling in ball mill. *Expert Systems with Applications*, 37(7), 5246-5258. doi:<http://dx.doi.org/10.1016/j.eswa.2009.12.077>
- Sun, X., Sakai, M., & Yamada, Y. (2013). Three-dimensional simulation of a solid-liquid flow by the DEM-SPH method. *Journal of Computational Physics*, 248(0), 147-176. doi:<http://dx.doi.org/10.1016/j.jcp.2013.04.019>

- Tabil, L., Sokhansanj, S., & Tyler, R. (1997). Performance of different binders during alfalfa pelleting. *Canadian Agricultural Engineering*, 39(1), 17-23.
- Takeuchi, H., Nakamura, H., Iwasaki, T., & Watano, S. (2012). Numerical modeling of fluid and particle behaviors in impact pulverizer. *Powder Technology*, 217, 148-156.
- Tamura, M., Watanabe, S., Kotake, N., & Hasegawa, M. (2014). Grinding and combustion characteristics of woody biomass for co-firing with coal in pulverised coal boilers. *Fuel*, 134(0), 544-553. doi:<http://dx.doi.org/10.1016/j.fuel.2014.05.083>
- Tanaka, T. (1972). Scale-Up Formula for Grinding Equipment Using Selection Function. *Journal of Chemical Engineering of Japan*, 5(3), 310-313. doi:10.1252/jcej.5.310
- Tang, J., Zhao, L.-j., Zhou, J.-w., Yue, H., & Chai, T.-y. (2010). Experimental analysis of wet mill load based on vibration signals of laboratory-scale ball mill shell. *Minerals Engineering*, 23(9), 720-730. doi:<http://dx.doi.org/10.1016/j.mineng.2010.05.001>
- Temmerman, M., Jensen, P. D., & Hebert, J. (2013). Von Rittinger theory adapted to wood chip and pellet milling, in a laboratory scale hammermill. *Biomass and Bioenergy*, 56, 70-81.
- Tijsskens, E., Ramon, H., & Baerdemaeker, J. D. (2003). Discrete element modelling for process simulation in agriculture. *Journal of Sound and Vibration*, 266(3), 493-514. doi:[http://dx.doi.org/10.1016/S0022-460X\(03\)00581-9](http://dx.doi.org/10.1016/S0022-460X(03)00581-9)
- Too, C. L., Yusof, Y. A., Chin, N. L., Talib, R. A., & Aziz, M. G. (2012). Size reduction of selected spices using knife mill: Experimental investigation and model fitting. *Journal of Food Agriculture & Environment*, 10(1), 102-106.
- Topell Energy. (2014). What is Torrefaction. Retrieved from <http://www.topellenergy.com/technology/what-is-torrefaction/>
- Tumuluru, J. S., Sokhansanj, S., Wright, C. T., Boardman, R. D., & Yancey, N. A. (2011). *A review on biomass classification and composition, co-firing issues and pretreatment methods*. Paper presented at the Proceedings of the American Society of Agricultural and Biological Engineers Annual International Meeting.
- Tumuluru, J. S., Tabil, L. G., Song, Y., Iroba, K. L., & Meda, V. (2014). Grinding energy and physical properties of chopped and hammer-milled barley, wheat, oat, and canola straws. *Biomass and Bioenergy*, 60(0), 58-67. doi:<http://dx.doi.org/10.1016/j.biombioe.2013.10.011>
- UNFCCC. (2016). The Paris Agreement. Retrieved from http://unfccc.int/paris_agreement/items/9485.php
- Uslu, A., Faaij, A. P. C., & Bergman, P. C. A. (2008). Pre-treatment technologies, and their effect on international bioenergy supply chain logistics. Techno-economic evaluation of torrefaction, fast pyrolysis and pelletisation. *Energy*, 33(8), 1206-1223. doi:10.1016/j.energy.2008.03.007
- Van Dam, J. E., van den Oever, M. J., Teunissen, W., Keijsers, E. R., & Peralta, A. G. (2004). Process for production of high density/high performance binderless boards from whole coconut husk: Part 1: Lignin as intrinsic thermosetting binder resin. *Industrial Crops and Products*, 19(3), 207-216.
- van den Broek, R., Faaij, A., & van Wijk, A. (1996). Biomass combustion for power generation. *Biomass and Bioenergy*, 11(4), 271-281. doi:[http://dx.doi.org/10.1016/0961-9534\(96\)00033-5](http://dx.doi.org/10.1016/0961-9534(96)00033-5)
- van der Stelt, M. J. C., Gerhauser, H., Kiel, J. H. A., & Ptasinski, K. J. (2011). Biomass upgrading by torrefaction for the production of biofuels: A review.

- Van Essendelft, D., Zhou, X., & Kang, B.-J. (2013). Grindability determination of torrefied biomass materials using the Hybrid Work Index. *Fuel*, 105, 103-111.
- Van Loo, S., & Koppejan, J. (2007). *The handbook of biomass combustion and co-firing*. Earthscan.
- Vassilev, S. V., Baxter, D., Andersen, L. K., Vassileva, C. G., & Morgan, T. J. (2012). An overview of the organic and inorganic phase composition of biomass. *Fuel*, 94(0), 1-33. doi:<http://dx.doi.org/10.1016/j.fuel.2011.09.030>
- Verkoeijen, D., A. Pouw, G., M. H. Meesters, G., & Scarlett, B. (2002). Population balances for particulate processes—a volume approach. *Chemical Engineering Science*, 57(12), 2287-2303. doi:[http://dx.doi.org/10.1016/S0009-2509\(02\)00118-5](http://dx.doi.org/10.1016/S0009-2509(02)00118-5)
- Vogel, L., & Peukert, W. (2003). Breakage behaviour of different materials—construction of a mastercurve for the breakage probability. *Powder Technology*, 129(1–3), 101-110. doi:[http://dx.doi.org/10.1016/S0032-5910\(02\)00217-6](http://dx.doi.org/10.1016/S0032-5910(02)00217-6)
- Vogel, L., & Peukert, W. (2005). From single particle impact behaviour to modelling of impact mills. *Chemical Engineering Science*, 60(18), 5164-5176. doi:10.1016/j.ces.2005.03.064
- Vorobyev, A. (2012). *A Smoothed Particle Hydrodynamics Method for the Simulation of Centralized Sloshing Experiments*.
- Walker, W., Lewis, W., McAdams, W., & Gilliland, E. (1923). Principles of chemical engineering, 1923: McGraw-Hill Inc., New York.
- Wang, G., Zhao, K., Li, X., Li, L., & Wang, J. (2012). Arrangement optimization of hammers and fenders on Scrap Metal Shredder using ant colony algorithms. *JVC/Journal of Vibration and Control*, 18(5), 659-670.
- Wang, H., Jia, M.-p., Huang, P., & Chen, Z.-l. (2010). A study on a new algorithm to optimize ball mill system based on modeling and GA. *Energy Conversion and Management*, 51(4), 846-850. doi:<http://dx.doi.org/10.1016/j.enconman.2009.11.020>
- Wang, J., Yu, H. S., Langston, P., & Fraige, F. (2011). Particle shape effects in discrete element modelling of cohesive angular particles. *Granular Matter*, 13(1), 1-12. doi:10.1007/s10035-010-0217-4
- Wang, Y., & Mora, P. (2009). The ESYS_particle: a new 3-D discrete element model with single particle rotation *Advances in Geocomputing* (pp. 183-228): Springer.
- Webb, P. A. (2001). *Volume and density determinations for particle technologists*.
- Weerasekara, N. S., Powell, M. S., Cleary, P. W., Tavares, L. M., Evertsson, M., Morrison, R. D., . . . Carvalho, R. M. (2013). The contribution of DEM to the science of comminution. *Powder Technology*, 248, 3-24. doi:10.1016/j.powtec.2013.05.032
- Williams, O. (2016). *On biomass milling for power generation*. University of Nottingham.
- Williams, O., Eastwick, C., Kingman, S., Giddings, D., Lormor, S., & Lester, E. (2015). Investigation into the applicability of Bond Work Index (BWI) and Hardgrove Grindability Index (HGI) tests for several biomasses compared to Colombian La Loma coal. *Fuel*, 158(Supplement C), 379-387. doi:<https://doi.org/10.1016/j.fuel.2015.05.027>
- Womac, A., Igathinathane, C., Bitra, P., Miu, P., Yang, T., Sokhansanj, S., & Narayan, S. (2007). Biomass pre-processing size reduction with instrumented mills. *parameters*, 17, 20.

- Wood, C. J., Summers, G. H., Clark, C. A., Kaeffer, N., Braeutigam, M., Carbone, L. R., . . . Narbey, S. (2016). A comprehensive comparison of dye-sensitized NiO photocathodes for solar energy conversion. *Physical Chemistry Chemical Physics*, *18*(16), 10727-10738.
- World Coal Association. (2014). Coal and Electricity. Retrieved from <http://www.worldcoal.org/coal/uses-of-coal/coal-electricity/>
- Yamada, Y., & Sakai, M. (2013). Lagrangian–Lagrangian simulations of solid–liquid flows in a bead mill. *Powder Technology*, *239*, 105-114.
- Yan, W., Acharjee, T. C., Coronella, C. J., & Vásquez, V. R. (2009). Thermal pretreatment of lignocellulosic biomass. *Environmental Progress & Sustainable Energy*, *28*(3), 435-440. doi:10.1002/ep.10385
- Zhang, M., Song, X., Zhang, P., Pei, Z. J., Deines, T. W., & Wang, D. (2012). Size Reduction of Cellulosic Biomass in Biofuel Manufacturing: A Study on Confounding Effects of Particle Size and Biomass Crystallinity. *Journal of Manufacturing Science and Engineering*, *134*(1), 011009-011009. doi:10.1115/1.4005433
- Zhang, Y. G., Wu, Q. H., Wang, J., Oluwande, G., Matts, D., & Zhou, X. X. (2002). Coal mill modeling by machine learning based on onsite measurements. *Energy Conversion, IEEE Transactions on*, *17*(4), 549-555. doi:10.1109/TEC.2002.805182
- Zhou, Y., Liu, Y., Tang, X., Cao, S., & Chi, C. (2014). Numerical investigation into the fragmentation efficiency of one coal prism in a roller pulveriser: Homogeneous approach. *Minerals Engineering*, *63*, 25-34.
- Zhu, M. (2014). *Fluid-structure interaction analysis with the particle finite element method*. (Doctor of Philosophy), Oregon State University. Retrieved from <https://ir.library.oregonstate.edu/downloads/sb397b49r>
- Zhu, M., & Scott, M. H. (2014). Modeling fluid–structure interaction by the particle finite element method in OpenSees. *Computers & structures*, *132*(0), 12-21. doi:<http://dx.doi.org/10.1016/j.compstruc.2013.11.002>
- Zwart, R. (2012). *Production of Solid Sustainable Energy Carriers from Biomass by Means of Torrefaction, Deliverable No. D6.1: Description of existing handling and storage facilities and the associated issues*. Retrieved from https://sector-project.eu/fileadmin/downloads/deliverables/SECTOR_D6.1.pdf